MODULATIONS OF PHOTOPHYSICAL PROPERTIES OF FLUOROGENIC DYES THROUGH SUPRAMOLECULAR INTERACTION AND THEIR APPLICATIONS

By

Goutam Chakraborty

CHEM01201404011

Bhabha Atomic Research Centre, Mumbai

A thesis submitted to the

Board of Studies in Chemical Sciences

In partial fulfillment of requirements

for the Degree of

DOCTOR OF PHILOSOPHY

of

HOMI BHABHA NATIONAL INSTITUTE

April, 2019

Homi Bhabha National Institute

Recommendations of the PhD Viva Voce Committee

As members of the Viva Voce Committee, we certify that we have read the dissertation prepared by Shri **Goutam Chakraborty** entitled **"Modulations of Photophysical Properties of Fluorogenic Dyes through Supramolecular Interaction and Their Applications"** and recommend that it may be accepted as fulfilling the thesis requirement for the award of Degree of Doctor of Philosophy in Chemical Sciences.

Chairman - **Dr. S. K. Nayak, (Ex-BARC)**		**Date:** 07/08/2019
Guide/Convener - **Prof. A. K. Ray, (Ex-BARC)**		**Date:** 07/08/2019
Examiner - **Prof. Anindya Datta, (IIT Bombay)**		**Date:** 07/08/2019
Co-guide - **Dr. Haridas Pal, (BARC)**		**Date:** 07/08/2019
Member 1- **Dr. Sukhendu Nath, (BARC)**		**Date:** 07.08.19
Member 2 - **Dr. J. Mohanty, (BARC)**		**Date:** 07.08.2019
Member-3 - **Dr. P. A. Hassan, (BARC)**		**Date:** 07.08.2019

Final approval and acceptance of this thesis is contingent upon the candidate's submission of the final copies of the thesis to HBNI.

We hereby certify that we have read this thesis prepared under our direction and recommend that it may be accepted as fulfilling the thesis requirement.

Date: 07-08-2019

Place: BARC, Mumbai

07/08/19
Signature
Guide

07/08/2019
Signature
Co-Guide

STATEMENT BY AUTHOR

This dissertation has been submitted in partial fulfillment of requirements for an advanced degree at Homi Bhabha National Institute (HBNI) and is deposited in the Library to be made available to borrowers under rules of the HBNI.

Brief quotations from this dissertation are allowable without special permission, provided that accurate acknowledgement of source is made. Requests for permission for extended quotation from or reproduction of this manuscript in whole or in part may be granted by the Competent Authority of HBNI when in his or her judgment the proposed use of the material is in the interests of scholarship. In all other instances, however, permission must be obtained from the author.

Goutam Chakraborty

DECLARATION

I, hereby declare that the investigation presented in the thesis has been carried out by me. The work is original and has not been submitted earlier as a whole or in part for a degree / diploma at this or any other Institution / University.

Goutam Chakraborty

List of Publications arising from the thesis

Journal

1. "Interaction of a Triaryl Methane Dye with Cucurbit[7]uril and Bovine Serum Albumin: A Perspective of Cooperative versus Competitive Bindings", **G. Chakraborty**, A. K. Ray* and H. Pal*, *Chemistryselect*, **2018,** 3, 1088-1096.

2. "A highly fluorescent turn-on probe in the near-infrared region for albumin quantification in serum matrix", **G. Chakraborty**, A. K. Ray, P.K.Singh*, H. Pal*, *Chem. Commun.,* **2018**, 54, 8383-8386.

3. "Non-covalent interaction of BODIPY-benzimidazole conjugate with bovine serum albumin- A photophysical and molecular docking study", **G. Chakraborty**, A. K. Ray, P. K. Singh*, H. Pal*, *J. Photochem. Photobiol., A,* **2019,** 377, 220-227.

4. "A styryl based fluorogenic probe with high affinity for a cyclodextrin derivative", **G. Chakraborty**, A. K. Ray, P. K. Singh*, H. Pal* *Org. Biomol. Chem.* **2019**, 17, 6895-6904.

Symposia/Conference

1. "Improved photophysical characteristics of aqueous Rhodamine-B by interaction with host Sulfobutylether-β-cyclodextrin for use in dye lasers, **G. Chakraborty***, P. K. Singh, A.K. Ray and H. Pal", National *Laser Symposium*-26, **2017**.

2. "Interaction of Crystal violet and it's BSA complex with Cucurbit[7]uril - A competitive supramolecular interaction study", **G. Chakraborty**, A. K. Ray and H. Pal, *Trombay Symposium of Radiation and Photochemistry (TSRP),* **2018.**

Other publications

5. "Supramolecularly Assisted Modulation of Optical Properties of BODIPY−Benzimidazole Conjugates", S. S. Thakare, **G. Chakraborty**, P. Krishnakumar, A. K. Ray, D. K. Maity, H. Pal,* N. Sekar*, *J. Phys. Chem. B.,* **2016**, 120, 11266−11278.

6. "pH-Responsive Interaction of Fluorogenic Antimalarial Drug Quinine with Macrocyclic Host Cucurbit[7]uril: Modulations in Photophysical and Acid-Base Properties", D.R. Boraste, **G. Chakraborty,** A. K. Ray, G. S. Shankarling*, H. Pal*, ChemistrySelect, **2017,** 2, 5128– 5142.

7. "Modulation of the photophysical properties of β-substituted BODIPY dyes", A. B. More, **G. Chakraborty,** S. Mula, A. K. Ray and N. Sekar, J. Fluoresc. 28(1), **2018**, 381-392.

8. "Modulation of optical properties of BODIPY fluorophore via intramolecular charge transfer", S.S.Thakare, **G. Chakraborty,** S. Mula, A. More, A. K. Ray, S Chattopadhyay and N. Sekar, J. Lumin., **2018**, 194, 622–630.

9. "Proton Induced Modulation of ICT and PET Processes in an Imidazo-phenanthroline Based BODIPY Fluorophores", S.S.Thakare, **G. Chakraborty**, S. Kothavale, S. Mula, A. K. Ray and N. Sekar, J. Fluoresc, **2018**, 27 (6), 2313–2322.

10. "Supramolecular Host-Guest Interaction of Antibiotic Drug Ciprofloxacin with Cucurbit[7]uril Macrocycle: Modulations In Photophysical Properties and Enhanced Photostability", D.R. Boraste, **G. Chakraborty**, A. K. Ray, G.S. Shankarling, H. Pal*, *J. Photochem. Photobiol.,* A, **2018**, 358, 26–37.

Goutam Chakraborty

Dedicated to My Beloved Mother, Father, Sweet Sisters,

Respected Teachers and Mentors

ACKNOWLEDGEMENTS

I would like to take this opportunity to thank everyone, who supported me throughout in my work for this thesis. First of all, I wish to begin by expressing my sincere and deepest gratitude to my guide, Dr. Alok K. Ray and my co-guide Dr. Haridas Pal, who aspired to me every single moment of my work by their guidance, constant encouragement, and motivation. From my guide Dr. Alok K Ray, I learnt the ability to keep calm and patience during an experiment. On the other hand, from Dr. Haridas Pal, I learnt how to execute a problem and not to leave the job unless and until it is finished properly. I was fortunate enough to work with these two persons and their wide knowledge and logical way of thinking and reasoning on scientific problems greatly helped me during the work. I am thankful to both of them for sharing their knowledge and scientific understanding during the fruitful discussions with me throughout the work. Each and every time, during discussion with either of my guide or co-guide, I always learnt new things and scientific inputs which helped me a lot in my experiments.

I am privileged to thank Dr. Prabhat. K. Singh, for his unstinted support and encouragement. I am sincerely thankful to him for introducing me to the realm of supra-biomolecular chemistry. Without his support and help it would have been a very difficult for me to a give a proper shape of my thesis well with in time.

I would like to express my sincere regards and deepest appreciation to M B Saiprasad for his continuous and priceless support towards purchasing the necessary items, instruments and chemical for my Ph.D work.

I am grateful to Dr. M. Sayed, Dr. S. Adhikari, Mr. Sudip Gorai, Dr. Somyaditya Mula, Mr. Mrunesh Koli, Dr. Khsama Roy, etc. for their moral support, stimulating discussions and constructive criticisms, which have substantially helped me in my research work.

I also gratefully acknowledge the cooperative attitude and support provided by all the members of L&PTD. Their spirited research oriented approach has always been a source of inspiration and moral booster.

It gives me immense pleasure to thank the respected and distinguished members of the doctoral committee, Dr. S. K. Nayak (Cahirman), Dr. Sukhendu Nath (Member), Dr. P. A. Hassan (Member) and Dr. J. Mohanty (Member) for their critical reviews and suggestions during the progress reviews and pre-synopsis presentation.

I cannot imagine my current position without the blessings of my teachers, and will always be indebted to them. Mostly, I would like express my deepest love and respect to Shri. Rathindranath Majumber (Former Headmaster Shantinagar Vidyamandir, Burnpur, Asansol) who planted the seed of interest in Chemistry inside me from the very first time it was introduced to our study.

Most importantly, I owe my heartfelt gratitude to my mother, who never lost her hope in me. Even though in my hardest time, she always stood by me and gave constant support and encouragement so that I can move forward. It is her blessing that I could fulfill my dream of completing Ph.D. I am also thankful to my father, who always supported me during hardest days of research work.

Finally, I would like to express my endless thanks and appreciations to my two beautiful and loving sisters, who always loved, cared, supported and encouraged me to achieve my goals.

April, 2019

Goutam Chakraborty, L&PTD, BARC, Mumbai

CONTENTS

SYNOPSIS

Supramolecular chemistry plays a vital role in realizing various exotic three dimensional structures through noncovalent interactions that can bring out many interesting applications in wide areas like pharmaceuticals, therapeutics, nanotechnology, sensing, optical switches, functional materials, and so on.[1-10] In supramolecular host-guest complex the formations, molecular recognitions of constituent hosts and guests play the important role. Best molecular recognition occurs in nature between substrate-enzyme pairs, leading to ultra stable complex formation with association or binding constant (K_a) as high as 10^{16}-10^{21} M^{-1}. For artificial host-guest systems, K_a values typically range between 10^3-10^6 M^{-1}, though in some specific cases K_a can become as high as about 10^{11}-10^{17} M^{-1}.[10]

Cyclodextrins (CDs), calixarenes, cucurbit[n]urils (CBn), etc. are important synthetic macrocyclic hosts in supramolecular studies. On complexation with these hosts, the characteristics of guest molecules can be altered exceptionally, modeling their photophysical, acid-base and other properties, and marking them immune towards external reactants as well as photo-thermal-degradations.[10-14] Among various macrocycles, the CBn and CD hosts have been used extensively in supramolecular chemistry due to their reasonable bio-compatibility and low toxicity. In recent years host-guest studies involving different CD derivatives have gained immense momentum due to ready availability, easy synthesis, high solubility and low biotoxicity of these macrocycles.

Host-guest studies involving interactions of chromophoric dyes with biomolecules like proteins (HSA, BSA, globulin), RNA, DNA, etc. have also drawn immense research interests in supramolecular chemistry.[15-22] Binding with biomolecules can induce significant changes in the photophysical properties of the chromophoric guests. Thus, binding to DNA causes an enormous fluorescence enhancement for ethidium bromide dye which have been exploited extensively to study binding of other chromophores to DNA using competitive binding

methodology.[19,20] Similarly for BSA and HSA proteins, 8-anilinonaphthalene-1-sulfonic acid (ANS) dye has been recognized as the best probe for qualitative and quantitative determination of these proteins.[21,22]

In the present study we have investigated supramolecular host-guest interactions of various chromophoric dyes involving both biomolecular hosts (BSA and HSA) and synthetic macrocyclic hosts (CB7 and βCD derivatives). Our efforts have been to understand the mode of binding in the host-guest systems and the effect of such binding on the photophysical properties of chromophoric dyes, aiming to find their possible applications. Results obtained in the preset study have been discussed in this thesis. For convenience of presentation, the thesis has been divided into seven chapters and the contents in different chapters are briefly as follows.

Chapter 1: ***Introduction to Supramolecular Chemistry and Fluorescence Spectroscopy***

In this introductory chapter of the thesis, various aspects of supramolecular chemistry have been discussed briefly, mentioning different noncovalent interactions involved in the supramolecular host-guest complex formations, discussing the uses of such system chemical and biological sciences and bringing out the usefulness of such systems in the areas of photochemical sciences. A brief account on the fluorescence spectroscopy has also been provided in this chapter with emphasis on selection rules for electronic transitions and different photophysical pathways associated with excited chromophoric molecules. The host-guest systems chosen in the present investigation are also introduced in the present chapter along with a brief note on the objective and motivation of the present study.

Chapter 2: ***Materials, Methods and Instrumentations***

The properties and applications of the chromophoric dyes and the host molecules used in the present study (cf. Chart 1) have been discussed briefly in this chapter. Working

principles of various spectrometric techniques and other measuring instruments used in the present study have also been described in this chapter with necessary details.

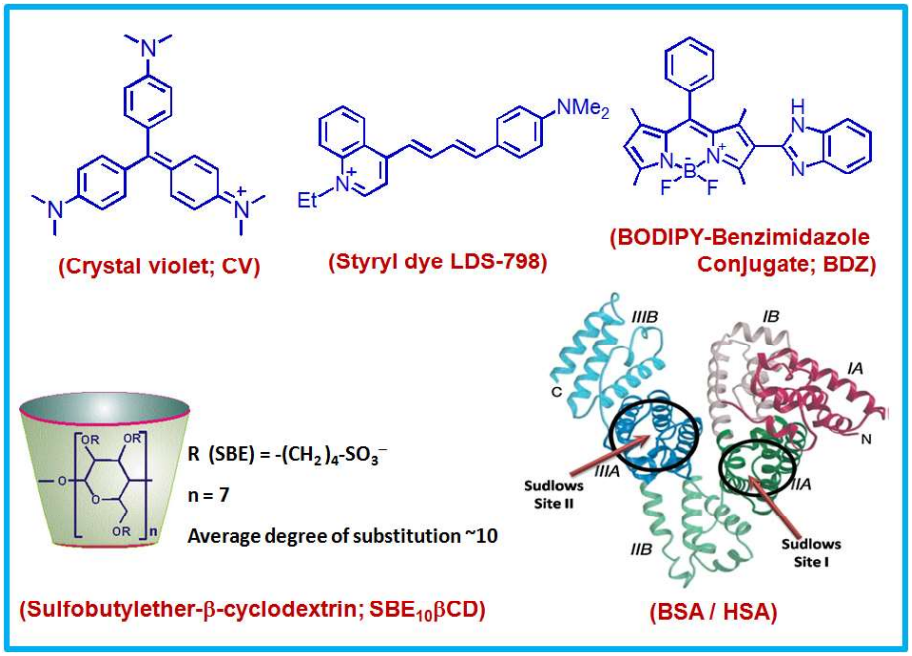

Chart: 1. Chemical structures of the chromophoric dyes and the schematics of the macrocyclic and biomolecular hosts used in the present study.

Chapter 3: *Interactions of a Triaryl Methane Dye with Cucurbit7uril and Bovine Serum Albumin Hosts - A Perspective of Cooperative versus Comparative Bindings*

Detail study on the interactions of a triphenyl methane (TPM) dye, crystal violet (CV), with a macrocyclic host CB7 and a biomolecular host BSA has been presented in this chapter.[23] A homologues TPM dye, brilliant green (BG), was shown earlier to undergo cooperative binding with CB7 and BSA host.[24] In this study our interest was thus to see if CV interacts in a cooperative or competitive manner with CB7 and BSA hosts and thus to understand whether cooperative binding is just specific to BG dye or a general phenomena for the TPM dyes. Independent binding of CV with CB7 occurs with a moderate K_a value (~6.3×10^3 M^{-1}) causing only a few fold of fluorescence enhancement of the dye, as only one of the three flexible arms of CV is encapsulated by CB7 cavity. On the contrary, independent binding of CV with BSA occurs with a very high K_a value (~$3.2 \times 10^5 M^{-1}$) and a large

enhancement in fluorescence intensity (~100 folds), supporting complete entrapping of CV by BSA binding pocket. Addition of CB7 to CV-BSA complex results in a substantial reduction in fluorescence intensity, whereas addition of BSA to CV-CB7 complex causes an a significant increase in the fluorescence intensity. The effective K_a values for titration of CV-CB7 complex by BSA or CV-BSA complex by CB7 are much lower (~1.2×10^4 M^{-1} and ~4.3×10^3 M^{-1}, respectively) compared to those for CV-BSA and CV-CB7 binary systems. It is concluded from the observed results that CV undergoes competitive binding with CB7 and BSA hosts than the cooperative binding reported for homologue BG dye.[23] It appears from the observed results that while comparable K_a values for BG-CB7 and BG-BSA binary systems support a cooperative binding, the large difference of K_a values for CV-CB7 and CV-BSA binary systems (by ~50 fold) actually favors a competitive binding over a cooperative binding. Present results provide a clue towards designing of suitable ternary systems with either cooperative or competitive bindings to achieve best effects in drug formulation and drug delivery mechanisms.

Chapter 4: ***Supramolecular Interaction of Near Infrared Fluorescent Probe LDS-798 With a Highly Substituted Anionic β-Cyclodextrin Derivative.***

This chapter describes interaction of a styryl dye, LDS-798, with polyanionic macrocyclic host sulfobutylether-βCD (SBE_{10}βCD). LDS-798 fluorescence undergoes substantial enhancement (~70 fold) on its binding to SBE_{10}βCD cavity. The K_a value for the LDS-798-SBE_{10}βCD system is estimated to be very high (~1.6×10^6 M^{-1}), apparently the highest reported till date involving a CD derivate. With the SBE_{10}βCD host, while the sulfobutylether groups at its host portals extend the host cavity for better encapsulation and improved hydrophobic interaction for the dye, the polyanionic charges on the host portals provide additional strong electrostatic interaction for the cationic LDS-798, causing exceeding high K_a value and large enhancement in the fluorescence intensity. The strongest binding in

the LDS-798-SBE_{10}βCD system is further corroborated by negligible effects on the K_a value by the presence of the competitive guests like lithocholic acid and adamentyl hydrochloride. The LDS-798-SBE_{10}βCD system is found to be very sensitive to external stimulus like salt concentration, temperature and pH. The strongest binding of LDS-798 with polyanionic SBE_{10}βCD host and the exceptional response of the dye-host complex to external stimuli like temperature, ionic strength, etc. makes this system an excellent choice for its utilization as a supramolecular sensor for temperature, polarity, and so on.

Chapter 5: ***Interaction of a BODIPY-Benzimidazole Derivative with Serum Albumin: A Photophysical Investigation***

This chapter describes interaction of a BODIPY-benzimidazole conjugate dye (BDZ) with BSA host. Due to strong hydrophobic characteristics, BDZ is insoluble in water. To avoid dye aggregation, thus, present study was carried out in 20% ethanolic PBS solution. In BDZ, there is an intramolecular charge transfer (ICT) from benzimidazole to BODIPY unit causing the dye very weakly fluorescent. Addition of BSA to BDZ solution results in a substantial fluorescence enhancement along with a notable blue shift (from 545 nm to 531 nm). While reduced structural flexibility and ICT process for bound dye inside BSA pocket decreases non-radiative deexcitation and hence a large increase in fluorescence intensity, the lower micropolarity at the binding site causes the observed blue shift. Binding of BDZ with BSA is quite strong, with K_a as ~1.8×10^4 M^{-1}. Competitive interactions in the presence of warfarin (binder for Sudlow's site-I) and ibuprofen (binder for Sudlow's site-II) suggest that BDZ binds preferentially to Sudlow's site-II of BSA. Molecular docking study further confirms this binding interaction. Observed results suggest the potential of the BDZ-BSA system for uses in fluorogenic sensor applications.

Chapter 6*: Interaction of LDS-798 (Styryl-11) Dye with BSA Protein - Highly Fluorescent Turn-On Probe in the Near Infrared Region for Albumin Quantification*

This chapter presents the interaction of biologically important dye LDS-798 with BSA and HSA hosts.[25] The dye in aqueous solution is almost non-fluorescent due to its large structural flexibility and its ability to undergo twisted intramolecular charge transfer (TICT) in its first excited state. Addition of BSA to LDS-798 solution results in an exceptional fluorescence turn-ON with ~500 fold enhancement for 10 μM dye in the presence of ~300 μM BSA. Similar results are also obtained on interaction of LDS-798 with HSA. Largely reduced structural flexibility, micropolarity and TICT formation imposed by the dye confinement into BSA/HSA cavity results in the large modulations observed in the photophysical properties of LDS-798 dye. The K_a values for LDS-798-BSA and LDS-798-BSA systems are found to be very high, ~1.27x0^4 M^{-1} and ~1.86x10^4 M^{-1}, respectively. Competitive binding experiments using warfarin (binder for Sudlow's site-I) and ibuprofen (binder for Sudlow's site-II) reveals that LDS-798 binds preferentially to Sudlow's site-I of the BSA host.

Binding of LDS-798 to BSA/HSA proteins is only negligibly affected by the presence Na^+, K^+, Ca^{2+}, HPO_4^-, Cl^-, amino acids, porphyrins, etc. suggesting the interaction very specific and useful for qualitative/quantitative estimation of albumins. Increase in emission intensity for LDS-798 is found to be linear up to ~50 μM albumin concentrations suggesting the limit of detection (LOD) is found to be ~48 nM. Quantification efficiency of the system has also been checked in urine matrix and 5% fetal bovine serum (FBS) and results are found to be very satisfactory.

In order to find practical application of the studied system, quantification of albumin has also been carried out in four different blood serum samples of normal persons. Obtained results are compared and validated with a known spectrophotometric method of albumin

estimation using bromophenol blue as the probe. The results from the two independent methods are compared by unpaired student t-test that show an insignificant variation between the two methods.

In effect, the LDS-798 dye is realized as a very selective and sensitive fluorescent turn-ON probe in the much desired near IR region, which registers ~500 fold emission enhancements, the highest reported so far, in the response to BSA/HSA. Notwithstanding other reports, as a sensor probe, LDS-798 offers several advantages such as label free operation, high sensitivity and selectivity and most importantly giving emission in the biologically advantageous red region that involves minimum auto fluorescence, high light penetration and low tissue damage. Present probe can suitably detect and quantify albumins in actual serum samples. Easy commercial availability of the probe is an additional advantage, as tedious and time-consuming synthetic efforts can be avoided, and thus can have a large impact on albumin sensing in clinical applications.

Chapter 7: ***Summary and Future Outlook***

This is the concluding chapter of the thesis. In this chapter we have summarized the results obtained from different studies carried out in the PhD program. Future perspectives of the research work carried out in the PhD program have also been provided in this chapter based on the results obtained from the present study and the possible follow-up studies in the subject area. Briefly, the supramolecular host-guest interactions involving chromophoric dyes as the guests and macrocyclic molecules and bio-macromolecular systems as the hosts have many prospects for their applications in optical sensing, drug formulations, drug delivery, nanotechnology, therapeutics and many others, and this research area is quite interesting, challenging and highly prospective in diverse areas of contemporary chemical sciences.

References

1. Amabilino, B. D.; Smith, D. K.; Steed, J. W. *Chem. Soc. Rev.* **2017**, *46*, 2404.
2. Katdare, A.; Chaubal, M. V. Excipient development for pharmaceutical, biotechnology, and drug delivery systems. *CRC Press, New York, 2006*.
3. Qu, D. H.; Wang, Q., C.; Zhang, Q. W.; Ma, X.; Tian, H. *Chem. Rev.* **2015**, *115 (15)*, 7543.
4. Xue, M.; Yang, Y.; Chi, X.; Yan, X.; Huang, F. *Chem. Rev.* **2015**, *115 (15)*, 7398.
5. Del Valle, E. M. M. *Process Biochemistry* **2004**, *39* 1033.
6. Monti, S.; Mane, I. *Chem.Soc.Rev.* **2014**, *43*, 4051.
7. Ding, C.; Zhu, A.; Tian, T. *Acc. Chem. Res.* **2014**, *47*, 20.
8. Yang, Y. W.; Sun, Y. L.; Song, N. *Acc. Chem. Res.* **2014**, *47* 1950.
9. Onogi, S.; Shigemitsu, H.; Yoshii, T.; Tanida, T.; Ikeda, M.; Kubota, R.; Hamachi, I. *Nat. Chem.* **2016**, *8*, 743.
10. Sayed, M.; Pal, H. *J. Mater. Chem. C* **2016**, *4*, 2685.
11. Sayed, M.; Jha, S.; Pal, H. *Phys. Chem. Chem. Phys.* **2017**, *19*, 24166.
12. Boraste, D. R.; Chakraborty, G.; Ray, A. K.; Shankarling, G. S.; Pal, H. *ChemistrySelect* **2017**, *2*, 5128
13. Boraste, D. R.; Chakraborty, G.; Ray, A. K.; Shankarling, G. S.; Pal, H. *J. Photochem. Photobiol. A: Chem.* **2018**, *358*, 26.
14. Gavvala, K.; Sengupta, A.; Hazra, P. *ChemPhysChem* **2013**, *14*, 532
15. Sayed, M.; Shinde, K.; Shah, R.; Pal, H. *ChemistrySelect* **2016**, *1*, 989.
16. Naveenraj, S.; Anandan, S. *J. Photochem. Photobiol. C: Photochem. Reviews* **2013**, *14*, 53.
17. Bayraktutan, T.; Meral, K. *Phys. Chem. Chem. Phys.* **2016**, *18*, 23400.

18. Solomonov, A. V.; Rumyantsev, E. V.; Kochergin, B. A.; Antinab, E. V. *Biophysics* **2014**, *59, No. 1*, 35.

19. Garbett, N. C.; Hammond, N. B.; Graves, D. E. *Biophysical Journal* **2004**, *87*, 3974.

20. Olmsted, J.; Kearns, D. R. *Biochemistry* **1977**, *16*, 3647.

21. Kumar, D.; Banerjee, D. *Clinica Chimica Acta* **2017**, *469* 150.

22. Schoeeky, K. H.; Verges, M.; Esqulvel, A. L.; Chavarria, M. A. *Clin. Chem.* **1987**, *33*, 223.

23. Chakraborty, G.; Ray, A. K.; Pal, H. *ChemistrySelect* **2018**, 3, 1088.

24. Bhasikuttan, A. C.; Mohanty, J.; Nau, W. M.; Pal, H. *Angew. Chem. Int. Ed.* **2007**, *46*, 4120.

25. Chakraborty, G.; Ray, A. K.; Singh, P. K.; Pal, H. *Chem. Commun.*, **2018**, 54, 8383.

LIST OF ABBREVIATIONS

A	Absorbance
BDZ	BODIPY-benzimidazole
BG	Brillinat green
BODIPY	4,4-difluoro-4-bora-3a,4a-diaza-s-indacene
BSA	Bovine serum albumin
CBn	Cucurbit[n]uril
CD	Cyclodextrin
CV	Crystal violet
DFT	Density functional theory
DNA	Deoxyribonucleic acid
FBS	Fetal bovine serum
FWHM	Full-width at half-maximum
HOMO	Highest occupied molecular orbitals
HSA	Human serum albumin
LUMO	Lowest unoccupied molecular orbital
IC	Internal conversion
ICT	Intramolecular charge transfer
IR	Infra-red
IRF	Instrument response function
ITC	Isothermal titration calorimetry
LA	Lithocholic acid
LE	Locally excited
LED	Light emitting diode
MALDI	Matrix-assisted laser desorption/ionization

MCP	Multi channel plate
MRI	Magnetic resonance imaging
MW	Molecular weight
NMR	Nuclear magnetic resonance
O.D.	Optical density
PBS	Phosphate buffer saline
PMT	Photo multiplier tube
SS	Steady state
SBEβCD	Sulfobutylether β-cyclodextrin
TCSPC	Time correlated single photon counting
TMS	Tetramethylsilane
TOF	Time of flight
TICT	Twisted intramolecular charge transfer
TR	Time resolved
UV	Ultra violet

LIST OF FIGURES

LIST OF TABLES

CHAPTER-1

INTRODUCTION TO SUPRAMOLECULAR CHEMISTRY AND FLUORESCENCE SPECTROSCOPY

1.1. Introduction of Supramolecular Chemistry

Supramolecular chemistry has been drawing a significant interest for more than a century due to the exceptional outcomes and applications in various fields of basic as well as applied science. Any kind of noncovalent interaction is the basis of supramolecular chemistry and plays an important role in determining the three dimensional structure with the constituent molecular units leading to unique properties of the assemblies formed. Although supramolecular chemistry has been explored and applied in various fields for more than a century, the subject has been put forward in its modern perspectives only in 1978 by Lehn,[1, 2] who defined, supramolecular chemistry is the subject that extends beyond the chemistry of the molecules as such. According to him, "Supramolecular chemistry" is the "chemistry of molecular assemblies and of the intermolecular bonds." Classic explanations of supramolecular chemistry describe it as "chemistry beyond the molecule," "the chemistry of the noncovalent bond," and "non molecular chemistry." Different noncovalent interactions like electrostatic, ion-dipole, dipole-dipole, van der Waals, hydrophobic, hydrogen-bonding, π–π stacking etc. singly or in combination result in the formation of the supramolecular assembly/complex. Thus, any material which is formed via non-covalent interaction can be termed as supramolecule but specifically supramolecule mean the super molecule i.e., a large molecular entity formed via molecular recognition between the smaller molecular building blocks leading to the formation of well-defined organized architecture. Due to the comparatively weak nature of the non-covalent interactions, the formation of supramolecular assemblies is dynamic in nature and these assemblies are capable of displaying complete

reversibility in their behaviour. Hence, the presence of external stimuli can significantly modulate the construction, dissociation and reconstruction of the supramolecular assemblies.[3] The most attractive feature of the supramolecular complexes is the nature of the supramolecular entities vastly different than the constitutional blocks.[4] This aspect of supramolecular system has attracted substantial attention in all branches of science including chemistry, medical science, biology, material science, pharmaceutical science, molecular engineering and so on, to explore the intricate details of various supramolecular systems keeping in view of their widespread applications in diverse areas like functional materials, catalysis, electronic devices, drug formulation, sensors, medical diagnostics, and so on.[2, 3, 5-21] Very recently it has been reported that the properties of the supramolecular entities can be tuned by controlling the thermodynamics of the formation process.[22-24] It has also been found that non-covalent interaction enables the fusion of liquid crystalline and inorganic materials properties that can produce materials having properties that are similar to the harder pure material.[25] Hamachi and co-workers recently reported that the two different peptides are capable of self-assembling into a different type of supramolecular nano fibers.[26] In the living world, functioning of the genetic information carrier, DNA, are mainly governed by the structural motifs created by involving appropriate base pairs through non-covalent hydrogen bonding supramolecular interactions and also the molecular recognition of enzymes on their substrates, transportation of nutrients, hormones, drugs and all are mainly governed through various supramolecular interactions. To understand the different thermodynamic parameters that govern the molecular arrangement of a particular supramolecular system in three dimensional spaces or to enhance the stability of a system by improving molecular recognition between the constituents, the role of non-covalent interactions is significant. The interaction of different guest molecules with suitable macrocyclic host cavities has been the area of extensive investigation in supramolecular chemistry whereby the physicochemical properties

of the guest molecules can be modulated quite extensively for their improved applications. These modulations can arise in regard to their photochemical properties, photophysical characteristics, conformational selectivity, thermal stability, water solubility, de-aggregation, desorption from surface adhesions, and so on.[10, 27-51] In the literature, modulations in the photophysical properties, e.g. altering absorption/emission peak positions, in fluorescence quantum yields, fluorescence life times, vibration/rotational relaxation rates, etc., of various chromophoric dyes (guests) on their binding with macrocyclic molecular cavities (hosts) have been investigated very extensively, exploring the usefulness of such modulations in diverse applications.[32, 34-36, 47-61] For many chromophoric dyes, along with the modulations in their photophysical properties, there are also substantial changes in their acid-base properties through host-guest interactions, causing their pK_a values to shift largely either upward or downward, which are often useful in stabilizing dyes/drugs in their proactive forms and also in controlling the binding/release mechanisms of dyes/drugs between macrocyclic host carriers and targeted biological/bio-macromolecular systems.[17, 32, 35, 56, 62-64]

1.2. Different forces in supramolecular chemistry

Generally, all kinds of forces which do not involve in the formation of covalent bond come in the category of non-covalent interaction or forces. Electrostatic, ion-dipole, dipole-dipole, π-π stacking, cation-π, anion-π, coordinate bond, halogen bond, hydrogen bond, Van der Waals force, hydrophobic interactions all fall under noncovalent interaction. Depending upon the interacting units or molecules these forces acquire a definite range which can be increased or decreased with the help of external means due to the reversible nature of these interactions. Some of these interactions and their typical interaction energies are listed below for quick comparison:

Table: 1.1. List of the different interactions in supramolecular chemistry.[65]

Sl No.	Type of interaction	Interaction energies ($kJmol^{-1}$)	Examples
1	Electrostatic or ion-ion	100-350	NaCl, KCl etc.
2	Coordinate bonds	100–300	$[Fe(CN)_6]^{4-}$
3	Ion–dipole	50–200	Na^+-crown ether complex
4	Hydrogen bonds	4–120	HF, Carboxylic acid dimer
5	Cation–π and anion–π interactions	5–80	$+N(CH_3)_4$.toluene
6	Dipole–dipole interactions	5–50	-C≡N
7	Halogen bonds	10-50	Sulfur-iodine complex
8	π-π interactions	2-50	Xanthne, BODIPY dyes etc.
9	Van der Waals interaction	<5	Host-guest inclusion complexes

1.2.1. Electrostatic interaction

This is the strongest known non-covalent interaction and operative in a long range between two oppositely charged entities. The electrostatic interaction is generally non-directional in nature and found in the isotropic lattice. The force of attraction between two oppositely charged entities is governed by the following equation:

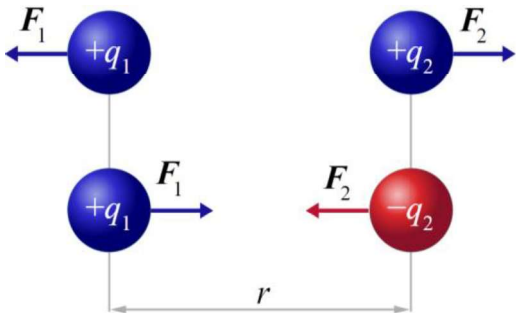

Figure: 1.1. Schematic of electrostatic interaction between two charged particles (taken from Google) .

$$F = \frac{q_1 q_2}{4\pi\varepsilon_0 r^2} \tag{1.1}$$

where, q_1 and q_2 are the charge of the interacting entities, ε_0 is the permittivity of the medium and r is the distance between the two dielectric species.

Generally, the interaction of cationic dye molecules like rhodamines, hemicyanines, coumarins and many others with poly-substituted anionic hosts like sulfated cyclodextrins, sulfobutylether beta-cyclodextrins or sulfonate calixarenes are the suitable examples where electrostatic interaction plays a significant role to provide stability of the supramolecular complex formed.

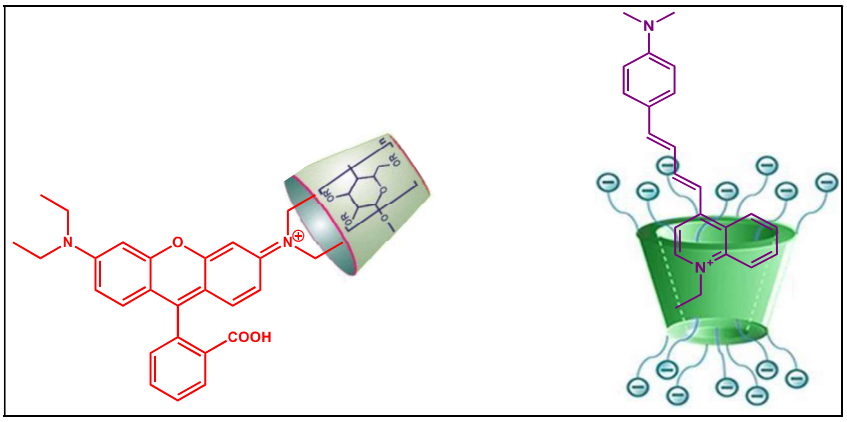

Figure: 1.2. Electrostatic interaction between dyes (rhodamine-B and LDS-798) (guest) and substituted β-cyclodextrin derivatives (hosts).

1.2.2. Ion-dipole and dipole-dipole interaction

Ion-dipole interaction is the force of attraction operative between a completely charged (positive or negative) entity and a dipolar molecule. This is generally weaker force as compared to the ion-ion type of electrostatic force but has the potential to determine the geometry, property and selectivity between the interaction pairs. Crown ethers interacting with different alkali metal ions fall in this category. The ion-dipole interaction can be quantitatively expressed as:

$$F = \frac{q_1 q_2}{4\pi\varepsilon_0 r^4} \qquad (1.2)$$

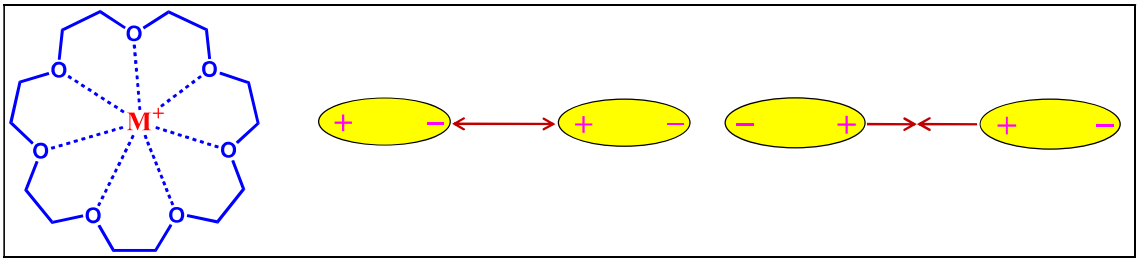

Figure: 1.3. Schematic of ion-dipole and dipole-dipole interactions.

On the other hand, the dipole-dipole interaction is operative between two dipolar molecules. Nature wise it can be attractive, which stabilizes the molecular ensembles leading to the large supramolecular entity or repulsive that destabilizes a supramolecular entity leading to the dissociation of the supramolecular architecture. This interaction is even weaker than ion-dipole type of electrostatic interaction and is governed by the following equation:

$$F = \frac{q_1 q_2}{4\pi\varepsilon_0 r^6} \tag{1.3}$$

1.2.3. Coordinate bonds

Coordinate bonds are mostly formed between transition metals having incompletely filled d-or f-orbitals with electron rich ligands. The coordination bonds have enormous applications in supramolecular chemistry and strength wise it is almost similar to the ion-ion interaction. Depending upon the nature of the interacting ligand, availability of the vacant d or f orbitals, size of the metal ions and so on the strength of coordination bond varies from 100-300 $kJmol^{-1}$ which is quite significant and has a dramatic effect on the geometry and three dimensional arrangements of the molecular subunits in a supramolecular complex.[66-68] The presence of labile or inert coordination bonds in a supramolecular complex allows it to undergo self modulation until a thermodynamically stable product is achieved.[69] Thus, coordinate bonds contribute to improve the properties of the supramolecular complex formed between metal ions and ligands.

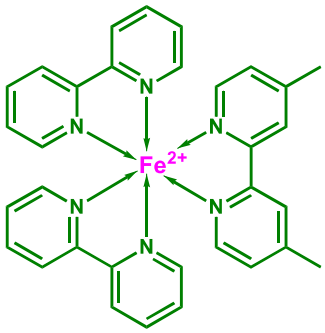

Figure: 1.4. Coordinate bonds of $[Fe(bpy)_2]^{2+}$ complex.

1.2.4. Hydrogen bonds

When hydrogen is directly attached to a highly electronegative element like F, O, N in a covalent bond, the bonding electrons get attracted towards electronegative element due to electron withdrawing tendency of the F, O or N and thereby making the hydrogen partially positive in nature. This partially positively charged hydrogen then forms a weak to a comparatively stronger electrostatic bond with the electron rich or electronegative part of the nearby or surrounding molecules. This weak directional electrostatic interaction is known as hydrogen bond. The energy of a hydrogen bond can vary from 4-120 $kJmol^{-1}$ depending upon the surrounding molecules and the nature of the electronegative element/atom directly attached to the hydrogen atom.[65] Hydrogen bond is often termed as the "master key" of supramolecular complexation. The importance of hydrogen bond in supramolecular complexation cannot be overlooked during explaining the structure and three dimensional arrangements of the biomolecules. The π-π stacking and H-bonding between its complementary base pairs in the double helical structure of DNA, the genetic information carrier, provides a substantial stability to the three-dimensional frameworks. The hydrogen bonding is actively responsible for the transport properties of different enzymes, hormone and other nutrients that regulate many sophisticate biological activities in situ.[70-75] H-bonding is also responsible for aggregation, stimuli responsive behavior of different dye molecules in most of the host-guest interactions.[76-79]

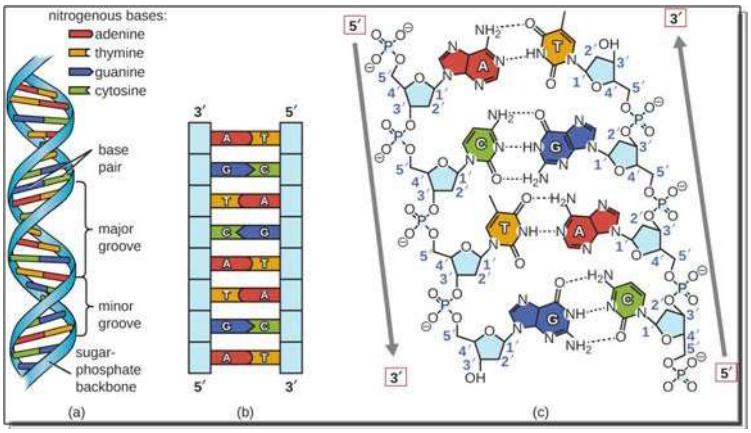

Figure: 1.5. H-bond between double helical strands of DNA.

1.2.5. π-π interaction

When the molecules which are rich in π-electron clouds come in close vicinity of each other, an organized supramolecular entity is formed via π-π interaction, generally known as π-π stacking. The formation of the supramolecular entities involving π-electron cloud can have three possible orientations which are face to face, end-to face and tilted T-shape. The first two types are generally termed as the H-aggregates whereas the later one is known as J-aggregates [ref]. The π-π stacking plays an important role in governing the optical properties of many dyes (like, BODIPY, rhodamines, coumarins and so on). It may be noted that the π-surfaces tend to self-organize into either herringbone or a stacked motif in solid state.

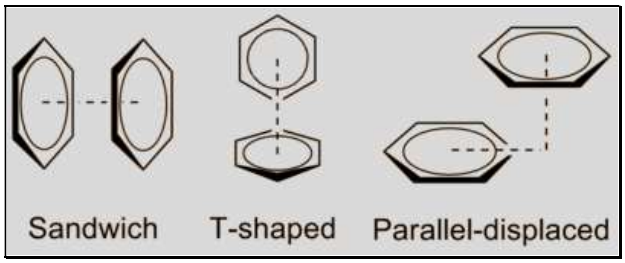

Figure: 1.6. π-π interaction between aromatic rings.

1.2.6. Hydrophobic interaction

It is the most important force that governs the formation of a supramolecular complex especially when the case is host-guest type of complex formation. Generally, host molecules

(e.g, cucurbiturils, cyclodextrins, calixarenes and so on) contain water molecules inside their cavity and the release of the high energy strained water molecules from the host cavity during inclusion of the guest molecule into the host cavity results in a substantial change in entropy or enthalpy during complexation depending upon the nature of the interacting host and guest pair, which drives the thermodynamics of the host-guest complexation.[33, 59, 80-87] It has been shown quite quantitatively by computational and experimental studies that the number of the water molecules and the deficiency of the hydrogen bonding of the encapsulated water molecules determine the overall gain in the potential energy for the formation of the host-guest inclusion complex.[87, 88] The energy of the encapsulated water molecules decrease with increase in the size of the host cavity due to the increase or improvement of the hydrogen bonding network between the trapped water molecules and the encapsulated water molecules tend to achieve the energy of the bulk water molecules. In case of smaller dimension cavity, the energy of the individual water molecule is higher but the total energy change is small due to the fewer number of the water molecules released during guest inclusion. Whereas the energy of the individual water molecules are smaller in case of the hosts with very larger cavity size and the energy released upon guest encapsulation is nominal. Thus, there is an optimization of the guest cavity size that can produce a large change in the potential energy by releasing encapsulated water molecules during inclusion complex formation.[59, 88]

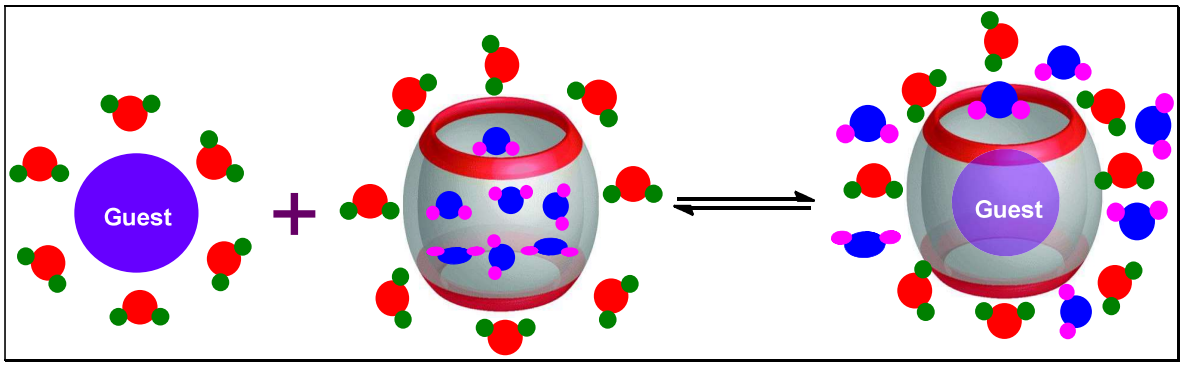

Figure: 1.7. Release of high energy encapsulated water molecules during host-guest inclusion complex formation between organic guest and cucurbit[7]uril.

1.2.7. Van der Waals interaction

This is the weakest of all of the forces responsible for the formation of supramolecular complexes. In the case of host-guest chemistry, formation of the inclusion complex is also driven by Van der Waals interaction between the guest molecule and the host cavity but the overall effect of Van der Waals force on supramolecular complexation is limited due to its very short range of operation. Typically, strength of Van der Waals force is <5 $kJmol^{-1}$.

1.3. Thermodynamic in supramolecular chemistry

Quantitative description of the formation of supramolecular complex can never be elucidated only on the basis of the type of interactions between the building units**.** The change of free energy (ΔG^0), enthalpy (ΔH^0) and entropy (ΔS^0) during complexation provide quantitative means in explaining the formation of the organized, stable three dimensional constructions for supramolecular complexes. In case of host-guest chemistry, along with the above-mentioned factors, association constant or binding constant (K_b) between host and guest pair provides a crucial information regarding the formation probability, stability and also improved property of the formed host-guest complex.[5, 89]

From Van′t Hoff's equation we have,

$$\Delta G^{o} = -RT \ln K \tag{1.4}$$

On the other hand, the relationship between free energy, enthalpy and entropy is given by Gibbs-Helmholtz equation,

$$\Delta G^{o} = \Delta H^{o} - T\Delta S^{0} \tag{1.5}$$

where, T is the temperature during supramolecular complexation.

The formation of a supramolecular complex is associated with the many new non-covalent bonds among the constituent units at the expense of the dissociation of many non-covalent bonds preexisting with the host and the guest molecules. Thus, the change in

enthalpy can easily be estimated by measuring the changes in the overall bond strengths or energies during supramolecular complexation. The formation process of a supramolecular complex can be termed as endothermic (ΔH^0 = +ve) or exothermic (ΔH^0 = –ve) depending on the change in the heat content during the process. On the other hand, entropy provides the measure of randomness in a particular ensemble. From eqn. 5 we find that the greater the entropy of a system, lower will be the free energy of the complexation process and hence greater will be the stability. In a system or ensemble, entropy is the result of the molecular translation (S^0_{trans}), vibration (S^0_{vib}), rotation (S^0_{rot}), symmetry (S^0_{sym}) and even due to the mixing (S^0_{mix}) of different components with each other. Among all these entropies the contribution from the change in the molecular translation and rotation have marked effect on the supramolecular complex formation as the complexation leads to drastic change in molecular agility of all the smaller constitutional units in a supramolecular complex. These contributions lead to the substantial change in translational entropy (ΔS^0_{trans}) and rotational entropy (ΔS^0_{rot}), whereas, the contribution from the entropy change in molecular vibration (ΔS^0_{vib}) has a very marginal effect in governing the formation of a supramolecule. Thus, it is the change in translational entropy (ΔS^0_{trans}) and the rotational (ΔS^0_{rot}) entropy that govern the formation of supramolecular complex specifically when the case is host-guest type of complexation process.[65]

1.3.1 Enthalpy and entropy driven process

As discussed in the earlier section, formation of a supramolecular entity is dependent on the overall change in free energy, enthalpy and entropy of the system. But the dependence on the thermodynamic parameters of the supramolecular entities changes from one system to

another. In some cases supramolecular complexation is solely dependent on the change in enthalpy, depending upon the type of the bonds involved during the formation of the supramolecule, resulting the molecular recognition of the interacting species.[90, 91] Generally, when the formation of the supramolecular complex mainly proceed via strong electrostatic interaction, the process of formation of the complex is mainly governed by the change in enthalpy, as substantial amount of the heat change takes place through the bonds formation between the building units. The formation of strong host guest complexes involving cationic dyes and anionic hosts, such as avidin-biotin interaction, are the predominantly enthalpy driven process.[90, 91] However, if the non-covalent interaction is mainly hydrogen bonding or hydrophobic in nature, the main driving force of the complexation process is determined by the change in the entropy, as there is a marginal change in the heat content of the system during the formation of the supramolecules.[92, 93] Formation of host-guest supramolecular complex involving neutral guest and cyclodextrins, protein-ligand complexation etc. are primarily the entropy driven process, as this type of host-guest complex results in the release of high energy water molecules from the guest cavity leading to the increase in the overall entropy of the system.[94-96] In general, majority of the supramolecular complexation proceeds through entropic gain rather than enthalpy consideration.

1.4. Supramolecular chemistry in fluorescence spectroscopy

Supramolecular chemistry has found gradually increasing applications in the field of fluorescence spectroscopy for the past few decades. Starting from the improvement of the fluorescence quantum yield, improved laser property of the dyes like rhodamine, coumarin, BODIPY, hemicyanine, oxazine etc., fluorogenic metal sensing, in situ imaging and

quantification of different biomolecules like protein, DNA, enzymes etc., fluorescence modulation through host-gust supramolecular complexation is a hot topic in the research area for the chemists, biologists, and biochemists. The popularity and the use of the host-guest chemistry in photosciences, especially in fluorescence spectroscopy have been increased enormously due to the high sensitivity of the fluorescence detection and unique properties of the supramolecular systems like their (i) ease of application, (ii) reversibility, (iii) easy tuning and (iv) immediate response towards external stimulus etc., are helpful for diverse applications. [3, 4, 23, 35, 63, 96-99]

1.5. Introduction to fluorescence spectroscopy

Fluorescence spectroscopy has gathered quite an extensive scientific attention for the past few decades**.** Earlier the use of fluorescence spectroscopy was limited to only biochemists and biophysicists but recently the field of fluorescence spectroscopy has expanded to all areas of basic as well as applied sciences. Fluorescence spectroscopy which includes steady-state emission, time resolved fluorescence, single molecule detection and so on; is one of the major realm of research and extensively applied in medical diagnostics, biotechnology, metal sensing, bio-imaging, in situ quantification of proteins, DNA sequencing, flow cyctometry, forensics, genetic analysis etc., are the few important examples.[96, 100-106] Not only the application of fluorescence spectroscopy that attracted scientists of various parts of the world; also the ease of applicability, non-destructive methodology, fast response, fast data acquisition, high sensitivity make fluorescence technique one of the major blessing to the scientific field. The use of fluorescence method has discarded the use of radio tracers which were used for the most of the biological imaging purposes, making the technique more safe, inexpensive and non-hazardous in nature.[107]

1.5.1. Science behind emission spectroscopy

Generally emission of light from an electronically excited molecules or species is known as luminescence. Depending upon the involvement of the excited electronic state from which electron transition to the ground state takes place, the phenomenon of luminescence has been divided into two categories; (i) fluorescence, when the electronic transition takes place from an excited state to a ground state of the same spin i.e, singlet to singlet and (ii) phosphorescence, when emission of light occurs due to the electronic transition from a triplet excited state to singlet ground state i.e., transition takes place between the states of different spin multiplicity, which is a forbidden transition according to the selection rule (will be discussed later). For this reason, fluorescence takes place in faster time scale of nano seconds while phosphorescence is a much slower emission process and takes place in a time scale of microsecond onwards.[107]

When light is incident on a material, the electromagnetic field of the incident radiation causes a perturbation in the electronic cloud of the molecules (or atoms or ions) in the material along the light path which results in the modulation of oscillating dipole in the molecules. [note: in the g.s., molecule is an oscillating dipole) When the frequency of the oscillating dipole resonates with the natural frequency of the molecules which is nothing but the energy difference between two electronic states, the photon incident on the molecule gets absorbed and the molecule is excited to higher energy level, i.e.

$$\nu = \frac{E_2 - E_1}{h} = \frac{\Delta E}{h} \tag{1.6}$$

where, E_1 is the energy of the ground state and E_2 is the energy of the excited state and h is Plank's constant.

Thus, the process in which molecules absorb radiation of suitable energy to get excited to the higher energy level is known as absorption. Excited molecules can spontaneously emit light to undergo de-excitation to the ground state, resulting either fluorescence or

phosphorescence emission, as discussed before. It is to be noted here that transition from the excited state to ground state can also be induced by the presence of the radiation of the same frequency and the process is called as the stimulated emission, which is the governing phenomenon to achieve laser action.

1.5.2. Types of electronic transitions in organic molecules

The probability of the electronic transition depends on the energy of the absorbed radiation and the nature of the molecular orbitals participating during the excitation or emission process. Different types of transitions in molecular systems are designated by the Kasha's rule, proposed by the American spectroscopist, Michael Kasha in 1950. In general; depending on electronic occupancy, symmetry and energy; organic molecules have three types of molecular orbitals which are formed due to the overlap of the atomic orbitals of the constituent atoms. The different molecular orbitals are (i) bonding orbitals (σ and π), (ii) anti-bonding orbitals (σ^* and π^*) and (iii) non-bonding orbitals (n). Again depending on the occupancy of the electrons, these orbitals can be divided into two categories; (a) those occupied by the pair of electrons namely highest occupied molecular orbitals (HOMO) and sequentially lower energy occupied orbitals like HOMO-1, HOMO-2, etc., and (b) those unoccupied by electrons namely lowest unoccupied molecular orbital (LUMO) and the sequentially higher energy unoccupied orbitals like LUMO+1, LUMO+2, etc. Based on Kasha's rule different electronic transitions in a molecular system can be represented by the following schematic diagram (Fig. 1.8).

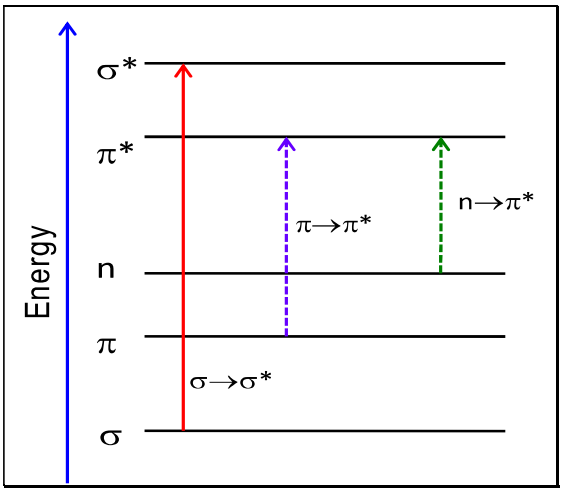

Figure: 1.8. Energy diagram of the molecular orbitals and different types of electronic transitions taking place in an organic molecule.

As indicated from Fig.1.9, depending upon the energy of the absorbed light, three possible electronic transitions in an organic molecule are energetically ordered as $n\rightarrow\pi^* < \pi\rightarrow\pi^* < \sigma\rightarrow\sigma^*$. As it is quite evident from the above energy diagram that the transition between non-bonding HOMO to π^* anti-bonding LUMO is the lowest energy transition. However, considering the orbital/spatial symmetry, the probability of this transition is very poor. Hence, although this transition takes place at lower energy than $\pi\rightarrow\pi^*$, the intensity of this transition is very poor. The transition between π bonding orbital to π^* anti-bonding orbital takes place at relatively higher energy, but the symmetry consideration makes this transition highly allowed and so the intensity (oscillator strength) of this transition is quite high in nature. In most of the organic molecules whatever spectra we encounter is mainly due to π to π^* transition and the energy of this transition lies in the visible region of the molecular spectrum. Additionally when organic molecules contain both the electron donating and withdrawing group with the chromophoric moiety, special type of electronic transitions can take place; depending on the geometry, conjugation, electron potential of the donating and the accepting groups. These special type of electronic transitions are divided into two categories, (i) intramolecular charge transfer (ICT), occurs through bonds between the donor and the

acceptor groups and (ii) intermolecular charge transfer (ICT), occurs through space between the donor and the acceptor groups.[107, 108] Both of these electronic transitions depend upon the solvent polarity and found to be intensified with the increase in solvent polarity. Generally, ICT bands shift towards the longer wavelength side with the increasing polarity of the medium.[63, 108-110]

1.5.3. Multiplicity of different electronic energy states in organic molecules

The spin multiplicity of the energy states of molecular orbitals is an important governing factor for the probability of electronic transition from one energy state to another. The spin multiplicity is given as (2S+1), where S is the total spin quantum number. Thus, for a singlet state (2S+1) = 1, which is possible when S = 0, indicating that the two electrons present in a particular energy state of the molecule have opposite or anti-parallel spin. On the other hand, for a triplet state (2S+1) = 3, which is possible when both the electrons in the same energy state of the molecule have the same spin or the parallel spin giving rise to S = 1. Almost for all the molecules ground state is generally singlet state as both the electrons occupy the same molecular orbital with opposite spins and this energy state is denoted as S_0. All the singlet states other than the ground state (S_0) are the excited singlet states where two electrons occupy two different molecular orbital with opposite spins and are denoted as S_1, S_2, S_3 and so on, with increasing energy. Similarly triplet states are those in which two electrons occupy two different molecular orbitals with similar spins and are denoted as T_1, T_2, T_3 and so on, with their increasing energy relative to the ground state (S_0) of the molecule. It is to be noted that the energy of a triplet state is always lower than that of the corresponding singlet state, which is in accordance to the Hund's rule of the maximum multiplicity and the spin correlation of the two paired and unpaired electrons dictates this energy ordering. Due to the parallel spins of the two electrons in the two molecular orbitals, electronic repulsion is much less in the case of the triplet energy states as compared to the situation with the two electrons

of the opposite spins in the singlet energy states. Hence, a triplet state always comes at a lower energy position than the corresponding singlet state.

1.5.4. Franck-Condon Principle

To understand how electronic transitions from one energy level to the other in a molecular system take place during absorption or emission process, the Franck-Condon principle is a very important concept to be considered. According to Franck-Condon principle, the transition of electrons from one electronic energy state to another is too rapid that there is hardly any change in the internuclear separations during transition. This can be explained on the basis of huge mass difference between electrons and nuclei of the atoms. Electrons are more than thousand times (to be precise 1837 times) lighter than even the proton nucleus. Hence, there is hardly any change in the internuclear separation as the electron is promoted from the initial to the final energy state during the process of electronic transition (by absorption or emission). In terms of the potential energy surface of the electronic states, Franck-Condon principle can be presented schematically as shown in Fig. 1.10 and can be stated as: "Electron transitions occur vertically between the two potential energy surfaces involved."

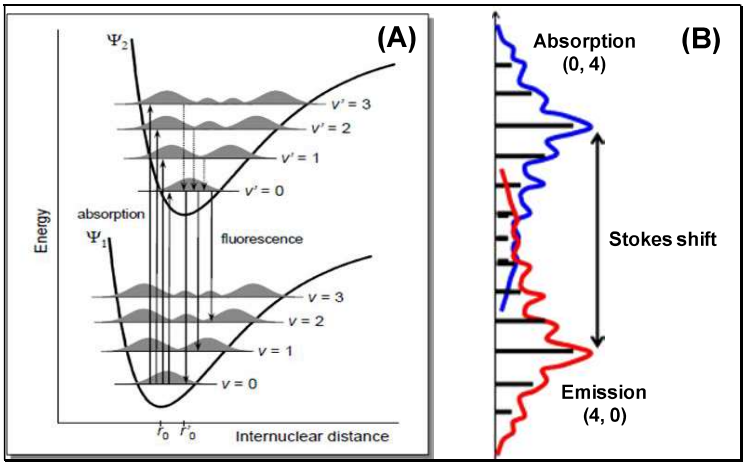

Figure: 1.9. (A) Schematic presentation of electronic transition following absorption, emission according to Franck-Condon principle and **(B)** Intensity changes of different vibrational bands in the absorption and fluorescence spectra based on Franck-Condon Principle.

The intensity of the electronic transition between two energy states depends on the probability of finding the molecules in the two vibrational levels accessible vertically in the initial and the final electronic states, respectively. For a particular inter-nuclear separation, if the wave functions of the two vibrational levels of the initial and the final electronic states, respectively, have a better spatial overlap, the associated electronic transition will be of stronger intensity. However, if the spatial overlap of the two vibrational states involved in the electronic transition is poor, the transition will be of weaker intensity. Figure 1.9 illustrates the electronic transitions for the absorption and emission process according to the Franck-Condon principle, depicting the differences in the spatial overlap of the associated vibrational wave functions and the consequent changes in the intensity of the vibration bands in the absorption and emission spectra. It is to be mentioned that if the equilibrium inter-nuclear separation in the initial and the final electronic states remains the same (i.e. $r_o = r_1$), the intensity associated with the 0-0 vibrational transition will be the highest among other vibrational bands involved in the electronic spectra.

1.5.5. Jablonski diagram

Jablonski diagram provides qualitative information of the different de-excitation processes occur in a molecular system following its excitation by absorption process. Fig.1.10 represents a typical Jablonski diagram which shows different electronic levels according to the increasing energy and with different multiplicity. S_0 is the ground state of the fluorophore whereas, S_1, S_2.....S_n are the first, second to nth excited state with singlet multiplicity and T_1 and T_2 represents the first and second triplet states, respectively. When a fluorophore molecule absorb a photon of energy which matches exactly to the difference between the ground state to the any of the excited state in the singlet manifold, the fluorophore gets excited and is often represented as M*. Each of the electronic levels is subdivided into a number of vibrational

levels and the distribution of the fluorophore molecules in the vibrational levels is governed by the Boltzmann distribution.

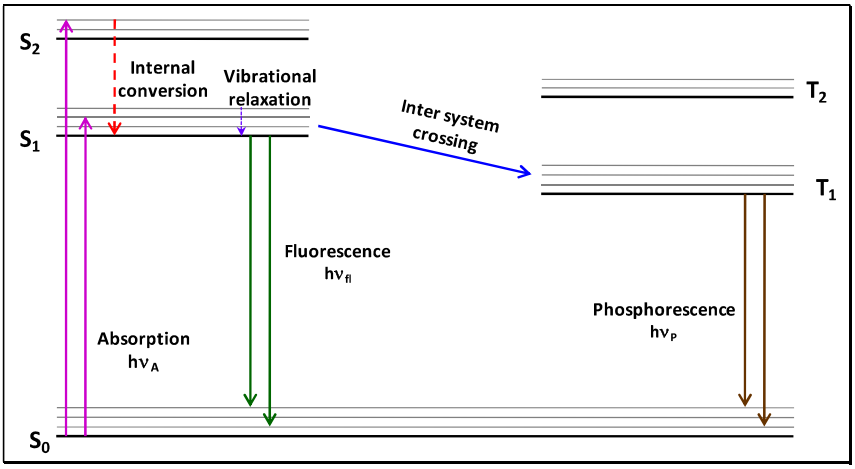

Figure: 1.10. Jablonski diagram showing different energy states and de-excitation processes following light absorption by a molecular system.

The de-excitation of the excited molecule created by the absorption process is divided into two broad categories: (i) radiative pathways, which involves the emission of light during de-excitation and (ii) non-radiative pathways, which is the result of depopulation of the excited state molecules without emission of light. Fluorescence is a process where de-excitation takes place via emission of light and this occurs through the electronic states of same multiplicity, i.e., from S_1 to S_0, which is allowed according to selection rule (will be discussed later) and hence, takes place within the time scale of few nanoseconds. However, in addition to fluorescence, there are many non-radiative processes that can take place simultaneously in the excited S_1 state and those are vibrational relaxation (time scale: 10^{-11}s to 10^{-9} s), internal conversion (10^{-12} s or less) and intersystem (S_1 to T_1) crossing (10^{-10} s to 10^{-8} s). The rate of these non-radiative processes especially can vary depending upon the surrounding environment of the fluorophore. It is to be noted that there are certain luminescent molecules that can show emission due to the electronic transition from the first triplet state (T_1) to the singlet ground state (S_0) of the molecules. This phenomenon is known as

phosphorescence. Phosphorescence is a spin forbidden transition and hence, occurs generally in the time scale of microseconds or longer.

1.6. Different laws governing photochemical processes

1.6.1. Grothus-Draper law

This law is often considered as first law of photochemistry which states that "Only the light or photon that is absorbed by the system can lead to a chemical change."

1.6.2. Stark-Einstein law

This law is regarded as the second law of photochemistry. According to this law, "Only one photon is absorbed per reacting molecule undergoing a photochemical reaction." Though Stark-Einstein law is in general followed in most of the photochemical processes, there are however, some exceptions to this law, especially when more than one photon is absorbed by a molecule to undergo photochemical change. One of the examples of the deviation of this law is the bi-photonic absorption leading to the ionization of a molecule.

1.6.3. Lambert-Beer law

This is the most important law for quantitative understanding of the absorption process. It relates the attenuation of light intensity as the light beam travels through a medium. Lambert's law states that the fractional absorption of light intensity ($-\Delta I/I$, where I is the incident intensity) by a material sample is directly proportional to its thickness (path length). However, almost a century later August Beer discovered that the fractional attenuation of light intensity is proportional to the concentrations of the absorbing species present in the material sample. The combination of these two observations is generally termed as the Lambert-Beers law which states that "The fractional light absorbed by a material is directly proportional to the concentration of the absorbing species and the thickness of the absorbing medium."

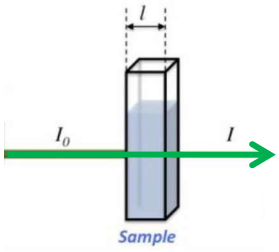

Figure: 1.11. Absorption of light by the sample solution.

Suppose the decrease in the light intensity is dI for the incident light of intensity I after passing through the sample of path length dl and concentration of the absorbing species is C. Hence, the mathematical expression for the Lambert-Beer law would be,

$$\frac{-dI}{I} = \alpha C dl \quad \text{where, } \alpha \text{ is the proportionality constant.} \qquad (1.7)$$

Integrating both sides we have,

$$\ln \frac{I_0}{I} = \alpha C l \qquad (1.8)$$

$$\text{or, } \log \frac{I_0}{I} = \frac{\alpha}{2.303} C l \qquad (1.9)$$

$$\text{or, } \log \frac{I_0}{I} = \varepsilon C l \qquad (1.10)$$

$$\text{or, } A = \varepsilon C l \qquad (1.11)$$

Here, ε is called the molar absorptivity or the molar extinction coefficient at a particular wavelength, A is called the absorbance which is also often designated as the optical density (O.D.) of the sample.

In order to fulfil the Lambert-Beer's law, the following conditions must be satisfied:

- The medium or the sample must be homogeneous.
- The sample solution must be clear which means that there should not be turbidity that gives rise to scattering of the incident light.

- The sample should not undergo any kind of aggregation, degradation, or chemical changes.
- The concentration of the sample must be reasonably at the lower side, because at higher concentrations the linearity of the Lambert-Beer's law generally deviates to a significant extent.

1.7. Selection rule of electronic transitions in molecular systems

Following quantum theory, it is the square of the transition moment integral that governs the probability of a given electronic transition. The transition moment integral can be expressed by the following equation,[111]

$$|\mu_{ab}| = \int \psi_a \hat{\mu} \psi_b d\tau \qquad (1.12)$$

ψ_a and ψ_b are the wave functions of the initial and the final electronic states and $\hat{\mu}$ is the dipole moment operator. The nature of distribution of the electronic cloud in the two electronic states decides the value of the dipole moment integral. For a feasible electronic transition, the value of $|\mu_{ab}|$ should have a non-zero value and the intensity of the electronic transition increases with increasing $|\mu_{ab}|$ value. By the quantum chemical consideration of the electronic states involved in the transition, the value of the dipole moment integral can be known and hence the probability of the electronic transition. The ideal conditions of zero or non-zero value of μ_{ab} provide us the useful information of the electronic transition which leads to the development of selection rules for the allowed transitions, which are listed as follows:

(i) $\Delta\Lambda = 0, \pm 1$; i.e. the change in the total orbital angular momentum quantum number should be zero or ± 1 during the electronic transition involving two electronic states.

(ii) $\Delta S = 0$ i.e. there should not be any change in the total spin angular momentum quantum number during an electronic transition. Hence, the transition between two singlet states or two triplet states are allowed. The transition between singlet to triplet or vice versa is accordingly

the forbidden processes. However, some perturbations like spin-orbital coupling can give rise to the relaxation of this rule, causing a weak and delayed transition between singlet and triplet states.

(iii) Total symmetry involving two electronic states and the electric field of the interacting light photons should be conserved during electronic transition. Thus, according to this rule $n \rightarrow \pi^*$, $\pi \rightarrow \sigma^*$ and $n \rightarrow \sigma^*$ are the forbidden transitions.

Although selection rules provide us the general idea about the relative intensities of different electronic transitions in the chromophoric molecules, they are not followed strictly in the actual systems. This is due to the much more complexity of the electronic states in the chromophoric molecules which is beyond the considerations of quantum mechanical calculations. Thus, the transitions which are forbidden according to the selection rules are often prevailed in the electronic spectra. However, intensity of the so called forbidden transitions is in general very weak. Basically selection rules provide us quantitative idea regarding the expected trends of the relative intensities for different electronic transitions possible in a chromophoric molecule.

1.8. Characteristics of the excited states of chromophoric molecules: Photophysical properties

When a molecule absorbs a light photon, it is promoted to a higher electronic state and the molecule is then called as the excited molecule (M*), which can behave differently than its ground state, participating in different photophysical and photochemical processes. The properties of the chromophoric molecules in regard to their absorption spectra, emission spectra, emission quantum yield (φ), excited state lifetime (τ), etc. are as a whole considered as the photophysical properties of the chromophoric systems. The details of these properties are discussed below:

1.8.1. Ground state absorption and steady state emission spectra

Ground state absorption spectra and steady state emission spectra provide us the information about the relative absorption and emission of light of different wavelengths by the chromophoric system under consideration. Absorption spectra are obtained by plotting the optical density (O.D) or absorbance (A) as a function of wavelength of the incident radiation, while the emission spectra are obtained by plotting the emission intensity against wavelengths of the emitted light. It is to be noted that while the intensity of the emitted light from the molecules depends on the wavelength of excitation; the position of the emission maxima or the overall shape/feature of the emission spectra usually remain unchanged with the excitation wavelength. In order to carry out any photophysical or photochemical study, it is always the first step to know the absorption and emission spectra of the chromophoric system. Although absorption is a universal phenomenon for chromophoric molecules, their emission is not. There are many examples where chromophoric molecules show only very weak emission or no emission though their absorption spectra are quite strong.

1.8.2. Emission quantum yield (φ)

The efficiency of the chromophoric molecules to undergo emission process is expressed by the parameter emission quantum yield (φ), which is defined as the number of the photons emitted over the number of photons absorbed by the molecules. Hence, mathematically φ can be written as,

$$\varphi = \frac{\text{total number of photons emitted}}{\text{total number of photons absorbed}} \qquad (1.13)$$

Alternatively, the emission quantum yield can also be defined as the rate of de-excitation of the excited molecules via radiative process over the sum of rates of all the de-excitation processes. Thus,

$$\varphi = \frac{k_r}{k_r + \Sigma k_{nr}}$$

(1.14)

where, k_r is the rate of radiative process and Σk_{nr} is the sum of all the non-radiative decay processes.

It is to be noted that the fluorescence quantum yield of a molecular system can never be more than unity, as evident from the equation (1.13) and (1.14). When the sum of the de-excitation rates via non-radiative processes is much less as compared to the radiative decay rate i.e. $\Sigma k_{nr} < k_r$, the fluorescence quantum yield tends to become unity. The organic molecules having φ close to unity are known as strong fluorophores (e.g. rhodamine-6G, Pyrromethene-546, Pyrromethene-567 etc.) whereas, the molecules with low value of φ are generally known as weakly fluorescent or non-fluorescent molecules. The chromophoric molecules for which φ is quite low under normal condition but the φ value increases largely on changing their microenvironments especially through their confinements, are in general designated as the fluorogenic molecules, having immense importance in photochemical science.

1.8.3. Excited state lifetime (τ)

Excited state lifetime is defined as the average time spent by the excited molecules before they undergo de-excitation via all possible de-excitation pathways. Since, both radiative and non-radiative processes in general follow the first order kinetics, the de-excitation rate for the excited state molecules can be expressed as,

$$\frac{dn(t)}{dt} = n(t)(k_r + \Sigma k_{nr})dt \qquad (1.15)$$

$$\text{or, } \frac{dn(t)}{n(t)} = (k_r + \Sigma k_{nr})dt \qquad (1.16)$$

Integrating both the sides we get, $n(t) = n_0 \exp(-t/\tau)$ (17)

where, n(t) and n_0 are the concentration of the excited species at time t and 0, respectively and and $\tau = 1/(k_r+\Sigma k_{nr})$ is the lifetime of the excited state molecules.

When $t = \tau$, $\frac{n(t)}{n_0} = \frac{1}{e} = 0.37$

Thus, from the mathematical point of view; fluorescence lifetime of an excited molecule is the time when population of the excited molecules have been reduced to 1/e or 37% of the initial population. In other words, τ is the lifetime by which 63% of the initial population has already undergone de-excitation.

The radiative decay rate constant k_r is the intrinsic property of an excited state molecule which does not depend significantly on the surrounding environment. On the other hand the sum of the rate constants of the non-radiative de-excitation processes, which is the combination of rate constants of internal conversion, intersystem crossing, vibrational-rotational relaxation, solvent effect and also on, is the extrinsic property and can be modulated by tuning the surrounding environment by several means. Supramolecular host-guest complexation is one of the unique ways to reduce the rate of non-radiative decay processes by encapsulating the guest molecules into the host cavities, because encapsulation of a guest effectively reduces its molecular agility responsible for the decay of its excited state via non-radiative decay processes.[29, 30, 33, 35, 56, 80, 82, 112-114]

1.9. Solvent and environmental effects on absorption and emission spectra

The local environment and solvent polarity substantially modulate the electronic distribution in the chromophoric molecules which results in the changes of the absorption spectra, emission spectra and lifetime of the fluorophores to a significant extent. Interaction of solvent with the chromophoric molecule can also change the rates of the non-radiative de-excitation processes making the fluorophores either more or less fluorescent in nature on changing the solvent properties.

1.9.1. Effect of solvent polarity

Emission spectra of any molecule always appear at the longer wavelength region as compared to the absorption spectra. This is due to the fact that prior to emission a fraction of the excited state energy of the molecules is lost by different non-radiative processes, one of which is the solvent relaxation process. When a molecule is excited to the first singlet state (S_1), it undergoes a very fast (within few picoseconds) vibrational relaxation to the lowest vibrational level of the S_1 state wherefrom the emission radiative transition to different vibrational levels of S_0 state takes place (According to Kasha's rule). However, if the fluorophore is excited to the higher electronic level, e.g. S_2, the fluorophore rapidly comes to the first excited state via non-radiative internal conversion (IC, $t=10^{-12}$s or less) prior to undergo emission process. Solvent polarity generally lowers the energy gap between excited and ground states by stabilizing the excited state more than the ground state. Typically the fluorophores which have higher dipole moment in the excited state (μ_E) than that of the ground state (μ_G), red shift in the emission maximum with increasing solvent polarity is observed. This is due to the gradually larger stabilization of the excited state of the molecule than the ground state.[107] On the other hand, there are some fluorophores having higher ground state dipole moment (μ_G) than the dipole moment in the excited state (μ_E). In these cases, the increase in the solvent polarity leads to a hypsochromic shift of the emission peak. This is because the greater stabilization of the ground state than that of the excited state results in the increase in the energy gap between the two states involved in the electronic transition during emission.[107] The fluorophore those are non-polar in nature, show only nominal changes in the emission characteristic with the changing solvent polarity. Unsubstituted aromatic hydrocarbons, the fluorophores having very less polarity difference between excited and ground states (e.g. BODIPY dyes) fall in this category.[115, 116]

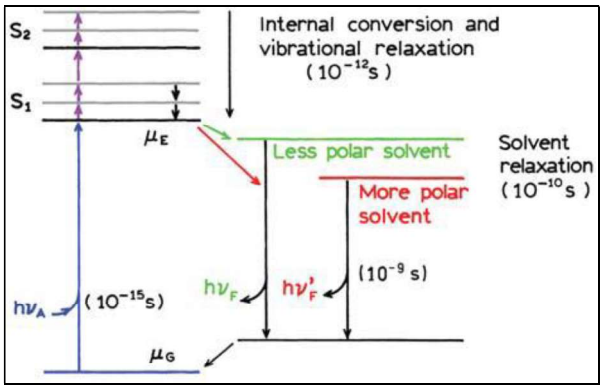

Figure: 1.12. Different process in sample solution.

The effect of solvent polarity on the energies of the electronic states is quantitatively shown in Fig. 1.12. It is clear from the above figure that the absorption process takes place within the time scale of femtoseconds and hence, the position of the fluorophore or the solvent molecules in the ground state and the excited state remains unchanged during absorption. This indicates that the fluorophore experiences the same local environment in the ground state and in the excited state immediately following excitation. This explains why the absorption spectra are insensitive to solvent polarity. Subsequently however, excited energy level undergoes substantial solvent relaxation, resulting a solvent polarity dependent shift in the emission spectra especially.

1.9.2. Effect of solvent viscosity

The increase in solvent viscosity does not have any marked effect on the absorption or emission spectra of a fluorophore but the excited state lifetime and the fluorescence quantum yield of the fluorophore increase significantly. With the increase in solvent viscosity, the molecular flexibility of the fluorophore reduces to a significant extent which in turn drastically reduces the non-radiative deactivation channels, which otherwise proceed through rotational relaxation, vibration relaxation, internal conversion and formation of twisted intramolecular charge transfer state (TICT).[117-121] Hence, the reduced Σk_{nr} leads to the increase in fluorescence quantum yield and excited state lifetime of the fluorophore as evident from the

eqn. (1.14) and eqn. (1.17). This phenomenon forms the basis of the flexible fluorophores to be used as the molecular rotors.

1.9.3. Spectral Shifts due to the other mechanisms

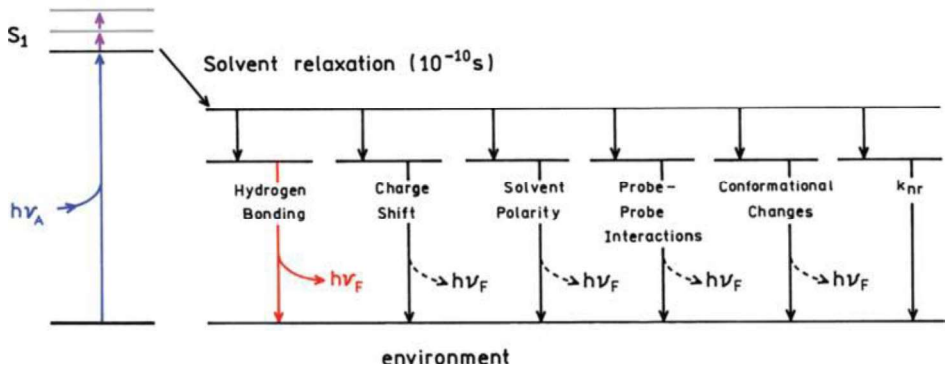

Figure: 1.13. Other interactions for the fluorophore present in solution.

It is not only the solvent polarity that results in the shifting of the emission spectra of a fluorophore, but there are many other intra and intermolecular interactions that can also cause shifts in the emission spectra of the molecules. When a fluorophore contains both electron donating group (like amino or hydroxyl group) and electron withdrawing group (like carboxylic acid, cyano group) simultaneously attached to the chromophoric moiety, there occurs a substantial charge separation in the excited state of the fluorophore. This phenomenon of the charge separation is known as intramolecular charge transfer (ICT or TICT), which is facilitated substantially on increasing the solvent polarity and becomes the lowest excited energy state. Whereas, the non-polar excited state of the fluorophore, which is commonly called as the locally excited (LE) state is the lowest energy state in the non-polar solvents. Thus, in addition to the general solvent effects, solvent medium can also govern the excited molecules to switch from one excited state to other, e.g. LE state to ICT or TICT states. There are also a huge number of examples where it is found that the presence the hydrogen bonding between the fluorophore and the solvent molecule can substantially change the spectral position of the fluorophore both in the case of absorption and emission.[122, 123]

Fluorophores containing electron donating groups like –NH_2, -OH, -NHR etc. form a very strong H-bonding in the ground state of the fluorophore, making the ground state more stable as compared to the excited state and hence, with the increasing strength of the H-bonding the energy difference between the ground state and the excited state increases leading to the blue shift in the absorption and emission maxima.[82, 122, 123] Again, a large spectral shift can also be observed due to the formation of the exciplex or excimer of the fluorophores where these excited complexes are emissive in nature.

1.10. Objective and outlook of the present work

Investigation of the effect of the macrocyclic and bio-macromolecular hosts on the photophysical and photochemical properties of different guests through host-guest supramolecular complexations is frequently been studied using various techniques which include UV-vis absorption, fluorescence, time resolved emission, NMR; isothermal titration calorimetry (ITC) and so on. Encapsulation of the guest into the host cavity leads to substantial modulations in the absorption, emission, lifetime, quantum yield, anisotropy, photo-degradation characteristics of the guest molecule which can be employed in different fields depending upon the requirements.[20, 28-30, 32, 34-37, 44-51, 53, 54, 56, 58, 61, 63, 82, 85, 95, 96, 124-133] It is observed that the properties of the guests can be tuned to differential extents by different hosts as per the requirements. The present thesis includes detailed studies on the modifications or improvements of the physicochemical properties of different guest molecules like crystal violet, BODIPY-benzimidazole, styryl-11 or LDS-798 dyes upon supramolecular complexation with various hosts like Cucurbit[7]uril (CB7), beta-cyclodextrin and its different analogues, bovine serum albumin (BSA), etc. As most of the guest molecules used in these studies have emission feature in the red or near-infra red region, we were prompted to explore the possible uses of the supramolecular complexation of these dyes with various hosts and quite satisfactorily found that the complexation of LDS-798 with BSA/HSA protein can be

employed for the quantification of the serum albumin in complex biological matrices (discussed later). The present studies have also explored how the degree of substitution of beta cyclodextrin (CD) scaffold results in substantial difference in the binding properties as well as in the modulations of the guest properties. Additional studies like the effect of ionic strength and changing the temperature on supramolecular complexations have also been explored in the present work. In these studies, we mainly used the spectroscopic techniques like ground state absorption, steady state fluorescence, time resolved emission (excited state lifetime, anisotropy) and ^{1}H NMR measurements. To support the obtained results from the spectroscopic techniques we have also used theoretical calculations, wherever possible, using either molecular docking or DFT calculations. The details of the studies carried out in the Ph.D. program are described in the following chapters.

CHAPTER-2

MATERIALS, METHODS AND INSTRUMENTATION

2.1. Introduction

To get the insights of host-guest supramolecular interactions and their possible applications, we studied several host-guest systems with various dyes such as crystal violet, BODIPY-benzimidazole conjugate and LDS-798 or styryl-11 as guests and different macrocyclic compounds including cucurbit[7]uril (CB7), β-cyclodextrin (CD) and its anionic derivatives, and the biomolecules like bovine serum albumin (BSA), human serum albumin (HSA) as hosts. The inclusion of the aforementioned dyes into the host cavity or binding pockets resulted in a substantial modulation in their physicochemical properties. While the changes in the ground state absorption and steady-state emission of guest dyes were measured by spectrophotometer and fluorimeter, respectively, the properties of their excited state (excited state lifetime and time resolved fluorescence anisotropy) were measured by time correlated single photon counting (TCSPC) set up. The locations or the mode of complexation in different host-guest systems were also recognized by nuclear magnetic resonance (NMR) technique. This chapter gives an overview of different guests and hosts used in the present studies along with various experimental techniques that have been employed to elucidate the objective of the present thesis.

2.2. Different guest molecules used during the present studies

2.2.1 Crystal Violet (CV)

The dye crystal violet (CV), whose chemical structure is shown in Fig. 2.1, is a homologue of the triaryl methane dyes. In the literature, the dye CV is emphasized as a useful chromophoric system for staining various bio-organisms, having potentials of being antifungal, antibacterial, anthelmintic and antiparasitic agent and is also effective in

photodynamic therapy. Due to its non-planar and non-rigid (flexible) structure, the excited state of CV relaxes very efficiently involving ultrafast non-radiative de-excitation pathways, making the free dye to be extremely weak in its fluorescence.[134-139] Upon inclusion into macrocyclic host cavities or incorporation into the bio-macromolecular binding sites, the dye, however, can display a large enhancement in its fluorescence intensity, due to reduction in its non-radiative deexcitation processes, caused by the restrictions imposed by the hosts on the flexibility of the dye, generalized as the confinement effects.[35, 63, 80, 82, 95, 96, 125, 140, 141] It is acknowledged in the literature that in the ground state CV molecules can exist in more than one conformational structures.[134-137, 139, 142, 143] A planer symmetric propeller structure where all the aryl groups at the central sp^2 carbon are rotated in the same sense (D_3 point group), is unambiguously established form X-ray crystallographic studies.[142, 143] While some studies suggest one of its conformer as a planer asymmetric propeller structure with one of the aryl group rotated in opposite sense than the other two aryl groups (C_2 point group), other studies propose it as a pyramidal symmetric propeller structure (C_3 point group), stabilized by the dye-solvent hydrogen bonding interaction at the central carbon atom of CV. It is suggested that the planar symmetric propeller structure is the most stable conformer of CV and accordingly it dominates over the other structure in the solution.

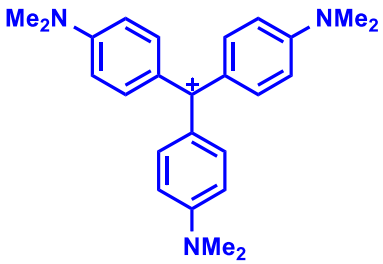

Figure: 2.1. Chemical structure of Crystal Violet (CV).

2.2.2. BODIPY-benzimidazole (BDZ)

4,4-Difluoro-4-bora-3a,4a-diaza-s-indacene and its derivatives, commonly know as BODIPY dyes, have a unique structural motif where two pyrrole units are linked together by a

BF_2 bridge. Compared to the other organic dyes, BODIPYs have several advantages in regard to their photophysical/photochemical properties, which include high molar absorptivity, high fluorescence quantum yield, very sharp absorption and emission profiles in the red spectral region, low photo bleaching tendency, low singlet-triplet conversion, easy tumability of physicochemical features by chemical modifications, and so on.[116, 144-147] Accordingly BODIPY class of the dyes are realized as excellent chromophoric molecules for their uses in various applications such as active medium in dye lasers, metal sensors, polarity sensors, bio-imaging applications, molecular logic gates, pH sensors, biological markers and so on.[116, 144-148] Although, BODIPYs have several advantages, their low aqueous solubility, small Stoke's shift and tendency to form aggregates in aqueous solution limit their uses in many cases. Thus, extensive research has been going on to improve the properties of BODIPY dyes to a large extent by chemical modifications at different positions of the BODIPY core.[148-153] One such modification is BODIPY-benzimidazole conjugate (BDZ), which is formed by substituting the hydrogen atoms at positions 2 and 8 of the BODIPY chromophore by benzimidazole and phenyl units respectively through suitable chemical reactions.[63, 154] Notably, the BDZ dye shows high sensitivity towards pH, polarity of the surrounding enviroment and excellent fluorescence turn on through host-guest interactions with macrocyclic and bio-macromolecular hosts, along with a favorable response towards external stimulus and all these charateristics have provided the present probe BDZ with additional advantages to be used as a biological probe.

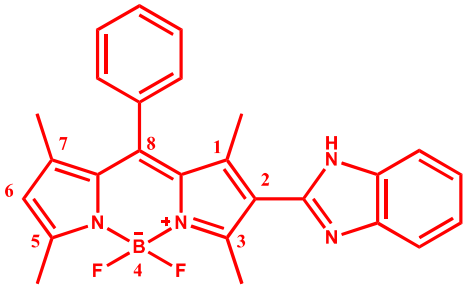

Figure: 2.2. Chemical structure of BODIPY-benzimidazole conjugate (BDZ).

2.2.3. Styryl-11 or LDS-798

Styryl-11 or LDS-798 [1-Ethyl-4-(4-(*p*-dimethylaminophenyl)-1,3-butadienyl)-quinolinum percholate] is a polar dye with a positively charged chromophore which is counter balanced by the presence of perchloratre ion. Over the years, LDS-798 has been used as a solvatochromic dye as well as in other biological applications such as determination of lipid structure, membrane potential, membrane permeability, vesicle trafficking, exocytosis and so on.[117, 155-157] Presence of electron donating dialkyl amino group and electron deficient quinolinium group in conjugation and also the rotation of $-N(CH_3)_2$ group around C–N bond or that of aniline group as a whole leads to the formation of twisted intramolecular charge transfer (TICT) structure in the excited state, rendering this dye to become extremely weak in fluorescence ($\varphi \sim 0.002$).[117, 155, 158] This property makes LDS-798 an excellent candidate to determine solvent polarity and viscosity thorough fluorescence modulations.[117] The non-fluorescent TICT form of excited LDS-798 is highly favorable in polar media but with a decrease in solvent polarity and an increase in solvent viscosity, the formation of TICT form becomes largely reduced and the dye becomes strongly fluorescent in nature.[96, 117, 155]

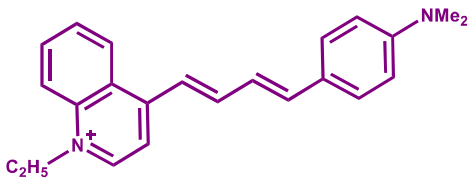

Figure: 2.3. Chemical structure of LDS-798 (Styryl-11).

2.3. Different hosts used in the present study

2.3.1. Cucurbit[7]uril (CB7)

Cucurbit[7]uril (CB7) is one of the most important member of the cucurbit[n]uril (CBn) class of the macrocyclic hosts, developed and identified in recent times. In 1905,

Behrend and coworkers first synthesized a white powder by condensation of paraformaldehyde with glycouril in acidic condition.[159-163] The formed product was found to be insoluble in water but weakly soluble in dilute acid or base. But for some reason, the Behrend group could not characterize the product in their work. In 1981, Mock et al. revisited the experimental procedure of Behrend and successfully synthesized, crystallized and characterized a macrocycle with six glycouril groups joint together by twelve methelene groups in a cyclic manner, to give a typical shape like a pumpkin. They named the product ‘‘cucurbituril’’ and the formed product was cucurbit[6]uril or CB[6]. Although initial discovery and separation of CB[6] was carried out earlier, it was the South Korean scientist Kimmon Kim who first in 2000 separated three new members of the CB[n] family members, CB[5], CB[7] and CB[8], containing 5, 7 and 8 glycouril units, respectively.[160]

Despite very recent entry of cucurbiturils in the realm of the host-guest chemistry as compared to the other macrocyclic hosts like cyclodextrin, calixarene, crown ethers and so on; cucurbit[n]urils have gathered the attention of many scientists in diverse fields all over the globe due to their specificity, selectivity, availability with various cavity sizes, possessing highly polar carbonyl portals, rigid hydrophobic cavity, high binding capacity, excellent biocompatibility, and so on.[31, 59, 61, 83, 163] Among the members of the CBn family; application, demand and usefulness of CB7 are increasingly growing day by day. CB7 shows excellent binding affinity towards most of the organic guests as the cavity dimension of CB7 matches quite well with the size of the organic guest molecules or their hydrophobic residues as compared to the other CBn members. Reasonably good water solubility (3-4 mM)[82, 125] of CB7 provides an added advantage for its uses in host-guest chemistry. CB7 forms very strong inclusion complex via strong ion-dipole interaction between its portal carbonyl groups and the cationic guests. Hydrophobic interaction provided by the CB7 cavity to the encapsulated hydrophobic residue of the guest molecules and the H-bonding between the carbonyl portals

of CB7 and the H-donor guests also often contribute largely to strengthen the inclusion complex formation. In most of the cases, CB7 forms stable 1:1 inclusion complexes with guest molecules, in which the binding constant between guests and CB7 often ranges from 10^3 to 10^{10} M^{-1}.[31, 59, 82, 83, 141] CB7 found to bind with ferrocene, ademantanes, diadamantanes with exceptionally high binding affinity and in some cases the reported affinities in such systems exceed the strongest non-covalent interaction of biotin–avidin pair found in nature.[59, 164] In addition to this, CB7 is also known for its application in the field of sensing, aqueous dye lasers, molecular logic gates, supramolecular catalysis, drug formulation, nano drug carrier, etc.[10, 14, 20, 27-31, 33-36, 48-51, 56-59, 61, 62, 80, 82, 83, 87, 124, 141]

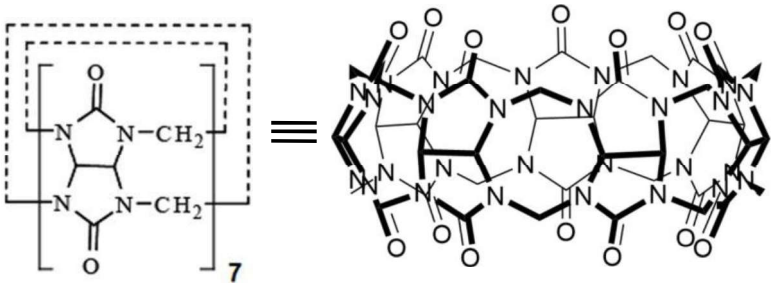

Figure: 2.4. Chemical structure of Cucurbit[7]uril (CB7).

The cavity size of the CBn hosts increases with the increase in the number (n) of the repetitive glycouril units while the height of the cavity remains constant for all the members of CBn family.[35, 59, 160, 165] Molecular dimension and the water solubility of the important CBn homologues are given in the Table 2.1.

Table: 2.1. Molecular dimensions and water solubility of CB[n] family members.[59, 82, 141, 165]

CB[n]	Outer diameter (Å)	Portal diameter(Å)	Cavity diameter(Å)	Height(Å)	Volume of the cavity(Å^3)	Solubility (mM)*
CB5	13.1	2.4	4.4	9.1	82	~3-4
CB6	14.4	3.9	5.8	9.1	164	0.02-0.03
CB7	16.0	5.4	7.3	9.1	279	20-30
CB8	17.5	6.9	8.8	9.1	479	0.075

(*) The solubility of CB[n] members is dependent on the pH, and ionic strength of the experimental solution.[161, 166, 167]

2.3.1A. Synthesis of cucurbit[7]uril (CB7)

Cucurbit[7]uril is a costly macrocyclic host and not easily available commercially. Based on the difficulties in availability of pure CB7 at expected time, we synthesized CB7 independently using the literature based method as shown in Scheme 2.1.[160]

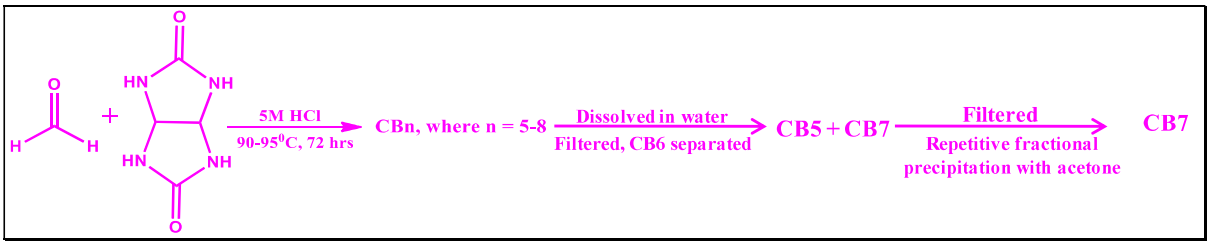

Scheme: 2.1. Synthesis scheme of CB7 macrocycle.

2.3.1B. Purification of Cucurbit[7]uril (CB7)

Reaction of glycouril with paraformaldehyde in presence of 12N HCl at 90-95^{0}C for about 100 hours results in the formation of a mixture of products that contains CB[6] as a major product (~75%) along with CB5 (~10%) and CB7 (~10-12%) as the minor products, in addition to a very small amount of CB8 (~0.02 %).

For isolation of CB7, ~50 gm of the reaction mixture was added to 2.5 liter of water with constant stirring to dissolve completely CB5 and CB7 and then the solution was filtered. The filtrate contained the mixture of CB5 and CB7 in the dissolved condition while the residue was composed of mainly CB6. The filtrate was concentrated and acetone was added into it to precipitate both CB5 and CB7. The precipitate was then dried and subjected to ^{1}H and ^{13}C NMR study to get a rough idea of the relative proportions of CB5 and CB7 in the mixture. After that, ~8.3 gm of the precipitate containing CB5 and CB7 was again dissolved in 450 ml of water, stirred to dissolve the precipitate followed by the addition of ~300 ml acetone into it to separate out the dissolved CB7. The turbid solution then filtered, dried to get

4 gm of the CB7 which was subjected to NMR study. NMR study revealed that the obtained precipitate was the pure CB7.

2.3.1C. Characterization of cucurbit[7]uril (CB7)

The purity characterization of the separated CB7, was carried out by two independent methods, (i) NMR study and (ii) MALDI-TOF analysis. In chemical characterization NMR study is an essential tool to get an idea about the structure and purity of the synthesized compound in a chemical reaction. Herein, we performed ^{1}H and ^{13}C NMR studies to get an idea about the composition and/or the purity of the CB7 synthesized by afore mentioned method. Although there is a subtle difference in NMR spectra of CB7 and CB5, the presence of the two homologues can easily be identified. For a CB7 sample, the doublet peak of two hydrogens of the methelene group barely show any difference in presence of CB5 but the methine hydrogen at the junction of the two rings gets heavily affected and shows broadening along with the appearance of another overlapping peak as shown in the Figure 2.5. After purification or removal of CB5 by repetitive and tedious fractional precipitation method, the apparent doublet peak of the methine hydrogens appears as a singlet with a sharp intensity. The characterization was further done by MALDI-TOF analysis where a peak of highest intensity at ~1185.5 corresponds to CB7 (M.W. of CB7 = 1163 + 23 for Na^{+}) whereas the peak of moderate intensity at ~1300 is due to the (M.W. of CB7 = 1163 + 137 for Cs^{+}). The low intensity peaks at the lower mass region come from the fragmentation of CB7 molecules under the experimental conditions.

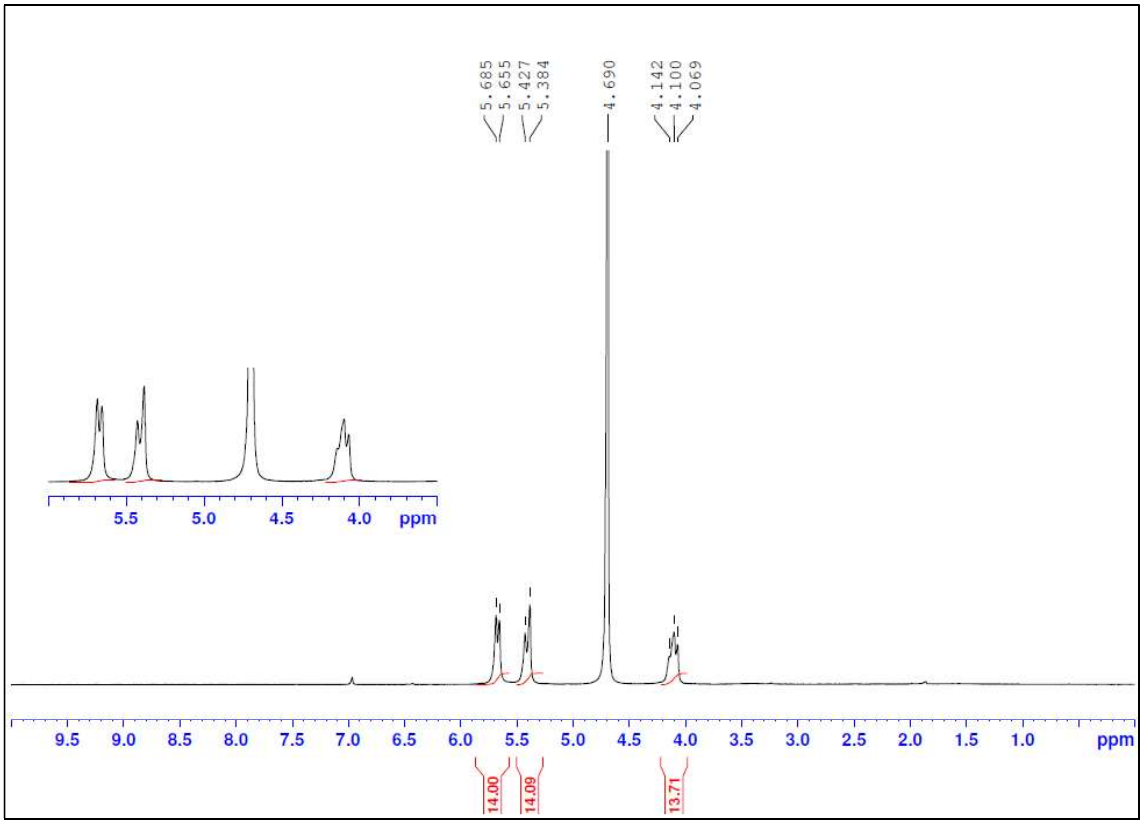

Figure: 2.5. [1]HNMR spectra of impure cucurbit[7]uril (CB7) with small amount of CB5.

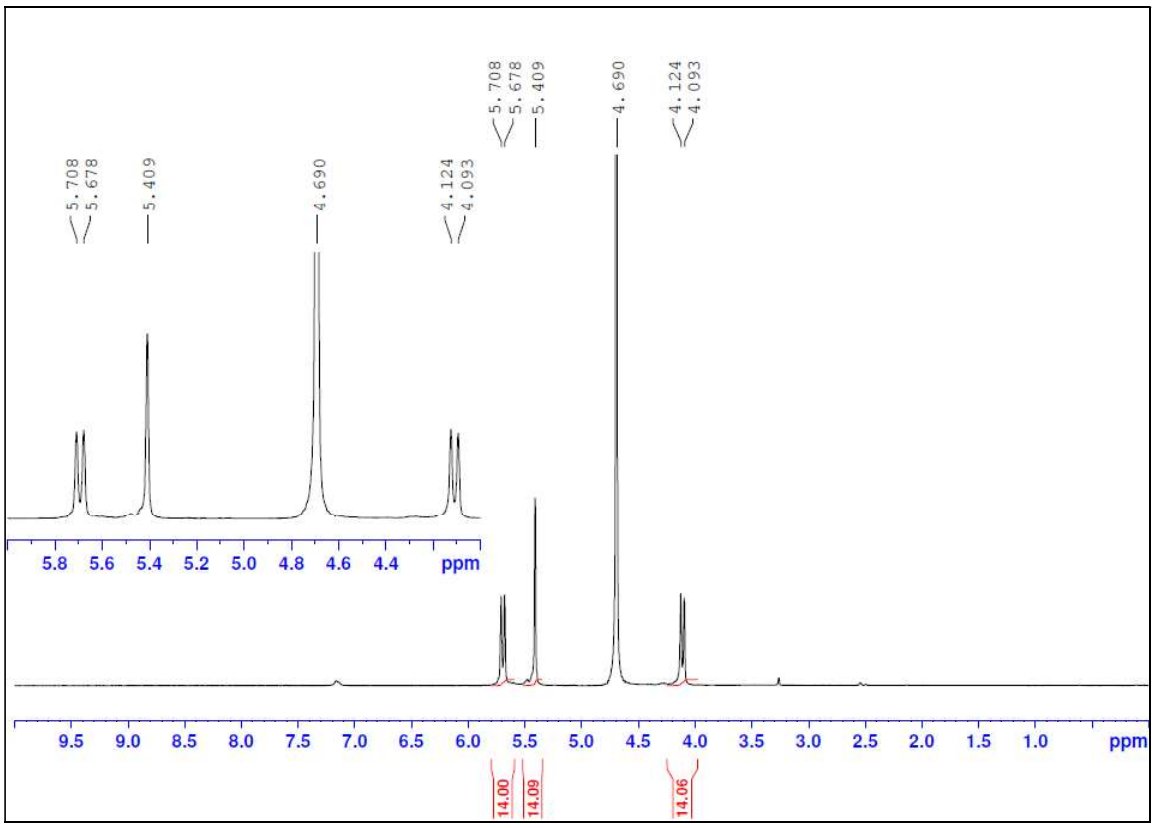

Figure: 2.6. [1]H NMR spectra of pure cucurbit[7]uril (CB7).

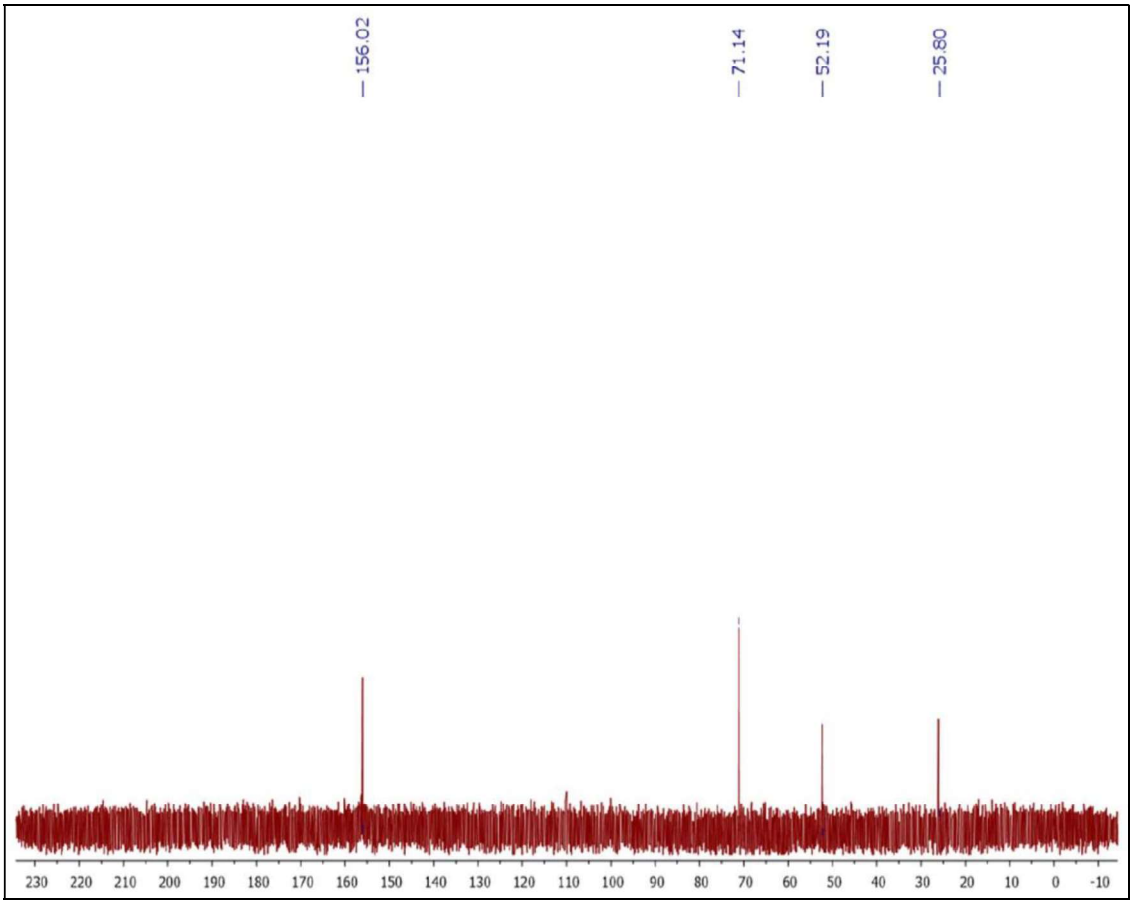

Figure: 2.7. ^{13}C NMR spectra of pure cucurbit[7]uril (CB7).

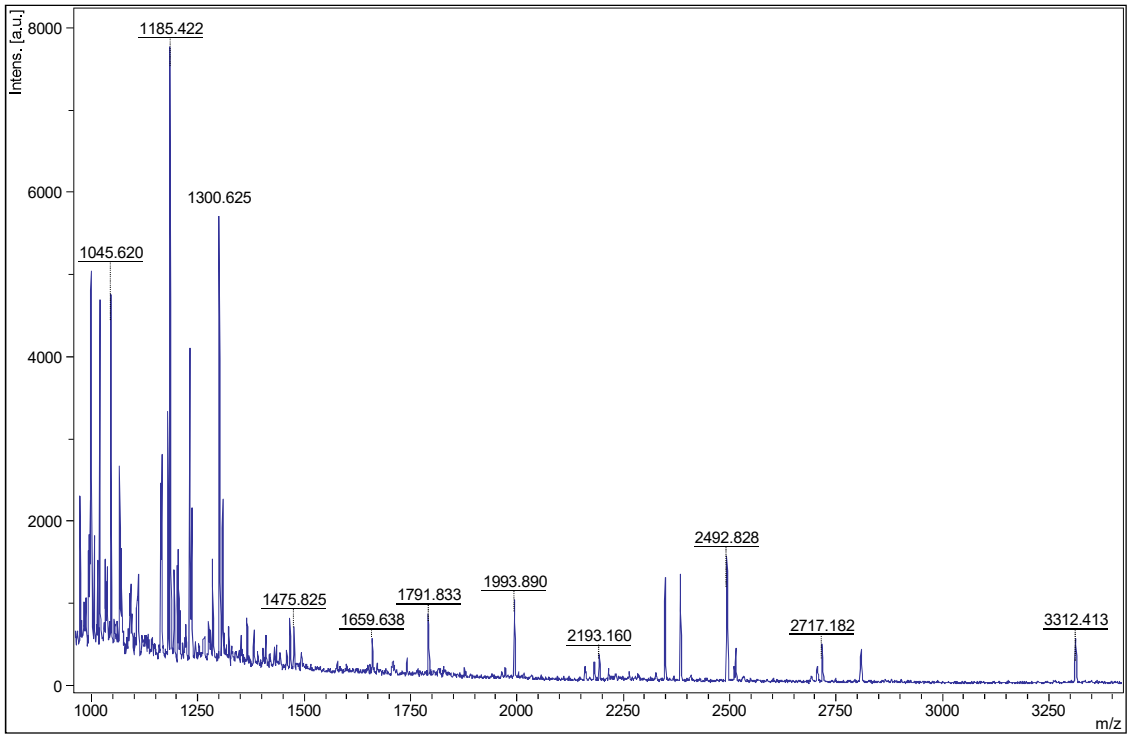

Figure: 2.8. MALDI-TOF spectra of cucurbit[7]uril (CB7).

2.3.1D. Purity determination of cucurbit[7]uril (CB7)

Generally, CB7 contains acid of crystallization, water of crystallization and some metal ions as impurity which get trapped during synthesis and isolation.[166] In addition, CB7 sample is very hygroscopic and often picks up atmospheric moisture.[168, 169] The removal of these impurities from a CB7 sample is often, cumbersome, difficult and time-consuming. These impurities present with the CB7 samples reduce the effective binding efficiency and cause the apparent molecular weight of CB7 to be always greater than the molecular weight of only CB7.[169] Thus, it is important to estimate the content of CB7 before subjecting the CB7 sample for any kind of semi-quantitative or quantitative study. Multiplication of the percentage of purity with the taken weight of the CB7 gives the actual measure of the working CB7 sample in the experiments or used to estimate the binding strength of CB7 with the guest molecules.

The purity of CB7 samples is determined by the spectrophotometric method established by Kaifer et al. using cobaltocene complex as guest.[169] Pure cobaltocenium hexafluorophosphate ($Cob^+PF_6^-$) is commercially available, easier to handle (not hygroscopic) and relatively cheap, which makes it an excellent guest for this analytical purpose. Cob^+ has very high affinity (mention K_b= 5.7x10^9 M^{-1} in 50 mM sodium acetate solution) towards CB7 and forms 1:1 complex.[170] With gradual increase in CB7 concentration to the solution containing cobaltocene complex, the optical density of the Cob^+ solution at 263 nm decreased and remained unchanged at the equivalence point.

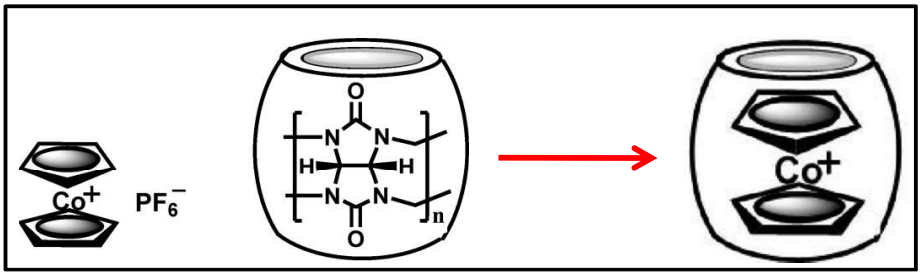

Figure: 2.9. Complexation of cobaltocene complex and cucurbit[7]uril (CB7).

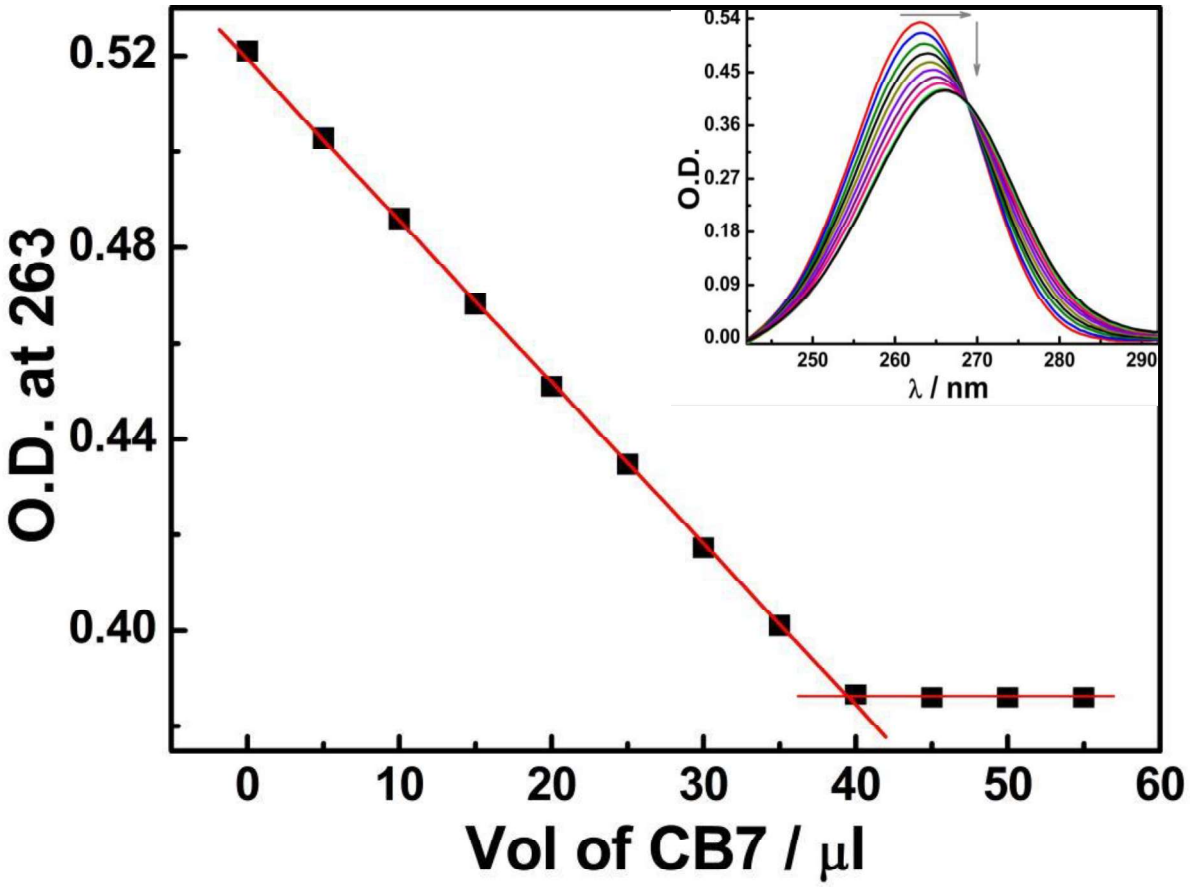

Figure: 2.10. Spectropohotometric purity determination of CB7 using cobaltocene complex.

The percentage purity of the CB7 sample was then determined by the following formula,[169]

$$\%p = \frac{MW.C.(v_i + v_e)}{m.\frac{v_e}{V}} x100 \qquad (2.1)$$

where, MW= Molecular weight of CB7 = 1163

C= concentration of the prepared cobaltocene complex= 15.35 µM

v_i = initial volume of the cobaltocene complex taken in the cuvette = 2 ml

v_e = volume of CB7 solution required for complete complexation = 39 µl

V = Volume of the Cobaltocene stock in which CB7 sample initially dissolved = 10 ml.

m = weight of CB7 taken in the stock solution = 9.4 mg.

In the present case, the determined purity of the synthesized CB7 sample (% p) was 77% by weight and the rest will be mainly due to water and acid of crystallization. Thus, content of

CB7 in this sample was considered as 77% by weight during its use for host-guest complexation studies.

2.3.2. β-Cyclodextrin (β-CD) and its sulfobutylether derivative (SBEβCD)

Among many macrocyclic hosts, cyclodextrin (CD) family of the molecules are realized as the important class of the hosts, which were first discovered in 1891.[171] Intramolecular transglycosylation reaction from degradation of starch by cyclodextrin glucanotransferase (CGTase) enzyme results in the formation of cyclodextrins.[172]. Cyclodextrins (CD) are cyclic oligosaccharides consisting (α-1,4)-linked α-D-glucopyranose units with a hydrophilic exterior and hydrophobic cavity providing a truncated cone shaped structure. The secondary hydroxyl groups in CD molecules extend from their wider rim while the primary hydroxyl groups extend from their narrow rim. Due to their good water solubility, low toxicity, excellent bio-compatibility, ready availability and cost effectiveness, CDs are the most celebrated hosts used in the pharmaceutical industry.[19, 42, 173-177] Cyclodextrins are used to reduce hydration, unwanted chemical susceptibility towards enzymatic actions and also enhance the bio-availability, water solubility, chemical compatibility, enzymatic stability and sometimes to improve the taste of the drug molecules.[42, 177, 178]

Amongst the parent CDs (α, β and γ-CD); β–CD comprising of seven glucopyranose units, has the cavity size most compatible to most of the dye/drug molecules. Its ready availability and low cost make β–CD to be used quite extensively in pharmaceutical industry.[42, 173, 178] However, its lower water solubility,[42, 82, 141, 173] low binding affinity (K_a mostly in the order of 10-10^3 M^{-1})[5, 42, 82, 140, 141] and also its significant toxicological effect often restrict the use of β–CD in many such applications.[42] Thus, an extensive research work went on to improve the water solubility and binding affinity of β–CD while reducing its toxicological effects. There has been extensive research work carried out by various scientists in different parts of the world to improve the properties of the CD molecules in general, by

incorporating different substituents for their hydroxyl hydrogens. Most of the substituted CD derivatives show improvements in many of their attributes as compared to the parent CD molecules. Amongst different substitutions, those with sulfobutylether (SBE) sulfonate groups markedly improve the water solubility of the CDs due to the change of the neutral form of the parent host molecules to ionic ones, which make them highly soluble in polar solvent like water. The presence of anionic sulfonate end groups in these substituted CDs makes them susceptible to bind with the cationic dyes/drugs very strongly, involving electrostatic interaction, along with the participation of the conventional hydrophobic interaction. The presence of the extended hydrophobic cavity provided by the sulfobutylether groups at the basic CD portals make these CD derivatives to hold guest molecules even stronger than the parent CD molecules.[46, 47, 179, 180] All these combined effects make the substituted anionic derivatives, especially the anionic SBEβCD derivatives to act as very effective hosts for host-guest supramolecular complexations.[179] It has been recently found that SBEβCD derivatives are well tolerated in humans and it causes no adverse effects on the kidneys or other organs following either oral or intravenous administration.[179, 180] It is realized that SBEβCD hosts are far the most promising candidate for interaction studies with compounds abundant in nitrogen containing moieties, since for theses guest molecules, besides molecular host-guest inclusion, electrostatic interactions can also contribute significantly for successful host-guest binding.[47, 179-181] The SBE substituted CD derivatives also possess low cell membrane disrupting effect.[179, 180] Studies on the effect of degree of SBE substitutions on β−CD has been carried out very elaborately and it has been found that among all the β−CD derivates the SBE_7βCD with 7 SBE substitutions displays the most effectiveness in general towards stable complexation with different dyes and drugs,[46, 47, 180-183] though in some limited cases higher order substitutions are also found to be more efficient than the SBE_7βCD derivative.

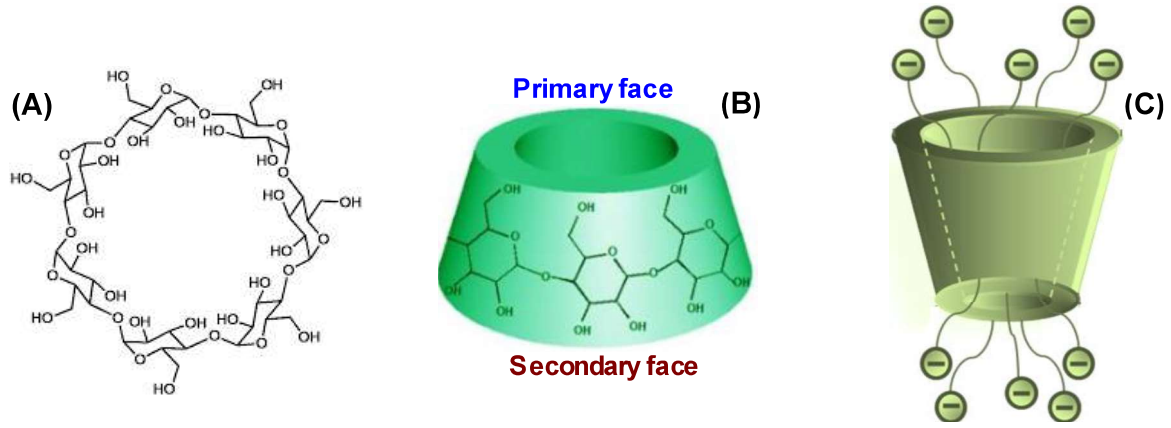

Figure: 2.11. (A) Chemical structure and **(B)** three dimensional presentation of β-CD and **(C)** SBEβCD hosts.

Similar to cucurbiturils, cyclodextrins are also categorized depending upon the number of glycosidic linkages present in their primitive structure. Cyclodextrins with six, seven and eight glucopyranose units are known as α-cyclodextrin, β-cyclodextrin and γ-cyclodextrin, respectively. The tabular form of the molecular dimension and the solubility of CD homologues are given in the Table 2.2.

Table: 2.2. Molecular dimensions and solubility of important CD hosts.[42, 82, 173]

Cyclodextrins	Outer diameter (Å)	Narrow rim diameter(Å)	Wider rim diameter(Å)	Height(Å)	Volume of the cavity(Å^3)	Solubility (mM)*
α-CD	14.6	4.7	5.3	7.9	174	120-150
β-CD	15.4	6.0	6.5	7.9	262	16.5
γ-CD	17.5	7.5	8.3	7.9	427	175
SBEβCD	15.4	6.0	6.5	7.9	-*	~600

(*) The volume of the SBEβCD cavity is far higher due to the presence of the extended sulfobutyl ether chains attached at the rims of the parent CD.

2.3.3. Bovine serum albumin (BSA) and human serum albumin (HSA)

Serum albumins are the important transport proteins present in the blood plasma that help in transporting essential analytes/drugs from one place to another inside the body. Albumin is a simple protein which is synthesized in the liver; contain only amino acids, without prosthetic groups (Cofactors) or other additives. Bovine serum albumin (BSA) is a

transport protein obtained from the blood plasma of cows. It is consisting of a single polypeptide chain composed of 583 amino acid residues with no carbohydrates attached. Due to structural resemblance with human serum albumin (HSA), the BSA is widely used as a model transport protein to investigate various drug–protein interactions.[50-58] BSA is fairly soluble in water with solubility as about 48 mg/ml and maintains a fairly stable structure in the pH range 5 to 8. Isoelectric point (pI) of BSA is 4.7, hence at the physiological pH (pH ~7.4) BSA surface is mainly negatively charged.[184-186] In the pH range of about 5 to 7, BSA structure contains 17 intra chain disulfide bridges and 1 free sulfhydroxyl (thiol) group. BSA is fairly fluorescent in nature ($\varphi \sim 0.15$) due to the presence of two tryptophan (Trp-134, Trp-212), twenty tyrosine and twenty-seven phenylalanine residues.[184-187] The BSA emission, however mainly comes from the tryptophan residues, due to the energy transfer from tyrosines and phenylalanines to tryptophan residues.[184-186] The studies on the interactions of different dye/drug molecules with BSA are very useful in understanding different binding mechanisms of the transport protein and also to reveal the implications of the various binding modes in regard to the availability and efficacy of the concerned dyes/drugs to the biological targets as well as for pharmaceutical, medicinal and other applications.[95, 96, 187-199]

Structurally BSA consists of three α-helical domains I, II, and III, oriented three dimensionally in space to give an equilateral triangle with sides of ~80 Å and a depth of ~30 Å.[184, 186, 187] Each domain is further divided into two sub-domains which are marked as sub-domain A and sub-domain B. Although BSA has almost nine different binding sites, two of these sites are realized to be the major binding pockets, one is denoted as the Sudlow's site I, situated at the sub-domain IIA, which is also often referred as the wafarin site; and the other one is designated as the Sudlow's site II, exists at the sub-domain IIIA, which is also often called the indole/benzodiazepine/ibuprofen binding site.[184-187] Site I is more voluminous and in this site the main operative force is hydrophobic interaction. Compared to site I, the site II

is less capacious in which the prevailing forces are combinations of hydrogen bonding, electrostatic interaction, van der Waals' force and hydrophobic interaction. If the binding analyte is hydrophobic in nature and large in size, it preferentially gets accommodated in the site-I of BSA. However, if the guest molecule is polar in nature and smaller in size, it is likely that the guest would be preferentially accommodated in site-II. BSA having almost 76% resemblance with human serum albumin (HSA).[184, 187] Binding interaction of different guests with BSA provides an idea about their behavior towards HSA as well. Important physicochemical parameters of BSA and HSA proteins are listed in Table 2.3 for quick reference.

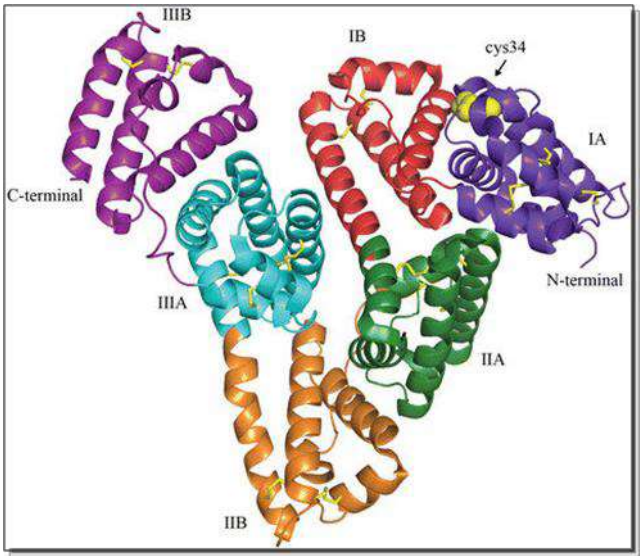

Figure: 2.12. Three-dimensional structure of serum albumin (SA).

Table: 2.3. The physicochemical properties of the serum albumins[185, 186]

Parameters	BSA	HSA
No. of Aspartic acid	40	36
No. of Tyrosine	20	18
No. of Phenylalanine	27	31
No. of Tryptophan	2 (Trp-134, Trp-212)	1 (Trp-214)
Calc. mol. mass (Da)	66411.17	66,438.41
Calc. net charge (pH 7)	−17	−15

Quantum yield (φ)	0.15	0.13
Intrinsic viscosity, η	0.0417	0.0426
Refractive index increment (578 nm) x 10^{-3}	1.909	1.8921
Isoelectric point	4.7	4.7
Estimated α helix, %	68	67
β form, %	17	10

2.4. Methods and Instrumentations

2.4.1. Ground State Absorption Studies using Spectrophotometer

To get the information on the ground state of a chromophoric molecule, absorption spectroscopy is a very important tool. The light absorbed is dependent on the nature of the absorbing species, which in turn depends on the ground state electronic configuration of the chromophore and its interaction with surrounding solvents and interacting molecular systems. Absorption spectrum of a chromophoric system is obtained by recording the light absorbed by the system as a function of wavelength of the incident radiation and the absorption maximum is designated as the wavelength at which the chromophoric molecule shows the maximum absorption or minimum transmittance of the incident light, denoted as λ_{max}. The position of the peak absorption of the chromophoric species may change depending on polarity, polarizability and H-bonding ability of the solvent medium. Hence, from the ground state absorption data one can get an idea about the interaction of the chromophoric system with the surrounding solvent environment.

As discussed in Chapter-1, according to the Lambert-Beer's law, absorbance (A) of a chromophoric system depends on the concentration (C) of the absorbing molecules present in the solution and the path length (l) used for the solution in the absorption measurement. Thus,

$$A = \varepsilon_{\lambda} Cl \tag{2.2}$$

where, ε_λ is the molar absorption co-efficient at wavelength λ.

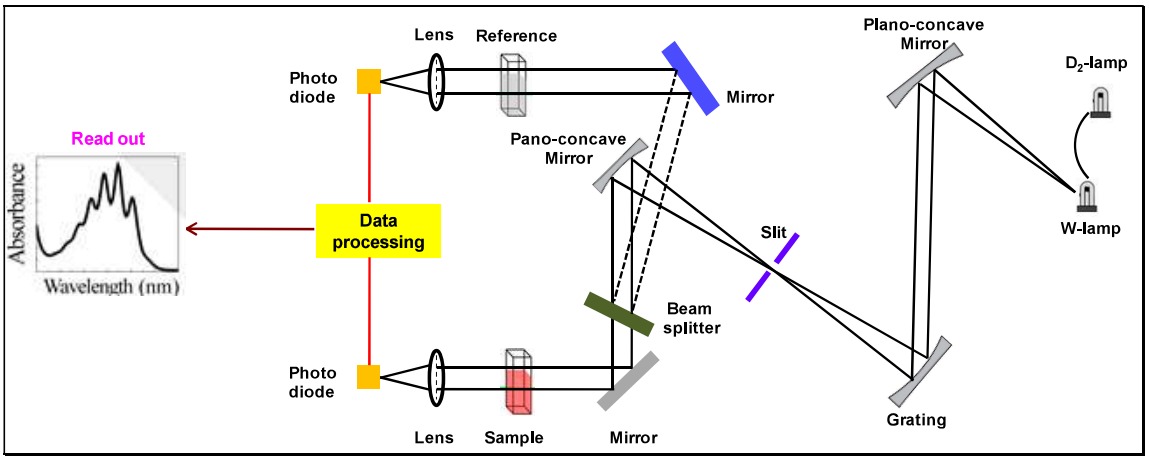

Figure: 2.13. Schematic presentation of a double beam UV-Vis spectrophotometer.

In the present study, ground state absorption studies were carried out using a Thermo-Scientific UV-vis spectrophotometer (model no-UV 2700) taking the sample solution in an optical quartz cell of 10 mm path length. The spectrophotometer covers a wide range of wavelength (from 200-1100 nm) with two light sources, one of which is the tungsten lamp which covers wavelength from 1100 nm to 330 nm and the other one is the deuterium lamp that covers the wavelength range of 330-200 nm. Silicon photodiodes are used as detectors with the minimum wavelength resolution of 0.2 nm and lowest measurable absorbance ~0.005. Schematic of spectrophotometer is shown in Fig. 2.13.

2.4.2. Steady-state fluorescence measurements using Spectrofluorometer

Fluorescence spectroscopy is a very useful and extremely sensitive technique to get precise information about the physicochemical processes occurring in the excited state of a fluorophoric system. Due to the ease of sample preparation, non-destructive nature of the technique, very low sample requirement, easy sample handling and high sensitivity, the demand of fluorescence spectroscopy increasing vary rapidly among chemists, biologists, pharmacologists and bio-chemists from different parts of the globe. The fluorophores emit light following their excitation with suitable wavelength of light and the emission spectra of the fluorophores are obtained by plotting the emitted light intensity of the fluorophoric system

as a function of the increasing wavelengths. The wavelength position of the emission peak (λ_{em}), intensity of the emission spectra and also the shape of the emission spectra are greatly influenced by the surrounding solvent/molecular environment.[107] In the present study, the steady-state (SS) fluorescence measurements were carried out using a Horiba fluoromax-4 spectrofluorimeter in a quartz cuvette of 1 cm x 1 cm optical windows. The sample solutions were excited at a suitable wavelength (λ_{ex}) of the light source and the emission from the samples were collected at the right angle configuration with respect to the excitation beam. The fluorimeter uses a high pressure (10 atm) and 150 watt continuous output Xe lamp as an excitation source and an R-928P photomultiplier tube (PMT) as the photodetector. The detector responds over a long range of wavelengths from 185 to 850 nm with dark current <1000 counts. The schematic of the spectrofluorimeter is given in Fig. 2.14 for a general understanding.

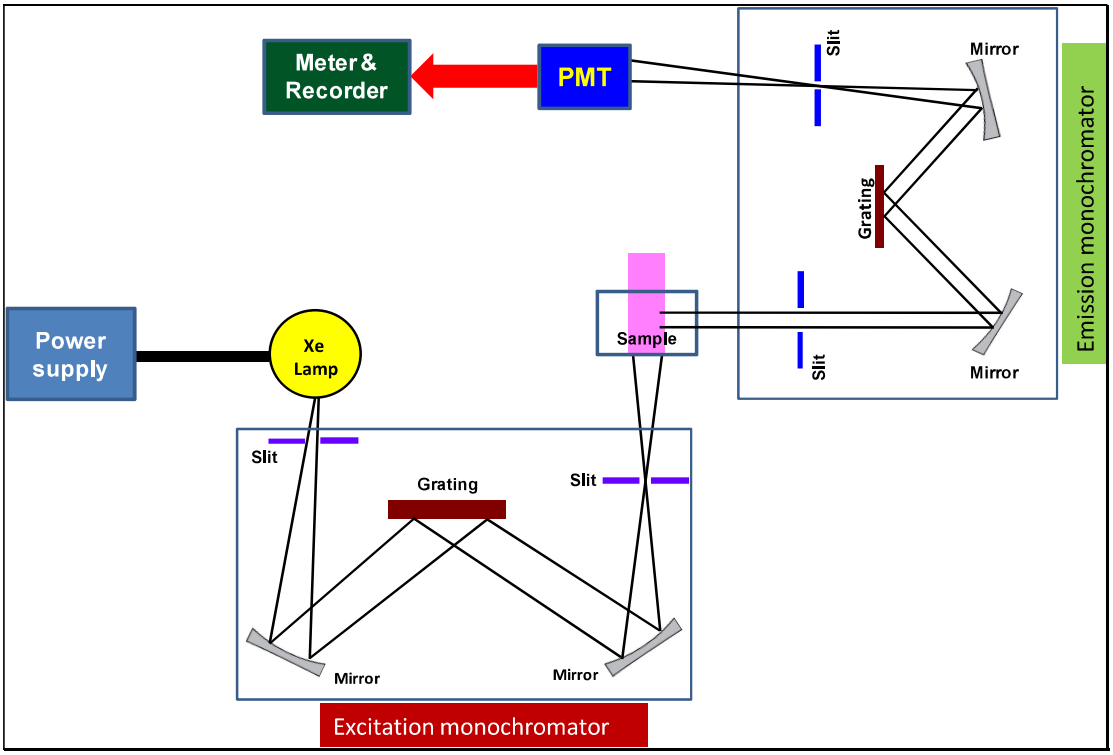

Figure: 2.14. Schematic presentation of a spectrofluorometer.

2.4.3. Fluorescence quantum yield measurement

As discussed in Chapter-1, fluorescence quantum yield (φ_{fl}) of a fluorophore is defined by the following equation,[107]

$$\varphi_{fl} = \frac{\text{Number of photons emitted}}{\text{Number of the photons absorbed}} \tag{2.3}$$

As the exact number of the photons absorbed or emitted by the sample is difficult to obtain, the quantum yield of a fluorophore is calculated using a comparative method [ref] in which the emission of the sample at a particular excitation wavelength is compared with a standard of known quantum yield (φ_{std}), whose absorption spectra matches quite well with the unknown sample. Thus, (φ_{fl}) can be obtained by using the following equation,[200]

$$\varphi_{fl} = \varphi_{std} \, x \left(\frac{Grad_{fl}}{Grad_{std}} \right) x \left(\frac{\eta_{fl}^2}{\eta_{std}^2} \right) \tag{2.4}$$

where, φ_{fl} = Quantum yield of the fluorophore, φ_{std} = Quantum yield of the standard, $Grad_{fl}$ and $Grad_{std}$ are the gradient or slope from the plot of integrated fluorescence intensity vs absorbance of the fluorophore, η_{fl} and η_{std} are the respective refractive indices of the solvents used for the solution of the fluorophore and the standard.

2.4.4. Excited-state lifetime measurement

Measurement of excited state lifetime is a useful methodology to get insights of different photochemical and photophysical processes taking place in the excited state of a fluorophore. The dynamics and kinetics of the deactivation of excited fluorophores via radiative and non-radiative pathways can be quantitatively calculated using the value of the excited state lifetime. On using ultra-short excitation pulse, the fluorophore molecules are promoted to excited state with an instantaneous population of n_0. Since, the decay of an excited molecule is a random phenomenon; the de-excitation of the excited fluorophore molecules should follow the same probability for a given time window following the

excitation pulse. Thus, the decay of the excited molecules follows the first order kinetics and can be expressed as following equation,[107]

$$\frac{dn}{dt} = -(k_r + k_{nr})n(t) \tag{2.5}$$

$$n(t) = n_0 \exp(-t/\tau) \tag{2.6}$$

where, n_0 *and* $n(t)$ are the number of the excited molecules at time 0 and t following the excitation pulse, k_r and k_{nr} are the respective radiative and non-radiative decay rate constants and $\tau = (k_r+k_{nr})^{-1}$, called the excited state lifetime. In the actual experiments, it is generally very difficult to calculate the number of the excited molecules; however, at any point of time, the intensity of the emitted light by the fluorophoric system is directly proportional to the number of the excited molecules present at that time. Hence, to get a practical useful rate equation for molecules; the number of excited molecules is replaced by the time dependent intensity and the rate equation is thereby modified as,

$$I(t) = I_0 \exp(-t/\tau) \tag{2.7}$$

where, I_0 *and* $I(t)$ are the intensity at time 0 and t respectively and τ is the fluorescence lifetime, which is explicitly expressed as,

$$\tau = \frac{1}{k_r + k_{nr}} \tag{2.8}$$

To be mentioned that τ is expressed by eqn. (2.8) is actually the statistical average of the times spent by the ensemble of the excited fluorophores. Since the emission is a statistical phenomenon, any isolated excited molecule can emit a photon at any time following its excitation and the time-dependent probability of its emission is in effect represented by the fluorescence intensity decay of the ensemble of the excited molecules.

For a fluorophore having lifetime in the picosecond to nanosecond range, the most widely used technique to record fluorescence intensity decay is the time-correlated single

photon counting (TCSPC) technique. In all of our present studies, we have used a TCSPC set up from Horiba Jobin Yvon IBH, U.K (model data hub station) to record fluorescence decay traces of the samples. In the majority of the present studies, a 445 nm pulsed diode laser (pulse width 120 ps, pulse repetition rate 1 MHz) was used as the excitation light source whereas in some of the specific cases, e.g. with crystal violet dye as the fluorophore; the used excitation source was a 594 nm nano LED (pulse width ~800 ps, pulse repetition rate 1 MHz). The fluorescence decays were in general recorded at the respective emission maxima of the dye and/or the dye-host complexes. Emission was detected using a micro channel plate photomultiplier tube (MCPPMT) based detection module (IBH, U.K), attached with a peltier cooling system. The detector covered a quite large spectral range (~300 nm to 800 nm) of response. A light scatterer (suspension of TiO_2 powder in water) was used to record the instrument response function (IRF) for the present TCSPC setup. The full-width at half-maximum (FWHM) of a typical IRF was found to be about 120 ps on using 445 nm diode laser and about 800 ps on using 594 nm nano LED. Fluorescence decays were always recorded at magic angle condition. The data analyzing software version DAS-6 from IBH was used for the re-convolution analysis of the observed decays, following suitable exponential function to obtain best fits for the decays. The goodness of the fits and consequently the mono or multi-exponential natures of the decays were judged based on the reduced chi-square (χ^2) values and the distribution of the weighted residuals among the data channels. For a good fit, the χ^2 value was close to unity and the weighted residuals were distributed randomly around zero line among the data channels. In the cases where the decay traces follow a multi-exponential function as given by the following form,[107, 201]

$$I(t) = \Sigma a_i \exp(-t/\tau_i) \tag{2.9}$$

The mean fluorescence lifetime $<\tau>$ of the chromophoric system was calculated according to the following equation,

$$< \tau >= \sum A_i \tau_i \text{ , where } A_i = \alpha_i \tau_i / \sum \alpha_i \tau_i \qquad (2.10)$$

Block diagram of a typical TCSPC set up is shown in Fig. 2.15.

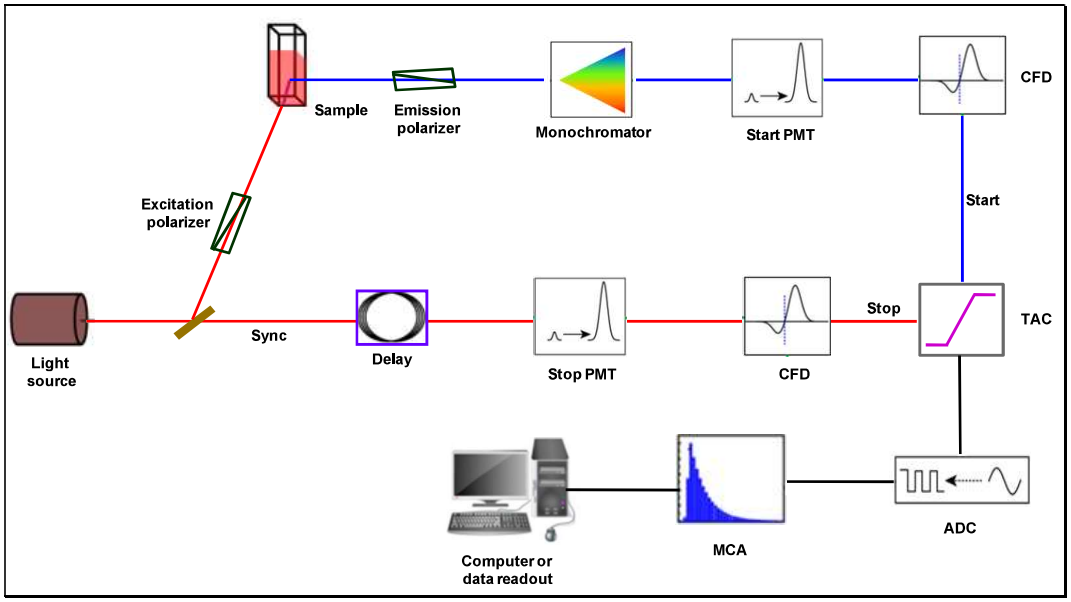

Figure: 2.15. Schematic presentation of a TCSPC setup.

2.4.5. Fluorescence anisotropy measurements

The photoselective excitation of the fluorophore molecules by polarized light is the basis of fluorescence anisotropy measurements. In an isotropic/homogeneous solution, all the fluorophore molecules and accordingly their electronic transition dipoles are randomly oriented. To be mentioned that within its molecular framework each fluorophore has a fixed absorption and emission transition dipoles, oriented in definite directions with respect to the molecular axis and there is a defined angular separation (β) between the absorption and the emission dipoles. During absorption process, the photons which have electric vectors aligned parallel to the absorption transition dipole of the fluorophore molecules are preferentially absorbed by the fluorophore molecules. Therefore, upon excitation with plane polarized light, one selectively excites those fluorophore molecules that have their absorption transition dipoles oriented parallel or nearly parallel to the electric vector of the excitation light beam. If θ is the angle between the transition dipole of the molecule and the electric field vector of the

light, the probability of absorption of a photon by the molecule becomes proportional to cosθ. Hence, absorption is maximum when $\theta=0^0$ and no absorption when $\theta=90^0$.

During emission also, the probability of emission of a photon with its electric field parallel to the emission transition dipole of the excited molecule is the maximum and with the electric field perpendicular to the emission transition dipole is zero. Accordingly, the emission arises from an ensemble of polarized excited molecules, created by a plane polarized excitation light is anisotropic in nature. In a dilute solution, where the fluorophore molecules are significantly away from each other, depolarization of the excited molecules via energy transfer is negligible and thus the decay of the initially created fluorescence anisotropy can take place mainly through the rotational relaxation of the excited molecules. The rate of the rotational diffusion of the excited fluorophore molecules thus, effectively determines the time-dependent decrease of the fluorescence anisotropy, represented by the observed fluorescence anisotropy decay. Since, the diffusive motion is strongly dependent on the size and shape of the fluorophore molecules, the viscosity and/or rigidity of the surrounding environment and the temperature of the solution, the fluorescence anisotropy decay is also accordingly dependent on these parameters. The measurement of fluorescence anisotropy of a fluorophore in a supramolecular host-guest system is a very effective tool to get an idea about the formed host-guest complexes. Complexation between the fluorophore and the host increases the effective hydrodynamic volume of the fluorophore significantly which in turn slows down the depolarization process quite substantially. Hence, rotational relaxation time (τ_r) of the fluorophore, as measured in terms of the fluorescence anisotropy decay time constant, increases significantly as compared to that of the free molecules.

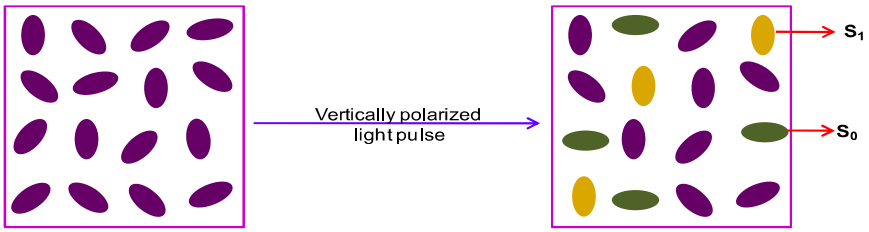

Figure: 2.16. Generation of anisotropy from an isotropic solution of a fluorophore by polarized light excitation.

Both steady-state and time-resolved fluorescence spectrometers can be used to measure anisotropy. In steady-state measurement, the fluorophore is excited with a continuous beam of plane polarized light, and the intensity of emission is recorded with both parallel and perpendicular polarization of the emitted light with respect to the vertically polarized excitation light. A steady-state situation is achieved by the sample almost instantaneously when the sample is exposed to the continuous beam of light. On the other hand, in the time-resolved measurement, the sample is excited with a vertically polarized pulsed excitation light source and two fluorescence decays are collected with emission polarization parallel ($I_{\parallel}$) and perpendicular ($I_{\perp}$) to that of the excitation polarization. Figure 2.17 gives the schematic of a typical fluorescence anisotropy measurement set up. In this set up, a vertically polarized light is used for the sample excitation. The electric vector of the excitation light is oriented parallel to the vertical direction or z-axis and the emission is measured through a polarizer suitably oriented with respect to the excitation polarizer. The emission intensity obtained at the parallel position of the emission polarizer with respect to the excitation polarizer, is denoted by $I_{\parallel}$. Similarly $I_{\perp}$ is the emission intensity obtained at the perpendicular position of the emission polarizer with respect to the excitation polarizer. As the response of the monochromator and photodetector is different for the light with parallel and the perpendicular polarization, a correction factor, known as G–factor, is generally applied especially for the perpendicular component, to rectify the polarization bias of the overall detection set up. G-factor is not a

constant for all measurements but changes with monitoring emission wavelength of the measurement. Mathematically the steady-state anisotropy can be expressed as,[107]

$$< r >= \frac{I_{II} - GI_{\perp}}{I_{II} + 2GI_{\perp}} \tag{2.11}$$

where, the correction factor G, is obtained independently by keeping the excitation polarizer horizontal and measuring emission intensities with emission polarizer vertical (I_{HV}) and horizontal (I_{HH}) respectively, whereby, G-factor is estimated as $G = I_{HV}/I_{HH}$. It is worth mentioning that anisotropy is a dimensionless quantity as the difference in intensity ($I_{\parallel} - GI_{\perp}$) is normalized with respect to the total intensity ($I_{\parallel} + 2GI_{\perp}$) of the sample. Similar to the steady-state anisotropy, time-resolved fluorescence anisotropy is expressed as,

$$r(t) = \frac{I_{II} - GI_{\perp}}{I_{II} + 2GI_{\perp}} \tag{2.12}$$

Here, G-factor is estimated similarly to steady-state measurements, keeping the excitation polarization horizontal and integrating the decays $I_{HV}(t)$ and $I_{HH}(t)$ such that,

$$G = \frac{\int I_{HV}(t)dt}{\int I_{HH}(t)dt} \tag{2.13}$$

The steady-state fluorescence anisotropy is simply an average of the time-resolved anisotropy, weighted by the intensity decay of the sample. Thus, the relationship between steady-state and time-resolved fluorescence anisotropy can be expressed as,

$$< r >= \frac{\int_0^{\infty} r(t)I(t)dt}{\int_0^{\infty} I(t)dt} \tag{2.14}$$

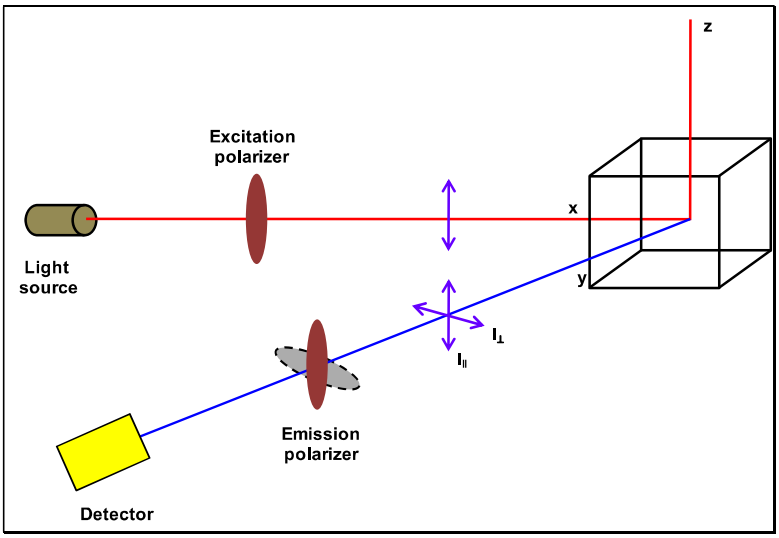

Figure: 2.17. Schematic presentation of fluorescence anisotropy measurement.

Similar to the overall fluorescence decay following ultra-short excitation, the anisotropy decay also follows a first order kinetics and can be expressed simply by the following equation (2.15),

$$r(t) = r_0 \exp(-t/\tau) \qquad (2.15)$$

where, r_0 = the initial anisotropy i.e. the anisotropy created immediately after the irradiation with a δ-excitation pulse. Substitution of I(t) and r(t) from the equations 2.9 and 2.14 and performing integration we get,

$$< r >= r_0 \left(\frac{\tau_r}{\tau_r + \tau_f} \right) \qquad (2.16)$$

The above equation is valid only in the cases of the single exponential decays of the fluorescence intensity [I(t)] or anisotropy [r(t)]. In many real systems, however, the intensity and anisotropy decays cannot be accounted by using the single exponential function. Hence, in many such cases the intensity and/or anisotropy decays are analyzed conveniently by using either bi- or tri-exponential functions. In host-guest complexation, a fluorophore can be present either in free state or in the bound form with the host. In these cases, the analysis of the anisotropy decay is often done following bi-exponential fitting to get information about

the extent of host-guest interaction and also to understand about the surrounding environment of the fluorophore on its binding with the host molecules. The bi-exponential decay of fluorescence intensity can be expressed as,[107]

$$I(t) = a_1 \exp(-t/\tau_{f1}) + a_2 \exp(-t/\tau_{f2}) \quad (2.17)$$

where, τ_{f1} and τ_{f2} are the two components of lifetimes of the fluorophore, representing two different conformers, structures, or environment of fluorophore and a_1 and a_2 are their respective pre-exponential factors. Similarly, the bi-exponential anisotropy decay can be expressed as,

$$r(t) = r_0[b_1 \exp(-t/\tau_{r1}) + b_2 \exp(-t/\tau_{r2})] \quad (2.18)$$

where, b_1 and b_2 are the anisotropy contribution originated from the fluorophores present in two different conformations, structures, or environment with the respective relaxation times τ_{r1} and τ_{r2}. The intensity and anisotropy decays with more than two exponentials can be expressed as,

$$I(t) = \Sigma a_i \exp(-t/\tau_{fi}) \quad (2.19)$$

$$r(t) = r_0[\Sigma b_i \exp(-t/\tau_{ri})] \quad (2.20)$$

The interpretation of the decay parameters from these types of multi-exponent decays is very difficult and requires a number of pre-assumption and intuitions. Hence, in such cases, to get better understanding of the surroundings of the fluorophores under investigations, we need to rely on results from other complementary techniques.

2.4.6. Application of NMR spectroscopy in host-guest study

To get the qualitative as well as quantitative idea about the chemical structure of the organic compounds and complex reaction mechanisms in chemistry, biochemistry, pharmacology, etc. nuclear magnetic resonance (NMR) spectroscopy is an essential technique.

Nuclear magnetic imaging (MRI) is a form of the NMR technique that has proven to be very powerful tool in modern days' medical science to get precise information about the body parts under observation.

In NMR study, a radiofrequency wave is absorbed by the nuclei of a chemical system that are having permanent nuclear magnetic moment and this absorption occurs in the presence of an appropriate applied external magnetic field. The basic criterion of an atomic nucleus to respond in NMR study is that the nucleus should posses a nonzero nuclear spin angular quantum number (I), which is related to the spin angular momentum (m) by the following relation,[202]

$$m = \sqrt{I(I+1)}\hbar \tag{2.21}$$

According to the quantum mechanics, there are (*2I+1*) quantized components of the spin angular momentum along the z axis and can be represented as,

$$m_z = m_I\hbar \text{ where, } m_I = I, (I-1), \ldots\ldots\ldots\ldots, -I. \tag{2.22}$$

The spin quantum number I can be zero, integer or half-integer and only those nuclei having I > 0, can have non-zero spin angular momentum. The nuclei with odd number of protons or neutrons or both can have non- spin angular momentum. However, those nuclei having even number of protons and neutrons posses spin angular momentum = 0. The most common nuclei which are diagonized in NMR spectroscopy are: ^{1}H (I = 1/2), ^{13}C (I = 1/2), ^{14}N (I = 1), ^{31}P (I = 1/2), ^{19}F (I = 1/2), ^{23}Na (I = 3/2), ^{35}Cl (I = 3/2), etc.

The presence of a non-zero spin of the positively charged nucleus gives rise to a magnetic moment for the nucleus, denoted as μ. Similar to the spin angular momentum, μ can also posses (*2I+1*) quantized component along an arbitrary z axis and can be expressed as,

$$\mu_z = \gamma_I m_z = \hbar\gamma_I m_I \text{ and } m_I = I, (I-1), \ldots\ldots\ldots\ldots, -I. \tag{2.23}$$

where, γ_I is a constant which is known as the gyromagnetic ratio. The estimation of γ_I is not possible theoretically, however, it is possible to be determined experimentally. In other way

the μ_z can be expressed in terms of the nuclear g-factor and the nuclear magneton which can be obtained theoretically. Thus,

$$\mu_z = g_I \mu_N m_I \tag{2.24}$$

where,

$$\mu_N = \frac{e\hbar}{2m_p} \tag{2.25}$$

m_p is the mass of proton and e is the electronic charge and the value of μ_N is 5.051 x 10^{-27} JT^{-1}. Hence, from the above equation it is obvious that gyromagnetic ratio is related to g_I and μ_N by the following equation.

$$\gamma = \frac{g_I \mu_N}{\hbar} \tag{2.26}$$

In the presence of the applied external magnetic field (H) along z, the interaction of the (2I+1) number of the different components of μ will be different and hence, these components experience different interaction energies from each other which can in general be expressed as,

$$E_{m_I} = -m_z H = -g_I \mu_N m_I H \tag{2.27}$$

In the proton NMR study, the value of m_I can be either +1/2 or −1/2 and hence the corresponding interaction energies for the proton nucleus under the applied magnetic field H will be,

$$E_{1/2} = -\frac{1}{2} g_I \mu_N H \tag{2.28}$$

$$E_{-1/2} = \frac{1}{2} g_I \mu_N H \tag{2.29}$$

Thus, there is a difference or splitting of the two energy states of a proton which is given as,

$$\Delta E = g_I \mu_N H \tag{2.30}$$

It is evident from the eqn. 2.30 that the splitting of the two energy states increases as we increase the strength of the applied magnetic field H. With such a splitting of energy states,

the nuclei can now absorb a radiofrequency for which frequency exactly matches with the energy difference between the upper and lower energy state of the nucleus, i.e. when a resonance condition is achieved, which is the basic principle of nuclear magnetic resonance (NMR) spectroscopy.

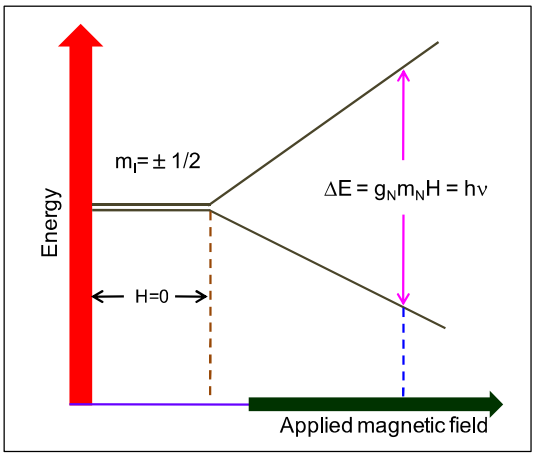

Figure: 2.18. Energy splitting of the two nuclear states in presence of applied external magnetic field.

From the discussion so far, apparently, it may seem that all the proton nuclei under the external magnetic field will have the same resonance frequency. However, in real systems, this is not the case. Actually, in the presence of the applied magnetic field, the electrons around the nucleus give rise to small additional magnetic field which usually acts opposite to the applied magnetic field. The magnitude of this induced magnetic field by the surrounding electrons depends on the distribution of the electrons in the molecular orbitals around the NMR active nucleus and hence, the same nucleus (here proton) under the influence of the different chemical environment will absorb different frequency of the electromagnetic radiation. This effect of the induced local magnetic field on the nucleus under observation is commonly referred as shielding and de-shielding effects. If the nucleus is shielded i.e. if the density of electrons surrounding the nucleus is high, the nucleus experiences a relatively reduced external magnetic field and the frequency of the radiowave required to resonate will be less. This phenomenon is known as upfield shift. The reverse phenomenon occurs where

the density of electrons surrounding the nucleus is less and the phenomenon is called the downfield shift.

Generally, in NMR spectroscopy, to make the measurement independent of the applied magnetic field, the resonance frequencies are expressed in terms of a relative quantity, called chemical shift (δ), which is defined as,

$$\delta = \frac{\nu - \nu_0}{\nu_0} \text{ x } 10^6 \text{ ppm} \qquad (2.31)$$

where, ν and ν_0 are the resonance frequency of the nucleus under observation and the standard nucleus respectively, under the same applied field.

In proton NMR, tetramethylsilane [TMS, $Si(CH_3)_4$] which has 12 equivalent protons is used as the NMR standard or reference. As the protons in TMS are highly shielded, the value of ν_0 is very low (highly upfielded) and by definition the δ value is zero. By convention, NMR spectra are plotted with increasing δ value from right to left. Thus, from the values of δ it is possible to predict the surrounding chemical environment of a particular proton which in turn provides valuable information regarding the structure of the compound.

In supramolecular host-guest chemistry, NMR spectroscopy provides very useful information about the mode of the complexation process. The binding between host and guest significantly alters the electronic environment around the protons of the host and guest molecules under study and hence the NMR signals before complexation and after complexation differ from each other to a considerable extent. This is the basis of NMR spectroscopy used in the host-guest study.[17, 20, 203-208] NMR spectroscopy is used to elucidate the stoichiometry of the host-guest complex, the binding site of the guest molecule, the preferential orientation of the guest molecule included in the host cavity, the binding or relocation of guest from one host to the other, effect of structural alteration of host or guest on their host-guest binding and so on.[17, 20, 203-208] Generally, in host-guest complexation study, the

changes in the proton NMR signals of guest molecule are considered to simplify the observation while the changes in the proton NMR signals of the host makes the interpretation quite difficult as the number of the proton nucleus present in the host molecule is quite high as compared to the guest molecule. When a part of the guest molecule undergoes inclusion into the guest cavity, the protons belonging to that part usually display upfield in NMR signals due to the shielding effect imparted by the host cavity. Similarly, downfield shift is usually observed for the protons belonging to the part of the guest molecule that remains outside the host cavity but placed quite near to the host cavity portals, due to the electron withdrawing effect of the host terminals. Factors like electrostatic or ion-dipole interaction, H-bonding, π-π stacking also contribute to the observed shifts in the NMR signals.[20, 209-211] Thus, by observing the changes in the NMR signals, useful information on the supramolecular host-guest complexation can be obtained very convincingly. Although in all our host-guest studies we relied mainly on the photophysical changes of the chromophoric guest molecules, in number of cases we also carried out ^{1}H and/or ^{13}C NMR study to unambiguously understand the mode of binding with host-guest complexes formed.

CHAPTER - 3

INTERACTION OF A TRIARYL METHANE DYE WITH CUCURBIT[7]URIL AND BOVINE SERUM ALBUMIN: A PERSPECTIVE OF COOPERATIVE VERSUS COMPETITIVE BINDINGS

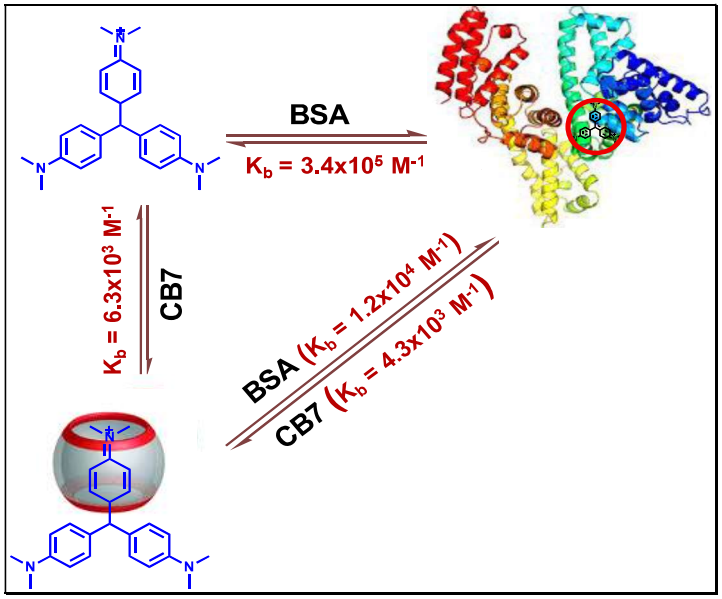

3.1. Introduction

Molecular assembly formation through non-covalent interactions involving ion-dipole, dipole-dipole, H-bonding, π-π stacking, hydrophobic and other weak forces is the backbone of the vast subject area designated as the supramolecular chemistry.[1-4, 6, 7, 9, 11, 23, 66, 68, 69] Jean-Marie Lehn defined,[1] supramolecular chemistry as the subject that extends beyond the chemistry of the molecules as such. The role of supramolecular chemistry is quite crucial in determining structural motifs and their activity in various biological systems as well as in many artificially produced molecular assemblies.[8, 13-15, 21, 212, 213] In supramolecular chemistry the physicochemical properties of the guest molecules can be modulated quite extensively for their improved applications by noncovalent interaction with suitable macrocyclic host

molecules.[30, 33, 82, 140, 214-216] Along with modulation in photochemical properties of the guest molecules, supramolecular complexation also often leads to the improvement of the conformational selectivity, thermal stability, water solubility, de-aggregation, desorption from surface adhesions, and so on.[29, 48, 51, 82, 141, 205, 217-219] In the literature, modulations in the photophysical properties, e.g. in fluorescence intensity, quantum yields of fluorescence, excited state lifetimes, vibration/rotational relaxation rates, etc., of various chromophoric dyes (guests) on their binding with macrocyclic molecular cavities (hosts) have been investigated very extensively, exploring the usefulness of such modulations in different field of science.[14, 29, 30, 32-37, 41, 44, 46, 47, 56-59, 61, 63, 80, 82, 86, 95, 96, 125, 175] In addition to photophysical properties, for chromophoric molecules having prototropic properties, there are also substantial changes in their acid-base characteristics through host-guest interactions, causing their pK_a values to shift largely either upward or downward, which are often useful in stabilizing dyes/drugs in their proactive forms and also in controlling their binding/release mechanisms between macrocyclic hosts used as carriers and biological/bio-macromolecular systems considered as targets.[17, 32, 57, 114, 220-223]

In the supramolecular host-guest studies, the cyclodextrin (CD), calix[n]arene (CXn) and cucurbit[n]uril (CBn) families of the macrocyclics have been extensively used to understand the modulations in the photophysical and acid-base properties of various chromophoric guest molecules.[20, 27, 29, 30, 32-36, 38, 40, 43-51, 56, 58, 61, 63, 80, 82, 95, 124, 125, 162, 168, 175, 224] Among various macrocyclic hosts, the CBn families of the macrocycles have attracted enormous research interests in the literature during about last two decades, due to their number of favorable characteristics in regard to host-guest interactions.[14, 28-36, 48, 49, 56, 57, 59, 61, 80, 83, 86, 124, 159, 162, 164, 167] In CBn family, CB7 is realized to be the most useful host in supramolecular chemistry. CB7 has quite a rigid macrocyclic structure (*cf.* Scheme 3.1) comprising of moderate cavity dimensions and it has reasonably good water solubility (3-4

mM in un-buffered water).[82, 141, 159, 165, 214, 225] As already discussed in Chapter 2, CB7 can undergo quite efficient host-guest inclusion complex formation with most organic dyes/drugs involving non-covalent hydrophobic, ion-dipole, dipole-dipole and H-bonding interactions.[10, 14, 20, 27-32, 34-36, 48-51, 56-58, 60-62, 83, 87, 88, 162-165, 168, 215, 216] The binding interactions are often quite strong when the guest molecules are cationic in charge or have substantial charge transfer character. Additionally, CB7 has been realized to show reasonably low toxicity and display quite good compatibility with biological systems suitable for various applications.[10, 14, 20, 27-32, 34-36, 48-51, 56-58, 60-62, 83, 87, 88, 162-165, 168, 215, 216]

Proteins are the most essential ingredients in living organisms.[184, 186-191, 197, 226-230] Different proteins can bind specific analytes quite selectively in biological systems due to their unique primary, secondary and tertiary structures. For example, hemoglobin and myoglobine can selectively bind and transport oxygen to the cells in the body through blood plasma. On the other hand, serum albumins are the important transport proteins present in the blood plasma that help in transporting essential analytes/drugs from one place to another inside the body. It helps in maintaining the water balance between the tissues. The detailed discussion on the structural, chemical, biological and binding properties of bovine serum albumin (BSA; *cf.* Scheme 3.1B) has already been discussed in Chapter-2. It is well documented in literature that interaction of serum albumin with various analytes leads to modulation in fluorescence characteristics of the bound species. Among the many other analytes, crystal violet is one such molecule that shows an enormous enhancement in its fluorescence properties upon binding with host cavities.

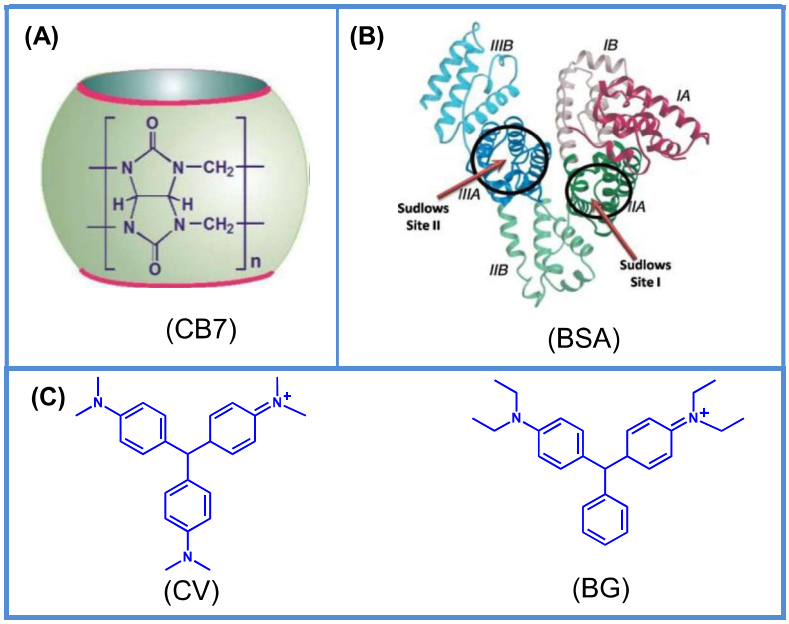

Scheme: 3.1. (A) Schematic presentation of the macrocyclic CB7 host cavity. **(B)** The ribbon representation of the heart shaped structure of a BSA molecule. Different sub-domains in the BSA structure and its two Sudlow's sites (conventional dye/drug binding pockets) are marked for quick visualization. **(C)** Chemical structures of the two triaryl methane dyes, crystal violet (CV) and brilliant green (BG), as considered for comparison in the present study with respect to their cooperative and/or competitive interactions with CB7 and BSA hosts.

Crystal violet (CV; *cf.* Scheme 3.1C) is a homologue of triaryl methane dyes. It possesses a highly flexible structure and hence from the excited electronic state its energy relaxes very fast through non-radiative decay channels, making the dye highly non-fluorescent in nature.[134, 135, 137, 138, 142, 143, 231, 232] By formation of inclusion complex with macrocyclic hosts or biomolecules, CV shows substantial enhancement in fluorescence intensity owing to the decrease in structural flexibility of the dye inside the host cavity.[82, 133, 137, 141, 233] Along with many uses, as discussed in Chapter-2, CV is useful as a chromophoric system for staining various bio-organisms.[133, 134, 137, 233]

Few years back, Bhashikuttan et al.[217] reported that a triaryl methane dye, brilliant green (BG), undergoes a strong cooperative interaction, simultaneously binding to both CB7 cavity and BSA binding pocket, causing an exceptionally large fluorescence enhancement in a cumulative manner compared to what observed for the BG-CB7 and BG-BSA binary systems independently. For a quick comparison, the chemical structure of the dye BG is also shown in

Scheme 1C along with that of the dye CV. Inspired by this unusual cooperative effect reported for BG-CB7-BSA ternary system,[217] we were curious to understand if such cooperative binding is specific only for BG dye or it is a general phenomenon for the triaryl methane dyes. Hence, in the present study, we have investigated the interaction of CV, with CB7 and BSA independently and also with the simultaneous presence of both CB7 and BSA in aqueous solution of CV. Interestingly, the outcomes of the present study are distinctly different, indicating the most commonly encountered competitive interactions of both CB7 and BSA hosts towards the CV dye in the CV-CB7-BSA ternary system, than the earlier observed cooperative interaction as reported for the BG-CB7-BSA system.[217] The detailed study carried out on the CV-CB7-BSA system is systematically presented in this chapter along with the comparison of the results with those reported for BG-CB7-BSA system, to understand the possible reason for the completely contrasting interaction patterns of the two analogous and structurally very similar triaryl methane dyes.

3.2. Materials and Methods

Crystal violet (CV) sample was purchased from SRL, India, and was purified further by solvent extraction method whereby the aqueous solution of CV was extracted with ether to remove small amount of non-polar impurities from the solution and subsequently drying the aqueous phase at ~80^{o}C in a rotavapor to obtain solid CV in pure form. BSA sample (pH 6-7 fraction, purity > 98%) was obtained from SRL, India, and used without further purification. CB7 sample was synthesized in-house following reported procedure.[160] ^{1}H NMR and ^{13}C NMR spectra were used to characterize the synthesized CB7. Further, the content of CB7, in the synthesized sample with acid and water of crystallization, was checked using cobaltocenium cation complexation study.[169] All the aqueous solutions during the experiments were prepared by using nanopure water from a Millipore Elix 3/A10 water purification system (conductivity less than 0.1 μS cm^{-1}). The studies involving BSA were carried out in 10 mM

PBS buffer at pH 7.4. To avoid any dye aggregation and inner filter effect, all the photochemical measurements were done using very low dye concentration (~1.5 μM).

Ground state absorption studies were carried out using a Thermo-Scientific UV-vis spectrophotometer in an optical quartz cell of 10 mm path length. The Steady-state (SS) fluorescence measurements were carried out in a Horiba fluoromax-4 spectrofluorimeter using a 1 cm x 1 cm quartz cuvette. The absorbance changes with the added hosts were found to be comparatively less at 565 nm and hence, in steady state measurements the dye solutions were excited at 565 nm to minimize the effect of absorbance towards observed fluorescence changes. Single Photon Counting (TCSPC) spectrometer obtained from Horiba Jobin Yvon IBH, U.K was used for the time-resolved (TR) fluorescence measurements. A pulsed LED of 594 nm (pulse width ~800 ps; repetition rate 1 MHz) was used as the excitation source and the fluorescence decays were recorded at the emission maximum of the dye (~630 nm) using a microchannel plate photomultiplier tube (MCPPMT) based detection module (IBH, U.K.). Aqueous suspension of TiO_2 powder was used as light scatterer to record the instrument response function (IRF). The full-width at half-maximum of a typical IRF was about 800 ps. Observed decays were in general analyzed as a sum of exponentials (eqn. 2.9, Chapter 2).[107, 201] All the measurements in the present study were carried out at ambient temperature, i.e. at 25±1°C.

3.3. RESULTS AND DISCUSSION

3.3.1. Ground State Absorption and Steady-State Fluorescence Studies on the Interaction of CV Independently with CB7 and BSA Hosts

In aqueous solution CV (1.45 μM) shows a broad absorption band in the 450 to 660 nm regions with peak position at about 590 nm and a significantly strong shoulder band at around 537 nm.[133-135, 137, 142, 143, 231-233] The changes in the absorption spectra for the aqueous solution of CV (1.45 μM) with the increasing concentration of CB7 host are shown in Figure

3.1A. For the initial additions of up to ~21 μM of CB7, the absorption spectra of CV undergo a small blue shift (~3 nm) along with a small decrease in the peak absorbance. Following these initial changes, however, on further increasing the CB7 concentration (up to about 0.76 mM), the absorption spectra of the dye show an intriguing reversal in the changes, experiencing a red shift of ~3 nm in the peak position along with a significant increase in the peak absorbance. On the other hand, at the 537nm shoulder band, the absorbance shows a continuous decrease throughout the CB7 additions, especially at the blue edge of the band (*cf.* Inset of Figure 3.1A), making the spectra to become gradually more shaper with the increase in CB7 concentration. From these observations, it can be suggested that there are apparently two kinds of interactions for CV with the CB7 host, one indicated to be happening preferentially at the lower CB7 concentrations, while the second is indicatively taking over as the dominant interaction as the host concentration is made reasonably higher.

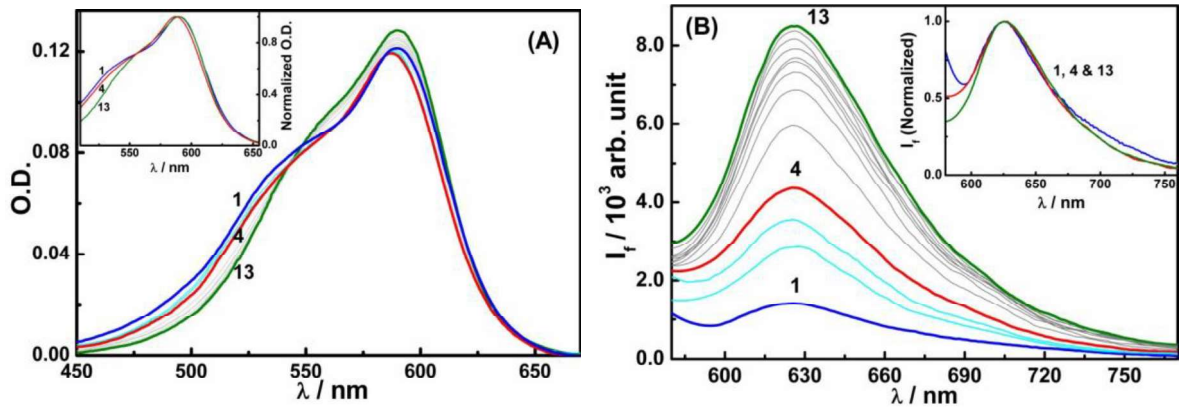

Figure: 3.1. **(A)** Absorption spectra and **(B)** steady-state emission spectra (λ_{ex} = 565 nm) of CV (1.45 μM) with the increasing CB7 concentration; 1) Blue: CV only, 4) Red: CV with 21 μM CB7, and 13) Green: CV with 0.76 mM CB7. **Inset of (A):** Absorption spectra 1, 4 and 13, plotted after peak normalization, to understand the spectral changes occur at the lower and higher CB7 concentrations. **Inset of (B):** Fluorescence spectra 1, 4 and 13, plotted after peak normalization, indicating that there is no observable shift in the peak position.

As discussed in the Chapter-2, the ground state CV molecules in solution adopt two conformational structures.[134, 135, 137, 142, 143, 231, 232] One conformer of CV is unambiguously established to be the planer symmetric propeller structure (all the three aryl substituents of central sp^2 carbon are rotated in the same sense; D_3 point group) through X-ray

crystallographic studies.[142, 231] The three-dimensional arrangements in the other conformations are still quite controversial. While some studies suggest it as a pyramidal symmetric propeller structure (*C3* point group) supported by dye-solvent hydrogen bonding interaction at the central carbon atom, other studies suggest it as a planer asymmetric propeller structure (one of the aryl substituents of central sp^2 carbon is rotated in opposite sense than the other two substituents; *C2* point group). It is understood that the planar symmetric propeller conformation of CV is the energetically most stable structure in the ground state and accordingly it dominates in the solution over the other structures.[231] It is also realized that the symmetric propeller structure of CV (D_3 point group) has a sharper absorption spectrum with relatively stronger peak at around 590 nm and relatively weaker shoulder band at around the 537 nm shoulder band as compared to the energetically less stable conformer of CV (either *C2* or *C3* point group).[231]

From the observed results in Fig. 3.1A, we feel that there is the exo-complex formation at the lower CB7 concentrations, whereby the cationic CV dye gets electrostatically bound at the highly polarizable portals of the CB7 host involving ion-dipole interaction, and in this case the bound dye apparently prefers to adopt a pyramidal conformation than the planer symmetric conformation. The process of exo-complex dominates at the lower CB7 concentrations since the formation of the exo-complex can take place at either of the CB7 portals, whereas the inclusion complex formation is not substantial due to less availability of the CB7 host.

At the higher CB7 concentrations, there is a larger availability of the CB7 host and the interaction is suggestively switches from the exo-complex to the formation of the inclusion complex, as supported by the better stability of the inclusion complexes than the exo-complexes. In the inclusion complex, we feel that the planer symmetric conform of the dye will be encapsulated more preferentially into the CB7 cavity than the other conform of the dye

due to the steric reasons, and accordingly the absorption spectra of the dye is expected to become more intense, sharper and relatively red shifted at the higher CB7 concentrations,[231] as observed experimentally. Apparently, there is a significant conformational preference for the CV dye for its inclusion into the CB7 cavity, which is suggested quite convincingly from the absorption results.

The changes in the steady-state (SS) fluorescence spectra of CV (1.45 μM) in aqueous solution with the increasing CB7 concentration are shown in Fig. 3.1B. As mentioned before, free CV is extremely weak in fluorescence due its high molecular flexibility.[134, 135, 137, 142, 143, 231, 232] Thus, in the absence of CB7, CV shows very weak emission (quantum yield ~10^{-5})[134] in the 580 to 780 nm region, with a peak at around 626 nm. With gradual addition of CB7, the fluorescence intensity of CV systematically increases, up to about 6 folds, without any observable shift in the peak position (*cf.* Inset of Figure 3.1B). Observed results indicate a reasonably strong interaction of the dye with the CB7 host. To be noted that unlike in absorption studies, no contrasting reversal is observed in the fluorescence properties of the dye as the CB7 concentration is gradually increased in the solution. These observations apparently indicate that the CV-CB7 inclusion complex formation is mainly responsible for the observed fluorescence enhancement in the present system and the role of exo-complex which is indicated in the absorption study, is negligible here in the fluorescence results. This is expected because the flexibility of CV would not be restricted that substantially in the exo-complex, as the dye is quite loosely bound to the CB7 portals.[47, 82, 141, 216] On increasing the CB7 concentration, the flexibility of CV becomes largely reduced, as the binding interaction systematically switches from exo to inclusion complexes causing the fluorescence intensity of the dye to enhance significantly, as observed experimentally.

Figure 3.2A shows the changes in the absorption spectra of CV (1.45 μM) in aqueous solution with the gradual addition of BSA (up to about 18 μM). As indicated from the figure

3.1A, till about 3.36 μM BSA concentrations, there is a small decrease in absorbance which is accompanied with a small red shift (~2 nm) in the peak absorption. However, with further increase in BSA concentration (from ~3.6 μM to ~18 μM), the peak absorbance increases quite substantially along with an additional red shift in the peak position by ~3 nm. The blue edge of the 537 nm shoulder band of the absorption spectra, however, gradually decreases for the entire concentration range of BSA used (*cf.* Inset of Figure 3.2A). Accordingly, similar to the CV-CB7 system, for the CV-BSA system also the final absorption spectrum becomes much sharper than that of the free dye. It is clearly indicated from the absorption studies that similar to the CV-CB7 system, in the CV-BSA system also there are two distinct types of dye-host interactions, one is preferred at the lower BSA concentrations and the other supersedes the previous as the BSA concentrations is reasonably increased in the solution.

Figure 3.2B shows the changes in the SS fluorescence spectra for CV (1.45 μM) with the increasing BSA concentrations. While the fluorescence intensity for CV in the absence of BSA is expectedly weak,[133-135, 137, 142, 143, 232, 233] it undergoes a massive enhancement (up to about 100 folds) with the addition of BSA in the solution. Evidently, the much higher enhancement in emission intensity for the CV-BSA system than in the CV-CB7 system (up to about 6 folds) clearly suggests that the binding of CV is much stronger with the BSA binding pocket than with the CB7 cavity. The fact that unlike in absorption studies, there is no contrasting modulations in the fluorescence characteristics at the lower and higher BSA concentrations apparently suggests that the CV-BSA inclusion complex is the main contributor for the observed enhancement in the emission intensity.

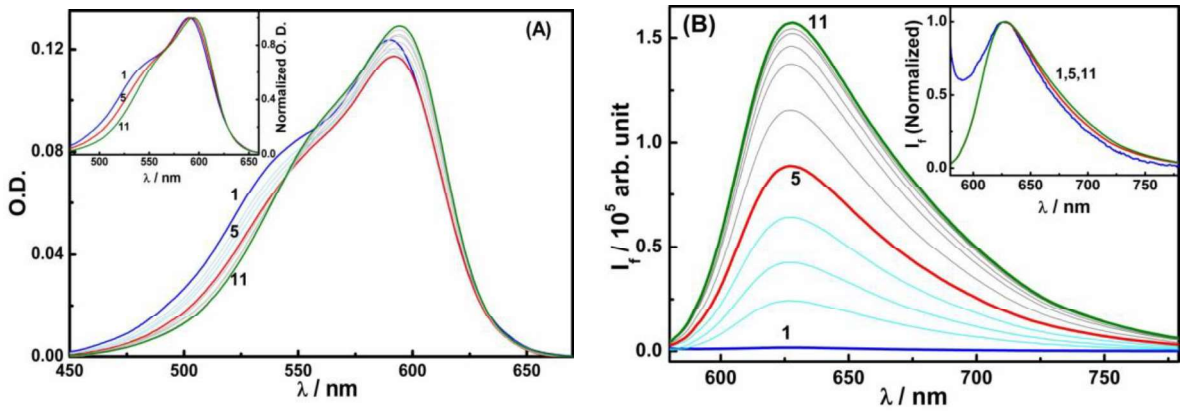

Figure: 3.2. (A) Absorption spectra and **(B)** fluorescence spectra (λ_{ex} = 565 nm) of CV (1.45 μM) with the increasing BSA concentration; 1) Blue: CV only, 5) Red: CV with 3.36 μM BSA, and 11) Green: CV with 15.4 μM BSA. **Inset of (A):** Absorption spectra 1, 5 and 11 are plotted after peak normalization to understand the comparative spectral changes under lower and higher BSA concentrations. **Inset of (B):** Fluorescence spectra 1, 5 and 11, plotted after peak normalization, indicating that there is no observable shift in the peak position.

The isoelectric point (pI) of BSA is ~4.7[184-186] and hence, at the experimental pH of 7.4 the BSA would possess significant negative charge on its surfaces.[184-186] Thus, we feel that at lower BSA concentrations, the cationic CV dye preferentially binds to the BSA surface to form exo-complex quite in a nonspecific manner as the entrapment of CV molecules into the BSA binding pockets would not be substantial in this situation due to less availability of the host molecules. The flexibility of the surface-bound CV molecules is not reduced to any significant extent as the dye molecules are substantially exposed to the bulk aqueous phase and thus, they cannot contribute any appreciably to the fluorescence enhancement. However, at the higher BSA concentrations, due to availability of a large number of the host molecules, the CV-BSA exo-complex preferentially switches to the more stable CV-BSA inclusion complexes, where the flexibility of the entrapped dye molecules is greatly reduced, causing a huge enhancement (~100 times) in the fluorescence intensity (*cf.* Figure 3.2B).

Among the two major dye binding sites, BSA has a relatively more capacious and flexible binding site at sub-domain IIA (Sudlow's Site I) as compared to its other binding site at sub-domain IIIA (Sudlow's Site II). Site I of BSA is known to bind the dye molecules involving mainly the hydrophobic interactions. Considering the molecular flexibility,

bulkiness and three reasonably hydrophobic aryl substituents attached to the central (sp^2) carbon atom, we feel that the binding/entrapping of CV would occur more preferentially into the capacious and flexible Sudlow's Site I of the BSA molecule than to the less capacious and less flexible Sudlow's Site II, though small extent of non-specific binding of CV into the latter site cannot be disregarded completely. From the consideration of the results from the absorption studies (*cf.* Inset of Figure 3.2A) we found that on binding to BSA the absorption spectrum of the dye eventually becomes much sharper than that of the free dye, suggesting the preferential binding of the symmetric propeller structure of the dye with BSA than that of the asymmetric/pyramidal structure.[134, 135, 137, 142, 143, 232] In short, there is apparently a significant extent of conformational preference for the CV dye for its binding to the BSA pocket.

3.3.2. Binding Constants for CV-CB7 and CV-BSA Binary Systems Following Fluorescence Titration Method

Estimation of the binding constant for supramolecular host-guest complexes can be determined by various techniques among which the fluorescence titration method is the most convenient and well adopted method, where analysis of the relative changes in the emission intensity of the guest dye as a function of the increasing host concentration provides the required binding constant. The fluorescence titration method has been employed in the present study to estimate the binding constant (K_b) values for the CV-CB7 and CV-BSA inclusion complexes. Fig. 3.3A and 3.3B, show the observed binding isotherms for the two respective systems. The analysis of the isotherms was done following 1:1 stoichiometric complexation model where fluorescence intensity changes (ΔI_f) are correlated with the host concentrations using the following relation,[27, 28, 30, 35, 49, 56, 59, 63, 80, 82, 96, 125, 141, 234]

$$\Delta I_f = \Delta I_f^{\infty}\left(1-\frac{\{K_b[Dye]_0 - K_b[H]_0 - 1\} + \sqrt{(K_b[Dye]_0 + K_b[H]_0 + 1)^2 - 4(K_b)^2[Dye]_0[H]_0}}{2[Dye]_0 K_b}\right) \quad (3.1)$$

Here, ΔI_f^{∞} = final change in the fluorescence intensity on complete complexation of the dye in the solution, $[Dye]_0$ = total dye concentration used, $[H]_0$ = total host concentration used in the solution at any given point. The estimated K_b values for the CV-CB7 and CV-BSA systems are $6.3x10^3$ M^{-1} and $3.4x10^5$ M^{-1}, respectively.

Since, CV being a cationic dye, it was expected that the inclusion complexes of the dye with the CB7 host will be very strong due to the participation of ion-dipole interaction between the negatively polarized portal of the host and cationic charge of the dye in addition to the usual hydrophobic interaction exerted by the host cavity.[10, 14, 20, 27-36, 48-50, 56, 57, 59, 61, 80-83, 86, 88, 159, 162, 164, 165, 169] But the K_b value of the CV-CB7 system is found to be reasonably low, 6.3×10^3 M^{-1}, compared to many other cationic organic dyes.[59, 80, 82, 88, 114, 141] This is understandably due to the presence of three flexible aryl arms of CV, which make the inclusion of any of its arms into CB7 cavity significantly hindered sterically. But this is not the case for CV binding into BSA binding pocket. For the CV-BSA system, the K_b value is found to be exceptionally high as the whole CV molecule can get entrapped into the BSA binding pocket. The much larger fluorescence enhancement observed for the CV-BSA system nicely corroborates with the estimated high K_b value for the CV-BSA system.

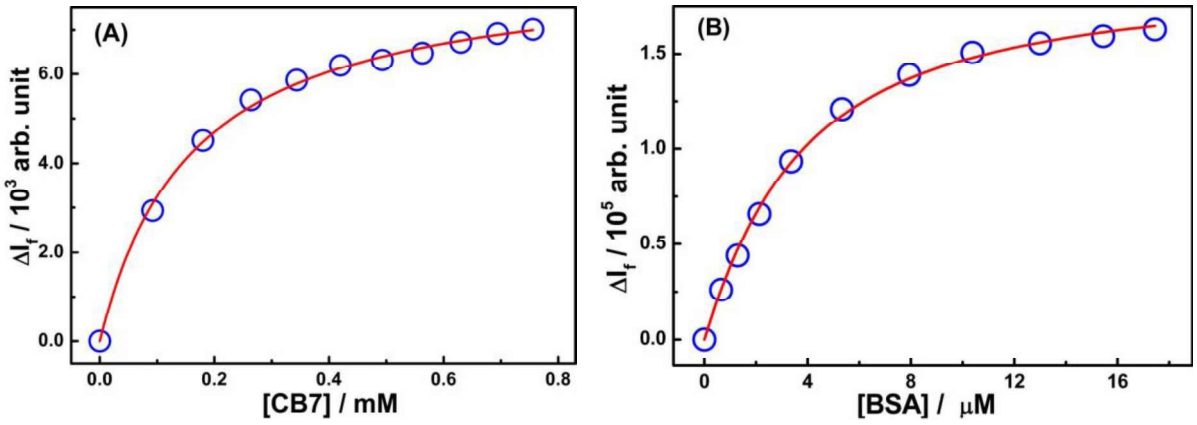

Figure: 3.3. Binding isotherms obtained for **(A)** CV-CB7 and **(B)** CV-BSA systems following fluorescence titration measurements and their nonlinear fittings following eq. 2, considering 1:1 binding model in both the cases. The CV concentrations in both the cases were 1.45 μM.

3.3.3. Job's Plot Studies for the estimation of stoichiometric compositions of Dye-Host complexes

To ascertain the stoichiometry of the formed host-guest complexes in the studied systems, we carried out Job's plot studies following photophysical measurements.[30, 63, 80, 96, 169, 235] Since the fluorescence enhancement is very large for the CV-BSA system, we could convincingly obtain the Job's plot following fluorescence studies, as shown in Fig. 3.4. To be mentioned here that to obtain quite appreciable changes in the fluorescence intensity to construct a reliable Job's plot, the sum of the concentrations of the dye and BSA were deliberately kept reasonably higher (9.2 μM). As indicated from Fig. 3.4, the maximum of the Job's plot for the CV-BSA system appears at a BSA mole fraction of about 0.5, supporting the 1:1 stoichiometery of the CV-BSA complex formed. For the CV-CB7 system, since the change in the fluorescence intensity of CV with the varying CB7 fraction in the solution was not that high, even on keeping the sum of the concentrations of the dye and CB7 host significantly higher, we could not obtain a reliable Job's plot for the CV-CB7 system even with our best efforts. The relatively weaker binding interaction and consequently the smaller changes observed in the fluorescence intensity for the CV-CB7 system do not allow us to construct a reliable Job's plot for the studied system.

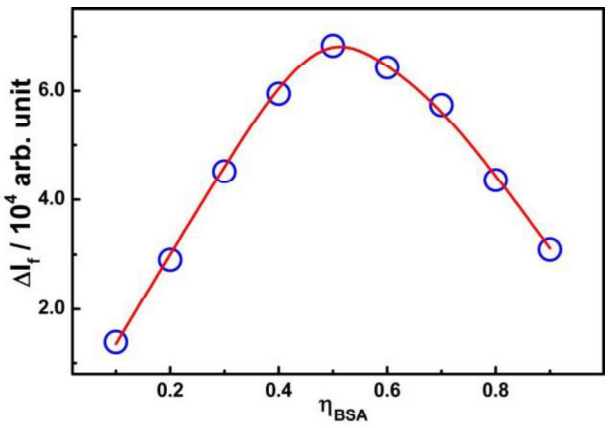

Figure: 3.4. The Job's plot constructed for the CV-BSA system (pH 7.4, 10 mM PBS), obtained through fluorescence intensity changes at 626 nm as a function of BSA mole fraction (η_{BSA}) in the solution, keeping the

sum of the concentrations of the dye and BSA as 9.2 μM. The circles are the experimental data points and the smooth curve is drawn through the data points just for a visual guide. Excitation wavelength was 565 nm.

3.3.4. Scatchard plot analysis for the CV-BSA system

To reveal the number of binding sites in the bio-macromolecular receptors for a studied dye/drug, the Scatchard plot analysis is the well utilized method.[134, 188, 236-239] George Scatchard first introduced this specific analysis method, in which the typical plot is constructed following the relation given as,

$$\frac{\bar{\nu}}{[D]} = nK_b - \bar{\nu}K_b \qquad (3.2)$$

where, $\bar{\nu}$ is the moles of dye/drug bound per mole of the receptor at any experimental condition, [D] is the free dye concentration at equilibrium, n is the maximum number of dye molecules that can bind to a receptor molecule and K_b is the binding constant. Fig. 3.5 shows the Scatchard plot for the CV-BSA system obtained by correlating the fluorescence titration data versus the number of moles of the bound dye. Though the correlation of the data in the obtained Scatchard plot is not very satisfactory, yet the plot apparently indicates the n value close to unity for the CV-BSA system along with a K_b value of about 4.2×10^5 M^{-1}, not very different from the K_b value obtained from the fluorescence titration analysis ($K_b = 3.4 \times 10^5$ M^{-1}; *cf*. Table 3.3). Thus, the present results support the preferential binding of CV to the sub-domain IIA (Sudlow's Site I) of the BSA molecule with a 1:1 stoichiometric composition.

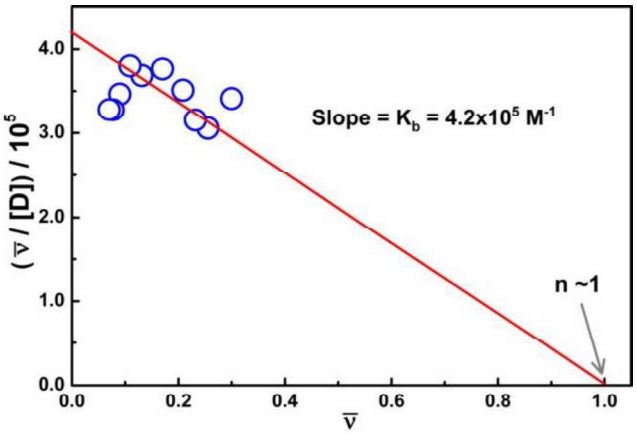

Figure: 3.5. Scatchard plot as obtained for the CV-BSA system using the same fluorescence titration data as shown in Fig. 3.4B. The plot apparently indicates an n value close to unity along with a K_b value of ~$4.2x10^5$ M^{-1}, quite in the same range as obtained from the fluorescence titration analysis (*cf.* Fig. 3.4B)

3.3.5. Time-resolved Fluorescence Studies on the Interaction of CV Independently with CB7 and BSA Hosts

As discussed earlier, due to very flexible molecular structure the fluorescence decay of free CV in solution occurs exceptionally fast, only in the ps time scales.[134, 135, 137, 142, 143, 232] Hence, with the limited time resolution of our present TCSPC setup (FWHM of IRF ~800 ps), the fluorescence decay recorded for free CV (in the absence of any host) was not possible to distinguish from the measured IRF (*cf.* Inset of Figure 3.6A). Although there was a reasonable SS-fluorescence enhancement observed for the CB7 bound CV the increase in fluorescence decay time for the same was not considerable enough to record the decay trace quite confidently rather it was found to be quite indistinguishable from that of the free CV and IRF of the present TCSPC setup (*cf.* Inset of Figure 3.6A). Thus, the observed fluorescence decays for both free CV and CV-CB7 complex could not be analyzed to obtain any reliable decay parameters. On the other hand, binding to BSA largely reduces the structural flexibility of CV complex which makes the observed fluorescence decay for CV-BSA reasonably long as compared to IRF, as shown in Figure 3.6A. The bi-exponential analysis of this decay trace satisfactorily provides the decay parameters which are listed in Table 3.1.

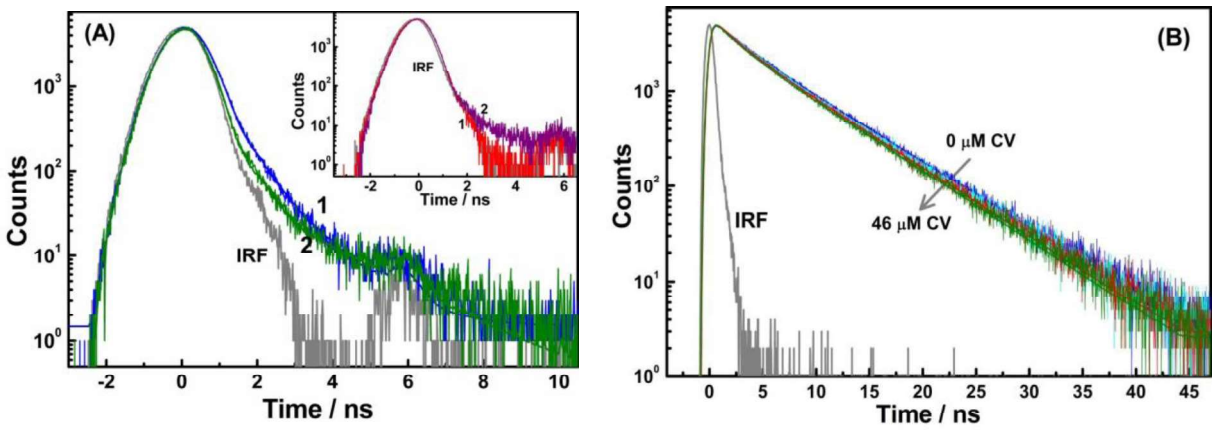

Figure: 3.6. (A) Fluorescence decay traces for (1) CV-BSA (Blue) and (2) CV-BSA-CB7 (Green) systems. Inset: Fluorescence decay curves for (1) CV only (Red) and (2) CV-CB7 system (Violet). λ_{ex} = 594 nm and λ_{em} = 627 nm. Concentrations of the concerned components were: [CV] = 1.5 μM, [BSA] = 23 μM and [CB7] = 1.0 mM. **(B)** Fluorescence decay curves for intrinsic emission of BSA (5 μM) in the presence of 0, 14, 30 and 46 μM CV concentrations; λ_{ex} = 292 nm and λ_{em} = 345 nm.

Table: 3.1. Fluorescence decay parameters for CV-BSA binary system (1.5 μM CV with 23 μM BSA) and CV-BSA-CB7 ternary system (1.5 μM CV with 23 μM BSA and 1 mM CB7). Samples were excited with 594 nm LED source and decays were recorded at 627 nm.

System	a_1 (%)	τ_1 / ns	a_2 (%)	τ_2 / ns	χ^2
CV-BSA	93.7	0.17	6.3	1.1	1.00
CV-BSA-CB7	95.2	0.06	4.8	1.1	1.09

As indicated from Table 3.1, the CV-BSA system shows its fluorescence decay with a major contribution (~93.7%) from a shorter lifetime component of τ_1 ~0.17 ns and a minor contribution (~6.3%) from a substantially longer component of τ_2 ~1.1 ns. As discussed earlier, in a solution, the dye CV exists in two conformational forms, the dominant one with a symmetric propeller structure and the minor one as an asymmetric/pyramidal propeller structure.[134, 135, 137, 142, 143] In addition to the structural flexibility, there is also a significant extent of twisted intramolecular charge transfer (TICT) process taking place in the excited state for both the CV conformers, and this TICT process is more proficient in the symmetric propeller conformer than in the other conformer.[134, 135, 137, 142, 143] As the non-radiative de-excitation channel for the excited dye is accelerated through TICT state formation, we infer that in the CV-BSA system the shorter 0.17 ns component is due to the BSA bound symmetric conformer and the longer 1.1 ns component is due to the BSA bound asymmetric/pyramidal conformer of the CV dye.

As discussed before, due to the large structural flexibility and the presence of three hydrophobic phenyl rings in CV, the dye molecules are expected to be entrapped more preferentially at the Sudlow's Site I (binding pocket IIA; *cf.* Scheme 3.1B) of the BSA host.

Since this binding site of BSA contains a tryptophan residue (Trp-212),[184-187, 197, 240] we expect that binding of CV would lead to some interaction of the bound dye with the Trp-212 residue of BSA, which can suitably be realized by monitoring the intrinsic fluoresce of BSA. In the SS fluorescence measurements, since the absorption band of BSA around 280 nm is strongly overlapped with one of the higher energy absorption band of CV, selective excitation of BSA was not possible and thus, we could not obtain any conclusive information from such a study. However, in the TR fluorescence measurements, it was possible to record convincingly the fluorescence decays for the intrinsic BSA emission at 345 nm, both in the absence and in presence of increasing dye concentration, as are shown in Figure 3.6B. The bi-exponential fittings of the decays were seen to be quite satisfactory and the estimated decay parameters thus obtained are listed in Table 3.2. It is evident from the observed results that there is a small reduction for both the lifetime components, which evidently supports our inference that the dye CV preferentially binds to the Sudlow's Site I of the BSA host (*cf.* Scheme 3.1B, binding pocket IIA).[184-188, 197, 241]

Table: 3.2. Fluorescence decay parameters for 5 μM BSA solution with varying concentration of CV. BSA solution was excited with 292 nm pulsed LED source and decays were monitored at 345 nm.

[CV] / μM	a_1 (%)	τ_1 (ns)	a_2 (%)	τ_2 (ns)	χ^2
0	13.3	2.32	86.7	6.29	1.11
14	11.3	1.84	88.7	6.06	1.14
30	12.4	1.78	87.6	5.98	1.22
46	12.4	1.62	87.6	5.89	1.24

3.3.6. ^{1}H NMR Studies on the Interaction of CV Independently with CB7 and BSA Hosts

To substantiate the results obtained from the photophysical studies, we also carried out ^{1}H NMR measurements for a CV (500 μM) solution in D_2O, both in the absence and in presence of 2.0 mM CB7 and the results are shown in Figure 3.7A and 3.7B, respectively.

There are three sets of signals for equivalent protons marked as H_a, H_b, H_c, respectively, in CV. Upon addition of CB7 to the CV solution, the H_a proton signal apparently undergoes a subtle upfield shift of ~0.04 ppm, but it suffers a significant broadening. This observation intuitively suggests the incorporation of any one of the aryl arm of CV with terminal $-N^+(CH_3)_2$ group into the CB7 cavity to form 1:1 inclusion complex, where the H_a protons are presumably placed quite close to the portal oxygen atoms of CB7 for a possible hydrogen bonding interaction and the positive charge on the $-N^+(CH_3)_2$ group can undergo reasonable ion-dipole interaction with the negatively polarized portal of the CB7 cavity. In the CV-CB7 system, the signal for the H_b protons of CV undergoes exceptionally large broadening in such a fashion that the signal apparently vanishes in the observed NMR spectra. H_c protons in the CV-CB7 system, suffers a large down-filled shift of ~0.746 ppm along with a small broadening of the signal. From these observations, we feel that the H_b protons of CV are deeply buried inside the CB7 cavity while the H_c protons are placed possibly just outside a portal of the encaging CB7 cavity. The observed broadening of the proton (H_a, H_b and H_c) peaks can be explained to dynamic nature of the inclusion complex formation with any one of the three symmetrical aryl groups of the CV in the NMR recording time scale. On the whole, the ^1H NMR results for the CV-CB7 system support the inclusion complex formation for CV with the CB7 host.

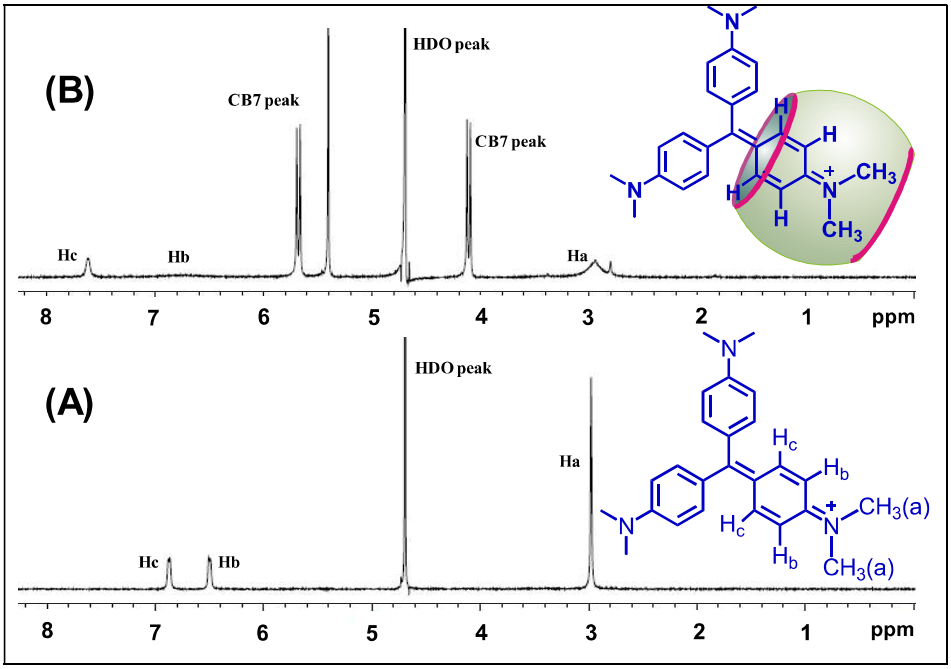

Figure: 3.7. ^{1}H NMR spectra for **(A)** CV (500 μM) only and **(B)** CV (500 μM) in the presence of CB7 (2 mM).

3.3.7. Ground State Absorption and SS Fluorescence Studies on the Simultaneous Interactions of CV Dye with CB7 and BSA Hosts

In this part of the study, the effect of BSA addition to the solution containing the preexisted CV-CB7 inclusion complexes (1.49 μM CV plus 733 μM CB7) have been investigated using absorption and fluorescence measurements. In the starting solution containing 1.49 μM CV and 733 μM CB7, all the dye molecules would almost exclusively bound to the CB7 host as the 1:1 inclusion complexes. With the incremental addition of BSA to the solution containing the preexisted CV-CB7 complexes, there occurs a small but systematic increase in the peak absorbance along with a small bathochromic shift in the peak position (~5 nm), as are shown in Figure 3.8A. The inset of Figure 3.8A shows the peak normalized absorption spectra corresponding to the starting CV-CB7 solution, the final solution obtained after addition of the highest BSA concentration (268 μM), and the final solution obtained earlier for the CV-BSA binary system (spectrum 11 in Figure 3.2A) for their direct comparison. It is evident from this comparison that while the 595 nm absorption peak

region of the spectrum for the CV-CB7-BSA ternary system resembles quite nicely with that of the CV-BSA binary system, the 537 nm shoulder region of the absorption spectrum for the CV-CB7-BSA ternary system, resembles more closely to that of the CV-CB7 binary system. From these observations, it is apparent that as the BSA host is gradually added to the solution of the preexisting CV-CB7 complex, the CV molecules show host selective relocation from the CB7 cavities and are relocated into BSA binding pockets.

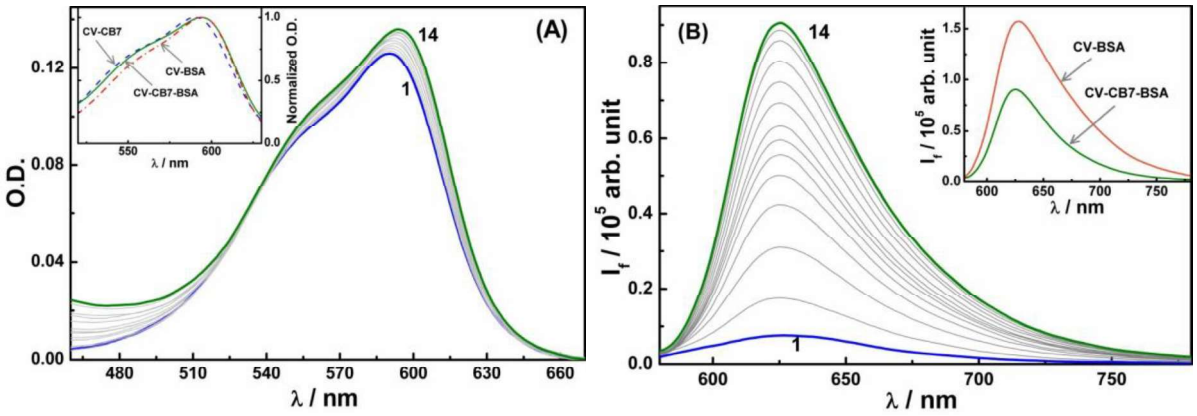

Figure: 3.8. **(A)** Absorption spectra and **(B)** emission spectra of CV(1.49μM)-CB7(733 μM) system with increasing concentration of BSA. 1) Blue: Initial CV-CB7 binary system and 14) Green: Final CV-CB7-BSA ternary system after addition of 268 μM BSA. **Inset of (A):** Comparison of the peak normalized absorption spectra of the final CV-CB7-BSA ternary system with the initial CV-CB7 binary system. Peak normalized absorption spectrum for the CV-BSA binary system is also plotted for a comparison. **Inset of (B):** Comparison of the fluorescence spectra of the final CV-CB7-BSA ternary system with that of the final CV-BSA binary system.

Changes in the fluorescence spectra with the stepwise addition of BSA to the solution of the CV-CB7 complex (1.49 μM CV and 733 μM CB7) are shown in Figure 3.8B. As evident from this figure, there is a gradual increase in the fluorescence intensity with an increase in the BSA concentration in the solution. The overall fluorescence enhancement for the dye in the present CV-CB7-BSA ternary system (compared to the free dye) is estimated to be about 72 times while the initial fluorescence enhancement for the dye in the starting solution with the CV-CB7 complex was about 6 folds (*cf*. figure 3.1B). It is evident that, the overall enhancement in the fluorescence intensity for the CV-CB7-BSA ternary system is significantly lower than that observed earlier for the CV-BSA binary system (i.e. about 100

folds; *cf*. figure 3.2B). In the inset of Figure 7B, the observed fluorescence spectra corresponding to the maximum fluorescence enhancements achieved in the cases of the CV-BSA binary system and the CV-CB7-BSA ternary system are shown for a comparison. Another important point to be noted that the concentration of BSA required to achieve saturation for CV-CB7-BSA ternary system is significantly high (~268 μM) as compared to the CV-BSA binary system (~18 μM). These results suggest that in the ternary system, there is a redistribution of CV between CB7 hosts indicating the competitive binding interaction of the dye with both the hosts as they are present simultaneously. Contrary to this result, for the homologous triaryl methane dye, brilliant green (BG), a cooperative interaction has been reported in the BG-CB7-BSA ternary system, where BG binds simultaneously with both CB7 and BSA hosts, forming the unique BG-CB7-BSA ternary complex, apparently due to entrapment of the whole BG-CB7 binary complex into the BSA binding pocket.[217] BG molecule consists of three aryl arms attached to the central carbon atom, one of which is a simple phenyl group while the other two arms are composed of the *para*-$N(C_2H_5)_2$ substituted phenyl groups.[217] Compared to BG, all the three aryl arms of CV are composed of the *para*-$N(CH_3)_2$ substituted phenyl groups (*cf*. Figure 1). Presumably both the dye CV and BG form 1:1 dye-CB7 inclusion complexes by the incorporation of one of their *para*-NR_2 substituted phenyl groups into the host cavity, proving a better host-guest binding interaction. The estimated K_b values for the 1:1 inclusion complexes for the CV-CB7 and BG-CB7 binary systems, are found to be about $6.3x10^3$ M^{-1} and $1.7x10^4$ M^{-1}, respectively. Relatively higher K_b value for BG-CB7 complex compared to the CV-CB7 complex is understandably due to the combined effect of the higher cationic charge at N atom in the CB7 enclosed $-=N^+(C_2H_5)_2$ group in BG than for the $=N^+(CH_3)_2$ group of CV (essential for better ion-dipole interaction; *cf*. Figure 6B) and the tighter binding of the larger *para*-$N(C_2H_5)_2$ substituted phenyl group of BG with the CB7 cavity compared to the relatively loose binding of the smaller *para*-$N(CH_3)_2$

substituted phenyl group of CV with the CB7 cavity (essential for better Van der Waals' interaction).

In the context of the competitive versus cooperative binding interactions in the presently considered dye-CB7-BSA ternary systems, we felt it necessary to compare not only the K_b values for the CV-CB7 and BG-CB7 inclusion complexes but also those of the CV-BSA and BG-BSA inclusion complexes involved in the respective dye-CB7-BSA ternary systems. To be noted that K_b values of the CV-BSA and BG-BSA inclusion complexes are estimated/reported to be about $3.4\text{x}10^5$ M^{-1} and $3.2\text{x}10^4$ M^{-1}, respectively. The relatively higher K_b value for CV-BSA complex than the BG-BSA complex is apparently due to the better fitting of the relatively smaller *para*-$N(CH_3)_2$ substituted phenyl groups of CV into the BSA binding pocket than the larger *para*-$N(C_2H_5)_2$ substituted phenyl groups of BG. Consequently, comparing all the K_b values of the associated dye-CB7 and dye-BSA inclusion complexes involved in the dye-CB7-BSA ternary systems, it apparently transpired that the comparable K_b values for the BG-CB7 and BG-BSA inclusion complexes perhaps made the situation for the BG-CB7-BSA ternary system quite conducive for the dye to undergo a cooperative binding involving both CB7 and BSA hosts simultaneously giving a more stabilized BG-CB7-BSA ternary complex than the overall stabilization that system could achieve through the formation of the individual BG-CB7 and BG-BSA binary complexes following competitive interaction modes. As the K_b values for the concerned CV-CB7 and CV-BSA binary complexes are largely different ($6.3\text{x}10^3$ M^{-1} and ~$3.4\text{x}10^5$ M^{-1}, respectively), for the CV-CB7-BSA ternary system, it is apparent that the cooperative interaction cannot possibly lead to any better stabilization for the CV-CB7-BSA ternary complex as compared to the overall stabilization of the respective CV-CB7 and CV- BSA binary complexes. Thus, it can be inferred from the obtained results for the CV-CB7-BSA and BG-CB7-BSA ternary systems that only such systems lead to the formation of the ternary complexes through a

cooperative interaction if the concerned K_b values for the respective binary complexes are quite comparable. On the contrary, the competitive supramolecular interactions will possibly dominate over the cooperatively formed ternary complexes if the K_b values for the concerned binary complexes are largely different from each other.

To get more insight of the competitive interactions in the CV-CB7-BSA ternary systems, we also carried out the ground state absorption and SS fluorescence studies in the reverse mode of the measurements, i.e. starting with a solution having the CV-BSA complexes initially (1.43 μM CV plus 30.2 μM BSA) and gradually adding CB7 into this experimental solution to understand the nature of interaction in the CV-BSA-CB7 ternary system. Observed results are shown in Fig.3.9A and 3.9B, respectively. As expected, in the present case, the fluorescence of the CV-BSA solution gradually suffers a quenching as CB7 is sequentially added to the experimental solution. Important point to be noted, that in spite of the substantial quenching, the final fluorescence intensity for the CV-BSA-CB7 ternary system still remains much higher than the total fluorescence enhancement achieved for the CV-CB7 binary system (cf. inset of Fig. 3.9B). It is thus clearly indicated that in the present CV-BSA-CB7 ternary system a good amount of CV still remains bound to the BSA host in the presence of the highest CB7 added, though a part of the CV had certainly been indicated to be released from the BSA pocket and got bound to the CB7 cavity. Therefore, the studies following this reverse strategy also it is clearly indicated that for the present CV-BSA-CB7 ternary system there is a competitive formation of both CV-CB7 and CV-BSA binary complexes, instead of the formation of the CV-CB7-BSA ternary complexes in a cooperative manner as otherwise observed for the BG-CB7-BSA system in the earlier report.[217] As competitive interactions are prevailed in the present ternary system, it is expected that the titration of the solution containing a binary complex initially and adding the second host sequentially would lead to a much lower K_b value than the value estimated for the direct titration of the dye solution by the

second host. Obviously, K_b value estimated in the case of cooperative interactions through titration involving ternary system, would be higher than that estimated for a binary system as reported earlier for the BG-CB7-BSA case.[217] With these perception, we also carried out the fluorescence titration studies involving the CV-CB7-BSA ternary system, following both CV-CB7 solution titrated by BSA and the CV-BSA solution titrated by CB7. The estimated K_b values from these titration studies along with those estimated for the binary systems independently are listed in Table 3. It is very evident that the K_b values are drastically reduced in the titration studies involving the CV-CB7-BSA ternary systems compared to the values estimated for the CV-CB7 and CV-BSA binary systems independently. These results are thus in direct support to the competitive interaction of CV with both CB7 and BSA hosts when both the hosts are simultaneously present in the experimental solution.

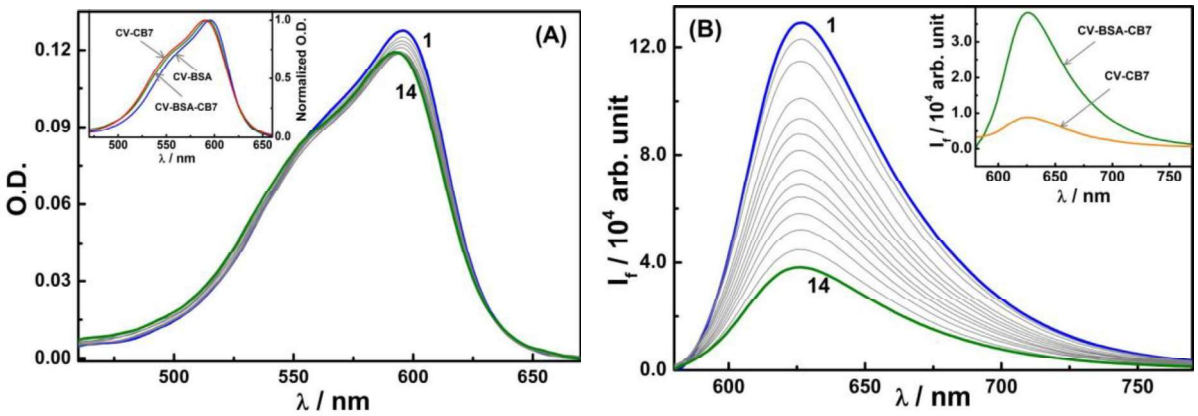

Figure: 3.9. (A) Absorption spectra and (B) SS fluorescence spectra (λ_{ex} = 565 nm) of CV (1.43 µM)-BSA (30.2 µM) system with increasing concentration of CB7. 1) Blue: Initial CV-BSA binary system and 14) Green: Final CV-BSA-CB7 ternary system after addition of 500 µM CB7. Inset of (A): Comparison of the peak normalized absorption spectra of the final CV-BSA-CB7 ternary system with the initial CV-BSA binary system. Peak normalized absorption spectrum for the CV-CB7 binary system is also plotted for a comparison. Inset of (B): Comparison of the fluorescence spectra for the final CV-CB7 and CV-BSA-CB7 system.

Table: 3.3. Binding constant values estimated for different combinations of the fluorescence titration studies involving the CV-CB7-BSA systems.

Mode of Titration	Estimated K_b value / M^{-1}
CV solution titrated with CB7	6.3×10^3

CV solution titrated with BSA	$3.4x10^5$
CV-CB7 solution titrated with BSA	$1.2x\ 10^4$
CV-BSA solution titrated with CB7	$4.3x10^3$

As competitive interactions are indicated to be prevailed in the presently studied CV-CB7-BSA ternary system, it is expected that the titration studies carried out on a solution containing one of the binary complex initially and gradually adding the other host of the concerned ternary system into this experimental solution would always lead to an apparent K_b value which would be much lower than the K_b value estimated independently for the direct titration of the respective dye-host binary system. Contrary to this, for the ternary system that display cooperative binding interactions, the K_b value estimated in the titration studies involving the ternary systems would always be higher than that estimated independently for the direct titration of the respective dye-host binary systems.[217] With these perspectives, we thus carried out the fluorescence titration studies for the CV-CB7-BSA ternary system, following both the initial CV-CB7 complex titrated by BSA and the initial CV-BSA solution titrated by CB7. The estimated K_b values from these titration studies along with those estimated directly for the dye-host binary systems are listed in Table 3. It is very evident that the apparent K_b values obtained from the titration studies involving the CV-CB7-BSA ternary systems are substantially reduced in comparison to the absolute K_b values estimated independently for the CV-CB7 and CV-BSA binary systems. These results are thus in direct support to the competitive binding interaction of the dye CV with both CB7 and BSA hosts, which is distinctly and contrastingly different than the cooperative binding interaction displayed by the homologous dye BG with the same CB7 and BSA hosts.

3.3.8. Time-resolved Fluorescence Studies for CV-CB7-BSA ternary systems

TR fluorescence measurements were carried out with the final solution of the titration study involving the CV-BSA-CB7 ternary system and the fluorescence decay thus obtained is

shown in Figure 3.6A along with that of final CV-BSA binary system for a comparison. Similar to the CV-BSA binary system, analysis of the decay trace of the CV-CB7-BSA ternary system has been done by a bi-exponential function for an acceptable analysis and the decay parameters thus obtained are listed in Table 3.2 for a comparison with those obtained for the CV-BSA binary system discussed before. To be mentioned that for the final solution of the CV-CB7-BSA ternary system where solution of CV-CB7 complex was titrated by BSA (*cf*. Figure 3.8B), the observed fluorescence decays was found to very similar to that of the CV-BSA-CB7 ternary system mentioned above (*cf*. Figure 3.9B).

As indicated from Figure 3.6A and Table 3.1, there occurs a drastic reduction of the shorter τ_1 component from ~0.17 ns to ~0.06 ns in the CV-BSA-CB7 system, which is just below the time resolution (~0.1 ns) of the present TCSPC setup. Interestingly, however, the longer τ_2 component for the studied ternary system remains very similar to that of the CV-BSA complex, i.e. ~1.1 ns, though its contribution reduces to a substantial extent. As discussed before, in the CV-BSA-CB7 ternary system, there is a competitive interaction of CV for both CB7 and BSA hosts. Thus, in the studied CV-BSA-CB7 ternary system, in the presence of the highest CB7 concentration used a large fraction of the initial CV-BSA complexes undergo disintegration and convert to the CV-CB7 complexes. As the fluorescence decay of these newly formed CV-CB7 complexes are faster than the time resolution of the present TCSPC setup, emission from these complexes effectively distorts the initial part of the measured fluorescence decay, causing the τ_1 component of the decay to appear as short as ~0.06 ns (*cf*. Table 3.1), apparently below the time resolution of our TCSPC setup. Compared to this τ_1 value, the τ_2 component, however, remains quite unchanged to ~1.1 ns, because this component basically represents the CV-BSA complexes still remains in the experimental solution. Overall thus, the observed TR fluorescence results for the CV-BSA-CB7 ternary

system clearly supports the competitive binding interaction of CV with both CB7 and BSA hosts when both of hosts are simultaneously present in the experimental solution.

3.4. Conclusion

Interaction of the triaryl methane dye CV with the macrocyclic host CB7 and the biomacromolecular binding target BSA has been investigated both in the dye-host binary systems and also in the dye-CB7-BSA ternary systems following ground state absorption as well as steady-state and time-resolved fluorescence studies. The large structural flexibility and ability to form twisted intramolecular charge transfer state (TICT) in the excited state make the free CV molecules in aqueous solution extremely weak in fluorescence while encapsulation into the host cavity leads to substantial enhancement of fluorescence property due to the structural confinement. While binding of CV into CB7 cavity results in the fluorescence enhancement by about 6 folds, the enhancement is as large as about 100 folds for the BSA bound CV, indicating a very strong binding of CV to the BSA binding pocket. This is in agreement with the larger K_b values estimated for the CV-BSA (K_b ~$3.4x10^5$ M^{-1}) system as compared to the CV-CB7 system (K_b ~$6.3x10^3$ M^{-1}). In both CV-CB7 and CV-BSA binary systems, the dye-host complexation is realized to be fomred through 1:1 stroichiometric inclusion complexation mainly, though at the very low host concentrations an indication of some exo-complex formation is also indicated for both the dye-host systems. Although there is substantial enhancement in fluorescence intensity when BSA added to the CV-CB7 system, the overall enhancement still remains much lower than that observed independently (~100 folds) for the CV-BSA binary system. The apparent K_b value estimated for CV-BSA-CB7 ternary system (K_b ~$1.2x10^4$ M^{-1}) is also found to be significantly lower than that obtained independently for the CV-BSA binary system (~$3.4x10^5$ M^{-1}). Similarly, when CB7 is gradually added to an initial solution containing the CV-BSA complex, the fluorescence intensity is seen to decrease quite substantially but the final intensity still remains much higher

than that observed independently for CV-CB7 binary system. The apparent K_b value estimated in this case (~4.3×10^3 M^{-1}) is again significantly lower than that obtained directly for the CV-CB7 binary system (~6.3×10^3 M^{-1}). All these observations clearly indicate a competitive binding interaction of CV when there is the simultaneous presence of both CB7 and BSA hosts. The competitive interaction observed for the triaryl methane dye CV in the dye-CB7-BSA ternary system is strikingly different than the cooperative binding interaction observed earlier for a homologous triaryl methane dye, BG, in the similar dye-CB7-BSA ternary system.[74] The distinctly different behaviors displayed by the CV-CB7-BSA and BG-CB7-BSA ternary systems may be accounted on the basis of the comparisons of the relative K_b values of the concerned dye-CB7 and dye-BSA binary systems involved in the respective cases. We infer from these comparisons that the situation becomes quite conducive for the cooperative interaction of the dye with the two hosts involved in the studied dye-CB7-BSA ternary system when the K_b values for the respective dye-CB7 and dye-BSA binary systems are quite comparable. However, when these K_b values are largely different, as in the case of CV-CB7-BSA ternary system, the cooperative interaction is not supported in the system rather in this case the competitive interaction of the dye with both the two hosts independently occurs resulting in the formation of both dye-CB7 and dye-BSA binary complexes in the solution. Observed results in the present study intuitively suggest a possibility of suitably selecting a dye-$(host)_1$-$(host)_2$ ternary system for a cooperative or a competitive interaction preferentially, based on the relative K_b values of the concerned dye-$(host)_1$ and dye-$(host)_2$ binary systems. While, cooperative interaction can understandably be utilized to achieve extraordinary photo and thermal stability for the dyes and drugs and also in achieving high sensitivity for the fluorogenic chromophoric dyes, the competitive interaction as observed in the CV-CB7-BSA system can certainly find its usefulness in drug formulations in enhancing

drug stability, drug solubility and so on, and also in realizing controlled drug delivery using macrocyclic host like CB7 as a useful drug nano-carrier.

CHAPTER-4

SUPRAMOLECULAR INTERACTION OF NEAR INFRA-RED FLUORESCENT PROBE LDS-798 WITH A HIGHLY SUBSTITUTED ANIONIC BETA-CYCLODEXTRIN DERIVATIVE

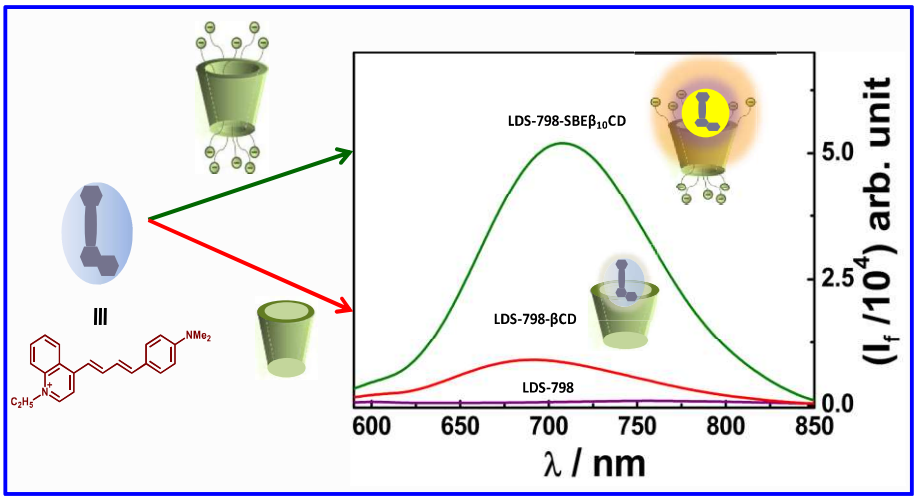

4.1. Introduction

Properties of supramolecular assemblies depend on their structure and the arrangement of the constitutional binding blocks in three dimensional spaces. In supramolecular chemistry, recognition among constituents plays the vital role in determining the three-dimensional structures of various assemblies formed via non-covalent forces of interactions and has direct or indirect influence in governing the features of these materials.[2-4, 6, 7, 9, 11, 12, 21, 23, 25, 66-68, 212, 242-244] The molecular recognitions between structural units are especially very important when the cases are the host-guest type of complexation processes. Better the molecular recognition, stronger is the complexation for the host-guest pair. The best molecular recognition occurs in nature between substrate and enzyme pairs, due to structural specificity towards each other, which leads to very stable host-guest type of supramolecular complexes (K_a in the order of 10^{16}-10^{21} M^{-1}).[5, 90, 91] There are also some cases where binding between a synthesized host and

a guest molecule is found to occur with exceptionally high binding affinity (K_a in the order of 10^{11}-10^{17} M^{-1}).[59, 82, 140, 141, 169, 170, 221] Many different classes of hosts are encountered in supramolecular chemistry among which the cyclodextrins and their derivatives, calixarenes and their derivatives and cucurbiturils are the most popular ones. These hosts can exceptionally modulate the properties of the guest molecules and have marked effects on the chemical and biological activities of the guest molecules, which are being exploited in various fields of science. Formation of stable host-guest pairs makes the guest molecules immune towards any external chemical as well as photochemical or enzymatic attack.[14, 15, 20, 32, 34, 48-51, 162, 230, 245] Depending upon cost effectiveness of the host, it's easy availability, compatibility and binding strength, various host-guest pairs are being explored for wide range of novel applications. These include their uses in supramolecular vesicles, fluorescence sensing, drug formulations, drug delivery, nanotechnology, catalysis, pharmaceuticals, optical sensors, on–off switches, food industry, photodynamic therapy, functional materials, dye stabilization, etc.[7, 8, 10, 14, 20, 25, 26, 30, 31, 33-36, 48-51, 56, 58-61, 80, 82, 83, 124, 168, 213, 215, 243, 246] Isaac et al. in 2005 demonstrated that cucurbit[7]uril (CB7) exhibits very high binding affinity towards guest molecules like adamantane and ferrocene derivatives.[159, 165] For example, CB7-adamantanes (K_a~10^{12}-10^{17} M^{-1}), and CB7-substituted amino ferrocences (K_a ~10^{11}-10^{15} M^{-1}) have registered the tightest binding constants reported till date.[59, 164, 169, 170, 247, 248] Among the other strong host-guest pairs to be cited are the cyclodextrin-adamantane derivatives (K_a~10^5-10^7 M^{-1}) and cyclodextrin-lithocholic acid (K_a~10^5-10^7 M^{-1}) pairs, having significantly large binding constants.[85, 249-252] Among various macrocyclic hosts, cucurbit[n]uril (CBn) and cyclodextrin (CD) class of macrocycles are the most studied hosts due to their bio-compatibility and low toxic effects. In the last few decades, there are an exceptional volume of studies carried out on parent CDs and different CD derivatives due to their ready availability, easy of synthesis, cost effectiveness and easy handling.

Parent CDs are cyclic oligosaccharides consisting of (α-1,4)-linked α-D-glucopyranose units, composing a hydrophilic exterior and a hydrophobic cavity interior to give a truncated cone shaped structure. Due to their reasonable water solubility, low toxicity, bio-compatibility and ready availability; CDs are the most celebrated hosts used for drug formulations.[42, 172, 173, 175, 177] As discussed already in Chapter-2, CDs are used in wide range of applications in different fields of science and amongst them, uses of CDs and their derivatives in pharmaceutical industry are especially notable.[42, 172, 173, 175, 177] In this respect, extensive research works have been carried out to improve the water solubility and binding affinity of βCD cavity while reducing its toxicological effects through suitable chemical modification. It is found that replacements of hydrogen atoms of the hydroxyl groups of parent βCD by sulfobutylether (SBE) groups result in substantial improvement in water solubility and binding strength of sulfobutylether β-cyclodextrin (SBEβCD) hosts as compared to parent βCD. The change of neutral form of the parent βCD to the anionic SBEβCD makes the substituted βCD highly soluble in polar solvent like water. The presence of anionic sulfonate end groups in the substituted βCD makes them to bind strongly with the cationic guests (dyes/drugs), through electrostatic interactions along with the involvement of the convention hydrophobic interactions.[46, 47] Further, the presence of extended sulfobutylether groups provides additional depth of the hydrophobic cavity to entrap the guest molecules more extensively with larger hydrophobic interactions.[46, 47] All these in combination make the substituted anionic SBEβCD derivatives as very effective hosts in supramolecular host-guest studies.

Based on the fact that the sulfobutylether substituted βCD derivatives interact with cationic guest molecules very efficiently and with the expectation that complexation of a styryl dye like LDS-798 with a SBEβCD host would emit strongly in the near IR region, which has added biological and experimental advantages,[253] we found our interest in the present study to explore the interaction of the cationic dye LDS-798 with the SBE_{10}βCD host

(having the average degree of sulfobutylether substitution as 10). Surprisingly, we found that the interaction of LDS-798 with SBE_{10}βCD host is exceptionally stronger as compared to the other CD hosts.

The dye LDS-798, also called styryl-11, falls under the category of hemicyanine dye, having a cationic quinolinium head group attached with the electron donating N,N-dimethyl aniline group via conjugation. Due to large structural flexibility, which is a common feature of the styryl dyes, and the possibility of intramolecular charge transfer from the aniline moiety to the quinolinium head group, especially in the excited state, the dye LDS-798 is highly non-fluorescent (quantum yield ~0.002) in the solvents with high dielectric constants.[117, 155, 254, 255] The dye however, can show a significant increase in its fluorescence properties (increase in fluorescence intensity, lifetime etc.) when the polarity, viscosity, temperature and pH of the surrounding micro environment changes.[117, 155, 158, 254, 255] Accordingly, LDS-798 serves as an excellent probe which has been used for several decades as a sensor to detect and estimate the changes in micro-polarity, pH, and viscosity of the surrounding environment.[96, 117, 155] LDS-798 is also a biologically important dye which is used to measure cell membrane permeability and cell electron potential.[96, 117, 155] Very recently it has been reported that LDS-798 can be used as an efficient fluorescent probe for qualitative and quantitative determination of albumins in complex matrices.[96] The emission in the near-IR region for LDS-798-complex and very strong binding of LDS-798 with SBE_{10}βCD derivative as found in this study, make the present host-guest system an attractive choice to explore in detail its possible applications in supramolecular fields, biological sensing and marker in the near IR region as well as applications as a sensor for pH, temperature, etc.

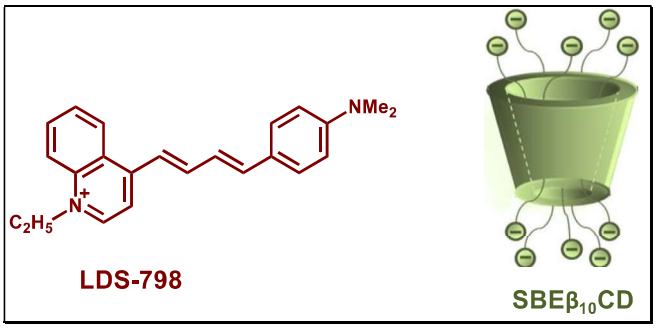

Scheme: 4.1. Schematic presentation of LDS-798 and $SBE_{10}\beta CD$.

4.2. Materials and Methods

Laser grade 1-ethyl-4-(4-(p-dimethylaminophenyl)-1,3-butadienyl)-quinolinum percholate (LDS 798 or styryl 11) was procured from Lambda Physik, and Sulfobutylether β-cyclodextrin ($SBE_{10}\beta CD$; Average degree of substitution ~10; MW: 2717) was obtained from Cyclolab, Hungary and used as received. Lithocholic acid and adamantine hydrochloride were obtained from Sigma-Aldrich and used without any further purification. Concentration of LDS-798 in aqueous medium was determined from its optical density using its molar absorptivity ($\varepsilon \sim 14400\ M^{-1}\ cm^{-1}$ at 500 nm).[96, 155] Nanopure water from a Millipore Elix 3/A10 water purification system (conductivity less than $0.1\mu S\ cm^{-1}$) was used for preparations of all solutions. In order to maintain the mono cationic form of the prototropic dye LDS-798,[96, 117] all the experiments were carried out at pH ~7. The adjustment of the pH was done using dilute solutions of NaOH and HCl. All the measurements were carried out at ambient temperature, i.e. at 25±1°C.

Ground state absorption studies were carried out using a Thermo-Scientific UV-vis spectrophotometer in an optical quartz cell of 10 mm path length. Steady-state (SS) fluorescence measurements were carried out using a Horiba fluoromax-4 spectrofluorimeter in 10 mm x 10 mm quartz cuvette. During the fluorescence studies the dye samples were excited at 500 nm, which is the peak position of the absorption spectra for the aqueous LDS-798. Time-resolved (TR) fluorescence measurements were carried out using a Time Correlated

Single Photon Counting (TCSPC) spectrometer, obtained from Horiba Jobin Yvon IBH, U.K. In TCSPC measurements, a 445 nm pulsed diode laser (pulse width 120 ps and repetition rate 1 MHz) was used as the excitation source and the fluorescence decays were recorded at the emission maximum of the dye-$SBE_{10}\beta CD$ complex (~715 nm) using a micro channel plate photomultiplier tube (MCP-PMT) based detection module (IBH, U.K.). Other details have already been discussed in Chapter-2

4.3. Results and Discussion

4.3.1. Steady-State Fluorescence Studies

LDS-798 is highly non-fluorescent in nature due to its large structural flexibility and its ability to undergo twisted intramolecular charge (TICT) state formation in the first excited state through twisting of its aniline moiety out of the molecular plane.[256, 257] While large structural flexibility of LDS-798 helps to channelize the excited state energy via non-radiative process though molecular vibration and rotation, formation of its TICT state provides an additional non-radiative route for the dye molecules to dissipate their excited state energy causing enhanced non-radiative process. It has been acknowledged in the recent literatures that the fluorescent intensity/quantum yield of LDS-798 decreases drastically with the increasing solvent polarity and decreasing solvent viscosity.[96, 117, 155, 254, 255] The solvents of low viscosity are not capable enough to restrict the molecular flexibility of the dye molecules whereas in the solvents of high polarity or dielectric constant, the propensity of formation of the polar TICT state in the first excited state gets amplified, rendering the LDS-798 molecules to become almost non-fluorescent in nature.

Aqueous solution of LDS-798 shows a very weak and broad emission band in the range of 640-850 nm, with maximum around at 765 nm. However, incremental addition of $SBE_{10}\beta CD$ to the aqueous solution of 3.5 μM LDS-798 at pH 7 results substantial changes in fluorescence properties, as are shown in Fig. 4.1A. The enormous blue shift (~ 51 nm i.e.,

from 765 nm to 714 nm) in emission maxima along with phenomenal increase in emission intensity (~70 folds), which find saturation at ~26 μM of SBE_{10}βCD, indicates a very strong interaction of LDS-798 with the applied host SBE_{10}βCD.

The increase in emission intensity of LDS-798 on interaction with SBE_{10}βCD can be understood as a combination of three effects. Firstly, the structural confinement imposed by the host cavity to the encapsulated dye molecule largely reduces the molecular flexibility of the dye, which contributes to reduce the non-radiative decay through molecular vibrations and rotations. Secondly, the rigid cavity of the host largely minimizes the ability of the excited dye molecules to undergo TICT state formation and hence inhibits the additional non-radiative decay of the excited dye molecules through TICT mediated pathway. Finally, reduced micro-polarity of the guest cavity as compared to bulk aqueous medium additionally helps in improving the fluorescence yield of the dye by decreasing the propensity of polar TICT state formation for the excited dye molecules. Thus, the drastic reduction in the rate of the non-radiative process imposed by the host cavity through the above mentioned effects makes the dye molecules to acquire a substantial improvement in their fluorescence properties in the presence of the host molecules. The large blue-shift observed in the emission spectra is understandably due to the result of strong solvatochromic behavior of LDS-798 and indicates that LDS-798 experiences a significantly reduced micro-polarity when the dye is transferred from the bulk aqueous phase to the cavity of the SBE_{10}βCD host.

It is evident from the Fig. 4.1A that the changes in fluorescence properties of the dye attain a kind of saturation at a very low SBE_{10}βCD concentration (~26 μM). This clearly suggests a very strong interaction between cationic LDS-798 and anionic SBE_{10}βCD host, understandably due to strong electrostatic interaction in addition to the conventional hydrophobic interaction exerted by the host cavity. The extended hydrophobic cavity due to the presence of the sulfobutylether groups at the CD portals provides an additional strength

towards the hydrophobic binding of the dye to the host cavity. Thus, a collective effect of strong electrostatic interaction along with the enhanced hydrophobic interaction rendered by the extended $SBE_{10}\beta CD$ cavity helps the dye molecules to bind very strongly with the host cavities.

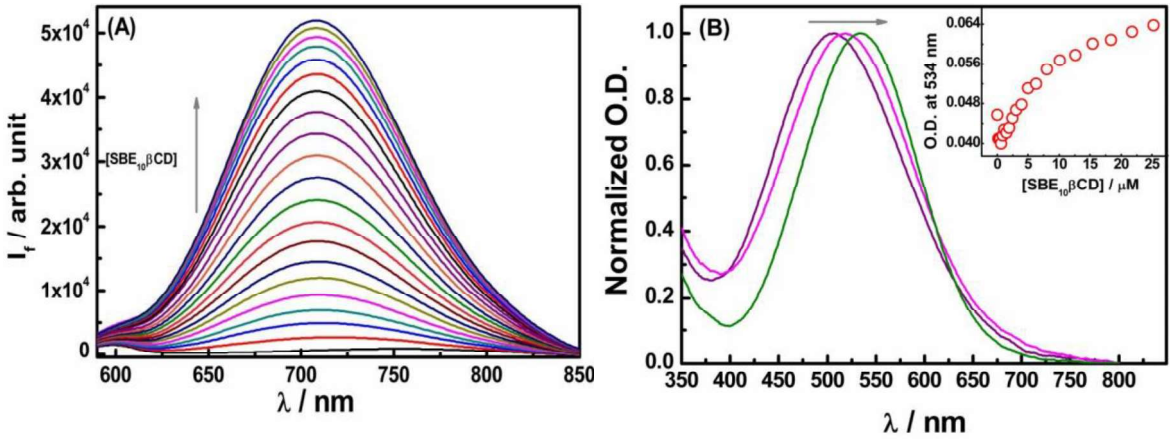

Figure: 4.1. (A) Fluorescence spectra of 3.5 μM LDS-798 with the increasing $SBE_{10}\beta CD$ concentration from 0 μM to 26 μM [λ_{ex} = 500 nm, pH ~7.0] and **(B)** Normalized absorption spectra of 3.5 μM LDS-798 with the $SBE_{10}\beta CD$ concentration 1) 0 μM, 2) 0.6 μM and 3) 26 μM. Inset of (B) shows the OD changes at 534 nm as a function of the $SBE_{10}\beta CD$ concentration.

4.3.2. Ground-State Absorption Studies

Aqueous solution of LDS-798 shows a broad absorption band with peak at ~500 nm. Gradual addition of $SBE_{10}\beta CD$ host to 3.5 μM LDS-798 aqueous solution, maintained at pH 7, shows a notable change in the absorption profile of the dye, as shown in Fig. 4.1B. Initially with the increasing host concentration up to 0.6 μM, there occurs a significant decrease in peak absorption along with a notable bathochromic shift in the absorption spectra. Beyond 0.6 μM $SBE_{10}\beta CD$, however, with the gradual increase in the host concentration, there occurs a much large bathochromic shift along with a substantial increase in the peak absorption of the dye. The reversal in the absorption changes for LDS-798 dye upon gradual addition of the host indicates the involvement of two different kinds of interactions, which are modulated significantly with the changing host concentration in the solution.

Initial dip in absorbance for LDS-798 in the presence of up to ~0.6 μM SBE_{10}βCD is possibly due to host assisted aggregation of the dye, is a phenomenon encountered very often involving oppositely charged hosts and guests, on keeping host concentration relatively low.[47, 95, 97, 235] In the present study, LDS-798 is a cationic dye; whereas SBE_{10}βCD is a highly negatively charged macrocyclic host due to the presence of 10 sulfobutylether groups at the portals. Thus, multiple dye molecules are expected to be electrostatically attracted by the negatively charged portals of the hosts, leading to dye aggregation, assisted by substantial charge neutralization effect and this is expected to be dominated at the lower host concentrations where availability of host is limited enough to support enough inclusion complex formation. Suggested dye aggregation at lower host concentration is further supported by the effect of added NaCl salt in the solution whereby the absorbance of the dye decreases drastically more along with a substantial red shift for the absorption peak position (discussed in section 4.3.8)

For the LDS-798-SBE_{10}βCD system, as the concentration of the host is made beyond 0.6 μM; the initially formed dye aggregates gradually suffer disintegration and undergo inclusion complex formation with the host molecules, stabilized by strong electrostatic interaction in addition to the enhanced hydrophobic interaction of the host cavity. Accordingly there occurs a significant increase in the absorbance for the dye along with an additional red shift of the peak position. The red shift of the absorption maxima of LDS-798 in the presence of the host indicates that the dye molecules are transferred from polar bulk water to the less polar or non-polar hydrophobic cavity of the host. The red shift in the absorption maxima with the reduction in the polarity of the solvent is a quite common feature for the charged push-pull polyenes (for example LDS-798), which has been theoretically substantiated by the work of Hynes and co-workers.[258]

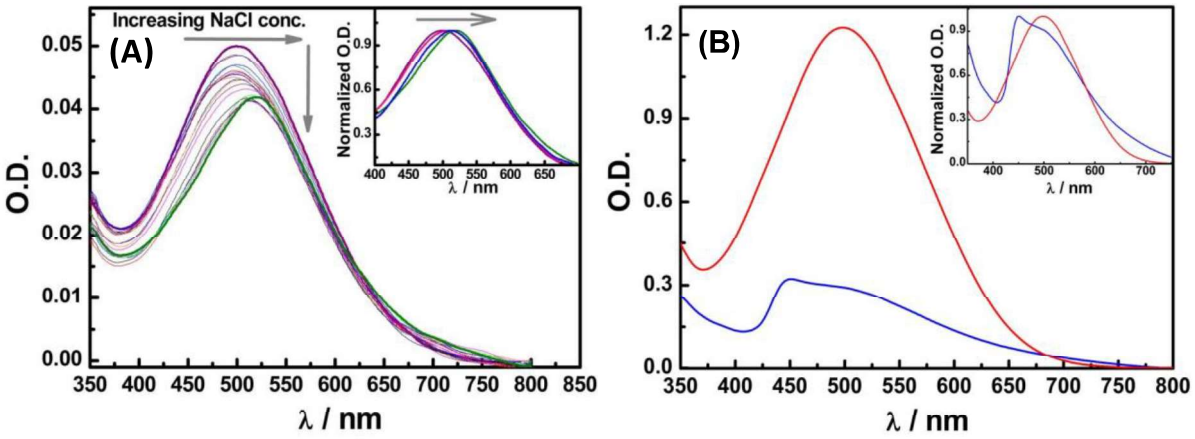

Figure: 4.2. (A) Absorption spectra of 3.5 μM LDS-798 with the increasing NaCl concentration from 0 M to 1M at pH ~7.0. [**Inset**: Normalized absorption of 3.5 μM LDS-798 showing the gradual red shift of absorption maxima with increasing NaCl concentration] and **(B)** Absorption spectra of 95 μM LDS-798 in the absence of 1M NaCl (red) and in the presence of 1M NaCl (blue) at pH ~7.0 [**Inset**: Normalized absorption of 95 μM LDS-798 in the absence of 1M NaCl (red) and in the presence of 1M NaCl (blue) NaCl concentration]

4.3.3. Determination of Stoichiometry for the LDS-798- $SBE_{10}\beta CD$ Complex

Stoichiometry of host-guest complex is generally determined by the Job's plot analysis where the changes in the physical properties (viz, enthalpy change, change in chemical shift, absorbance, emission intensity and so on) of the guest molecule are plotted against the mole fraction of the host or the guest used, keeping the sum concentrations of the host and guest constant in the experimental solutions.[33, 35, 63, 80, 95, 96, 169, 235] When the binding between host and guest is sufficiently strong and the host-guest complexation brings out notable changes in physical property, Job's plot analysis can provide satisfactory and reliable information about the stoichiometry of the host-guest complex. Fluorescence changes are usually being much larger than the other physical properties towards the addition of the hosts to the guest solutions; it is a quite common practice to use the changes in fluorescence intensity against the mole fraction of the host to construct the Job's plot for many host-guest systems.[33, 35, 95, 96, 235]

In our present study, although both the absorption and fluorescence properties of LDS-798 show considerable changes upon host addition, we used the changes in fluorescence intensity for the determination of the stoichiometry of the complex through Job's plot method

(*cf.* Fig. 4.3), because unlike absorbance changes that show a reversal in characteristics, the fluorescence changes for the present system follow a systematic increasing trend. As expected, determination of stoichiometry from the changes in the absorbance values might possibly lead to a misleading result and therefore it was not attempted.

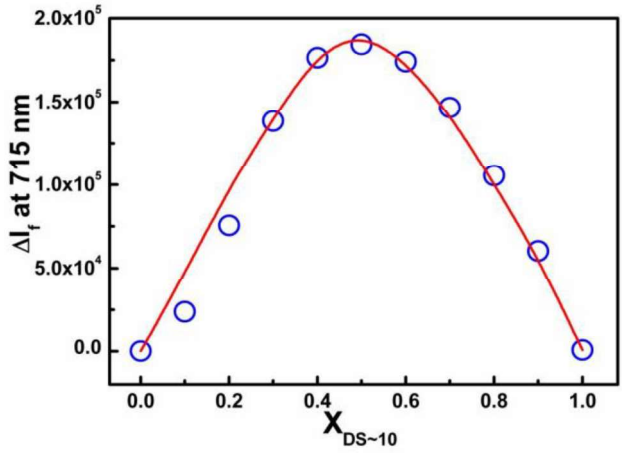

Figure: 4.3. Job's plot for LDS-798- $SBE_{10}\beta CD$ system at pH 7, obtained by plotting the relative changes in fluorescence intensity ($\Delta I_f = I_{LDS798\text{-}SBE10\beta CD} - I_{LDS798\text{-}water}$) at 715 nm against the $SBE_{10}\beta CD$ mole fractions used. The circles are the experimental data points. Smooth curve is drawn just for a visual guide. The sum of the concentrations of LDS-798 and $SBE_{10}\beta CD$ was kept constant at ~45 μM.

From the Fig 4.3 it is clear that when the relative changes in fluorescence intensity is plotted against continuous variation of mole fraction of the host, an inverted plot with maximum at 0.5 of the x-axis results. This clearly suggests the preferential formation of host-guest complex with 1:1 composition. It is to be noted that the sum concentrations of the host and the guest LDS-798 kept sufficiently high (~45 μM) to get substantial fluorescence changes for the reliable construction of the Job's plot.

4.3.4. Determination of the Binding Constants

To obtain quantitative estimate of the binding affinity between the applied host and the guest molecules, it is essential to determine the binding constant [K_b; also called the association constant (K_a)] of the complexation process. Binding constant provides us an idea about the stability of the complex formed between the host and the guest. The plot of the

changes in physicochemical properties for a fixed concentration of guest in the solution against the increasing concentration of the host produces necessary binding isotherm. A suitable nonlinear fitting of the obtained binding isotherm following an adequate mathematical equation depending upon the stoichiometry of the complexation provides the estimate of the binding constant for the complexation process.

As mentioned earlier, among all the physical properties, since the fluorescence intensity changes are often much larger than the other properties, the binding constant for host-guest system is often measured following the fluorescence intensity changes of the probe against the changing host concentration, a methodology commonly called the fluorescence titration method.[27, 28, 33, 35, 46-51, 63, 80, 82, 95, 96, 114, 141, 164, 217, 245]

In the present study, the binding isotherm of LDS-798-SBE_{10}βCD system was obtained by plotting the relative changes in the fluorescence intensity at 715 nm for a 3.5 μM dye solution with increasing host concentration up to 26 μM (*cf.* Fig. 4.4) and subsequently fitting the binding isotherm using eqn.4.1, a standard relation applicable for 1:1 complexation process. Observed binding isotherm indicates a kind of saturation of the changes in the fluorescence intensity in presence of quite a low concentration of the host (~26 μM), implying a very strong binding between dye LDS-798 and SBE_{10}βCD. This is understandably due to strong electrostatic interaction between cationic LDS-798 with the negatively charged sulfonate groups at the portal of the SBE_{10}βCD host along with conventional hydrophobic interaction exerted by the host cavity.

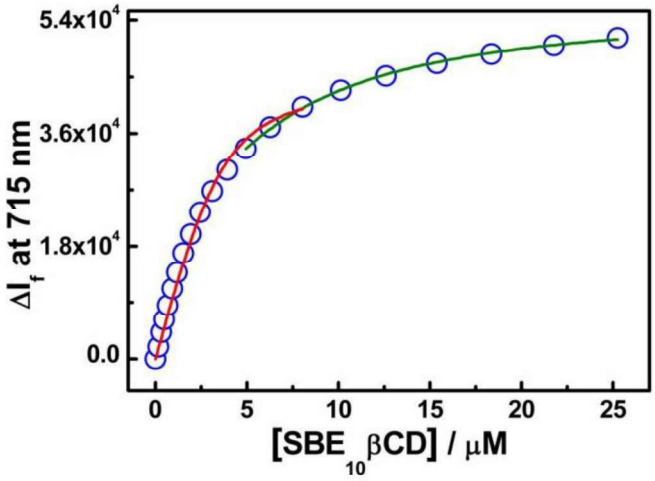

Figure: 4.4. Binding isotherm of LDS-798- $SBE_{10}\beta CD$ system at pH 7, obtained by plotting the relative changes in fluorescence intensity at 715 nm against the increasing concentration of $SBE_{10}\beta CD$. The circles are the experimental data points and the smooth curves are the segmental fitting of the isotherm following eqn. 4.1.

$$\Delta I_f = I_f^{\infty}\left(1-\frac{\{K_b[Dye]_0 - K_b - 1\}+\sqrt{(K_b[Dye]_0 + K_b[H]_0 + 1)^2 - 4(K_b)^2[Dye]_0[H]_0}}{2[Dye]_0 K_b}\right) \quad (4.1)$$

It is to be noted from the Fig 4.3 that the analysis of the binding isotherm using equation 4.1 of 1:1 binding model does not give a proper fitting over the entire concentration range of the host concentration. This definitely indicates the involvement of two consecutive binding modes operative for the system with the changing host concentration. Accordingly, in the present case, the binding isotherm has been analyzed in segmental manner, one for the lower host concentration region and the other for the higher host concentration region. Thus, for the lower host concentration region (up to 8 μM), the use of equation 4.1 for 1:1 binding model gives a very nice fitting and yields binding constant for the initial complexation as K_{b1} ~(1.64±0.6)x10^6 M^{-1}, which is found to be one of the highest for any dye/drug and β–cyclodextrin complex reported till date.[5, 82, 140, 141] For the higher host concentration region also the changes in emission intensity against host concentration was fitted similarly following equation 4.1. However, in this case, 5 μM host concentration was taken as the off set in the X-axis and the corresponding emission intensity change for the dye was taken as the offset in the Y-axis to fit the titration data. Resulted fitting yields the second step of the binding constant as

K_{b2} = (1.84±0.12)x10^5 M^{-1}. Hence, it is indicated that the formation of second complex in the later stage is almost one order of magnitude slower as compared to the first one. We infer that this second step represents a higher order of complex formation, possible at much higher concentration of the host used than the first one. This may be the possible reason why the second complex formation does not give its signature in the observed Job's plot. Following the analysis of the binding isotherm, we may conclude that at 26 µM concentration of SBE_{10}βCD the overall stoichiometry of the LDS-798- SBE_{10}βCD complex is effectively 1:2.

4.3.5. Excited State Lifetime Measurement

In order to get insights of the supramolecular host-guest complexations, the time resolved fluorescence measurements to estimate the excited state lifetimes are the most important and useful methods. As already discussed, free LDS-798 is a quite non-fluorescent in nature due to its large structural agility which disposes its excited state energy via molecular vibration and rotation and also due to its ability to form TICT state in its first excited.[96, 117, 155, 254, 255] Thus, the combined effect of molecular flexibility and propensity to form TICT state in its first excited state makes the free LDS-798 quite non-emissive in nature and its fluorescence decay becomes unusually fast.

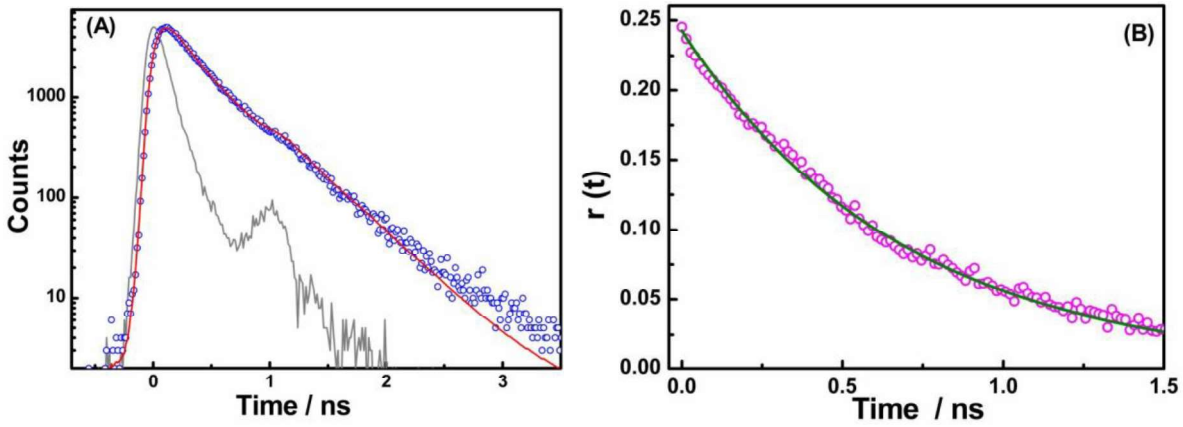

Figure: 4.5. (A) Fluorescence decay and **(B)** anisotropy decay curves of 10 µM LDS-798 in presence of 230 µM SBE_{10}βCD at pH 7. The grey line represents the instrument response function (IRF). (λ_{ex} = 445 nm diode laser source, λ_{em} =715 nm).

The excited state life time of free LDS-798 in aqueous medium is reported to be extremely short (~24 ps),[117, 155, 254, 255] which is well below the instrument response time (IRF) of our TCSPC setup (~120 ps). Accordingly, we could not record the fluorescence decay of free LDS-798 reliably to estimate its lifetime. However, in the presence of ~230 μM SBE_{10}βCD to the aqueous solution of 10 μM LDS-798, maintained at pH 7, results a substantial enhancement in the fluorescence lifetime of the dye. The large structural confinement and also the reduced propensity of TICT state formation due to lower micro-polarity imposed by the host cavity as compared to the dye in bulk water results a phenomenal increase of the excited state lifetime of the dye. This large increase in excited state lifetime of LDS-798, in the presence of SBE_{10}βCD, is in consistent with the increase in emission intensity in the steady state results as discussed earlier. The fitting of the decay trace for the LDS-798-SBE_{10}βCD system in the present case (*cf.* Fig. 4.5A) follows a bi-exponential fitting yielding a shorter lifetime component (36.5 %, 0.11 ns) and a longer lifetime component (63.5 %, 0.4 ns), providing an average lifetime value of ~ 0.26 ns. The bi-exponential decay kinetics has been attributed to the fact that during the relaxation on the potential energy surface, where the radiative decay constant becomes dependent on the phenyl bond twisting angle, the emission from different positions on the excited state potential energy surface results different time constants, which effectively causes the observed decay to become quite non-single exponential in nature. To be mentioned that the bi-exponential decay trace of LDS-798 is a very common feature as previously reported in the literature.[96, 117]

4.3.6. Time-Resolved Anisotropy Measurement

Time-resolve anisotropy is another significant tool to get information about the surrounding environments of the probe under investigation. In the anisotropy measurements, the probe molecules are excited with a plane polarized short light pulse. In solution phase, the probe molecules are randomly oriented with respect to each other. However, upon excitation

with the polarized light pulse, the excited probe molecules get selectively aligned to the direction of the oscillating electric field of the light pulse. After withdrawal of the light pulse, the molecules start to randomize their arrangements in a time dependent manner, following a definite rotational relaxation time. Depending on the changes in the rotational relaxation time we get the information about the modulations in the microenvironment of the probe. The rotational relaxation time (τ_r) depends on the rotational diffusion coefficient (D_r) of the probe, which in turn depends on several factors like temperature (T), viscosity (η) of the medium and the hydrodynamic volume of the probe (V) following relations as given below.

$$\tau_r = 1/6D_r \text{ where, } D_r = \frac{RT}{6V\eta} \quad (4.2)$$

Due to non-fluorescent nature and very short excited state lifetime, the fluorescence anisotropy decay and hence the rotational relaxation time of free LDS-798 could not be measured in the present study. Nevertheless, considering its molecular structure, the rotational relaxation time of LDS-798 is expected to be ~150 ps or less in the aqueous medium under the experimental condition.[63, 96] As shown in Fig. 4.5B, addition of ~230 μM $SBE_{10}\beta CD$ to aqueous solution of 10 μM LDS-798, results a substantial increase in the rotational relaxation time which becomes easily measurable in our experimental setup. The single exponential fitting of the observed fluorescence anisotropy decay results a rotational relaxation time of ~680 ps. This huge increase in rotational relaxation time in the presence of $SBE_{10}\beta CD$ host clearly indicates the formation of LDS-798- $SBE_{10}\beta CD$ inclusion complex, which causes substantial increase in hydrodynamic volume of the dye and accordingly a large retardation in the rotational relaxation rate.

4.3.7. Temperature Dependent Emission and Life Time Measurement Studies

To check the effect of temperature on the complexation process, we have carried out temperature dependent emission studies for the LDS-798- $SBE_{10}\beta CD$ system following both

steady-state and time resolved fluorescence measurements. In the present study, we checked the effect of temperature on emission of 10μM LDS-798 in the presence of 48μM SBE_{10}βCD.

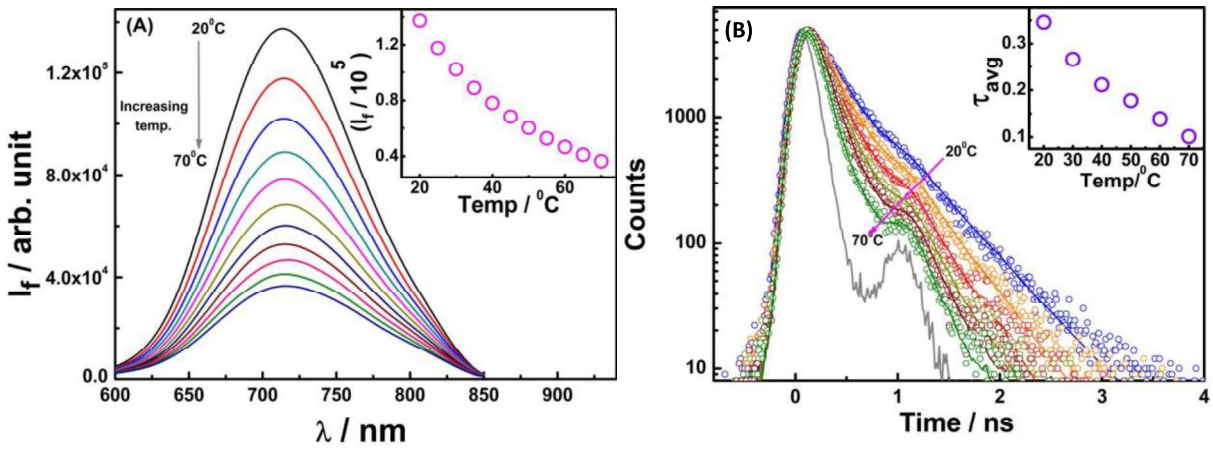

Figure: 4.6. (A) Effect of increasing temperature on emission intensity of 10 μM LDS-798 in the presence of 48 μM SBE_{10}βCD at pH 7 (λ_{ex} = 500 nm) [Inset shows the relative changes in emission intensity at the emission peak maxima (~715 nm) of the complex with the increasing in temperature from 20^{0}C to 70^0 C) and **(B)** Effect of temperature on fluorescence decay traces of 10 μM LDS-798 in the presence of 230 μM SBE_{10}βCD at pH 7, temperature was varied from 20^{0}C to 70^0 C (λ_{ex} = 445 nm diode laser source, λ_{em} =715 nm). The grey line represents the instrument response function (IRF).

Table: 4.1. Lifetime of LDS-798-SBEβCD complex at different temperature

Sl No.	Temp (^{0}C)	τ_1 (ns)	τ_2 (ns)	a_1 (%)	a_2 (%)	χ^2	τ_{avg} (ns)
1	20	0.16	0.49	43.7	56.3	1.24	0.35
2	30	0.10	0.39	42.6	57.4	1.36	0.27
3	40	0.08	0.33	47.5	52.5	1.24	0.21
4	50	0.086	0.30	57.3	42.7	1.39	0.18
5	60	0.07	0.27	65.8	34.2	1.4	0.14
6	70	0.05	0.255	75.0	25.0	1.13	0.10

As shown in Fig 4.6A, gradual increase in temperature from 20^{0}C to 70^{0}C results in substantial decrease (~3.8 folds) in emission intensity in the steady-state measurements. Similarly, in time-resolved measurements (shown in Fig. 4.6B), the increase in temperature leads to enormous decrease in the excited state lifetime of the formed complex. Increase in temperature accelerates the thermal agitation in the molecules which in turn increases the molecular flexibility by increasing vibrational and rotational motions, making the excited

probe molecules to de-excite rapidly through non-radiative process. Further, increase in temperature destabilizes the dye-host complexes promoting their disintegration. Thus, the decrease in fluorescence properties with increase in temperature in the studied system may be explained in terms of the weakening of the binding interaction along with the acceleration of the non-radiative de-excitation process. It is to be noted that when temperature restored to initial value of 20^0C, emission intensity and excited state lifetime reverted back to their initial values due to decrease in the destabilization effects. Thus, the remarkable temperature sensitivity of the LDS-798-SBE_{10}βCD complex makes the present system a promising probe for its usage in temperature sensing applications.

4.3.8. Effect of Increasing Ionic Strength

Supramolecular host-guest complexes are formed via reversible non-covalent interactions amongst which hydrophobic interaction, dipole-dipole interaction, ion-dipole interaction, electrostatic interaction and hydrogen bonding play significant roles.[3, 5, 6, 8, 23, 82, 91, 141, 212] When the guest molecule is mainly hydrophobic in nature (aqueous solubility is less) and the main operative force during supramolecular complexation with the host is hydrophobic interaction, the increase in concentration of salt or ionic strength of the solution increases the binding between guest and the host molecules.[180] With increase in salt concentration, the polarity or dielectric constant of the medium becomes higher and thus the hydrophobic dye molecules cannot remain in the water phase but prefer to be transferred to the less polar or hydrophobic host cavity, leading to an increased binding interaction.[180] On the other hand, when the interactions between the host and the guest molecules are ion-dipole/dipole-dipole or electrostatic in nature, the increased salt concentration results in a substantial decrease in the interaction between the oppositely charged constituents in the complex, which ultimately reduces the binding between the guest and host molecules.[20, 180, 235]

In the present LDS-798-SBE_{10}βCD system, the effect of salt concentration has been investigated by gradually increasing NaCl salt concentration in the solution containing the fully complexed LDS-798-SBE_{10}βCD complex. As shown in Figs 4.7A and 4.7B, in both fluorescence and absorption studies we find a substantial decrease in the complexation process in the presence of the salt.

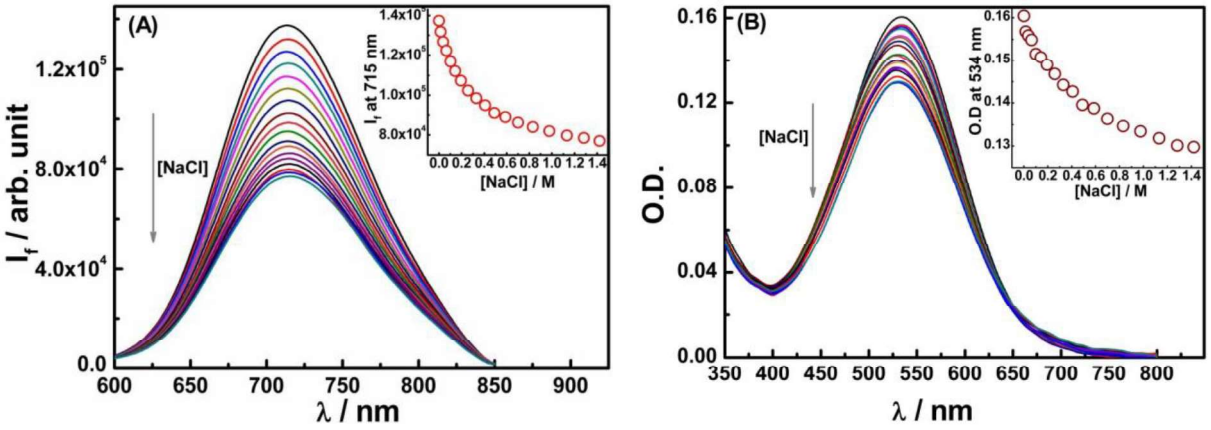

Figure: 4.7. Effect of increasing salt concentration on **(A)** emission intensity of 10 μM LDS-798 in the presence of 48 μM SBE_{10}βCD at pH 7 (λ_{ex} = 500 nm); [Inset shows the relative changes in emission intensity at the emission peak at ~715 nm of the complex with an increase in NaCl concentration from 0 to 1.4 M]. **(B)** Effect of increasing salt concentration on the absorption spectra of 10 μM LDS-798 in the presence of 48 μM SBE_{10}βCD at pH 7; [Inset shows the relative change in absorbance at the peak position at ~534 nm of the complex with an increase in NaCl concentration from 0 to 1.4 M].

The complex between LDS-798 and SBE_{10}βCD mainly formed via electrostatic interaction between the cationic dye molecule with the poly-anionic terminal sulfonate groups of the host, SBE_{10}βCD, along with the hydrophobic interaction imposed by the guest cavity. With increase in NaCl concentration, the positively charged Na^+ ions come into the competition with the cationic dye molecules towards the negatively charged sulfonate terminals of the host and at a relatively high concentration of the salt, the Na^+ ions mask most of the anionic sulfonate groups of the SBE_{10}βCD host for substantial electrostatic interaction with the cationic dye. This reduction in electrostatic interaction results a decrease in the stability for the dye-host complex leading to the dissociation of the initially formed complex,

as evident from the decrease in the fluorescence intensity of the dye with the increase in the NaCl concentration in the solution. In ordered to get more insight information about the effect of ionic strength on the system under investigation, we also performed ground state absorption study of 10 μM LDS-798 in the presence of 48 μM SBE_{10}βCD at pH 7. As shown in Fig. 4.7B, with increase in salt concentration from 0 to 1.4 M, there occurs a phenomenal decrease in absorbance at ~534 nm which corresponds to the disintegration of the LDS-798-SBE_{10}βCD complex. This result from absorption study nicely corroborates with the result obtained from the steady state fluorescence study, indicating the increasing probability of rupture of the host-guest complex with the increasing salt concentration.

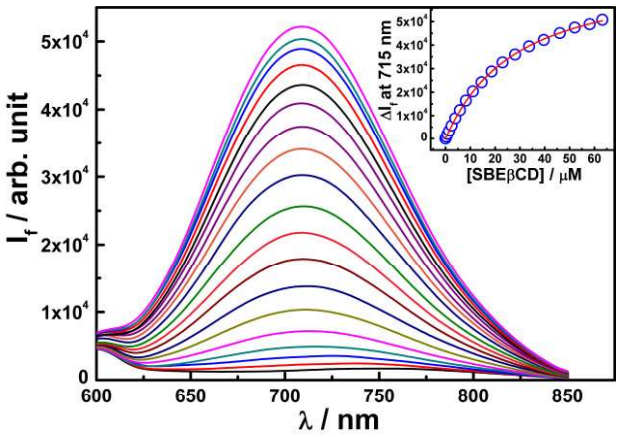

Figure: 4.8. Fluorescence spectra of 3.5 μM LDS-798 with increasing SBE_{10}βCD concentration in the presence of 1M NaCl at pH 7 (λ_{ex} = 500 nm). Inset shows the binding isotherm obtained by plotting the relative intensity changes at 715 nm. The isotherm was fitted with 1:1 binding model.

To get the quantitative measure for the salt effect on the LDS-798-SBE_{10}βCD complexation process, we performed the fluorescence titration study for 3.5 μM LDS-798 solution as a function of increasing concentration of SBE_{10}βCD in the presence of 1 M NaCl. It is found that in the presence of 1M NaCl, the SBE_{10}βCD concentration required to achieve saturation in the fluorescence changes for 3.5 μM LDS-798 solution is much higher than that required for the same LDS-798 solution in the absence of NaCl (*cf.* Fig. 4.8). This is quite expected, because the presence of high concentration of Na^+ ions introduces a competition

with the cationic dye molecules for binding to the anionic hosts present in the solution. The presence of Na^+ ions largely masks the negative charges at the terminal sulfonate groups of the host molecules through screening effects, which are responsible to reduce the electrostatic interaction of the cationic dye LDS-798 with the $SBE_{10}\beta CD$ host and thereby to reduce the complexation probability between the dye and the host molecules. When the change in the emission intensity was fitted with the 1:1 binding model (*cf.* eqn. 4.1), the binding constant (K_b) at this situation is estimated as ~$(3.87\pm0.6)x10^4$ M^{-1}., which is ~40 fold lower than the value obtained (K_b ~$1.6x10^4M^{-1}$) in the absence of NaCl. Thus, destabilization of the complex or the reduced propensity of the complex formation with the increasing ionic strength clearly indicates the predominance of the electrostatic interaction during the supramolecular host-guest complexation between LDS-798 and $SBE_{10}\beta CD$.

4.3.9. Effect of Competitive Binder towards LDS-798-$SBE_{10}\beta CD$ Complex

It is known in the literature that lithocholic acid and 1-adamantylamine hydrochloride bind to the cyclodextrin cavity with the highest ever observed binding constant (K_b), in the order of 10^6-10^7 M^{-1}.[85, 249-252] Hence, to substantiate our inference that the binding of LDS-798 with the substituted cyclodextrin ($SBE_{10}\beta CD$) host is the strongest found till date, we were interested to see if the binding of LDS-798 with $SBE_{10}\beta CD$ remains unaffected or hardly gets affected in the presence of the strongest binders like lithocholic acid or adamantylamine hydrochloride, as would be expected for the strongest dye-host binding in the studied system.

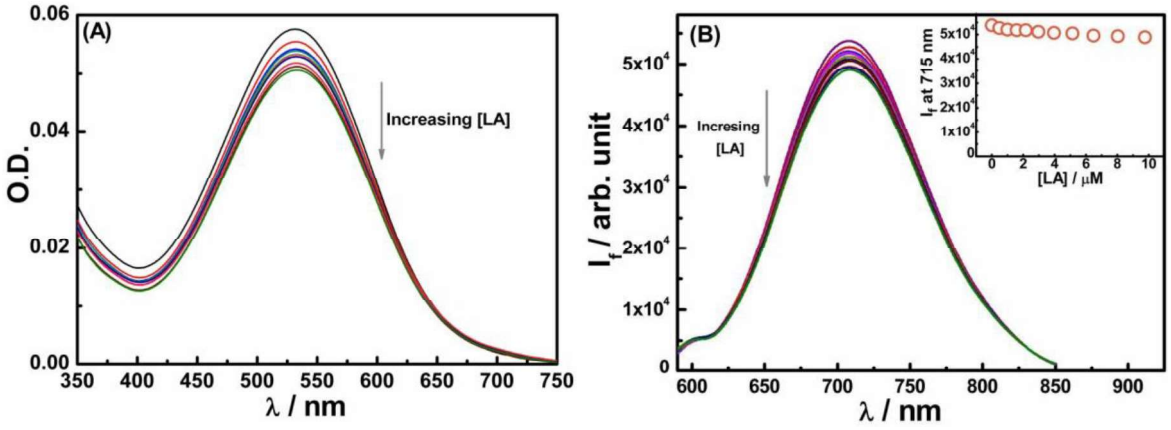

Figure: 4.9. Effect of increasing lithocholic acid (LA) concentration on **(A)** absorption and **(B)** emission characteristics of 3.5 μM LDS-798+32 μM SBE_{10}βCD complex (λ_{ex} = 500 nm).

Fig. 4.9A and 4.9B show the changes in the absorption and emission profiles of the complex, formed in the solution containing 3.5 μM LDS-798+32 μM SBE_{10}βCD upon gradual increase in concentration of lithocholic acid. If lithocholic acid had the higher binding affinity than LDS-798 towards the SBE_{10}βCD, substantial changes (more precisely decrease) would have been expected by the presence of lithocholic acid both in the absorption and emission intensity of the complex. But the observed changes/decrease in the absorption and emission intensity of the complex are found to be very nominal even up to a concentration of lithocholic acid which is three times higher than the LDS-798 concentration used for the study. This observation clearly suggests that the binding of LDS-798 with SBE_{10}βCD is so strong that even lithocholic acid, which is known as one of the strongly binding guest to the cyclodextrin cavity,[252] is unable to replace the LDS-798 dye from the cavity of the SBE_{10}βCD host. A very similar observation is also made when the experiments were performed using another strongly binding agent 1-adamantylamine hydrochloride[85, 249, 251] under identical condition (Fig. 4.10). These results indicate the highest binding affinity of LDS-798 towards SBE_{10}βCD, because of the strong electrostatic interaction between cationic LDS-798 with poly-anionic SBE_{10}βCD, along with the extensive hydrophobic interaction provided by the extended host cavity due to the presence of the sulfobutyl ether groups at the portals of the studied host.

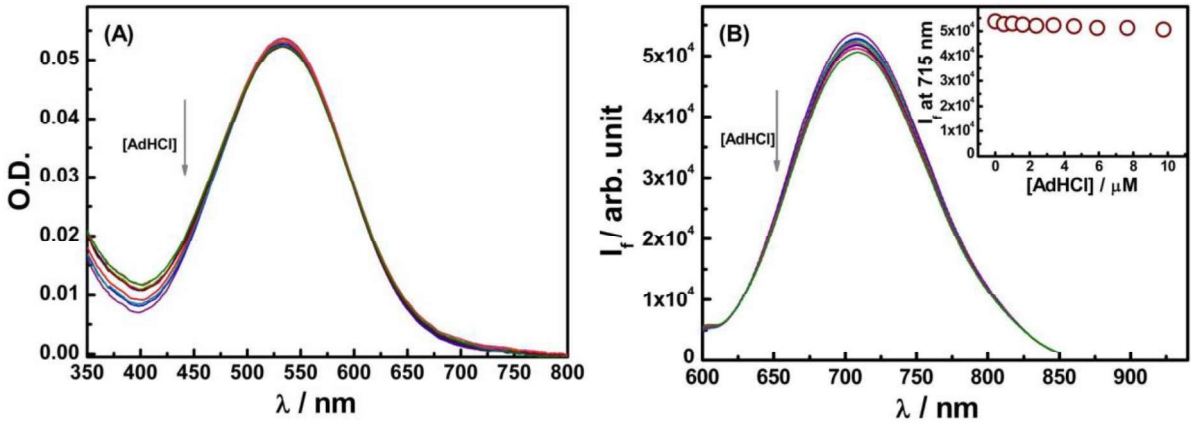

Figure: 4.10. Effect of increasing concentration of adamantylamine hydrochloride (AdHCl) concentration on **(A)** absorption and **(B)** emission characteristics of 3.5 μM LDS-798+32 μM SBE_{10}βCD complex (λ_{ex} = 500 nm).

4.4. Conclusion

Supramolecular interaction of LDS-798 with SBE_{10}βCD host has been found to be the strongest (K_a~$1.6x10^6M^{-1}$) reported till date involving cyclodextrins and their derivatives as the hosts. The marginal reduction in fluorescence properties in the presence of competing agents like lithocholic acid and adamentylamine hydrochloride further supports the strongest binding affinity of LDS-798 with SBE_{10}βCD. The structural confinement effect and reduced propensity of TICT state formation in the first excited state imposed by the host cavity upon LDS-798 substantially improve the fluorescence characteristics of the probe. The strong electrostatic interaction between cationic LDS-798 dye and polyanionic SBE_{10}βCD host along with the conventional hydrophobic interaction helps the dye molecules to bind with the host cavity very strongly. The LDS-798-SBE_{10}βCD complex found to be very sensitive towards external stimulus like temperature and ionic strength. Increase in ionic strength to the solution of LDS-798-SBE_{10}βCD complex results a notable reduction in fluorescence characteristics due to the masking effect rendered by the positively charged cations of the salt to the negatively charged terminal sulfonate groups that substantially reduces the electrostatic interaction between positively charged dye molecules and the negatively charged hosts. There occurs an enormous reduction in fluorescence intensity and excited state lifetime of the dye

complex with increasing temperature, due to destabilization of the dye-host complex and the increasing molecular agility at elevated temperatures. Hence, the highest binding of the LDS-798 probe with the substituted polyanionic cyclodextrin derivative $SBE_{10}\beta CD$ and the exceptional response of the dye-host complex towards the external stimulus like temperature and ionic strength makes this dye-host pair quite a good choice as prospective temperature sensor, polarity sensor and so on.

CHAPTER-5

NON-COVALENT INTERACTION OF BODIPY-BENZIMIDAZOLE MOLECULAR CONJUGATE WITH BOVINE SERUM ALBUMIN- A PHOTOPHYSICAL AND DOCKING STUDY

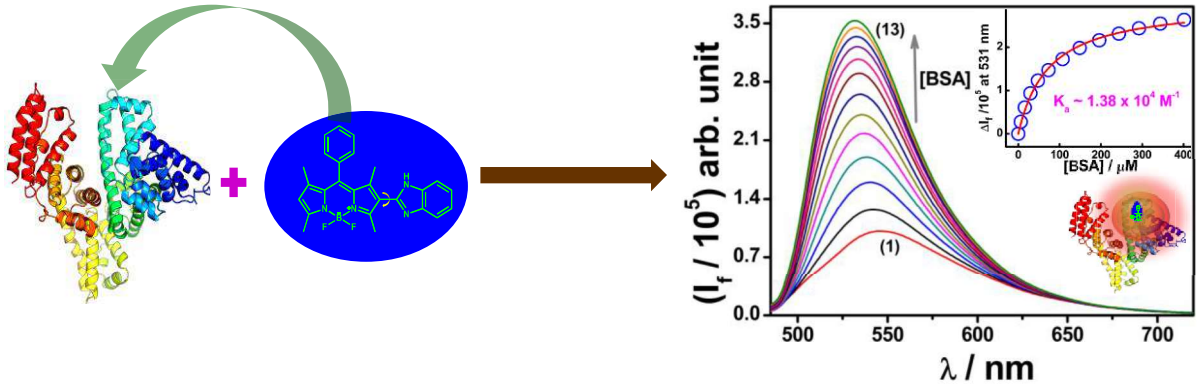

5.1. Introduction

Non-covalent interactions play a significant role in living orgamism. In fact, one of these primordial interactions, namely, hydrogen bonding, between the DNA base pairs, has helped mother nature to realize and evolve the mysterious processes of life on planet Earth. The prominence of non-covalent interactions cannot be discarded while exploring the chemical and biological processes. Supramolecular interactions are in general the non-covalent interactions, which deal with precisely organized structural molecular assemblies formed between constituent units. Hydrophobic interaction, hydrogen bonding, ion-dipole interaction, electrostatic interaction, π-π stacking, etc., fall under the umbrella of the non-covalent interactions and play a significant role in detretmining the thermodynamic parameters that govern the molecular arrangements of the supramolecular systems in three dimensional space.[6, 23] There have been extensive ongoing reasearch for the past few decades, targeting to improve the photophysical properties of different chromophores through their

binding to various biological agents, for their applications in various filelds of science.[10, 14, 20, 27-30, 32-35, 44-51, 54, 56-58, 61, 62, 80, 130-132, 159, 162, 168, 174, 199, 215, 217, 245, 251, 259-261] Enhancement in fluorescence yield and lifetime, inhibiting aggregation, controlling conformational relaxations, enhancing photochemical stability, increasing solubility, improving bio-availability of drugs, modulating acid-base properties (pK_a shift) etc., are few noteworthy properties of the guest molecules that have been attracted by many researchers to achieve through host-guest interactions.[32, 33, 35, 48, 51, 56, 63, 80, 82, 173, 221, 262] Among various biological agents, one of the most popular and studied system in this regard, is the bovine serum albumin (BSA) protein. BSA, is obtained from the blood plasma of cow. It is found to be moderately soluble (~ 50 mg/ml) in deionized water and possesses fairly stable structure in the pH range 5 to 8.[186, 187] Three dimansional structure of BSA contains three α-helical domains, I, II and III; each of these domains is further divided into two subdomains A and B, respectively. In the BSA structure, there are many non-specific binding sites to accommodate guest dyes or drugs via non-covalent interactions. Based on Sudlow's classification/observation however, most of the drugs/ligands are specifically bound in either of the two principal binding sites of BSA, designated as Sudlow's site-I (situated at domain IIA) and Sudlow's site-II (situated at domain IIIA). Sudlow's site-I, is more voluminous and binds guest molecules via hydrophobic interaction mainly. Whereas, Sudlow's site-II, is less capacious and the prevailing binding forces at this site are hydrogen bonding, electrostatic interaction, hydrophilic interaction as well as hydrophobic interactions.[184, 187] Several studies have however revealed that all different ligand binding instances cannot just be accounted based on Sudlow's classification. Thus, recent studies have identified a third binding site located at subdomain IB (site IB), which acts as a third major binding site in BSA for various analytes. Accordingly, in a detailed study involving 149 different ligand-albumin complexes and using X-ray crystallographic data

it has been indicated that atleast 49% of the ligands have significant affinity towards site IB of the BSA protein.[263]

Serum albumins are the transport proteins that bind to various hormone, enzymes, nutrients, etc., and help in the transportation of the species from one part of the body to another.[191, 226, 228, 264] Water balance between the tissues and mainatance of the pH of blood are also two other major activities where serum albumins are directly involved. Due to the close structural similarity of BSA with human serum albumin (HSA), BSA has been used extensively as a model for HSA to investigate various drug-protein interactions which help in understanding the in situ binding and transport mechanism of various analytes with serum albumin.[185, 187, 265] It has been well documented in literature that interaction of BSA with different dyes/drugs results in substantial changes in their physicochemical properties which have been exploited extensively in the field of chemistry, biology, microbiology, medicinal chemistry and, so on.[187, 189, 191, 226, 228, 265-268]

Binding of BSA with different chromophoric dyes (rhodamine, crystal violet, cresyl violet, methyl orange, bromophenol blue, malachite green, LDS-798 and so on) have been studied extensively in the literature.[95, 96, 233, 269-272] In this context, an increasing number of reports have been published, over the years, claiming the use of BODIPY class of dyes as protein and DNA lebeling agents.[128, 273-277] The 4,4-difluoro-4-bora-3a,4a-diaza-s-indacene, commonly known as BODIPY, is the basic structural unit of an important class of organic dyes that have two pyrrole units linked together by a BF_2 bridge. As discussed in Chapter-2, due to thier many advantageous characteristics, essentially thier very sharp absorption and emission spectral profiles in the green-yellow-red region, the BODIPY dyes have been extensively used in various applications, such as, polarity sensors, bio-imaging, molecular logic gates, pH sensors, biological markers, dye lasers and so on.[106, 147, 278-282] The tendency of

the BODIPY dyes to form non-emissive aggregates, and their low solubility in aqueous medium, however, often hinder their usage in many of the biological applications. The chemical modifications of BODIPY scaffold at suitable position(s) can logically overcome some of these limitations encountered with known BODIPY dyes.[150, 153, 154, 283-287] One such modified BODIPY dye is the BODIPY-benzimidazole (BDZ) conjugate (*cf* Scheme 1), which is formed by the substitution of the hydrogen atom at positions 2 and 8 (meso) of the BODIPY core by a benzimidazole and benzene units, respectively, and was synthesized and reported in our earlier work.[63] We designated this dye as a BODIPY-benzimidazole (BDZ) conjugate. Such substitutions lead to high sensitivity of the concerned BDZ dye towards various environmental factors such as pH and polarity of the surrounding enviroment.[154] The dye also demonstrates excellent fluorescence turn-on response towards pH, which makes the dye a potential probe for various biological studies. It has been reported in our earlier work that BDZ and its higher analogue show excellent fluorescence turn-on response towards the hydrophobic cavity of the macrocyclic host molecules such as cucurbit[7]uril.[63] Inspired by these observations, in the present contribution, we have investigated the interaction of the synthesized BDZ dye with an important bio-macromolecule, BSA, using a variety of photophysical techniques such as ground-state absorption, steady-state fluorescence and time-resolved flouorescence studies, which are further substantiated following molecular docking calculations and analysis.

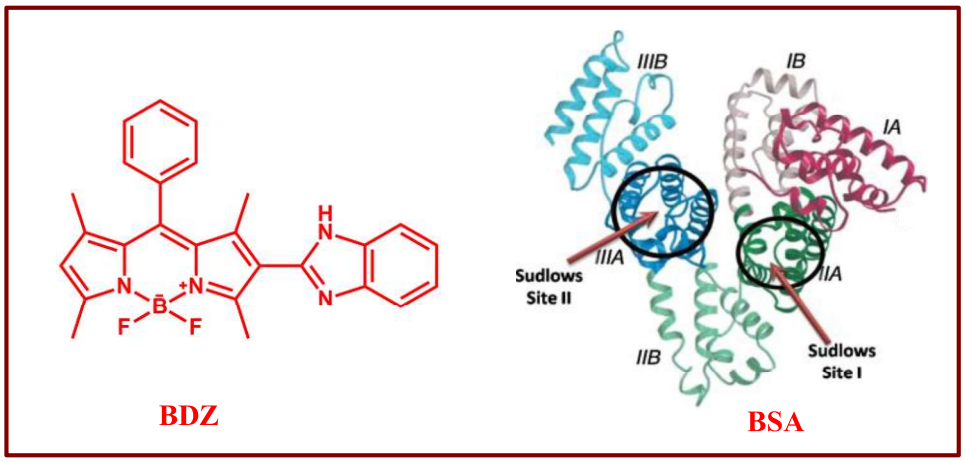

Scheme: 5.1. Chemical structure of BODIPY-benzimidazole conjugate (BDZ) and three-dimensional ribbon presentation of BSA protein indicating different binding sites.

5.2. Materials and Methods

In house synthesized, purified and characterized BDZ has been used in the present study.[63] The BSA sample (pH 7 fraction, purity > 99%) was obtained from Sisco Research Laboratory (SRL), India, and was used without further purification. Ibuprofen and warfarin were purchased from Sigma-Aldrich and were used as received. A very low concentration (~1 μM) of BDZ was used during all experiments, as BDZ is quite prone to undergo aggregation in aqueous solution, even at such low concentrations.[63] All the BDZ solutions in this study were prepared in 20% ethanolic PBS (10 mM) buffer solution, both to minimize the aggregation effect as well as to maintain the pH at ~7.4 for the experimental conditions. It is to be noted that the structural integrity of BSA protein remains intact at 20% ethanolic PBS.[288, 289] Nanopure water from a Millipore Elix 3/A10 water purification system (conductivity less than 0.1 μS cm^{-1}) was used for preparations of the sample solutions. All the measurements were carried out at ambient temperature, i.e. at 25±1°C.

Ground state absorption studies were performed using a Thermo-Scientific UV-vis spectrophotometer in an optical quartz cell of 10 mm path length. Steady-state (SS) fluorescence measurements were carried out using a Horiba fluoromax-4 spectrofluorometer

in 10 mm x 10 mm quartz cuvette. The dye samples were excited at 475 nm where the changes in the absorbance of the dye due to the complex formation with BSA is minimum. Time-resolved (TR) fluorescence measurements were carried out using a Time Correlated Single Photon Counting (TCSPC) spectrometer purchased from Horiba Jobin Yvon IBH, U.K. In TCSPC measurements, a 445 nm pulsed diode laser (pulse width ~100 ps and repetition rate 1 MHz) was used as the excitation source and the fluorescence decays were recorded at the emission maximum of the dye-BSA complex (~531 nm) using a micro channel plate photomultiplier tube (MCP-PMT) based detection module (IBH, U.K.). A suspension of TiO_2 powder in water was used as light scatterer to record the instrument response function (IRF). Observed decays were in general analyzed as a sum of exponentials (eq. 2.1, Chapter 2).

The fluorescence quantum yields (ϕ) of BDZ at different concentration of BSA were determined by comparing the integrated fluorescence intensities of the sample solutions with that of the BDZ in ethanol (ϕ=0.19) [154] as reference using the following equation,[107]

$$\phi_s = \phi_r \frac{I_s A_r n_s^2}{I_r A_s n_r^2} \qquad (5.1)$$

where, the subscripts s and r refer to the sample and the reference (BDZ in ethanol), respectively; I represent the integrated area under the emission band; A denotes the absorbance of the solution at the excitation wavelength and n is the index of refraction of the solvent.

Competetive binding experiments were performed with two well known BSA binding ligands, Ibuprofen and warfarin. For this purpose, the binding isotherm of BDZ-BSA system was obtained by plotting the relative changes in the fluorescence intensity, for a fixed concentration of BDZ dye and a fixed concentration of the ligand (Ibuprofen or Warfarin), while gradually increasing the BSA concentration in the solution.

Molecular docking calculations were performed using AutoDock Vina.[290] The crystal structure of BSA protein was taken from protein data bank (PDB: 4F5S).[291] Water molecules were removed and polar hydrogens were added for AutoDock software specific files. An optimized structure of BDZ (using Gaussian 03) was then docked onto BSA using AutoDock Vina. For the docking analysis, the grid size was set to 126 for each of the X-, Y-, and Z-axes, with a grid spacing of 1 Å. Discovery Studio Visualizer v16.1 software from Accelrys Software Inc. was used for visualization and schematic presentation of the docked conformations.

5.3. Result and Discussion

5.3.1. Ground-State Absorption Measurements

20% ethanolic buffer solution of BDZ shows a characteristic absorption band ranging from 450 nm to 560 nm with peak position around 510 nm. With gradual addition of BSA to the solution of 1 μM BDZ, notable changes in the absorption characteristics of the dye observed, as shown in Fig. 5.1A. It is evident from Fig. 5.1A that with incremental addition of BSA to 1μM dye solution there is a decrease in absorbance of the dye molecule along with a subtle red shift (~2 nm) in the peak position. With increasing BSA concentration, the dye molecules are moved from the high refractive index bulk water environment to the comparatively reduced refractive index pockets of BSA, which causes a reduction in the oscillator strength of the absorption process, resulting the hypochromic effect in the absorption spectra.[63] Though the extents of the changes in absorption features of the dye with the increasing BSA concentration are not large enough to be applied for any reliable quantitative analysis; it certainly provides an indication about the interaction of BDZ with BSA in 20% ethanolic PBS solution.

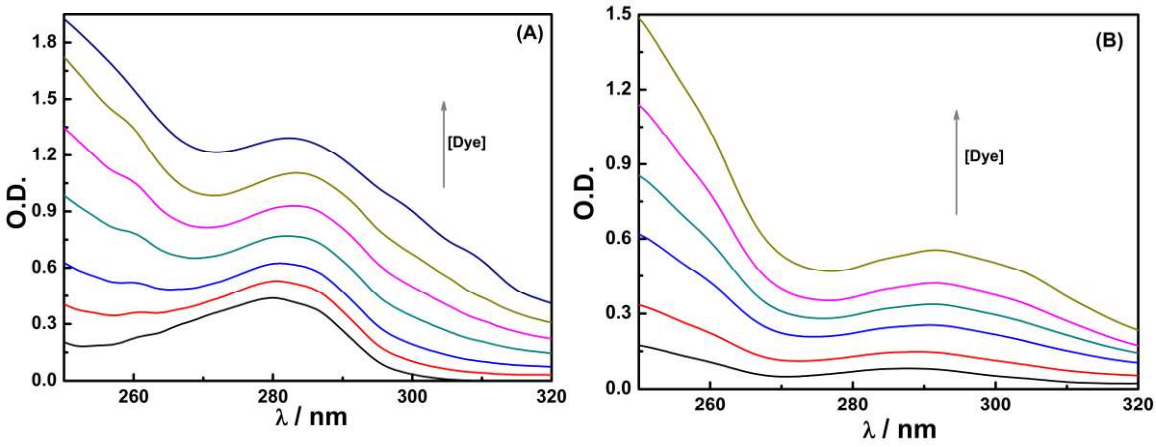

Figure: 5.1. (A) Absorption spectra of 10 µM BSA with increasing concentration of BDZ from 0 to 51 µM and **(B)** Absorption spectra of BDZ with increasing concentration of BDZ from 0 to 51 µM. [pH ~7.4 (20% ethanolic PBS)].

5.3.2. Steady-State Fluorescence Measurements

To obtain both qualitative and quantitative information on the host-guest binding, steady-state emission is a very useful technique. Emission from the BODIPY and their derivatives usually occur in the red side of the visible spectral region. It is acknowledged in the literature that with the increasing polarity of the solvent medium, fluorescence quantum yield of BDZ conjugates decreases.[109, 154] The large structural agility and ability to form weakly emissive intramolecular charge transfer (ICT) state, which gets amplified in a polar medium, provide additional pathways for the excited dye molecules to dissipate their excitation energy in non-radiative manner, causing the BDZ molecules to be meagerly fluorescent. Further, BDZ molecules are also reported to form non-emissive aggregates in aqueous solution even at a concentration as low as 1µM, which drastically reduces their fluorescence yield and interfere strongly in photophysical measurements.

In 20% ethanolic buffer solution, BDZ shows a characteristic emission band ranging from 490 nm to 700 nm with emission maximum at 545 nm. Incremental addition of BSA to the dye solution results into a significant increase in fluorescence intensity along with a gradual blue shift in peak position and the effects attains saturation at about 400 µM BSA, as

indicated from Fig 5.2B and the listed quantum yield values in Table 5.1. Decreased structural flexibility and reduced propensity of ICT formation for bound BDZ into the rigid and less polar BSA pocket results in a substantial increase in emission characteristics of the entrapped dye molecules. Further, the reduced micro-polarity, at the binding site of BSA, also reduces the tendency of formation of the weakly emissive ICT state which in turn causes an enhancement in emission intensity, as observed for BDZ in the presence of BSA. The observed hypsochromic shift of (~14 nm, from 545 nm to 531 nm) in the emission maxima of BDZ, on its binding to BSA, can be accounted on the basis of the decrease in the BDZ-water hydrogen bonding interactions and the reduced micro-polarity of the dye surrounding, as the dye molecules move from bulk polar water medium to less polar BSA pocket. The noteworthy changes observed in the emission features of BDZ, in presence of BSA, clearly indicate a strong interaction of BDZ dye with BSA protein.

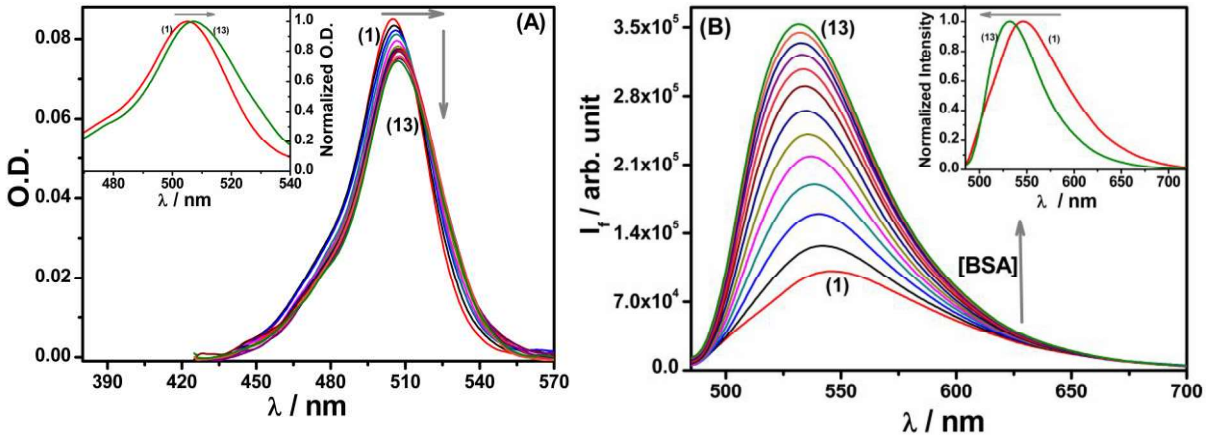

Figure: 5.2. (A) Absorption and **(B)** emission spectra of 1 µM BDZ with the increasing BSA concentration from 1) 0 to 13) 400 µM. [λ_{ex} = 475 nm, pH ~7.4 (20% ethanolic PBS)]. Insets: Normalized absorption and emission spectra of 1 µM BDZ with and without 400 µM BSA.

Table: 5.1. Variation of emission quantum yield of BDZ in water with increasing BSA concentration.

Conc. of BSA (µM)	Quantum yield (ϕ)
0	0.057
6	0.069

16	0.091
29	0.114
47	0.127
73	0.140
107	0.163
149	0.179
196	0.212
243	0.217
400	0.229

5.3.3. Determination of the Binding Constants

Supramolecular complexation process results from dynamic equilibrium between the interacting host and guest molecules and their association complex. Evaluation of the binding constant (K_b) for a supramolecular complexation process provides a quantitative measure of the stability for the complex formed between the interacting species. Fluorometric titration method has been realized to be the most suitable one among the various methods, due to its high sensitivity and easy implementation of the method, especially for the dye-host supramolecular interaction.[28, 30, 35, 49, 63, 82, 112, 114, 141, 164, 203, 217]

In the present study, the binding constant of BDZ-BSA system was obtained by plotting the relative changes in the dye fluorescence intensity at 531 nm, for a fixed concentration (1 μM) of BDZ dye while increasing BSA concentration up to 400 μM followed by the non-linear fitting of the obtained data (binding isotherm) using a 1:1 binding model.[234] The satisfactory fitting of the experimental data yielded the K_b value for the BDZ-BSA system to be (1.38±0.09) x10^4 M^{-1}, which indicates a strong complex formation of BDZ with BSA. The high K_b value of BDZ-BSA pair indicates a strong binding interaction of BDZ with BSA binding pocket, which is further supported by the molecular docking calculation discussed in the section 5.3.9. The dye binding with BSA largely hinders the structural mobility of the dye and hence decreases its non-radiative decay pathways significantly, making the bound dye to

be strongly fluorescent in nature. Logically, the binding constant of dye-BSA pair can also be evaluated by monitoring the changes in the intrinsic BSA emission with the increasing dye concentration. In the present study, however, the binding constant evaluation of BDZ-BSA system following intrinsic BSA emission could not be realized satisfactorily since the absorption spectrum of BDZ has significant overlap (cf. Fig 5.1A and 5.1B) with the absorption spectrum of BSA (250-325 nm), which makes the fluorescence changes of BSA (with varying BDZ) very difficult to be analyzed.

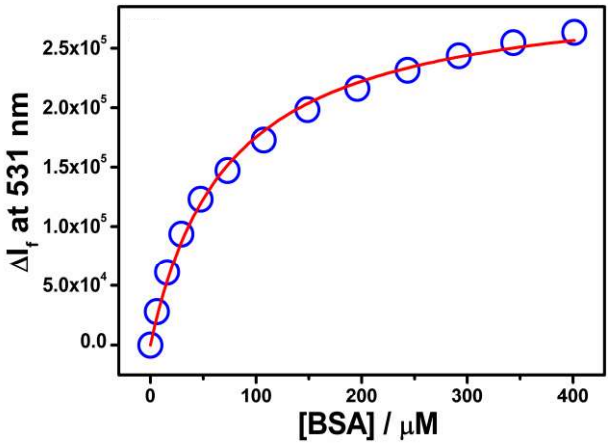

Figure: 5.3. Binding isotherm of BDZ-BSA system in 20% ethanolic buffer (pH~7.4), obtained by plotting the relative changes in fluorescence intensity of BDZ at 531 nm against the increasing concentration of BSA. The circles represent the experimental data points and smooth curve represents the fitting curve following 1:1 binding equation.

5.3.4. Excited-State Lifetime Measurement

To get valuable insights into the fate of the excited guest molecules upon host-guest complexation, time-resolved fluorescence measurements generally provide very useful information. As it is established in the literature,[63, 109, 154] a large structural mobility and the involvement of the weakly emissive ICT process, in the first excited state, between BODIPY chromophore and benzimidazole unit, makes the excited BDZ molecules to dissipate their excitation energy mainly through non-radiative processes, making the dye weakly fluorescent in nature.

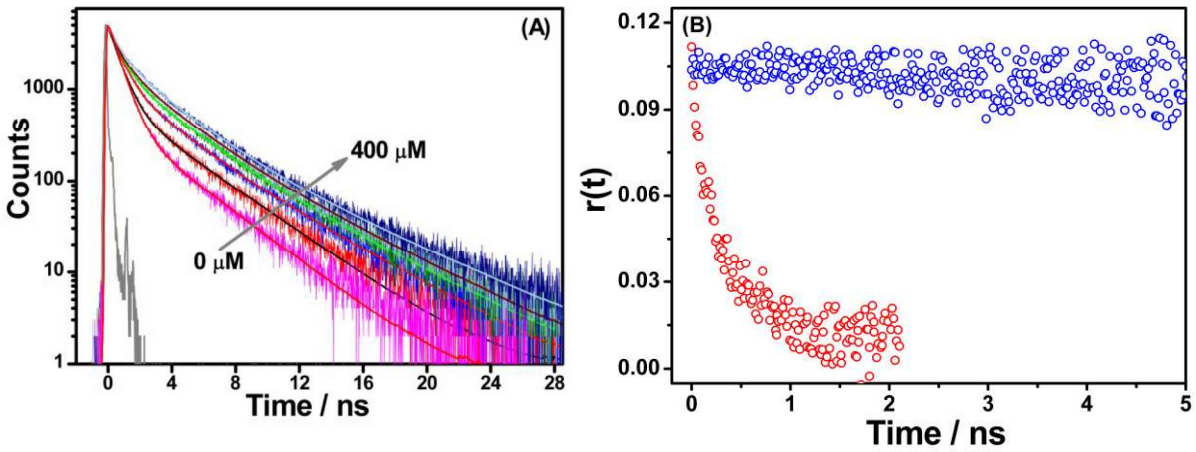

Figure: 5.4. (A) Fluorescence decay traces 1 μM BDZ with increasing concentration of BSA from 0 to 400 μM and **(B)** fluorescence anisotropy decay of 1 μM BDZ in presence of 400 μM BSA in 20% ethanolic PBS buffer (pH = 7.4). The grey line represents the instrument response function (IRF). (λ_{ex} = 445 nm, λ_{em} =531 nm).

Accordingly, the fluorescence decay trace of 1μM BDZ in 20% ethanolic buffer is found to be reasonably fast, showing a bi-exponential nature for the decay, having a fast component with 0.64 ns of major contribution (70.1%) and a reasonably long component of 3.26 ns with minor contribution (29.9%). The bi-exponential feature of the fluorescence decay of BDZ is mainly due to the presence of two conformational structures of the dye (with respect to the position of the N−H group of the benzimidazole unit relative to the BF_2 group) having significantly different lifetime values, arising due to the different extents of H-bonding interactions with the solvent molecules and the associated differences in the non-radiative de-excitation processes.[63] With stepwise addition of BSA to the dye solution, the lifetime values of both the conformers increase substantially with a noteworthy increase in the statistical weight of longer lifetime component (*cf.* Table 5.2). The structural rigidization and restriction towards ICT state formation, in the first excited state, imposed by the less polar and confined BSA cavity, largely retards the non-radiative decay processes, resulting an enhancement of the excited state lifetime values, and thus making the BDZ dye more emissive in nature, in the presence of BSA.

Table: 5.2. Fluorescence decay parameters of 1 μM BDZ in 20% ethanolic buffer (pH 7.4) with increasing BSA concentration from 0 to 400 μM. (λ_{ex} = 445 nm pulsed diode laser, λ_{em} = 531 nm).

Conc. of BSA (μM)	τ_1(ns)	τ_2(ns)	a_1 (%)	a_2 (%)	χ^2
0	0.64	3.26	70.1	29.9	1.02
7.9	0.65	3.56	57.0	43.0	1.18
23.3	0.69	3.69	45.3	54.7	1.3
52.1	0.73	3.80	37.8	62.2	1.44
97.2	0.80	3.88	34.7	65.3	1.54
156.9	0.85	3.95	33.8	66.2	1.68
240.7	0.91	4.04	34.1	65.9	1.77
328.2	0.93	4.10	34.5	65.5	1.77
397.1	0.95	4.12	34.8	65.2	1.85

5.3.5. Time-Resolved Fluorescence Anisotropy Measurement

We carried out time resolved fluorescence anisotropy measurements to get more information on the complexation dynamics of BDZ with the BSA host. Formation of the complexes between guest and host molecules substantially increases the effective molecular volume of the guest as compared to its free state.[30, 35, 56, 80, 96, 113, 114, 261] This increase in molecular volume largely slows down the rotational relaxation rate of the guest, resulting in the enhancement of the rotational relaxation time for the guest. In the present study, the fluorescence anisotropy decay of the free BDZ in 20% ethanolic buffer is found to be single exponential in nature (*cf*. Fig 5.4B), yielding the rotational relaxation time to be about 0.15 ns. However, in the presence of 400 μM BSA, the anisotropy decay becomes exceedingly slow. As evident from Fig. 5.4B, the time-dependent fluorescence anisotropy for BDZ-BSA system displays an insignificant decay within the experimental time-window, which cannot produce any meaningful estimate of rotational correlation time from the experimental data. Observation of such an ultraslow rotational relaxation rate is a representative of the formation of dye-BSA inclusion complex, where the rotational diffusion of the bound probe molecule is

exceedingly retarded. Thus, there is a good correlation between the steady-state emission and excited-state lifetime measurements where it is concluded that BDZ molecule undergoes strong complexation with BSA.

5.3.6. Effect of Ionic Strength on BDZ-BSA Complexation

The presence of electrostatic forces on the host-guest complexation process can be readily envisaged by observing the effect of ionic strength in the host-guest systems. The increase in the salt concentration or ionic strength of the solution markedly reduces the complexation process if the interaction between the host and guest is electrostatic or ion-dipole in nature.[180] This is also reflected clearly by the decrease in the binding constant of the complexation process in presence of the salt. When host is anionic and the guest is cationic in nature, as encountered in many host-guest systems, the cations from the added salt compete for the negatively charged host binding sites. Moreover, the added salt screens the electrostatic or ion-dipole interactions between the negatively charged host and the positively charged guest molecules, diminishing the binding interaction. Understanding the effect of ionic strength on the host-guest complexation is thus an important aspect in supramolecular chemistry.

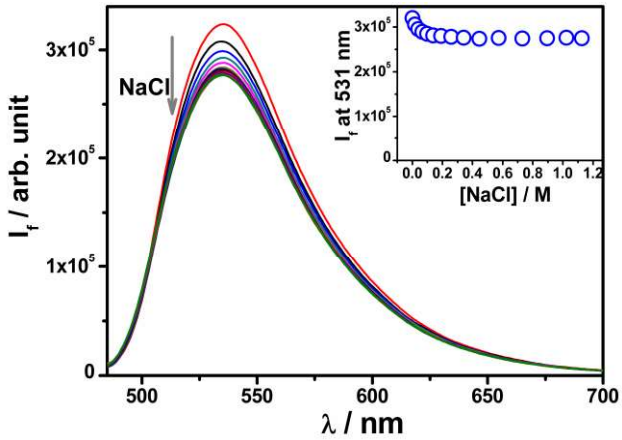

Figure: 5.5. Effect of increasing NaCl salt concentration (0 to1.2 M) on emission intensity of 1 μM BDZ in the presence of 105 μM BSA in 20% ethanolic PBS (λ_{ex} = 475 nm, pH 7.4)

In the present study, the increase in the NaCl salt concentration in the solution containing the BDZ-BSA complex results only a marginal reduction in the emission intensity as shown in Fig. 5.4. This subtle drop in fluorescence intensity for the dye-BSA complex for the initial NaCl concentration from 0 to 0.4 M (*cf*. Figure 5.5) can be attributed to the decrease in the water content around the binding site that selectively binds the BDZ molecule. It is to be noted that the increase in the salt concentration further, there is no significant effect on fluorescence intensity as well as on the position of the emission peak. Observed ionic strength dependent results effectively suggest that the binding between BDZ and BSA does not involve electrostatic or ion-dipole interaction, rather the dye binds to BSA pocket involving hydrophobic interaction predominantly.

5.3.7. Effect of Denaturing agent, Guanidine hydrochloride on BDZ-BSA Complexation

In order to get an idea about the binding of BDZ to a particular form of BSA i.e. to the natural form or denatured form, the emission characteristics of BDZ-BSA complex was monitored with increasing concentration of a denaturing agent like guanidinium hydrochloride (GndHCl). GndHCl at high concentration is known to rupture the secondary protein structure, making them randomly coiled, making most of the hydrophobic pockets present in the protein structure (in this case BSA) to become exposed to the bulk water,[184] thereby reducing both hydrophobic and electrostatic interactions for the guest molecules.

In the present study, it is observed that the gradual addition of GndHCl to 20% ethanolic PBS solution containing BDZ-BSA complex, resulted in a systematic reduction for the emission intensity of the dye, as clearly indicated from the plot in Fig. 5.5. Addition of GndHCl results in the unfolding of the secondary structures of BSA and hence the hydrophobic pockets, which are buried inside BSA molecules in the native form, get exposed to the bulk water. Thus, the dye molecules which were attached to the specific BSA pockets initially are easily released to the bulk aqueous phase in the presence of GndHCl, which

resulted in a dramatic reduction in the fluorescence intensity of the BDZ-BSA system. Observed results clearly indicate that BDZ selectively binds to the native form of the BSA as compared to its denatured form. Note that the decrease in emission intensity observed in the present system by addition of GndHCl might also be caused by the variation in pH of the solution caused by the addition of molar concentration of GndHCl into the solution, because BDZ dye is known to be a pH sensitive probe.[63, 109] To check this aspect, we recorded the changing pH of the solution by the addition of 7.5 M GndHCl, which resulted a lowering of pH by about 1.2 units (from 7.4 to 6.2). Interestingly, however, such a decrease in pH for BDZ solution in the presence of BSA actually leads to an increase in the fluorescence intensity of BDZ than decreasing (Fig. 5.7A and 5.7B).

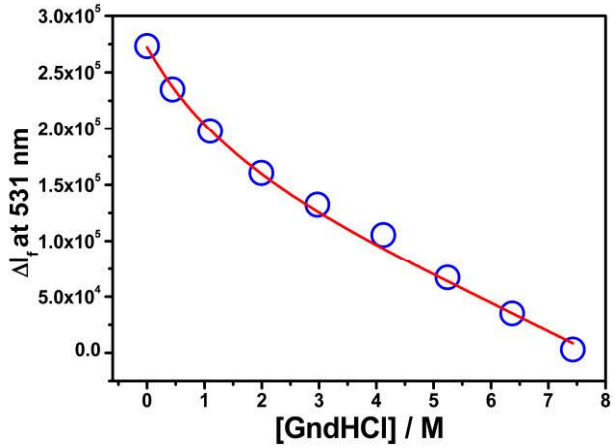

Figure: 5.6. Relative changes in emission intensity at 531 nm of 1μM BDZ-150μM BSA complex with increasing GndHCl concentration from 0 to 7.5 M in 20% ethanolic PBS (pH = 7.4, λ_{ex} = 475 nm).

Thus, the variation in pH (~1.2 unit) cannot account for the decrease in fluorescence intensity observed for BDZ-BSA system in the presence of GndHCl (*cf.* Fig. 5.6). We further checked if there was any specific quenching interaction for the free BDZ probe with GndHCl as a quencher that might contribute to the reduced fluorescence intensity observed for the BDZ-BSA system by the addition of GndHCl. However, the addition of GndHCl to the free BDZ probe actually leads to an increase in the emission intensity which can be attributed to the decrease in the pH as GndHCl is added to the solution. Therefore, it can be definitely

stated that observed results clearly indicate that BDZ selectively binds to the native form of the BSA as compared to its denatured form.

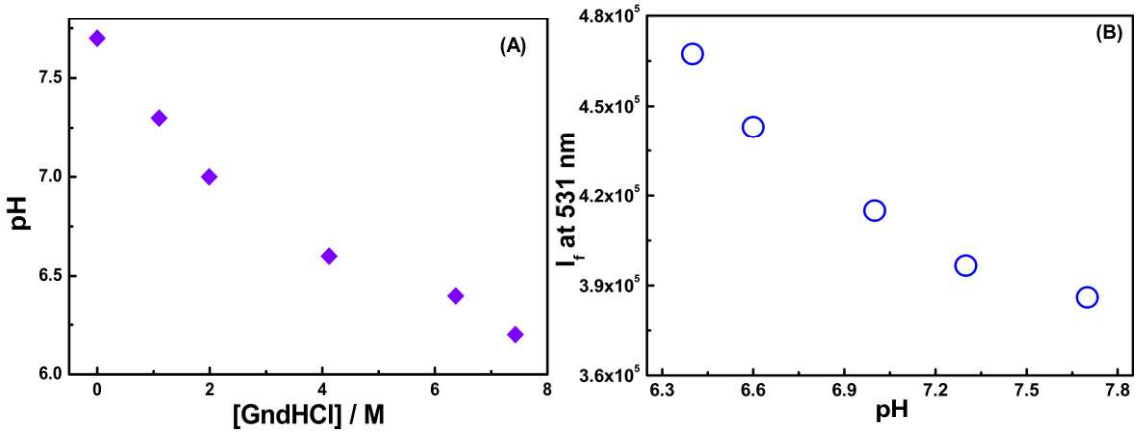

Figure: 5.7. (A) The changes in pH of blank 20% ethanolic PBS with increasing GndHCl concentration from 0 to 7.5 M and **(B)** Variation in intensity at 531 nm of 1µM BDZ-150µM BSA complex with change of pH of the solution from pH 7.4 to 6.2.

5.3.8. Molecular Docking Calculations and Competitive Binding Studies

Molecular docking calculations are frequently employed to gain important information regarding the preferred binding location in the host-guest systems, and provide important insights into the interaction forces responsible for the protein-ligand bindings. Thus, to get an idea about the most probable binding location for BDZ, in the 3-dimensional structure of BSA, we have performed molecular docking calculations for BDZ-BSA system using Autodock Vina. In the present case, the molecular docking calculations suggest site IB of BSA as the most preferred binding location for BDZ with the free energy of binding as −10 kcal/mole. The docked conformation of BDZ-BSA complex has been presented in Figure 5.6A, which was found to be stabilized by various non-covalent interactions (Figure 6B), such as van der Walls interaction, π-alkyl, amide-π stacking interaction along with π-anion and π-sigma interactions.

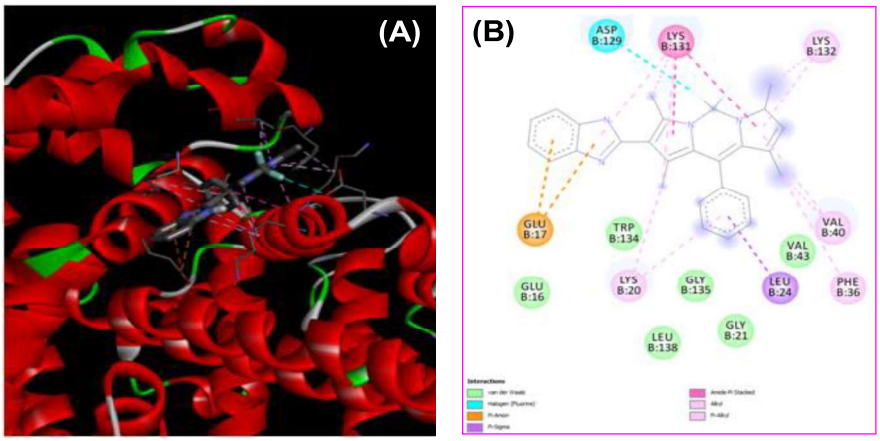

Figure: 5.8: (A) Binding site of BDZ in BSA. BDZ is shown in the ball and stick model. **(B)** Two-dimensional schematic diagram representing interactions between BDZ and neighboring residues of BSA.

To validate this binding picture obtained from molecular docking calculations, we have also performed some competitive binding experiments using the known albumin binding ligands, such as, warfarin and ibuprofen. As evident from Fig. 5.9; in the presence of the competitive binder warfarin, a selective binder for domain IIA (Sudlow's site-I) of BSA,[184, 186, 187] there is no apparent change in the binding isotherm for the BDZ-BSA pair. This observation suggests that BDZ dye does not have any reasonable binding affinity towards Sudlow site-I of BSA. On the contrary in presence of ibuprofen as the competitive binder, which is a selective binder to the domain IB of BSA, the binding isotherm for the BDZ-BSA system was found to be modulated quite significantly. The reduction in binding strength (from 1.38×10^4 M^{-1} to 8.2×10^3 M^{-1}) between BDZ and BSA in the presence of 200 μM ibuprofen evidently indicates the selectivity of BDZ binding into the domain IB of the BSA protein.

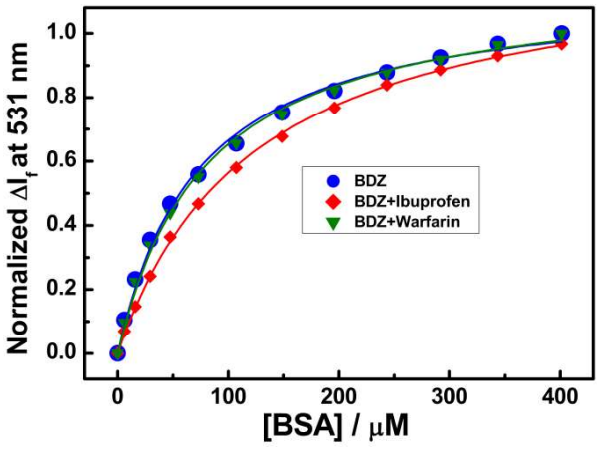

Figure: 5.9. Binding isotherm for BDZ-BSA system in the absence of any competitive binder (blue circle), in the presence of 200 μM warfarin as a competitive binder for domain IIA (Sudlow's site-I) (green triangles) and in the presence of 200 μM ibuprofen as a competitive binder for domain IB (red square) of the BSA protein.

5.4. Conclusion

Non-covalent interaction of synthesized BODIPY-benzimidazole conjugate (BDZ) dye with bovine serum albumin (BSA) has been investigated using a variety of photophysical techniques. BDZ found to interact quite strongly with BSA, as indicated from the high binding constant of (1.38±0.09) $x10^4$ M^{-1} for BDZ-BSA pair. The binding of BDZ with BSA causes significant enhancement in the emission intensity of the dye, attributed to the large structural immobilization of the dye inside the binding pocket of BSA as well as to the reduced propensity of the dye to form weakly emissive ICT state in the lower micro-polarity of the environment around the BSA binding cavity. These results were further supported by excited-state lifetime as well as by time-resolved anisotropy measurements. The binding of BDZ to BSA is suggested to be dominated by hydrophobic interaction as revealed from ionic-strength dependent measurements and molecular docking calculation which suggested the domain IB of BSA to be the most probable binding site for BDZ. Further, we have also established through guanidinium hydrochloride induced denaturation of BSA that the BDZ dye preferentially binds to the native form of the BSA as compared to its denatured form. The strong and selective binding of BDZ with BSA and its excellent fluorescence response towards the native form of BSA, make the studied BDZ-BSA system an efficient choice for bio-imaging study, identification of native structure of BSA protein, and to understand the transport mechanism of similar kinds of drugs and other metabolites with the serum proteins.

CHAPTER-6

A HIGHLY FLUORESCENT TURN-ON PROBE IN THE NEAR-INFRARED REGION FOR ALBUMIN QUANTIFICATION IN SERUM MATRIX

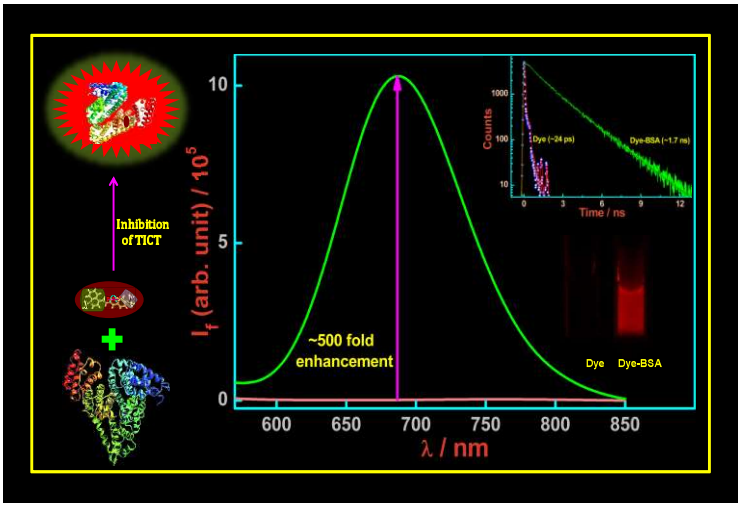

6.1. Introduction

In animal's circulatory system albumin is the most abundant protein, which is produced in the liver and mostly exists in plasma with a half-life of 19–21 days.[184-187] Albumin plays an important role to regulate the plasma osmotic pressure by maintaining the water equilibrium between tissues, and is crucially involved in the transport of various endogenous and exogenous ligands such as bilirubin, thyroxine, free fatty acids and a variety of drugs from one location to another in the body.[184-187, 191, 226, 228, 264, 266, 267] The optimum concentration of albumin (35–50 g/L in serum and ~ 30 mg/L in urine) is considered as a reliable marker of good health because of the involvement of albumin in various crucial biological processes.[292] The alteration of albumin concentration in body fluids gives an indication of progression of many human diseases like kidney failure, diabetes mellitus, hypertension, liver injury, post-menopausal obesity, etc.[293-296] While an increased level of albumin is an indication of kidney disease, a low level of albumin may cause cirrhosis, chronic hepatitis and liver failure.[227, 294] An unusual decrease in serum albumin concentration

points towards diabetes, as diabetes inhibits the metabolism of the serum protein.[227, 293, 295] Rapid decrease in serum albumin concentration also causes hemorrhea and burns, which ultimately lead to edema, if left untreated for a prolonged period.[227, 294] Thus, periodical quantification of serum albumin in body fluids is extremely necessary in order to maintain physiological activity uninterrupted. Serum composed of a variety of other components like fats, carbohydrates, hormones, peptides, growth factors, inorganic substances and so on [ref], which can interfere with the analysis and quantification of albumin. Hence, quantification of albumin is extremely important in biological matrices, which finds immense application in both clinical diagnosis and biomedical research. To determine albumin concentration in blood plasma, various methods have been employed, which include capillary electrophoresis, immunoassays, fluorimetry and colorimetry. Most of these methods suffer from lack of selectivity and require high precision instrumentation and lengthy procedures.[52, 126, 127, 192, 240, 259, 297-301] Fluorescence methods, however, provide an attractive and powerful tool by virtue of their excellent simplicity, selectivity, sensitivity, rapid response, non-destructive nature and very simple instrumentation. There are numerous examples documented in the literature mentioning about various fluorescent probe molecules, which display distinct changes in their fluorescence attributes, in response to albumin.[36, 52-55, 129-133, 199, 227, 233, 259, 261, 266, 270, 302-306] In this regard, fluorescent probes which are highly sensitive to the polarity and viscosity of the medium are quite attractive. For example, fluorescent probes which involve intramolecular rotation and weakly emissive charge transfer states can undergo large modulation in their emission yield upon reduction in the polarity and increase in the viscosity of the medium[29, 30, 33, 117, 155, 261, 307-309] and provide an important selection criterion for detection of albumins. However, a majority of these probes have their absorption and emission spectra in the UV-visible region, which suffer from the problems of severe auto-fluorescence from biological matrices, large scattering from tissue components and low photon penetration, leading to low

signal to background ratios and poor sensitivity. However, fluorescent probes emitting in the near IR region overcome many of these disadvantages and offer various advantages such as minimum auto-fluorescence by biomolecules, deep tissue penetration, low light scattering and minimum photo-damage to biological samples.[253] Thus, it is highly desirable to develop fluorescent probes for albumin detection in the near-IR region. Towards this aim, few fluorescent probes have been developed through dedicated synthetic attempts; however, a majority of them show limited enhancement in fluorescence intensity (turn-on response) in the presence of serum albumins when compared with their aqueous buffer solution.[54, 55, 130, 132, 134, 187, 227, 233, 259, 260, 269, 304, 306, 310] In this study, we report a styryl based molecule (LDS-798, see Scheme 6.1), which is commercially available in high purity and displays an exceptionally high fluorescence enhancement of ~500 fold in presence of albumin, the highest reported so far in the near-IR region, and most importantly enables quantification of albumin protein in the complex serum matrix.

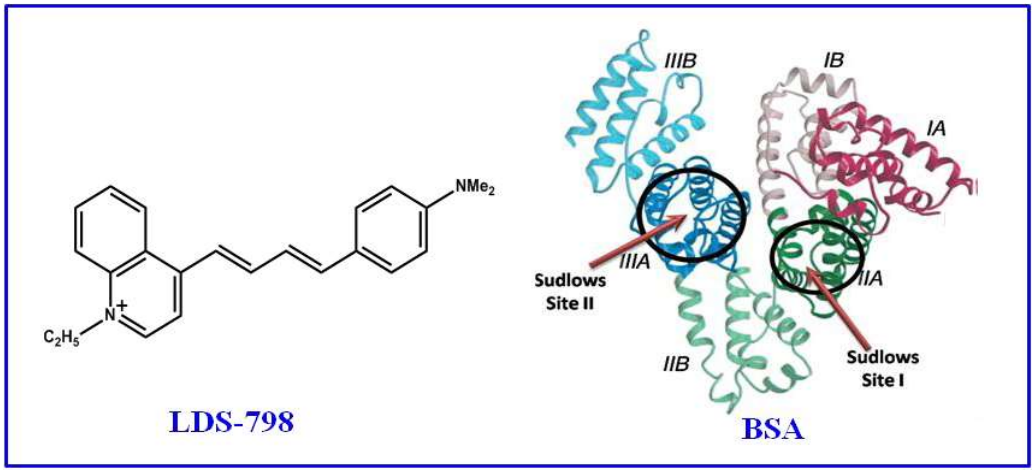

Scheme: 6.1. Schematic presentation of LDS-798 and Bovine Serum Albumin (BSA).

6.2. Materials and Methods

Laser grade 1-ethyl-4-(4-(p-dimethylaminophenyl)-1,3-butadienyl)-quinolinum percholate (LDS-798 or styryl-11) was procured from Lambda Physik, Germany and was used as received. BSA (pH 7 fraction, purity > 99%) was obtained from Sisco Research Laboratory

(SRL), India. Ibuprofen, warfarin, aspartic acid, cystein, lysine, histidine, hemoglobin, myoglobin, lysozyme from chicken egg white, trypsin from porcine pancreas, ovalbumin from chicken egg white, were procured from Sigma-Aldrich and were used as received. All the sample solutions were prepared in 10 mM aqueous phosphate buffer saline (PBS, pH ~7.4). Fetal Bovine Serum (FBS) was obtained from Himedia Laboratories (India) and was used as received. All the measurements were carried out at ambient temperature, i.e. at 25±1°C. Human blood serum samples were collected from BARC Hospital, Mumbai. Serum samples were treated following the well-known trichloroacetic acid-acetone method for further estimation of albumin content in human serum.[311] The human serum albumin (HSA) level in the serum samples, using LDS-798 as fluorescent probe, was estimated by the standard addition method. For the validation of the results obtained by LDS-798, the HSA level in the human serum samples were also estimated by a well-established photometric method which uses bromophenol blue dye as the probe.[271] The statistical analysis of the results obtained for human serum samples were performed using unpaired Student's t-test with the help of GraphPad software.

Ground state absorption studies were carried out using a Thermo-Scientific UV-vis spectrophotometer in an optical quartz cell of 10 mm path length. Steady-state (SS) fluorescence measurements were carried out using a Horiba fluoromax-4 spectrofluorimeter in 10 mm x 10 mm quartz cuvette. During the fluorescence studies, the LDS-798 dye samples were excited at 525 nm. Time-resolved (TR) fluorescence measurements were carried out using a Time Correlated Single Photon Counting (TCSPC) spectrometer obtained from Horiba Jobin Yvon IBH, U.K. In TCSPC measurements, A 445 nm pulsed diode laser (pulse width 120 ps and repetition rate 1 MHz) was used as the excitation source and the fluorescence decays were recorded at the emission maximum of the dye-BSA complex (~688 nm) using a

micro channel plate photomultiplier tube (MCPPMT) based detection module (IBH, U.K.). Further details of the TCSPC set up are provided in Chapter-2.

Determination of fluorescence quantum yield: The emission quantum yield (φ) of LDS-798-BSA complex was determined by comparing the integrated emission intensities of LDS-798-BSA complex with that of the LDS-798 in ethanol as reference (φ=0.0076)[155] using the following equation,[107]

$$\varphi_s = \varphi_r \frac{I_s A_r n_s^2}{I_r A_s n_r^2} \tag{6.1}$$

where, the subscripts r and s refer to the reference (LDS-798 in ethanol) and sample (LDS-BSA complex) respectively; 'I' represents the integrated area under the emission band; A denotes the absorbance of the solution at the excitation wavelength (λ_{ex} = 525 nm) and n is the refractive index of the solvent.

6.3. Result and Discussion

6.3.1. Ground-State Absorption Studies

Ground state absorption studies give an idea about the binding interaction between host and guest pair. In aqueous buffered solution the dye, LDS-798 displays an absorption band with maximum at ~500 nm. Upon gradual addition of BSA to LDS-798 solution, there is a large bathochromic shift (~40 nm), along with a slight reduction in the absorbance value (Fig. 6.1B). Interestingly, the red-shift observed in the absorption spectra is in contrast to the large blue shift observed in the emission spectra discussed latter. Such contrasting solvatochromism, though quite uncommon for most organic dyes, is seen to be observed sometimes, especially with charged push–pull polyenes (for example LDS-798), and has been explained in terms of the mixing of two valence bond states of the molecules, namely the D–Bridge–A+ and D+–Bridge–A.

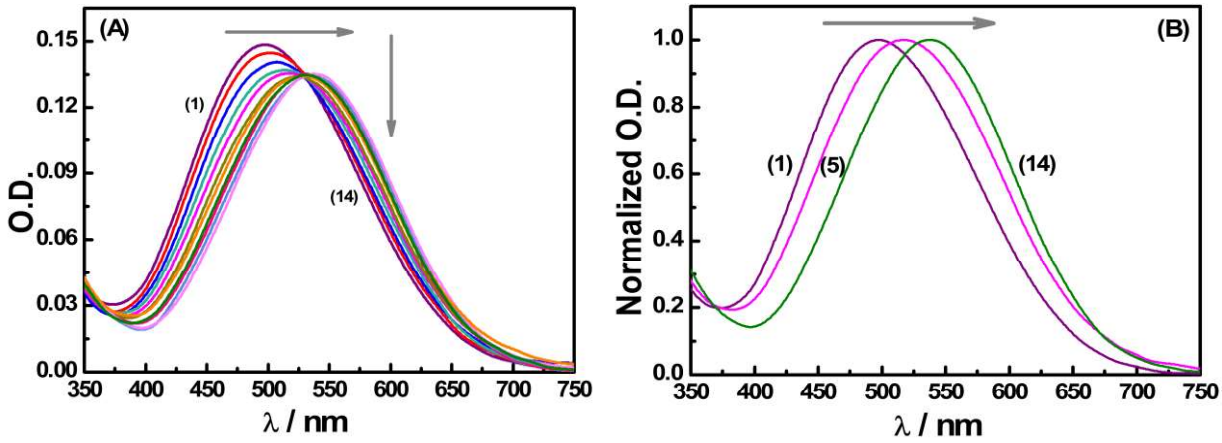

Figure: 6.1 (A) Absorption spectra of 10 µM LDS-798 upon increasing BSA concentration from (1) 0 to (14) 322 µM [pH = 7.4 (10 mM PBS)]. **(B)** Peak normalized absorption spectra of 10 µM LDS-798 in PBS at (1) 0 µM, (5) 50 µM and (14) 322 µM BSA.

6.3.2. Steady-State Fluorescence Studies

In aqueous solution, LDS-798 displays a very weak and broad emission band in the 600 to 850 nm region with a peak at ~763 nm. However, with gradual addition of BSA up to 300 µM to the PBS solution of 10 µM LDS-798, a large fluorescence enhancement (~500 fold) is observed along with a substantial blue shift (~75 nm, i.e. from 763 to 688 nm, *cf.* Fig. 6.1A) in the emission maxima. To the best of our knowledge, such enormous turn-on emission response towards BSA, which decides the sensitivity of a given probe, has not been reported so far for any fluorescent probe in the near or far-IR region. Due to its highly flexible structure and its ability to form a TICT state in its excited state, LDS-798 is almost non-fluorescent in aqueous solution. It is reported that styryl based dyes display very rich solvatochromism and the decrease in solvent polarity significantly enhances the fluorescence yield of these molecules.[117, 155, 254, 255] Very recently, it has also been reported that the fluorescence quantum yield of LDS-798 increases linearly with viscosity of the medium/solvent, when the polarity is kept constant.[117, 155] This suggests that the large amplitude conformational motions contribute significantly to the rate of non-radiative de-excitation process of the dye in aqueous solution.

Addition of BSA to the solution of LDS-798, results in the relocation of the dye molecules from the highly polar aqueous buffer medium to the relatively hydrophobic BSA

pockets of lower micro-polarity. Thus, on binding to the BSA pocket, the guest dye molecules experience a largely reduced polarity and restricted conformational flexibility. Hence, the enormous increase in the fluorescence intensity of LDS-798, in the presence of BSA, is attributed to the binding of the dye with the BSA molecule that leads to largely reduced structural flexibility of the dye, possibly inhibiting the formation of the non-fluorescent TICT state as well. Further, the large blue-shift in the emission spectra is in accordance with the strong solvatochromic behavior of LDS-798 and indicates that LDS-798 experiences a significantly reduced polarity when it is transferred from the aqueous phase to the BSA binding site.

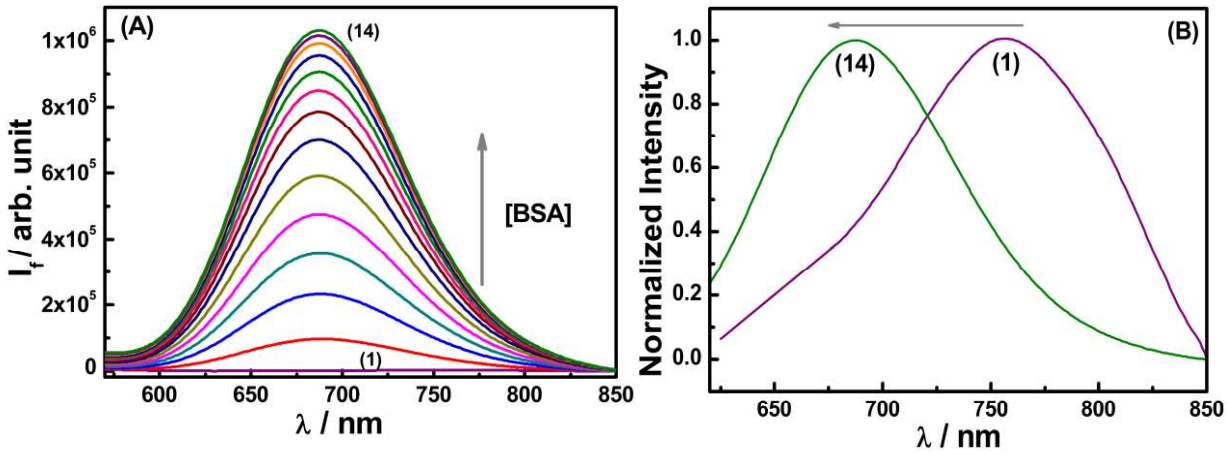

Figure: 6.2 (A) Fluorescence spectra of 10 μM LDS-798 upon increasing the BSA concentration from (1) 0 to (14) 322 μM [λ_{ex} = 525 nm, pH = 7.4 (10 mM PBS)]. **(B)** Peak normalized emission spectra of 10 μM LDS-798 in PBS at 0 and 322 μM BSA.

6.3.3. Determination of Stoichiometry of LDS-798-BSA complex

In our present study, both the absorption and fluorescence of LDS-798 show substantial changes upon host addition, but the changes in the emission intensity are exceptionally high. Hence, we used the changes in the fluorescence intensity for the determination of the stoichiometry of the LDS-798-BSA complex. By plotting the relative changes in the emission intensity against the mole fraction of BSA resulted an inverted Job's

plot with maximum at ~0.5 (*cf.* Fig. 6.2) of the x-axis, supporting the 1:1 stoichiometry of the LDS-798-BSA complex formed in the studied system.

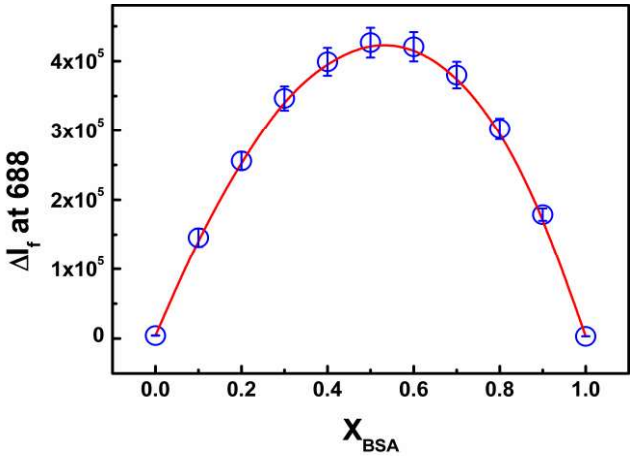

Figure: 6.3. Job's plot for LDS-798-BSA system obtained from the emission intensity changes ($\Delta I_f = I_{LDS798\text{-}BSA} - I_{LDS798\text{-}Buffer}$) at 688 nm as a function of the mole fraction of BSA (X_{BSA}). The sum of the concentrations of the LDS-798 and the BSA was kept at 20 μM.

6.3.4. Determination of the Binding Constants

As discussed in the previous chapters, binding constant in supramolecular chemistry is generally estimated by non-linear fitting of the changes in fluorescence intensity for a constant concentration of the probe in the solution as function of the changing concentration of the host.[14, 28, 30, 32-35, 59, 80, 82, 112, 124, 163, 164, 169, 217] In the present study, the non-linear fitting of the concentration dependent fluorescence changes (*cf.* Fig. 6.4A) using a 1:1 binding model yielded the binding constant of LDS-798-BSA complex as ~ (1.27±0.02) x10^4 M^{-1}, suggesting very strong binding affinity of LDS-798 for BSA host. For the present system, the limit of BSA detection in aqueous medium was calculated using the initial apparently linear region of the plot for 0 to 50 μM BSA concentration (*cf.* Fig. 6.4B) and found to be 48 nM.

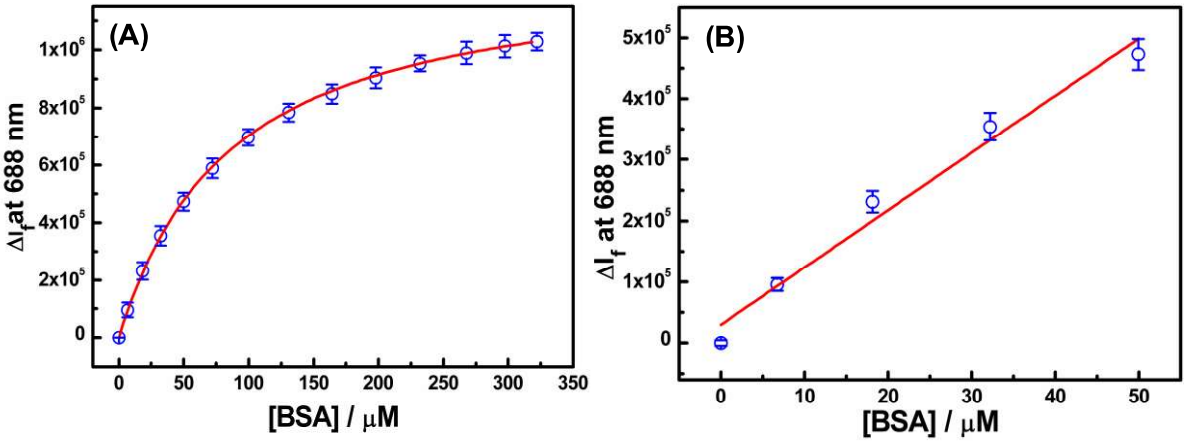

Figure : 6.4. (A) Binding isotherm for 10 μM LDS-798 with the increasing BSA concentration from 0 to 322 μM. **(B)** Apparently linear plot of the initial changes in the emission intensity of LDS-798 with the increasing BSA concentration in PBS solution (pH = 7.4). This plot is utilized for LOD determination, estimated to be 48 nM of BSA. (I_{688} = 9.386 x 10^3 [BSA/μM] + 29841, R^2 = 0.972).

Calculation of limit of detection (LOD) was doen using the following equation,

$$\text{LOD} = \frac{3\sigma}{s} = \frac{3\text{x}147.84}{9.386\text{x}10^3} = 47.25\text{nM} \qquad (6.2)$$

where, σ = standard deviation, which was obtained by taking 10 measurements of the 10 μM LDS-798 in buffer at identical condition and found to be 147.84, S = slope of the linear fit curve and is equal to be 9.386 x 10^3 M^{-1}.

Although LDS-798 shows enormously large fluorescence response towards BSA, to proceed more towards real applications, we checked the response of this probe towards human serum albumin (HSA). Therefore, we also tested the response of LDS-798 towards HSA (Fig. 6.5A), and the obtained binding constant ~(1.86±0.05) x $10^4 M^{-1}$, also found to be very similar to that obtained for BSA (*cf.* Fig. 6.5B).

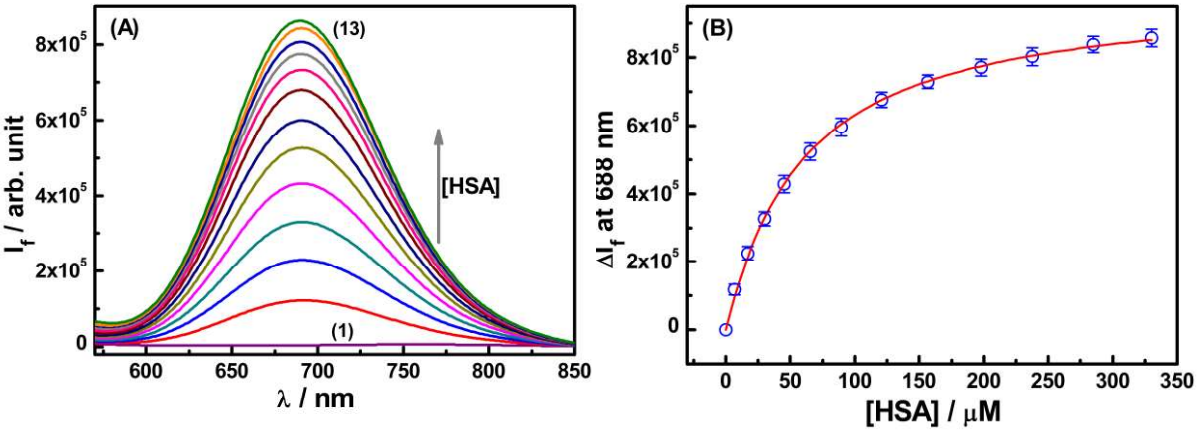

Figure: 6.5. (A) Fluorescence spectra of 10 μM LDS-798 upon increasing concentration of HSA from (1) 0 to (13) 330μM **(B)** Binding isotherm for 10 μM LDS-798 with the increasing HSA concentration from 0 to 330 μM [λ_{ex} = 525 nm, pH ~7.4 (10 mM PBS), blue circles denote the experimental data points and the red solid line indicates the fitting curve].

6.3.5. Excited-state Lifetime Measurements

To get an idea about its excited state dynamics of the BSA bound LDS-798, we performed excited state lifetime measurements of 10 μM LDS-798 in the presence and in the absence of 300 μM BSA in 10 mM PBS solution. In aqueous buffer solution, the fluorescence decay of free LDS-798 is exceedingly fast due to its large molecular flexibility and its ability in the excited state to undergo non-fluorescent twisted intramolecular charge transfer (TICT) state formation, which causes the excited LDS-798 molecules to dissipate their excited state energy very fast in non-radiative pathway, making the lifetime of the dye extremely short (~24 ps).[117, 155, 254, 255] Hence, the fluorescence decay of free LDS-798 in PBS buffer could not be recorded reliably using our TCSPC set up due to its limited time-resolution (0.12 ns). However, when BSA is added to 10 μM LDS-798 solution (in 10 mM PBS), the decay traces become drastically slower as shown in Fig. 6.6A. The bi-exponential fitting of the obtained decay trace of LDS-798-BSA system yielded two lifetime components; the major one of 1.92 ns with 83.5% contribution and the minor one of 0.62 ns with 16.5 % contribution. The average excited state lifetime of LDS-798, in the presence of BSA, is thus calculated to be about 1.7 ns. This drastic increase in the lifetime of LDS-798, in presence of BSA, is

corroborated to the huge emission enhancement observed in the steady-state emission measurements. The increase in the lifetime strongly suggests that the binding of LDS-798 to BSA substantially reduces the molecular flexibility as well as the propensity of the TICT state formation of the dye, resulting in a significantly reduced non-radiative decay rate of the excited dye upon its relocation from the bulk PBS solution (k_{nr} = 4.1 x 10^{10} s^{-1}) to the BSA binding pocket (k_{nr} = 5.1 x 10^{8} s^{-1}).

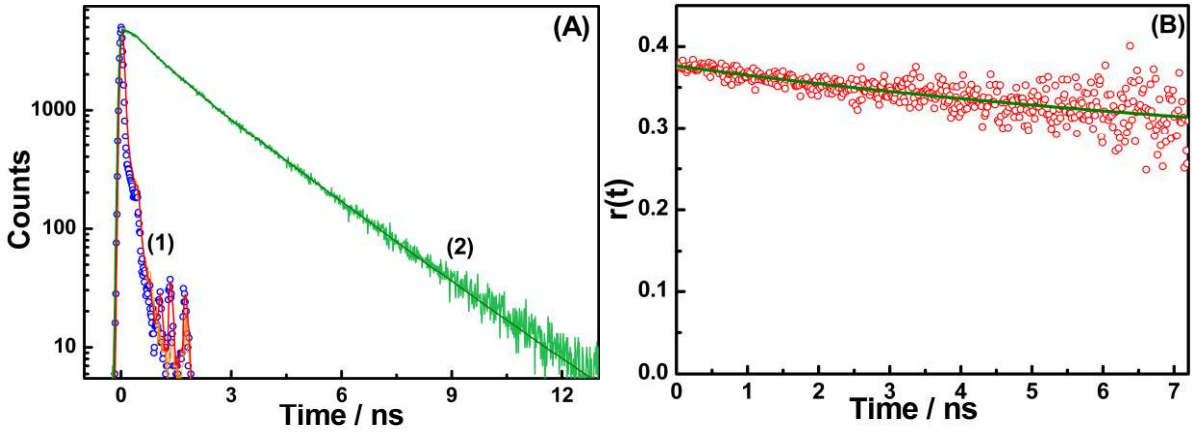

Figure: 6.6 (A) Fluorescence anisotropy decay of 10 µM LDS-798 in the absence (1) and presence (2) of 300 µM BSA. The blue dotted line represents the instrument response function (IRF). **(B)** Fluorescence anisotropy of 10 µM LDS-798 in the presence of 300 µM BSA (λ_{ex} = 445 nm, λ_{em} = 688 nm).

6.3.6. Time-resolved Fluorescence Anisotropy Measurement

Time resolved fluorescence anisotropy is also a sensitive tool to get crucial information on the complexation of the fluorescent probes with the host molecules.[33, 35, 46, 47, 63, 80, 112] While the fluorescence anisotropy decay of free LDS-798 in solution is extremely fast and could not be recorded using our TCSPC set up, the fluorescence anisotropy decay of LDS-798 in the presence of BSA becomes exceedingly slow (*cf.* Fig. 6.4B) indicating the BSA bound dye undergoes significant retardation in its rotational relaxation. Such slow fluorescence anisotropy decay suggests substantial confinement of the LDS-798 into BSA cavity. A single exponential fitting of the anisotropy decay trace yields a rotational correlation time > 6.7 ns, along with a large residual anisotropy, which suggests very restrictive rotation

of LDS-798 inside the BSA pocket. Though, the fluorescence anisotropy decay of free LDS-798 in the buffer medium could not be measured, yet on the consideration of the molecular dimensions of LDS-798 and the viscosity of the aqueous buffer medium, the rotational relaxation time of the free dye can be expected to be about 150 ps or less.[63] The strong rigidization of LDS-798 at the binding location in the protein pocket, as indicated by the anisotropy result, is consistent with the massive enhancement in the emission intensity and substantial retardation of the fluorescence decay dynamics of LDS-798 in the protein-bound state.

6.3.7. Competitive Binding Experiment and Molecular Docking Calculation

As discussed earlier, although BSA has many binding sites, it has two major binding pockets, which are denoted as Sudlow's site I (also called the warfarin site), situated in the sub-domain IIA, and Sudlow's site II (also known as the ibuprofen binding site) that exists in the sub-domain IIIA.[184-187] Site I is more spacious where the main operative force is hydrophobic interaction, and site II is less capacious in which the prevailing forces are hydrogen bonding, electrostatic interaction, van der Waals' forces and also hydrophobic forces.[184-187]

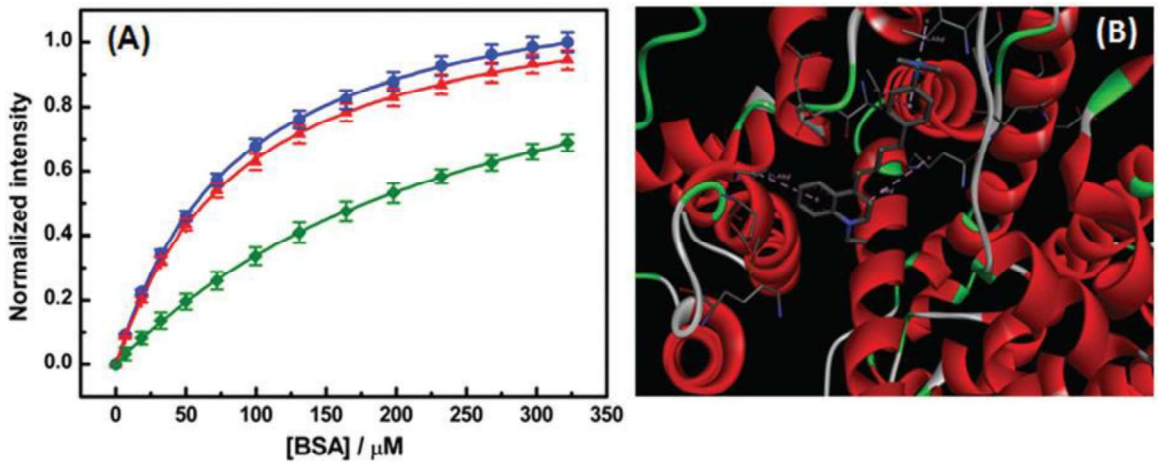

Figure: 6.7. (A) Normalized binding plots of 10 μM LDS-798 with BSA only (blue circles), in the presence of 100 μM ibuprofen (red triangles) and in the presence of 150 μM warfarin (green squares). **(B)** Molecular docking result showing the location of the binding site of the dye (LDS-798) in BSA.

Table: 6.1. Binding constant of LDS-798–BSA system in the absence and presence of the competitive binders.

System	Competitor	Binding constant (K_b)
LDS-798–BSA	—	(1.27±0.02) x 10^4 M^{-1}
LDS-798–BSA	100 μM ibuprofen	(1.23±0.02) x 10^4 M^{-1}
LDS-798–BSA	150 μM warfarin	(3.77±0.06) x 10^3 M^{-1}

Competitive binding experiments with ibuprofen (known binder to site-II) reveals very insignificant reduction in the binding constant of LDS-798 with BSA (Fig. 6.7A), whereas the presence of warfarin (known binder to site-I) leads to a substantial reduction in the binding affinity of LDS-798 to the BSA host (see Table 6.1). These results clearly suggest that LDS-798 predominantly binds to the Sudlow's site-I of BSA, which is known to bind relatively larger guest molecules. This is also nicely supported by molecular docking calculations which are frequently employed to gain important information regarding the preferred binding location, and the interaction forces responsible for the protein-ligand interactions. LDS-798 was found to bind to the Sudlow's site-I of BSA (Fig. 6.7B) with a binding energy of 6.4 kcal per mole. Molecular docking analysis suggests that π-alkyl and π-aryl interactions along with C–H–π bonds are among the prime contributors to the binding interaction between LDS-798 dye and BSA host.

6.3.8. Determination of pK_a value of LDS-798

Being a prototropic dye, LDS-798 shows changes in absorption and emission features depending upon the pH of the solution. Hence, it is needed to determine the acid dissociation constant (pK_a) value of LDS-798 by monitoring the changes in absorption or emission properties with the changing pH of the solution. The absorption and emission features of LDS-798 are found to be very sensitive below pH 5 and show a continuous variation upon changing

pH. Below pH 5, the fluorescence response of this probe decreases due to the changing protonation state of the probe, and such changes in emission feature against pH of the solution yielded the pK_a of this probe as 3.8 ± 0.2 (Fig. 6.8A), very similar to that reported in the literature [ref]. Again, for the practical applicability of a probe, the inherent response of the probe should be ideally invariant with pH over a broad pH range, covering the biological pH region. In this respect, the fluorescence response of this probe remains constant over a wide pH range of 5 to 10 (Fig. 6.8B). Thus, LDS-798 appears to be an ideal fluorescence probe for various biological studies.

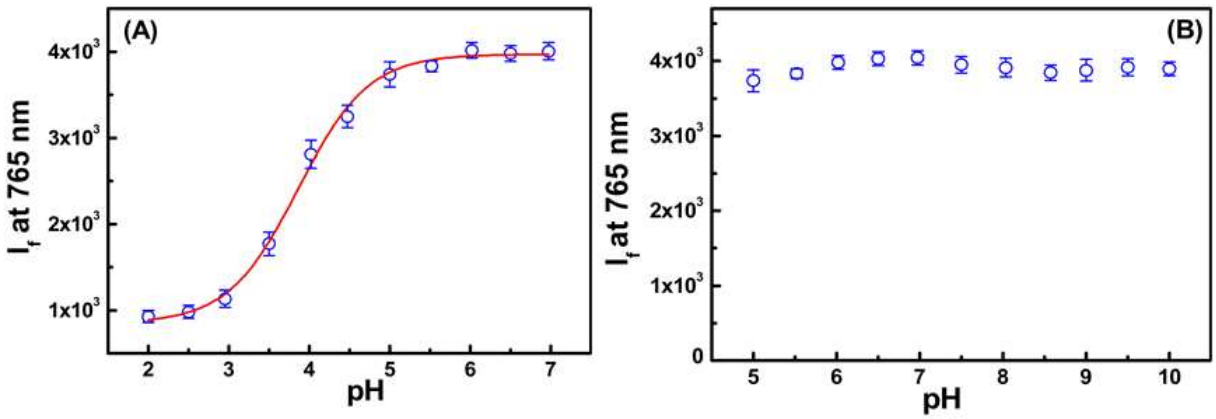

Figure: 6.8. (A) Dermination of pKa of 10 µM LDS-798 by plotting change in emission intensity (denoted by blue circles) with pH [red line indicates the fitting]. The pKa was calculated to be 3.8±0.2. **(B)** Variation of emission intensity of LDS-798 (10 µM) with pH of the medium for the pH range of 5 to 10.

6.3.9. Effect of guanidine hydrochloride on LDS-798-BSA complex

Another important aspect towards selectivity of LDS-798 in albumin detection is the condition that the probe should be selective to the native form of BSA and should not respond to the denatured form of BSA. To check this aspect, the denaturation of BSA was carried out with a well-known protein denaturant, guanidine hydrochloride (GndHCl), and the results are presented in Fig. 6.9. At high concentration, GndHCl ruptures the protein structure, making it randomly coiled. As a result, the hydrophobic pockets of BSA get exposed to the bulk solution. Accordingly, addition of GndHCl resulted in a dramatic reduction in the emission intensity of the LDS–BSA system. At higher concentrations (> 5 M) of GndHCl, complete

rupture of the BSA structure takes place and all the dye molecules are released into bulk water solution, causing a complete quenching of the fluorescence of the LDS-798–BSA system. Moreover, along with this decrease in emission intensity, the emission peak also gradually shifts from 688 nm to 750 nm, which also supports the nearly quantitative release of the dye from the BSA pocket into the bulk water.

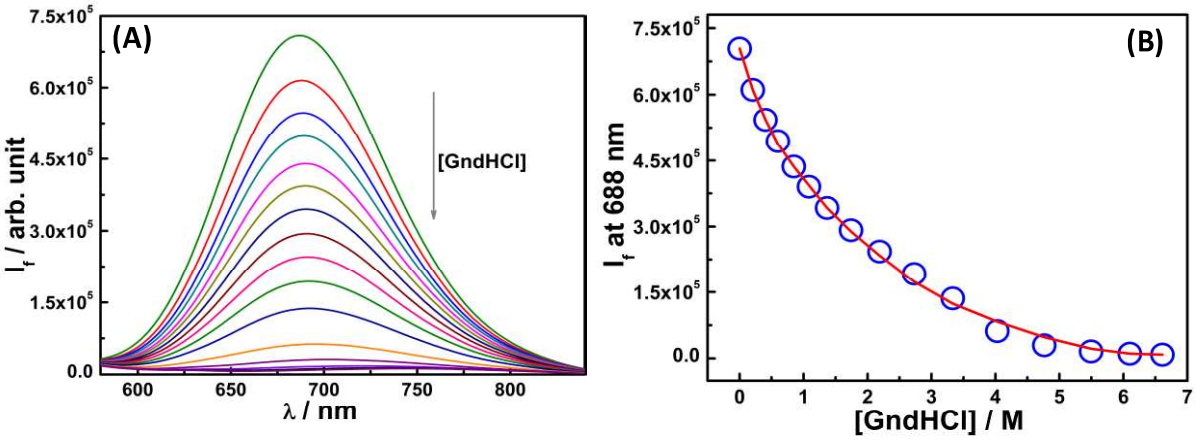

Figure: 6.9. Decrease of fluorescence intensity of 10 μM LDS-798+105 μM BSA complex with increasing concentration of GndHCl from 0 to 6.8 M. [λ_{ex} = 525 nm, pH ~7.4 (10 mM PBS)].

6.3.10. Selectivity of LDS-798 towards BSA

Selectivity is a very important criterion for the practical use of a probe as a sensor. For the present sensor probe, to evaluate the selectivity towards BSA, different biological agents (viz., proteins, porphyrins, amino acids) of the same concentration as BSA were tested for the fluorescence response of LDS-798. We also tested the responses of various inorganic substances (such as NaCl, KCl, $CaCl_2$, NaH_2PO_4) which are common inorganic constituents of human serum. Fig. 6.10 summarizes the results of these measurements. As evident from the figure, LDS-798 emission shows the largest response towards BSA, while the responses of the probe towards the other interfering analytes are either very small or insignificant. The binding of LDS-798 in the well-defined binding pocket of BSA presumably leads to such a large specificity. The present results suggest that LDS-798 is quite selective towards BSA.

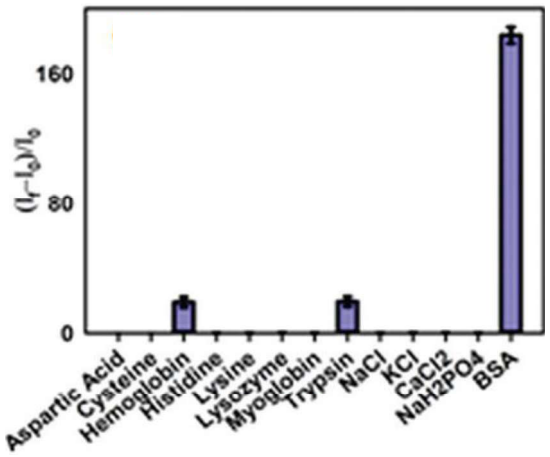

Figure: 6.10. Relative changes in the fluorescence intensity of LDS-798 (10 μM) upon addition of different proteins (20 μM), amino acids (20 μM) and various inorganic substances: NaCl (0.15 M), KCl (0.06 M), $CaCl_2$ (0.17 M) and NaH_2PO_4 (0.1 M); λ_{ex} = 525 nm and λ_{em} = 688 nm.

6.3.11. *In situ* Quantification of Serum Albumin by LDS-798 in Complex Serum Matrix

6.3.11A. Quantification of Albumin in 5% FBS Medium

To evaluate the practical usefulness of the studied system for albumin detection in real biological samples, we attempted to detect albumin in fetal bovine serum (FBS) using LDS-798. In 5% FBS containing LDS-798, the fluorescence intensity of LDS-798 increased linearly with increasing concentration of bovine serum albumin up to about 60 μM (Fig. 6.11B). The LOD in this case is found to be 1.6 μM, which is well within the biological concentration region of albumin in body fluids. It is to be noted that due to the presence of other biological components present in the FBS matrix, the initial counts of 10 μM LDS-798 in 5% fetal bovine serum (FBS) was quite high as compared to 10 μM LDS-798 in 10 mM PBS buffer only. Hence, the obtained LOD value in this case found to be lesser than that of the PBS buffer.

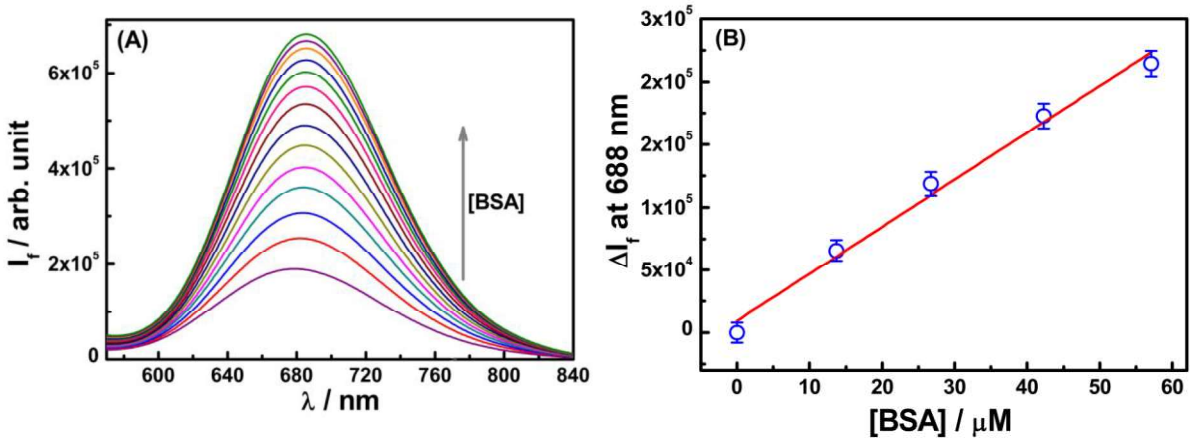

Figure: 6.11 (A) Fluorescence spectra of 10 μM LDS-798 upon increasing the BSA concentration from (1) 0 to (14) 330 μM in 5% FBS medium [λ_{ex} = 525 nm, pH = 7.4 (10 mM PBS)]. **(B)** Linear plot of the changes in the emission intensity of LDS-798 with the increasing BSA concentration from 0 to 57 μM in 5% FBS medium (pH = 7.4) used for LOD determination. (I_{688} = 3.742 x 10^3[BSA/μM] + 9625, R^2 = 0.986; LOD=1.57 μM.

6.3.11B. Quantification of Albumin in Urine Matrix

As discussed in the introduction section, alteration of concentration of albumin in human urine gives an indication of the diseases. Excess concentration of albumin in urine is an indication of kidney disease, albuminuria. Thus, it is quite mandatory to check the concentration of albumin in urine matrices on a regular basis. Based on this fact, we also attempted to detect HSA in human urine samples and the performance was found to be quite satisfactory. The LOD value of albumin in urine sample was found to be ~52 nM (*cf.* Fig. 6.12).

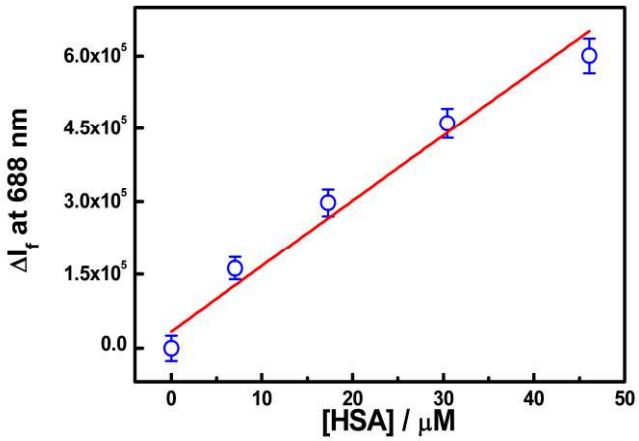

Figure: 6.12. Linear plot of the changes in the emission intensity of LDS-798 with the increasing HSA concentration from 0 to 50 μM in human urine (I_{688} = 1.34 x 10^4 [HSA/μM] + 33334, R^2 = 0.962; LOD = 52 nM).

6.3.11C. Quantification of Albumin in Human Serum Matrix

Finally, we attempted to estimate the HSA level in human blood serum. The HSA levels in the human serum samples were estimated by the standard addition method. The obtained results for the HSA levels in the human serum samples (normal person) are in very good agreement with the reported range of normal serum albumin concentrations in blood, and were further validated by a well-known spectrophotometric method which employs bromophenol blue dye for albumin quantification (*cf.* Fig. 6.13). Further, to validate our method, the statistical analysis of the obtained results was carried out using unpaired Student's t-test (Table 6.2). Comparison of the performance of LDS-798 probe with those of other near infrared dyes for albumin sensing are shown in Table 6.3. It is evident from this table that LDS-798 is one of the most sensitive probe for albumin sensing using fluorescence detection.

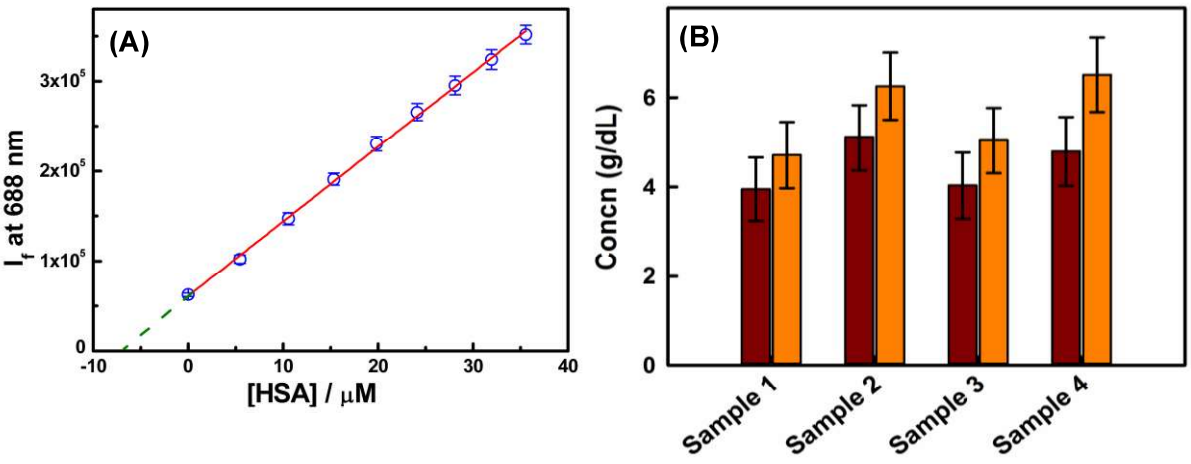

Figure: 6.13. (A) The standard addition calibration plot for HSA in 1% human serum sample. (B) Comparison of estimated HSA level in four different human blood serum samples (normal person) using LDS-798 (dark red) and a standard photometric method: Bromophenol blue method (Orange).

Table 6.2: Statistical test of estimation of HSA levels in four different human blood serum samples

Sample-1						
Method employed	**Mean**	**SD**	**SEM**	**N**	**P value**	**Inference**
LDS-798 method	3.95	0.71	0.355	4	0.1888 (> 0.05)	Difference is not statistically significant.
BPB method	4.71	0.74	0.370	4		
Sample-2						
LDS-798 method	5.10	0.73	0.365	4	0.0701 (> 0.05)	Difference is not statistically significant.
BPB method	6.25	0.75	0.375	4		
Sample-3						
LDS-798 method	4.03	0.74	0.370	4	0.1005 (> 0.05)	Difference is not statistically significant.
BPB method	5.04	0.73	0.365	4		
Sample-4						
LDS-798 method	4.80	0.77	0.385	4	0.0233 (< 0.05)	Difference is statistically significant.
BPB method	6.51	0.83	0.415	4		

Table: 6.3. Comparison of performance of different near infrared dyes for albumin sensing[53-55, 304, 312]

Sl. No.	**Dye/Probe**	**Emission maxima**	**Fluorescence enhancement**	**Detection limit**
1	Squarine based dye	674 nm	38 folds	140 nM
2	Derivative of 2-dicyanomethylene-3-cyano-4,5,5-trimethyl-2,5-dihydrofuran	660 nm	4.3 folds	0.61 µg/ml (9.2 nM)
3	Squarine derivative	660 nm	10 folds	22.4 nM
4	Merocyanine 540	580	35 folds	7.45 nM
5	aza-substituted benzothiazole squaraines	718 nm	400 folds	1.5 - 20 mg/ml (22.5 -300 nM)
6	**LDS-798**	**688**	**500 folds**	**48 nM**

6.4. Conclusion

In summary, we have identified a very selective and sensitive fluorescent turn-on probe in the much advantageous near IR region, which registers ~500 fold emission enhancement, the highest reported till date, in response to BSA. The specific binding of LDS-798 to site-I of BSA leads to large structural confinement which is additionally accompanied by significantly reduced micro-polarity that causes a large reduction in its propensity to form non-emissive TICT state, and thus all together results in a huge fluorescence enhancement for the probe. Notwithstanding other reports, as a sensor probe, LDS-798 offers several advantages such as label free operation, high sensitivity and selectivity and most importantly giving emission in the biologically desired red region. The present probe could suitably detect and quantify the albumin protein in human serum samples. The easy commercial availability of this probe in high purity provides an additional advantage, which makes tedious and time-consuming synthetic efforts avoidable, and thus can have a large impact on albumin sensing in clinical applications.

CHAPTER-7

SUMMARY AND FUTURE OUTLOOK

7.1. Introduction

In this concluding chapter, we briefly summarize all the major findings, applications and conclusions of the thesis. We also aim to provide a futuristic outlook, possible extensions and applications of the work carried out in the present thesis. The main goal of the work done in the present thesis was to understand the non-covalent interaction of different fluorogenic organic dyes with macroyclic hosts (viz, cucurbit7uril or cyclodextrins) and bio-macromolecular hosts (viz, BSA and HSA). The supramolecular host-guest interactions involving chromophoric dyes as the guests and macrocyclic molecules and bio-macromolecular systems as the hosts have many prospects for their applications in optical sensing, drug formulations, drug delivery, nanotechnology, therapeutics and many others, and this research area is quite interesting, challenging and highly promising in the realm of different filed of sciences such as chemistry, biology, bio-chemistry, pharmaceutical, material science, electronic and so on.

7.2. Chapter wise Summary and Future Directions

Initial part of Chapter-1 basically provides information on various aspects of supramolecular chemistry such as, different non-covalent forces operative in supramolecular chemistry and their strength in determining the construction of various supramolecular assemblies in three dimensional network and also about the thermodynamics involved during the formation of supramolecular entity, specially keeping in mind the host-guest systems. In the later part of this Chapter, we briefly discuss about the luminescence spectroscopy, highlighting different photophysical processes associated with the absorption and emission

processes of chromophoric molecules. A brief account on the selection rules associated with the electronic transitions has also been given in this chapter.

Chapter-2 mainly provides information on the synthetic procedure of some of the used guest (BDZ) and host (CB7), also highlights the notable properties and applications of the different guests (CV, BDZ, LDS-798) and hosts (CB7, β-CD, SBEβCD) involved in the present studies. This chapter also provides the necessary informations about the instrumentation and working principle of various spectrometric techniques (viz, UV-vis spectrophotometer, fluorometer, TCSPC, NMR) used in the present study.

In Chapter-3, the detail study on the interactions of a triphenyl methane (TPM) dye, crystal violet (CV), with a macrocyclic host CB7 and a biomolecular host BSA has been presented. A homologues TPM dye, brilliant green (BG), was reported in the literature to undergo cooperative binding with CB7 and BSA host, resulting a synergistic enhancement in the fluorescence properties of the dye. In the present study, we were interested to see whether CV interacts in a cooperative or competitive manner with CB7 and BSA hosts and thus to understand whether cooperative binding is just specific to BG dye or a general phenomena for the TPM dyes. CV is found to interact moderately with CB7 (K_b ~$6.3x10^3$ M^{-1}) causing only ~6 fold enhancement in fluorescence for the dye, due to the inclusion of only one of the three flexible arms of CV inside CB7 cavity. On the other hand, interaction of CV with BSA is very strong (K_b ~$3.2x10^5 M^{-1}$) leading to phenomenal enhancement (~100 fold) in fluorescence intensity. Addition of CB7 to CV-BSA complex results in a substantial reduction in fluorescence intensity, whereas addition of BSA to CV-CB7 complex causes a significant increase in the fluorescence intensity. The effective binding constant (K_b) for titration of CV-CB7 complex by BSA or CV-BSA complex by CB7 are much lower (~$1.2x10^4$ M^{-1} and ~$4.3x10^3$ M^{-1}, respectively) than those for CV-BSA and CV-CB7 binary systems. Thus, from the obtained results we concluded that CV undergoes competitive binding with CB7 and BSA

hosts than the cooperative binding displayed by the homologue dye BG. It appears from the observed results that binary systems with comparable K_b values, such as BG-CB7 and BG-BSA, makes the dye molecules to undergo cooperative binding in simultaneous presence of CB7 and BSA host, while the systems with large difference in K_b values, e.g. for CV-CB7 and CV-BSA binary systems (by ~50 fold), actually favors a competitive binding interaction over a cooperative binding. Present results provide a clue towards designing suitable ternary systems favoring either cooperative or competitive bindings to achieve best effects in drug formulation and drug delivery mechanisms.

In Chapter-4, we discussed the supramolecular interaction of a styryl dye, LDS-798, with polyanionic macrocyclic host sulfobutylether-βCD (SBE_{10}βCD). LDS-798 is a non fluorescent dye due to its large flexible structure, but it undergoes substantial fluorescence enhancement (~70 fold) on its binding to SBE_{10}βCD cavity. The K_b value for the LDS-798-SBE_{10}βCD system is estimated to be very high (~1.6×10^6 M^{-1}), apparently the highest for any fluorogenic molecules reported till date involving a CD derivate. The presence of negatively charged sulfonate end groups at the portals of SBE_{10}βCD host cause the cationic dye LDS-798 to interact very strongly with the host involving very strong electrostatic interaction. Further, the extended hydrophobic cavity of SBE_{10}βCD because of the butylether arms present at the SBE_{10}βCD portals provides improved hydrophobic interaction towards the encapsulation of LDS-798 into the host cavity. Thus, the combined effect of strong electrostatic interaction and improved hydrophobic interaction imparted by the SBE_{10}βCD towards LDS-798 is nicely corroborated with large K_b value and phenomenal enhancement in the fluorescence intensity of LDS-798 in the presence of SBE_{10}βCD. The strongest binding in the LDS-798-SBE_{10}βCD system is further corroborated by negligible effects observed on the K_b value by the presence of the competitive guests like lithocholic acid and adamentylamine hydrochloride. The LDS-798-SBE_{10}βCD system is found to be very sensitive to external stimulus like salt

concentration, temperature and pH. The strongest binding of LDS-798 with polyanionic $SBE_{10}\beta CD$ host and the exceptional response of the dye-host complex to external stimuli like temperature, ionic strength, etc. makes the studied system an excellent choice for its utilization as a supramolecular sensor for temperature, polarity, and so on.

Chapter-5 describes the non-covalent interaction of a BODIPY-benzimidazole conjugate dye (BDZ) with BSA protein. Due to strong hydrophobic nature, BDZ is insoluble in water and found to show high propensity of aggregation in aqueous solution. Thus, to avoid the aggregation of the BDZ during the experimental conditions, present study was carried out in 20% ethanolic PBS solution. The intramolecular charge transfer (ICT) from benzimidazole to BODIPY core makes the dye BDZ very weakly fluorescent in polar medium. With gradual addition of BSA to 20% ethanolic PBS solution of BDZ, results in a substantial fluorescence enhancement along with a notable blue shift of 14 nm (from 545 nm to 531 nm). Understandably, reduced structural agility and ICT process for bound dye inside rigid and less polar BSA pocket decreases the non-radiative deexcitation of the excited BDZ molecules causing a large increase in fluorescence intensity, along with a blue shift in the emission spectra. The non-linear fitting of binding isotherm using 1:1 binding model yields the binding constant of the BDZ-BSA system as $K_b \sim 1.38 \times 10^4\ M^{-1}$, which is quite strong and falls in the range of K_b values reported for many many dye -BSA systems. In the present case, the molecular docking calculations suggest site IB of BSA as the most preferred binding location for BDZ with the free energy of binding as −10 kcal/mole, which is further validated with the competitive binding experiments in the presence of warfarin (binder for site-IIA) and ibuprofen (binder for site-IB). Observed results suggest the potential of the BDZ-BSA system for uses in fluorogenic sensor applications in the visible region of the electromagnetic spectrum.

Chapter-6 presents the interaction of biologically important dye LDS-798 with serum albumins, BSA and HSA. The dye in aqueous solution is almost non-fluorescent due to its large structural flexibility and its ability to undergo twisted intramolecular charge transfer (TICT) state formation in its first excited state. Stepwise addition of BSA to LDS-798 buffer solution results in an exceptional fluorescence turn-on, with ~500 fold enhancement for 10 μM dye solution in the presence of ~300 μM BSA. Similar results are also obtained on interaction of LDS-798 with HSA. Large structural rigidization and reduced propensity of TICT state formation in the first excited state of LDS-798 inside the confined and lower micro-polarity BSA/HSA pocket results in the large modulations observed in the photophysical properties of LDS-798 dye. The K_b values for LDS-798-BSA and LDS-798-HSA systems are found to be very high, ~$1.27x0^4$ M^{-1} and ~$1.86x10^4$ M^{-1}, respectively. Competitive binding experiments using warfarin (binder for Sudlow's site-I) and ibuprofen (binder for Sudlow's site-II) reveals that LDS-798 binds preferentially to Sudlow's site-I of the BSA host, which is further validated by molecular docking calculation, showing the dye LDS-798 to bind at the Sudlow's site-I of BSA, with free energy of binding as –6.4 kcal/mole.

Binding of LDS-798 to BSA/HSA proteins is found to be very selective and gets hardly affected by the presence of Na^+, K^+, Ca^{2+}, HPO_4^-, Cl^-, amino acids, porphyrins, etc. This selectivity is very useful for the qualitative and quantitative estimation of albumins, even in complex matrices like FBS, urine, human serum matrix, etc. Increase in emission intensity for LDS-798 is found to be linear up to ~50 μM albumin concentrations, suggesting the limit of detection (LOD) as ~48 nM for BSA and 52 nM for HSA.

In order to find practical applicability of the studied system, quantification of HSA has also been carried out in four different blood serum samples of normal persons. Obtained results are compared and validated with a known spectrophotometric method of albumin estimation using bromophenol blue as the probe. The results from the two independent

methods are compared by unpaired student t-test, showing an insignificant variation between the two methods.

In effect, the LDS-798 dye is realized as a very selective and sensitive fluorescent turn-ON probe in the much desired near IR region, which registers ~500 fold emission enhancements, the highest reported so far, in the response to BSA/HSA. Notwithstanding other reports, as a sensor probe, LDS-798 offers several advantages such as label free operation, high sensitivity and selectivity and most importantly giving emission in the biologically advantageous red region that involves minimum auto fluorescence, high light penetration and low tissue damage. Present probe can suitably detect and quantify albumins in real serum samples. Easy commercial availability of the probe is an additional advantage, as tedious and time-consuming synthetic efforts can be avoided, and thus can have a large impact on albumin sensing in clinical applications.

With the summary of the present work, as presented so far in this Chapter-7, it can be realized that the present thesis made a reasonable contribution towards understanding the binding interaction of different fluorogenic dyes with some important macrocyclic molecules and bio-macromolecular hosts. It is highlighted that these interactions lead to significant modulation in the physicochemical properties of the dye, causing especially a large enhancement in the fluorescence intensity of the dyes. The key for any supramolecular host-guest system to be applied in the field of science is the selectivity, sensitivity and of course it's cost effectiveness. In these respects, all the host-guest systems studied in the present work display their prospects in different applications. Chemistry is full of surprises and synthetic organic chemistry has enormous possibilities of designing new compounds, which can have notable interactions with the different hosts depending on their stucture and hydrophobic/hydrophilic characteristics. The future perspective of the works carried out in this thesis would be to enhance the supramolecular interactions further through newly designed

and synthesized organic chromophoric dyes and suitably selected macrocyclic and bio-macromolecular hosts to achieve exceptionally large modulations in the photophysical properties of the dyes for their better implementations in the realm of chemical, biological and pharmaceutical sciences. Thus, there is lot of scope of this thesis for the identification of newer supramolecular host-guest system to bring out the futuristic applications of the host-guest chemistry in the benefit of the mankind.

References

1. J. M. Lehn, *Angew Chem. Int. Ed. Engl*, 1988, **27**, 89-112.
2. J. M. Lehn, *Angen. Chem. Int. Ed. Engl.*, 1990, **29** 1304-1319.
3. X. Yan, F. Wang, B. Zheng and F. Huang, *Chem. Soc. Rev.*, 2012, **41**, 6042–6065.
4. B. Rybtchinski, *ACS Nano* 2011, **5**, 6791–6818.
5. K. N. Houk, A. G. Leach, S. P. Kim and X. Zhang, *Angew. Chem. Int. Ed.*, 2003, **42**, 4872 – 4897.
6. J. M. Zayed, N. Nouvel, U. Rauwald and O. A. Scherman, *Chem. Soc. Rev.*, 2010, **39**, 2806–2816.
7. S. Monti and I. Manet, *Chem. Soc. Rev.*, 2014, **43**, 4051–4067.
8. X. Ma and Y. Zhao, *Chem. Rev.*, 2015 **115** 7794–7839.
9. G. V. Oshovsky, D. N. Reinhoudt and W. Verboom, *Angew. Chem. Int. Ed.*, 2007, **46**, 2366–2393.
10. B. C. Pemberton, R. K. Singh, A. C. Johnson, S. Jockusch, J. P. Da Silva, A. Ugrinov, N. J. Turro, D. K. Srivastava and J. Sivaguru, *Chem. Commun.*, 2011, **47**, 6323–6325.
11. Z. Zhang, Y. Luo, J. Chen, S. Dong, Y. Yu, Z. Ma and F. Huang, *Angew. Chem. Int. Ed.*, 2011, **50**, 1397–1401.
12. M. J. Frampton and H. L. Anderson, *Angew. Chem. Int. Ed.*, 2007, **46**, 1028 – 1064.
13. X. J. Loh, *Mater. Horiz.*, 2014, **1**, 185–195.
14. L. Wang, L.-l. Li, Y.-s. Fan and H. Wang, *Adv.Mater.*, 2013, **25**, 3888–3898.
15. Y. Zhao, F. Sakai, L. Su, Y. Liu, K. Wei, G. Chen and M. Jiang, *Adv. Mater.*, 2013, **25**, 5215–5256.
16. K. Liu, Y. Kang, Z. Wang and X. Zhang, *Adv. Mater.*, 2013, **25**, 5530–5548.
17. N. Saleh, A. L. Koner and W. M. Nau, *Angew. Chem. Int. Ed.*, 2008, **47**, 5398–5401.
18. G. Schaeffer, O. Fuhr, D. Fenske and J.-M. Lehn, *Chem. Eur. J.*, 2014, **20**, 179–186.

19. J. Zhang and P. X. Ma, *Adv. Drug Delivery Rev.*, 2013, **65**, 1215–1233.

20. M. Shaikh, J. Mohanty, A. C. Bhasikuttan, V. D. Uzunova, W. M. Nau and H. Pal, *Chem. Commun.*, 2008, 3681–3683.

21. Y. Hu, W. Yuan, N.-N. Zhao, J. Ma, W.-T. Yang and F.-J. Xu, *Biomaterials*, 2013, **34**, 5411–5422.

22. K. Ariga, J. Li, J. Fei, Q. Ji and J. P. Hill, *Adv. Mater.*, 2016, **28**, 1251–1286.

23. D. B. Amabilino, D. K. Smith and J. W. Steed, *Chem. Soc. Rev.*, 2017, **46**, 2404–2420.

24. N. J. V. Zee, B. Adelizzi, M. F. J. Mabesoone, X. Meng, A. Aloi, R. H. Zha, M. Lutz, I. A. W. Filot, A. R. A. Palmans and M. E. W., *Nature*, 2018, **558**, 100–103.

25. S. K. Nayak, M. Amela-Cortes, C. Roiland, S. Cordiera and Y. Molard, *Chem. Commun.*, 2015, **51**, 3774–3777.

26. S. Onogi, H. Shigemitsu, T. Yoshii, T. Tanida, M. Ikeda, R. Kubota and I. Hamachi, *Nat. Chem.*, 2016, **8**, 743–752.

27. M. Shaikh, S. D. Choudhury, J. Mohanty, A. C. Bhasikuttan and H. Pal, *Phys. Chem. Chem. Phys.*, 2010, **12**, 7050–7055.

28. D. A. Ivanov, N. K. N. Petrov, E. A. , M. V. Basilevsky, A. I. Vedernikov, S. P. Gromov and M. V. Alfimov, *J. Phys. Chem. A* 2011, **115**, 4505–4510.

29. N. Barooah, J. Mohanty, H. Pal and A. C. Bhasikuttan, *Org. Biomol. Chem.*, 2012, **10**, 5055–5062.

30. M. Gupta, D. K. Maity, M. K. Singh, S. K. Nayak and A. K. Ray, *J. Phys. Chem. B* 2012, **116**, 5551−5558.

31. E. Masson, X. Ling, R. Joseph, L. Kyeremeh-Mensah and X. Lu, *RSC Adv.*, 2012, **2**, 1213–1247.

32. K. Gavvala, A. Sengupta and P. Hazra, *ChemPhysChem* 2013, **14**, 532 – 542.

33. M. Gupta, D. K. Maity, S. K. Nayak and A. K. Ray, *J. Photochem. Photobiol., A*, 2015, **300** 15–21.

34. N. Barooah, A. Kunwar, R. Khurana, A. C. Bhasikuttan and J. Mohanty, *Chem. Asian J.*, 2017, **12**, 122 –129.

35. D. R. Boraste, G. Chakraborty, A. K. Ray, G. S. Shankarling and H. Pal, *ChemistrySelect*, 2017, **2**, 5128 - 5142.

36. J. Ca´ceres, J. Robinson-Duggon, A. Tapia, C. Paiva, M. Go´mez, C. Bohneb and D. Fuentealba, *Phys.Chem.Chem.Phys.* , 2017, **19**, 2574-2582.

37. Y. Liu, B. H. Han and Y. T. Chen, *J. Phys. Chem. B*, 2002, **106**, 4678-4687.

38. N. Basilio, V. Francisco and L. Garcia-Rio, *Int. J. Mol. Sci.*, 2013, **14**, 3140-3157.

39. M. YILMAZ and S. ERDEMIR, *Turk J Chem*, 2013, **37**, 558-585.

40. Y. X. Wang, Y. M. Zhang and Y. Liu, *J. Am. Chem. Soc.*, 2015, **137**, 4543−4549.

41. W. M. Nau and X. Zhang, *J. Am. Chem. Soc.* , 1999, **121**, 8022-8032.

42. E. M. M. Del Valle, *Process Biochem.*, 2004, **39** 1033-1046.

43. W. Yang and M. M. de Villiers, *The AAPS Journal* 2005, **7 (1)**, E241-E248.

44. S. Bakkialakshmi and T. Menaka, *Int.J. ChemTech Res.*, 2012, **4**, 223-231.

45. S. Siva, J. Thulasidhasan and N. Rajendiran, *Spectrochim. Acta, Part A*, 2013, **115** 559–567.

46. M. N. Shinde, A. C. Bhasikuttan and J. Mohanty, *ChemPhysChem*, 2015, **16**, 3425 – 3432.

47. M. Sayed, S. Jha and H. Pal, *Phys. Chem. Chem. Phys.*, 2017, **19**, 24166--24178.

48. J. Mohanty and W. M. Nau, *Angew. Chem. Int. Ed.*, 2005, **44**, 3750–3754.

49. J. Mohanty, H. Pal, A. K. Ray, S. Kumar and W. M. Nau, *ChemPhysChem*, 2007, **8**, 54–56.

50. R. Wang, D. Bardelang, M. Waite, K. A. Udachin, D. M. Leek, K. Yu, C. I. Ratcliffe and J. A. Ripmeester, *Org. Biomol. Chem.*, 2009, **7**, 2435–2439.

51. J. Mohanty, K. Jagtap, A. K. Ray, W. M. Nau and H. Pal, *ChemPhysChem*, 2010, **11**, 3333 – 3338.

52. B. N. G. Giepmans, S. R. Adams, M. H. Ellisman and R. Y. Tsien, *Science*, 2006, **312**, 217−224.

53. K. D. Volkovam, V. B. Kovalska, M. Y. Losytskyy, L. V. Reis, P. F. Santos, P. Almeida, D. E. Lynch and S. M. Yarmoluk, *Dyes Pigm.*, 2011, **90**, 41-47.

54. T. Bayraktutan and K. Meral, *Phys. Chem. Chem. Phys.*, 2016, **18**, 23400-23406.

55. X. Zeng, M. Ma, B. Zhu and L. Zhu, *Anal. Sci.*, 2016, **32**, 1291-1294.

56. N. Barooah, J. Mohanty, H. Pal and A. C. Bhasikuttan, *J. Phys. Chem. B* 2012, **116**, 3683−3689.

57. K. Gavvala, R. K. Koninti, A. Sengupta and P. Hazra, *Phys. Chem. Chem. Phys.* , 2014, **16**, 2823--2826.

58. L. Isaacs, *Acc Chem Res.*, 2014, **47**, 2052-2062.

59. K. I. Assaf and W. M. Nau, *Chem. Soc. Rev.*, 2015, **44**, 394--418.

60. T. Goel, N. Barooah, M. B. Mallia, A. C. Bhasikuttan and J. Mohanty, *Chem. Commun.*, 2016, **52**, 7306--7309.

61. S. Sinn and F. Biedermann, *Isr. J. Chem.*, 2018, **58**, 357 –412.

62. Y. V. Morimoto, S. Kojima, K. Namba and T. Minamino, *PLoS One*, 2011, **6**, e19598.

63. S. S. Thakare, G. Chakraborty, P. Krishnakumar, A. K. Ray, D. K. Maity, H. Pal and N. Sekar, *J. Phys. Chem. B* 2016, **120**, 11266−11278.

64. I. Ghosh and W. M. Nau, *dv. Drug Delivery Rev.*, 2012, **64** 764–783.

65. J. W. Steed and J. L. Atwood, *Supramolecular Chemistry*, 2nd ed., John Wiley & Sons, Ltd, Chichester, 2009.

66. N. L. Rosi, J. Eckert, M. Eddaoudi, D. T. Vodak, Kim J, M. O'Keeffe and O. M. Yaghi, *Science*, 2003 **300**, 1127-1129.

67. R. Kitaura, S. Kitagawa, Y. Kubota, T. C. Kobayashi, K. K., Y. Mita, A. Matsuo, M. Kobayashi, H. C. Chang, T. C. Ozawa, M. Suzuki, M. Sakata and M. Takata, *Science*, 2002 **298**, 2358-2361.

68. A. R. Millward and O. M. Yaghi, *J. Am. Chem. Soc.*, 2005, **127**, 17998-17999.

69. S. Sato, Y. Ishido and M. Fujita, *J. Am. Chem. Soc.*, 2009, **131** 6064–6065.

70. R. Itoh, *Supplement of the Progress of Theoretical Physics*, 1961, **17**, 69-79.

71. A. L. McClellan, *J. Chem. Educ.*, 1967, **44** 547-551.

72. G. A. Jeffrey, *Food Chem.*, 1996, **56**, 241-246.

73. H. Luecke and F. A. Quiocho, *Nature*, 1990, **347**, 402–406.

74. P. J. Goodford, *J. Med. Chem.*, 1985, **28**, 849-857.

75. B. Honig, K. Sharp and A. Yang, *J. Phys. Chem.*, 1993, **97**, 1101-1109.

76. T. E. Kaiser, H. Wang, V. Stepanenko and F. Würthner, *Angew. Chem. Int. Ed.*, 2007, **46**, 5541–5555.

77. M. R. Molla and S. Ghosh, *Chem. Eur. J.*, 2012, **18**, 1290–1294.

78. H. Lin, R. Camacho, Y. Tian, T. E. Kaiser, F. Wurthner and I. G. Scheblykin, *Nano Lett.*, 2010, **10**, 620-626.

79. F. Wurthner, T. E. Kaiser and C. R. Saha-Moller, *Angew. Chem. Int. Ed.*, 2011, **50**, 3376 – 3410.

80. M. Sayed, M. Sundararajan, J. Mohanty, A. C. Bhasikuttan and H. Pal, *J. Phys. Chem. B*, 2015, **119**, 3046−3057.

81. N. Rubio and A. L. Zanocco, *AFINIDAD LXXIII*, 2016, **573**, 69-74.

82. M. Sayed and H. Pal, *J. Mater. Chem. C*, 2016, **4**, 2685--2706.

83. J. Murray, K. Kim, T. Ogoshi, W. Yaod and B. C. Gibb, *Chem. Soc. Rev.*, 2017, **46**, 2479–2496.

84. J. Szejtli and T. Osa.

85. J. C. Harrison and M. R. Eftink, *Biopolymers*, 1982, **21**, 1153–1166

86. F. Biedermann, M. Vendruscolo, O. A. Scherman, S. A. De and W. M. Nau, *J. Am. Chem. Soc.*, 2013 **135**, 14879–14888.

87. F. Biedermann, V. D. Uzunova, O. A. Scherman, W. M. Nau and A. D. Simone, *J. Am. Chem. Soc.*, 2012, **134**, 15318−15323.

88. W. M. Nau, M. Florea and K. I. Assaf, *Isr. J. Chem.*, 2011, **51**, 559–577.

89. R. R. Krug, W. G. Hunter and R. A. Grieger, *Nature*, 1976, **261**, 566–567.

90. N. M. Green, *Biochem. J.*, 1963, **89**, 585–591.

91. O. Livnah, E. A. Bayer, M. Wilchek and J. L. Sussman, *Proc Natl Acad Sci U S A.*, 1993 **90**, 5076-5080.

92. H. Ohtaka, S. Muzammil, A. Schön, A. Velazquez-Campoy, S. Vega and E. Freire, *Int. J. Biochem. Cell Biol.*, 2004, **36**, 1787–1799.

93. I. Luque and E. Freire, *Proteins*, 2002, **49**, 181-190.

94. V. Khorwal, B. Sadhu, A. Dey, M. Sundararajan and A. Datta, *J. Phys. Chem. B*, 2013, **117**, 8603−8610.

95. G. Chakraborty, A. K. Ray and H. Pal, *ChemistrySelect*, 2018, **3**, 1088 – 1096.

96. G. Chakraborty, A. K. Ray, P. K. Singh and H. Pal, *Chem. Commun.*, 2018, **54**, 8383–8386.

97. N. H. Mudliar and P. K. Singh, *ACS Appl. Mater. Interfaces*, 2016, **8**, 31505-31509.

98. A. M. Desai and P. K. Singh, *Chem. Eur. J.*, 2019, **25**, 2035 – 2042.

99. A. M. Desai and P. K. Singh, *Sens. Actuators, B*, 2018, **277**, 205–209.

100. M. S. T. Gonçalves, *Chem. Rev.*, 2009, **109**, 190–212.

101. S. Wang, H. Liu, J. Mack, J. Tian, B. Zou, H. Lu, Z. Li, J. Jiang and Z. Shen, *Chem. Commun.*, 2015, **51**, 13389--13392.

102. S. I. Reja, I. A. Khan, V. Bhalla and M. Kumar, *Chem. Commun.*, 2016, **52**, 1182--1185.

103. D. Kim, S. W. Cho, Y. W. Jun and K. H. Ahn, *Bull. Korean Chem. Soc.* , 2017.

104. W. Xu, T. H. Kim, D. Zhai, J. C. Er, L. Zhang, A. A. Kale, B. K. Agrawalla, Y. K. Cho and Y. T. Chang, *Sci. Rep.*, 2013, **3 : 2255**.

105. M. E. Aliaga, L. Garcıa-Rıo, M. Pessego, R. Montecinos, D. Fuentealba, I. Uribe, M. M. Pastorc and O. G. Beltran, *New J. Chem.*, 2015, **39**, 3084-3092.

106. H. Li, P. Zhang, L. P. Smaga, R. A. Hoffman and J. Chan, *J. Am. Chem. Soc.*, 2015, **137**, 15628−15631.

107. J. R. Lakowicz, Principles of Fluorescence Spectroscopy. 3rd Edition, Plenumm Press, Springer, New York. 2006.

108. F. L. Arbeloa, J. B. Prieto, V. M. Martinez, T. A. Lopez and I. L. Arbeloa, *ChemPhysChem* 2004, **5**, 1762 – 1771.

109. S. S. Thakare, G. Chakraborty, S. Kothavale, S. Mula, A. K. Ray and N. Sekar, *J. Fluoresc.*, 2017, **27**, 2313–2322.

110. M. K. Singh, H. Pal, A. C. Bhasikuttan and A. V. Sapre, *Photochem Photobiol*, 1998, **68**, 32-38.

111. K. K. Rohatgi–Mukherjee, *fundamentals of Photochemistry*; Wiley Eastern Ltd: India, 1986.

112. M. Shaikh, J. Mohanty, M. Sundararajan, A. C. Bhasikuttan and H. Pal, *J. Phys. Chem. B*, 2012, **116**, 12450−12459.

113. M. Sayed, B. Krishnamurthy and H. Pal, *Phys. Chem. Chem. Phys.* , 2016, **18**, 24642--24653.

114. M. Sayed, K. Shinde, R. Shah and H. Pal, *ChemistrySelect*, 2016, **1** 989–999.

115. J. B. Prieto, F. L. Arbeloa, V. M. Martı´nez, T. A. Lopez and I. L. Arbeloa, *J. Phys. Chem. A*, 2004, **108**, 5503-5508.

116. A. Loudet and K. Burgess, *Chem. Rev.* , 2007, **107**, 4891-4932.

117. H. Doan, M. Castillo, M. Bejjani, Z. Nurekeyev, S. V. Dzyuba, I. Gryczynski, Z. Gryczynski and S. Raut, *Phys. Chem. Chem. Phys.*, 2017, **19**, 29934--29939.

118. A. Barik, M. Kumbhakar, S. Nath and H. Pal, *Chem. Phys.*, 2005, **315**, 277–285.

119. P. Dahiya, M. Kumbhakar, T. Mukherjee and H. Pal, *Chem. Phys. Lett.*, 2005, **414**, 148–154.

120. S. Corrent, P. Hahn, G. Pohlers, T. J. Connolly, J. C. Scaiano, V. Fornes and H. Garcia, *J. Phys. Chem. B*, 1998, **102**, 5852–5858.

121. N. Sarkar, A. Datta, S. Das and K. Bhattacharyya, *J. Phys. Chem.*, 1996, **100** 15483–15486.

122. S. Alex, H. L. Thanh and D. Vocelle, *Can. J. Chem.*, 1992, **70**, 880-887.

123. W. F. Forbes and J. F. Templeton, *Can. J. Chem.*, 1968, **36** 180-188.

124. S. S. Thomas and C. Bohne, *Faraday Discuss.*, 2015, **185**, 381–398.

125. D. R. Boraste, G. Chakraborty, A. K. Ray, G. S. Shankarling and H. Pal, *J. Photochem.Photobiol., A*, 2018, **358**, 26-37.

126. B. T. Doumas, W. A. Watson and H. G. Biggs, *Clin. Chim. Acta*, 1971, **31**, 87−96.

127. V. Bush and R. G. Reed, *Clin. Chem.*, 1987, **33**, 821−823.

128. J. Karolin, L. B.-A. Johansson, L. Strandberg and T. Ny, *J. Am. Chem. Soc.*, 1994, **116** 7801–7806.

129. J. Wang, Y. Guo, B. Liu, C. Cheng, Z. Wang, G. Han, J. Gao and X. Zhang, *J. Lumin.*, 2011, **131**, 231-237.

130. A. V. Solomonov, E. V. Rumyantsev, B. A. Kochergin and E. V. Antinab, *Biophys.*, 2014, **59, No. 1**, 35–42.

131. K. Jurek, J. Kabatc, K. Kostrzewska and M. Grabowska, *Molecules*, 2015, **20**, 13071-13079.

132. L. P. Jameson, N. W. Smith, O. Annunziata and S. V. Dzyuba, *Phys.Chem.Chem.Phys.*, 2016, **18**, 14182-14185.

133. M. Qin, T. Yin and W. Shen, *J. Dispersion Sci. Technol.*, 2016, **37**, 1623–1629.

134. M. S. Baptista and G. L. Indig, *J. Phys. Chem. B*, 1998, **102**, 4678-4688.

135. V. Sundström, T. Gillbro and H. Bergström, *Chem. Phys.*, 1982, **73**, 439−458.

136. S. Jockusch, H. J. Timpe, C.-H. Fischer and W. Schnabel, *J. Photochem. Photobiol. A: Chem.*, 1992, **63**, 217−226.

137. D. Ben-Amotz and C. B. Harris, *Chem. Phys. Lett.* , 1985, **119**, 305−311.

138. A. C. Bhasikuttan, A. V. Sapre and T. Okada, *J. Phys. Chem. A*, 2003, **107**, 3030−3035.

139. Y. Nagasawa, Y. Ando, D. Kataoka, H. Matsuda, H. Miyasaka and T. Okada, *J. Phys. Chem. A*, 2002, **106**, 2024−2035.

140. R. N. Dsouza, U. Pischel and W. M. Nau, *Chem. Rev.* , 2011, **111**, 7941–7980.

141. H. Pal, *Sci. Adv. Today*, 2016, **2**, 25257(25251)−25257(25222).

142. G. N. Lewis, T. T. Magel and D. Lipkin, *J. Am. Chem. Soc.*, 1942, **64**, 1774–1782.

143. Y. Maruyama, M. Ishikawa and H. Satozono, *J. Am. Chem. Soc.*, 1996, **118**, 6257–6263.

144. A. Kamkaew, S. H. Lim, H. B. Lee, L. V. Kiew, L. Y. Chung and K. Burgess, *Chem. Soc. Rev.*, 2012.

145. J. Banuelos, *Chem. Rec.*, 2016, **16**, 335–348.

146. T. Kowada, H. Maeda and K. Kikuchi, *Chem. Soc. Rev.*, 2015, **44**, 4953--4972.

147. N. Boens, V. Leen and W. Dehaen, *Chem. Soc. Rev.*, 2012, **41**, 1130–1172.

148. L. Wu and K. Burgess, *Chem. Commun.*, 2008, 4933–4935.

149. J. Han, O. Gonzalez, A. Aguilar-Aguilar, E. Pe˜na-Cabrera and K. Burgess, *Org. Biomol. Chem.*, 2009, **7**, 34–36.

150. C. Zhao, P. Feng, J. Cao, Y. Zhang, X. Wang, Y. Yang, Y. Zhang and J. Zhang, *Org. Biomol. Chem.*, 2012, **10**, 267–272.

151. V. Leen, V. G. Gonzalvo, W. M. Deborggraeve, N. I. Boens and W. Dehaen, *Chem. Commun.*, 2010, **46**, 4908–4910.

152. T. Rohand, M. Baruah, W. Qin, N. Boens and W. Dehaen, *Chem. Commun.*, 2006, 266-268.

153. R. B. Alnoman, P. Stachelek, J. G. Knight, A. Harriman and P. G. Waddell, *Org. Biomol. Chem.*, 2017, **15**, 7643–7653.

154. S. S. Thakare, G. Chakraborty, A. B. More, S. Chattopadhyay, S. Mula, A. K. Ray and N. Sekar, *J. Lumin.*, 2018, **194**, 622-630.

155. P. Sarkar, R. Luchowski, S. Raut, N. Sabnis, A. Remaley, A. G. Lacko, S. Thamake, Z. Gryczynski and I. Gryczynski, *Biophys. Chem.*, 2010, **153**, 61–69.

156. W. J. Betz, F. Mao and G. S. Bewick, *J. Neurosci.*, 1992, **12** 363–375.

157. W. J. Betz, F. Mao and C. B. Smith, *Curr. Opin. Neurobiol.*, 1996, **6**, 365–371.

158. R. Luchowski, Z. Gryczynski, P. Sarkar, J. Borejdo, M. Szabelski, P. Kapusta and I. Gryczynsk, *Rev. Sci. Instrum.*, 2009, **80**, 033109.

159. J. W. Lee, S. Samal, N. Selvapalam, H. J. Kim and K. Kim, *Acc. Chem. Res.*, 2003, **36**, 621-630.

160. J. Kim, I. N. Jung, S. Y. Kim, E. Lee, J. K. Kang, S. Sakamoto, K. Yamaguchi and K. Kim, *J. Am. Chem. Soc.*, 2000, **122**, 540-541.

161. A. I. Day, R. J. Blanch, A. Coe and A. P. Arnold, *J. Inclusion Phenom.Macrocyclic Chem.*, 2002, **43**, 247–250.

162. R. L. Halterman, J. L. Moore and L. M. Mannel, *J. Org. Chem.*, 2008, **73** 3266–3269.

163. H. Cong, X. L. Ni, X. Xiao, Y. Huang, Q. J. Zhu, S. F. Xue, Z. Tao, L. F. Lindoy and G. Wei, *Org. Biomol. Chem.*, 2016, **14**, 4335–4364.

164. L. Cao, M. Śekutor, P. Y. Zavalij, K. Mlinarić-Majerski, R. Glaser and L. Isaacs, *Angew. Chem., Int. Ed.*, 2014 **53**, 988-993.

165. J. Lagona, P. Mukhopadhyay, S. Chakrabarti and L. Isaacs, *Angew. Chem. Int. Ed.*, 2005, **44**, 4844 – 4870.

166. A. Day, A. P. Arnold, R. J. Blanch and B. Snushall, *J. Org. Chem.*, 2001, **66**, 8094−8100.

167. J. Zhao, H. J. Kim, J. Oh, S. Y. Kim, J. W. Lee, S. Sakamoto, K. Yamaguchi and K. Kim, *Angew. Chem. Int. Ed.*, 2001, **40**, 4233-4235.

168. S. Walker, R. Kaur, F. J. McInnes and N. J. Wheate, *Mol. Pharmaceutics*, 2010, **7**, 2166−2172.

169. S. Yi and A. E. Kaifer, *J. Org. Chem.*, 2011, **76**, 10275−10278.

170. W. Ong and A. E. Kaifer, *Organometallics*, 2003, **22** 4181–4183.

171. V. A., *Compt Rendu*, 1891, **112**, 536.

172. S. J., *Chem. Rev.*, 1998, **98** 1743–1754.

173. A. Rasheed, A. C. K. Kumar and V. V. N. S. S. Sravanthi, *Sci. Pharm.*, 2008, **76,** 567–598.

174. K. N. Baglole, P. G. Boland and B. D. Wagner, *J. Photochem. Photobiol., A*, 2005, **173**, 230–237.

175. T. Ogoshi and A. Harada, *Sensors*, 2008, **8**, 4961–4982.

176. M. Roux, B. Perly and F. Djedaini Pilard, *Eur Biophys J.*, 2007, **36**, 861–867.

177. T. Loftsson and D. Duchene, *Int J of Pharm.*, 2007, **329**, 1–11.

178. G. Crini, *Chem. Rev.*, 2014, **114**, 10940−10975.

179. S. Tongiani, T. Ozeki and V. J. Stella, *J. Pharm. Sci.*, 2009, **98**, 4769–4780.

180. V. Zia, R. A. Rajewski and V. J. Stella, *Pharm. Res.*, 2001, **18**, 667–673.

181. Y. Zhou, G. Zhang, Z. Wang, H. Wang, C. Dong and S. Shuang, *J. Inclusion Phenom.Macrocyclic Chem.*, 2006, **56**, 215–220.

182. H. Ueda, D. Ou, T. Endo, H. Nagase, K. Tomono and T. Nagai, *Drug Dev. Ind. Pharm.*, 1998, **24**, 863–867.

183. D. O. Thompson and A. K. Chaubal, M. V. .

184. D. C. Carter and J. X. Ho, *Adv. Protein Chem.* , 1994, **45**, 153−203.

185. T. P. Jr., All About Albumin: Biochemistry, Genetics, and Medical Applications, Academic Press, **First edition,** 1995.

186. T. Peters, 1995, 319–413.

187. S. Naveenraj and S. Anandan, *J. Photochem. Photobiol., C*, 2013, **14**, 53–71.

188. S. Ercelen, A. S. Klymchenko, Y. Mely and A. P. Demchenko, *Int. J. Biol. Macromol.*, 2005, **35**, 231−242.

189. G. J. Quinlan, G. S. Martin and T. W. Evans, *Hepatology*, 2005, **41**, 1211−1219.

190. J. Ghuman, P. A. Zunszain, I. Petitpas, A. A. Bhattacharya, M. Otagiri and S. Curry, *J. Mol. Biol.*, 2005, **353**, 38–52.

191. J. R. Simard, P. A. Zunszain, C. E. Ha, J. S. Yang, N. V. Bhagavan, I. Petitpas, S. Curry and J. A. Hamilton, *Proc. Natl. Acad. Sci. U. S. A.*, 2005, **102**, 17958−17963.

192. Y. Suzuki and K. Yokoyama, *J. Am. Chem. Soc.*, 2005, **127**, 17799−17802.

193. F. Yang, C. Bian, L. Zhu, G. Zhao, Z. Huang and M. Huang, *J. Struct. Biol.*, 2007, **157**, 348–355.

194. O. Lockridge, W. Xue, A. Gaydess, H. Grigoryan, S.-J. Ding, L. M. Schopfer, S. H. Hinrichs and P. Masson, *J. Biol. Chem.*, 2008, **283**, 22582–22590.

195. N. Seedher and M. Kanojia, *Chem. Biol. Drug Des.*, 2008, **72**, 290–296.

196. U. Kragh-Hansen, *Biochim. Biophys. Acta*, 2013, **1830**, 5535–5544.

197. A. A. Bhattacharya, S. Curry and N. P. Franks, *J. Biol. Chem.*, 2000, **275**, 38731−38738.

198. M. D. Meti, S. T. Nandibewoor, S. D. Joshi, U. A. More and S. A. Chimatadar, *J. Pharma. Anal.* , 2015, **5**, 249–255.

199. Q. Yang, Z. Ye, M. Zhong, B. Chen, J. Chen, R. Zeng, L. Wei, H. W. Li and L. Xiao, *ACS Appl. Mater. Interfaces*, 2016, **8**, 9629−9634.

200. *Jobin Yvon Ltd. 2 Dalston Gardens, Stanmore, Middlesex HA7 1BQ UK*.

201. D. V. O'Connor and D. Phillips, Time Correlated Single Photon Counting. Academic Press, New York. 1984.

202. P. W. Atkins, *Physical Chemistry*; Oxford University Press: Oxford, 1998.

203. J. Mohanty, A. C. Bhasikuttan, W. M. Nau and H. Pal, *J. Phys. Chem. B*, 2006, **110** 5132–5138.

204. S. D. Choudhury, J. Mohanty, H. P. Upadhyaya, A. C. Bhasikuttan and H. Pal, *J. Phys. Chem. B*, 2009, **113** 1891–1898.

205. J. Mohanty, S. D. Choudhury, H. P. Upadhyaya, A. C. Bhasikuttan and H. Pal, *Chem. Euro. J.*, 2009, **15**, 5215–5219.

206. C. Márquez, R. R. Hudgins and W. M. Nau, *J. Am. Chem. Soc.*, 2004, **126** 5806–5816.

207. S. D. Choudhury, J. Mohanty, H. Pal and A. C. Bhasikuttan, *J. Am. Chem. Soc.*, 2010, **132** 1395–1401.

208. C. Klöck, R. N. Dsouza and W. M. Nau, *Org. Lett.*, 2009, **11** 2595–2598.

209. J. Hu, Y. Cheng, Q. Wu, L. Zhao and T. Xu, *J. Phys. Chem. B*, 2009, **113** 10650–10659.

210. S. Sun, R. Zhang, S. Andersson, J. Pan, D. Zou, B. Åkermark and L. Sun, *J. Phys. Chem. B* 2007, **111** 13357–13363.

211. H. Lodish, A. Berk, C. A. Kaiser, M. Krieger, A. Bretscher, H. Ploegh, A. Amon and K. C. Martin, *Molecular Cell Biology*, 8th Edition, W. H. Freeman & Co. 2008.

212. H.-J. Schneider, *Applications of supramolecular chemistry for 21st century technology.* Taylor & Francis, Boca Raton, FL, 2012.

213. H. Bakirci and W. M. Nau, *Adv. Funct. Mater.*, 2006, **16**, 237–242.

214. A. C. Bhasikuttan, H. Pal and J. Mohanty, *Chem. Commun.*, 2011, **47**, 9959-9971

215. L. A. Baumes, M. Buaki, J. Jolly, A. Corma and H. Garcia, *Tetrahedron Lett.*, 2011, **52**, 1418−1421.

216. N. S. Moyon and S. Mitra, *J. Phys. Chem. B*, 2011, **115**, 10163–10172.

217. A. C. Bhasikuttan, J. Mohanty, W. M. Nau and H. Pal, *Angew. Chem. Int. Ed.*, 2007, **46**, 4120–4122.

218. W. M. Nau and J. Mohanty, *Int. J. Photoenergy*, 2005, **7**, 133–141.

219. M. Megyesi, L. Biczók and I. Jablonkai, *J. Phys. Chem. C*, 2008, **112**, 3410–3416.

220. R. K. Koninti, A. Sengupta, K. Gavvala, N. Ballav and P. Hazra, *Nanoscale* 2014, **6**, 2937–2944

221. I. Ghosh and W. M. Nau, *Adv. Drug Delivery Rev.*, 2012, **64** 764–783.

222. A. Praetorius, D. M. Bailey, T. Schwarzlose and W. M. Nau, *Org. Lett.*, 2008, **10**, 4089–4092.

223. H. Bakirci, A. L. Koner and T. Schwarzlose, *Chem. Eur. J.*, 2006, **12**, 4799–4807.

224. R. Ludwig and N. T. K. Dzung, *Sensors*, 2002, **2**, 397–416.

225. M. Shaikh, J. Mohanty, P. K. Singh, W. M. Nau and H. Pal, *Photochem. Photobiol. Sc.*, 2008, **7**, 408–414.

226. F. P. Nicoletti, B. D. Howes, M. Fittipaldi, G. Fanali, M. Fasano, P. Ascenzi and G. Smulevich, *J. Am. Chem. Soc.*, 2008, **130**, 11677−11688.

227. W. Li, D. Chen, H. Wang, S. Luo, L. Dong, Y. Zhang, J. Shi, B. Tong and Y. Dong, *ACS Appl. Mater. Interfaces*, 2015, **7**, 26094−26100.

228. J. R. Z. Simard, P. A.; Hamilton, J. A.; Curry, S. , *J. Mol. Biol*, 2006, **361**, 336−351.

229. J. P. Nicholson, M. R. Wolmarans and P. G. R., *Br J Anaesth*, 2000, **85**, 599–610.

230. U. Kraghhansen, V. T. Chuang and M. Otagiri, *Biol. Pharm. Bull.*, 2002, **25**, 695–704.

231. M. Ishikawa and Y. Maruyama, *Chemical Physics Letters*, 1994, **219**, 416–420.

232. D. F. Duxbury, *Chem. Rev.*, 1993, **93**, 381–433.

233. H. Xua, S. L. Gao, J. B. Lv, Q. W. Liu, Y. Zuo and X. Wang, *J. Mol. Struct.*, 2009, **919**, 334–338.

234. P. Thordarson, *Chem. Soc. Rev.*, 2011, **40**, 1305–1323.

235. A. A. Awasthi and P. K. Singh, *J. Phys. Chem. B*, 2017, **121**, 6208−6219.

236. Y. I. Henis and A. Levitzki, *Eur J Biochem.*, 1976 **71**, 529–532.

237. R. W. Kerwin and L. S. Pilowsky, *Euro. J. Nucl. Med.*, 1995, **22**, 699–710.

238. N. Düzgüneş and S. S. Nir, *Adv Drug Deliv Rev.*, 1999 **40**, 3–18.

239. T.-C. Chou, *Pharmacol. Rev.*, 2006, **58**, 621–681.

240. A. B. T. Ghisaidoobe and S. Chung, *Int. J. Mol. Sci.*, 2014, **15**, 22518−22538.

241. F. Chandra, K. Pal, S. Lathwal and A. L. Koner, *Mol. BioSyst.*, 2016, **12**, 2859–2866.

242. Y. H. Ko, E. Kim, I. Hwang and K. Kim, *Chem. Commun.*, 2007, **0**, 1305–1315.

243. O. Azzaroni, M. Mir and W. Knoll, *J. Phys. Chem. B*, 2007, **111**, 13499–13503.

244. F. Nouar, J. F.Eubank, T. Bousquet, L. Wojtas, M. J. Zaworotko and M. Eddaoudi, *J. Am. Chem. Soc.*, 2008, **130** 1833–1835.

245. Z. Miskolczy, M. Megyesi, G. Tárkányi, R. Mizseia and L. Biczók, *Org. Biomol. Chem.*, 2011, **9**, 1061–1070.

246. S. Li, I. W. Wyman, C. Wang, Y. Wang, D. H. Macartney and R. Wang, *J. Org. Chem.*, 2016, **81**, 9494-9498.

247. S. Moghaddam, C. Yang, M. Rekharsky, Y. H. Ko, K. Kim, Y. Inoue and M. K. Gilson, *J Am Chem Soc.*, 2011 **133**, 3570–3581.

248. S. Liu, C. Ruspic, P. Mukhopadhyay, S. Chakrabarti, P. Y. Zavalij and L. Isaacs, *J Am Chem Soc.*, 2005 **127**, 15959–15967.

249. R. F. Gomez-Biagi, R. B. C. Jagt and M. Nitz, *Org. Biomol. Chem.*, 2008, **6**, 4622–4626.

250. M. R. Eftink, M. L. Andy, K. Bystrom, H. D. Perlmutter and D. S. Kristolt, *J. Am. Chem. SOC.*, 1989, **111**, 6765–6112.

251. M. Paolino, F. Ennen, S. Lamponi, M. Cernescu, B. Voit, A. Cappelli, D. Appelhans and H. Komber, *Macromolecules*, 2013, **46** 3215–3227.

252. Z. Yang and R. Breslow, *Tetrahedron Lett.*, 1997, **38**, 6171–6172.

253. L. Yuan, W. Lin, K. Zheng, L. He and W. Huang, *Chem. Soc. Rev.*, 2013, **42**, 622–661.

254. R. Luchowski, P. Sarkar, S. Bharill, G. Laczko, J. B., Z. Gryczynski and I. Gryczynski, *Appl. Opt.*, 2008, **47**, 6257–6265.

255. R. Luchowski, Z. Gryczynski, P. Sarkar, J. Borejdo, M. Szabelski, P. Kapusta and I. Gryczynski, *Rev. Sci. Instrum.*, 2009, **80**, 033109(033101–033106)

256. X. Cao, R. W. Tolbert, J. L. McHale and W. D. Edwards, *J. Phys. Chem. A*, 1998, **102**, 2739–2748.

257. P. Fromberz and A. Heilemann, *J. Phys. Chem.*, 1992, **96**, 6864–6866.

258. D. Laage, W. H. Thompson, M. Blanchard-Desce and J. T. Hynes, *J. Phys. Chem. A*, 2003, **107**, 6032–6046.

259. M. H. Keefe, K. D. Benkstein and J. T. Hupp, *Coord. Chem. Rev.*, 2000, **205**, 201−228.

260. J. Jayabharathi, K. Jayamoorthy and V. Thanikachalam, *J. Photochem. Photobiol., B*, 2012, **117** 27–32.

261. N. H. Mudliar, B. Sadhu, A. M. Pettiwala and P. K. Singh, *J. Phys. Chem. B*, 2016, **120**, 10496−10507.

262. C. Hoskins and A. D. M. Curtis, *J. Nanomed. Res.*, 2015, **2**, 1–8.

263. F. Zsila, *Mol. Pharmaceutics*, 2013, **10**, 1668−1682.

264. O. K. Abou-Zied and O. I. K. Al-Shihi, *J. Am. Chem. Soc.*, 2008, **130**, 10793−10801.

265. Z. Liu and X. Chen, *Chem. Soc. Rev.*, 2016, **45**, 1432–1456.

266. Y. J. Hu, Y. Liu and X. H. Xiao, *Biomacromolecules*, 2009, **10**, 517−521.

267. J. Neuzil, S. R. Thomas and R. Stocker, *Free Radical Biol. Med.*, 1997, **22**, 57−71.

268. X. Li, S. Yu, Y. Lee, T. Guo, N. Kwon, D. Lee, S. C. Yeom, Y. Cho, G. Kim, J. D. Huang, S. Choi, K. T. Nam and J. Yoon, *J. Am. Chem. Soc.*, 2019, **141**, 1366–1372.

269. B. P. Kamat, J. Seetharamappa and D. Kovala-Demertzi, *J. Photosci.*, 2004, **11(2)**, 65–69.

270. H.-H. Cai, X. Zhong, P.-H. Yang, W. Wei, J. Chen and J. Cai, *Colloids Surf., A*, 2010, **372,** 35–40.

271. R. Flores, *Anal Biochem.* , 1978, **88**, 605–611.

272. K. H. Schoeeky, M. Verges, A. L. Esqulvel and M. A. Chavarria, *Clin. Chem.*, 1987, **33,** 223–226.

273. K. Tan, L. Jaquinod, R. Paolesse, S. Nardis, C. Di Natale, A. Di Carlo, L. Prodi, M. Montalti, N. Zaccheroni and K. M. Smith, *Tetrahedron*, 2004, **60**, 1099–1106.

274. R. P. Haugland, *Handbook of Fluorescent Probes and Research Chemicals*, 6th ed.; Molecular Probes: Eugene, OR. 1996.

275. M.-c. Yee, S. C. Fas, M. M. Stohlmeyer, T. J. Wandless and K. A. Cimprich, *J. Biol. Chem.*, 2005, **280**, 29053–29059.

276. R. W. Wagner and J. S. Lindsey, *Pure Appl. Chem.*, 1996, **68**, 1373–1380.

277. D. Dziuba, P. Jurkiewicz, M. Cebecauer, M. Hof and M. Hocek, *Angew. Chem. Int. Ed.*, 2016, **55**, 174–178.

278. Y. Wang, Y. Liu, J. Miao, M. Ren, W. Guo and X. Lv, *Sens. Actuators, B*, 2016, **226**, 364–369.

279. N. Dorh, S. Zhu, K. B. Dhungana, R. Pati, F. T. Luo, H. Liu and A. Tiwari, *Sci. Rep.*, 2015, **5,** 1-10.

280. M. Liras, J. B. Prieto, M. P. Sierra, F. L. Arbeloa, I. G. Moreno, A. Costela, L. Infantes, R.Sastre and F. A. Guerri, *Org. Lett.* , 2007, **9**, 4183–4186.

281. G. Ulrich, R. Ziessel and A. Harriman, *Angew. Chem. Int. Ed.*, 2008, **47**, 1184–1201.

282. A. Garcıa, R. Sastre, D. del Agua, A. Costela, I. G. Moreno, F. L. Arbeloa, J. B. Prieto and F. L. Arbeloa, *J. Phys. Chem. C* 2007, **111**, 1508–1516.

283. V. Leen, E. Braeken, K. Luckermans, C. Jackers, M. V. Auweraer, N. I. Boens and W. Dehaen, *Chem. Commun.*, 2009, 4515–4517.

284. A. Costela, I. Garcia-Moreno, M. Pintado-Sierra, F. Amat-Guerri, R. Sastre, M. Liras, F. L. Arbeloa, J. B. Prieto and I. L. Arbeloa, *J. Phys. Chem. A*, 2009, **113**, 8118–8124.

285. A. B. More, G. Chakraborty, S. Mula, A. K. Ray and N. Sekar, *J. Fluoresc.*, 2018, **28**, 381–392.

286. J. Shao, H. Sun, H. Guo, S. Ji, J. Zhao, W. Wu, X. Yuan, C. Zhangb and T. D. James, *Chem. Sci.*, 2012, **3,** 1049-1061.

287. M. Gupta, S. Mula, M. Tyagi, T. K. Ghanty, S. Murudkar, A. K. Ray and S. Chattopadhyay, *Chem. Eur. J.*, 2013, **19**, 17766−17772.

288. R. Liu, P. Qin, L. Wang, X. Zhao, Y. Liu and X. Hao, *J. Biochem. Mol. Toxicol.*, 2010, **24**, 66−71.

289. S. Yoshizawaa, T. Arakawab and K. Shirakia, *Int. J. Biol. Macromol.*, 2014, **68**, 169−172.

290. O. Trott and A. J. Olson, *J. Comput. Chem.*, 2010, **31**, 455−461.

291. A. Bujacz, *Acta Crystallogr., Sect. D: Biol. Crystallogr.*, 2012, **68**, 1278−1289.

292. *pathologyharmony.co.uk. Pathology Harmony. Retrieved 23 June 2013.*

293. C. E. Mogensen, W. F. Keane, P. H. Bennett, G. Jerums, H. H. Parving, P. Passa, M. W. Steffes, G. E. Striker and G. C. Viberti, *Lancet*, 1995, **346,** 1080−1084.

294. S. H. Murch, P. J. D. Winyard, S. Koletzko, B. Wehner, H. A. Cheema, R. A. Risdon, A. D. Phillips, N. Meadows, N. J. Klein and J. A. Walker-Smith, *Lancet*, 1996, **347**, 1299−1301.

295. C. E. Mogensen, R. Osterby, K. W. Hansen and E. M. Damsgaard, *Diabetes Care*, 1992, **15**, 1192−1204.

296. M. Dubniks, J. Persson and P. O. Grande, *Intensive Care Med.*, 2007, **33**, 293−299.

297. O. H. Lowry, N. J. Rosebrough, A. L. Farr and R. J. Randall, *J. Biol. Chem.*, 1951, **193**, 265−275.

298. M. M. Bradford, *Anal. Biochem.*, 1976, **72**, 248−254.

299. C. A. Royer, *Chem. Rev.*, 2006, **106**, 1769−1784.

300. I. Eryazici, C. N. Moorefield and G. R. Newkome, *Chem. Rev.*, 2008, **108**, 1834−1895.

301. R. Ghai, R. J. Falconer and B. M. Collins, *J. Mol. Recognit.*, 2012, **25**, 32−52.

302. K. Kanazaki, K. Sano, A. Makino, A. Takahashi, J. Deguchi, M. Ohashi, T. Temma, M. Ono and H. Saji, *J. Biomed. Opt.*, 2014, **19,** 096002(1-9).

303. R. Kumaran, M. Vanjinathan and P. Ramamurthy, *J. Lumin.*, 2015, **164**, 146–153.

304. X. Fan, Q. He, S. Sun, H. Li, Y. Pei and Y. Xu, *Chem. Commun.*, 2016, **52**, 1178–1181.

305. K. Jurek, J. Kabatc and K. Kostrzewska, *Color. Technol.*, 2016, **0**, 1–8.

306. X. Gu, Q. Chen and Z. Fang, *Dyes Pigm.*, 2017, **139**, 334–343.

307. C. M. Golini, B. W. Williams and J. B. Foresman, *J. Fluoresc.*, 1998, **8**, 395–404.

308. C. E. Kung and J. K. Reed, *Biochemistry*, 1989, **28**, 6678–6686.

309. R. O. Loutfy, *Macromolecules*, 1981, **14**, 270–275.

310. S. Ercelen, A. S. Klymchenko and A. P. Demchenko, *FEBS Lett.*, 2003, **538**, 25–28.

311. S. E. Michael, *Biochem. J.*, 1962, **82**, 212–218.

312. G. Wang, W. Xu, Y. Guo and N. Fu, *Sens. Actuators, B*, 2017, **245**, 932–937.